

THREE DIMENSIONAL ANALYSIS OF ROCKFILL DAMS UNDER GRAVITY LOADING

A THESIS

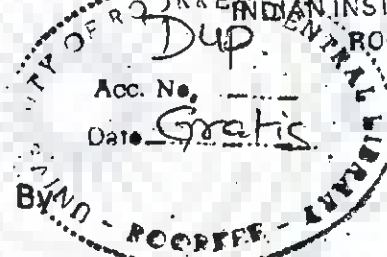
submitted in fulfilment of the
requirements for the award of the degree

of

DOCTOR OF PHILOSOPHY

in

WATER RESOURCES DEVELOPMENT CENTRAL LIBRARY
INDIAN INSTITUTE OF TECHNOLOGY
ROORKEE-247 667



910976

11-7-02

RAM PAL SINGH



WATER RESOURCES DEVELOPMENT TRAINING CENTRE
UNIVERSITY OF ROORKEE
ROORKEE-247667. (INDIA)

APRIL, 1991

CANDIDATE'S DECLARATION

I hereby certify that the work which is being presented in the thesis entitled " THREE DIMENSIONAL ANALYSIS OF ROCKFILL DAMS UNDER GRAVITY LOADING " in fulfilment of the requirement for the award of the Degree of DOCTOR OF PHILOSOPHY, submitted in the Department of Water Resources Development Training Centre of the University of Roorkee, Roorkee is an authentic record of my own work carried out during the period from May 1984 to March 1991 under the supervision of Dr. Bharat Singh and Dr. S.S. Saini.

The matter embodied in this thesis has not been submitted by me for the award of any other degree.

R. P. Singh

(RAM PAL SINGH)
(Candidate's signature)

This is to certify that the above statement made by the candidate is true and correct to the best of our knowledge.

S. S. Saini

(S. S. Saini)
Professor
Civil Engineering Department
University of Roorkee, Roorkee(U.P)
INDIA

Bharat Singh
(Bharat Singh)
Professor Emeritus
Water Resources Development
Training Centre
University of Roorkee,
Roorkee(U.P)
INDIA

ROORKEE

DATED : April 22 , 1991

The Ph. D. Viva - Voce examination of Sri Ram Pal Singh,
Research Scholar has been held on

Signature of Guide(s)

Signature of External Examiner(s)

ACKNOWLEDGEMENT

The author expresses his deep regards and sincere thanks to his supervisors, Dr. Bharat Singh, Professor Emeritus, Water Resources Development Training Centre and Dr. S. S. Saini, Professor of Civil Engineering, University of Roorkee, Roorkee for their inspiration, invaluable guidance and continuous encouragement during the course of investigations reported in the thesis.

The author is also grateful to the Director, Water Resources Development Training Centre, University of Roorkee for providing facilities for this study.

Thanks are also due to the staff of Roorkee University Regional Computer Centre and to Dr. Jia Lal in particular for their ever helping and cooperative attitude during the course of running the programs on DEC - 2050 system.

SYNOPSIS

The objective of this study is to carry out three dimensional sequential non-linear analysis of rockfill dams with central core for gravity loading. The dams have been considered to be located in valleys of different shapes to bring out the effects of valley width, valley slope and material properties on the stresses and deformations in them. Parameters of the valley under which a plane strain analysis of the maximum transverse section would be adequate to predict the response of the dam, have been brought out.

The canyon and section of a proposed 260 m high dam has been used in this study. The canyon has a valley width factor (top valley width to height ratio) of 2.25. Other valley shapes have been considered with valley width factors of 1.12, 4.5 and 9.0. The same transverse section has been used for all the three dimensional analyses and plane strain analysis to facilitate comparison of the results of 3-D and plane strain analyses.

The materials of the various zones (shell, transition and core) of the dam have been taken to exhibit non-linear behaviour. The hyperbolic model (16) has been adopted to model the stress strain behaviour of the materials. The weight of the dam is applied in six sequential stages to simulate the construction sequence. The dam is discretised into 98 number of 20-noded brick elements and consists of 724 nodes, each having 3 degrees of freedom, thus a total of 2172 degrees of freedom. For plane strain analysis of the maximum transverse section of the dam, 8-noded isoparametric elements have been used. The foundations and the abutments for all the analyses have been

taken as rigid.

A digital computer program has been developed to carry out the three dimensional sequential non-linear analysis of rockfill dams. The program uses residual force approach (56) to equilibrate the loads applied. The ratio of the norm of residual loads to that of the applied loads has been used as the criteria to stop further iterations. Another program to plot the results of all the 3-D analyses and plane strain analysis jointly or individually on a calcomp plotter has also been developed.

Study has also been made to assess separately the contribution of valley base width and valley wall slope in comparison to the effect of valley width factor. Three base widths of valley (20, 40 and 80 m) at a valley wall slope of 0.5H:1V, two base widths (40 and 80 m) at 1H:1V valley wall slope and 80 m base width at 2H:1V valley wall slope, have been taken.

The effect of core stiffness on the dam behaviour has also been studied with four values of core stiffness, keeping all other material properties unchanged, for one valley with valley width factor of 2.25. The effect of material properties on the performance of the dam due to change in valley width factor has also been studied at two different valley shapes with valley width factors of 2.25 and 4.50 respectively, each with two values of core stiffness.

The studies show that for dams situated in valleys with valley width factor β greater than or equal to 4.5, a plane strain analysis of the maximum transverse section is adequate

to accurately predict the stresses in the dam section. For displacements, however, the limiting valley width factor beyond which a 3-D analysis will not be required is 9. For narrow valleys significant differences in magnitudes of stresses and displacements are observed, with 3-D stresses and displacements being substantially lower than those given by plane strain analysis, and therefore a three dimensional analysis is a must for such valleys.

The effect of increase in valley base width on the stresses and displacements in the dam is more than that of the effect of valley wall slope. For the valley shapes studied, flattening of valley wall beyond 1H:1V at a constant valley base width does not significantly affect the stresses in the dam and the displacements are not affected beyond 2H:1V slope. The effect of valley wall slope goes on decreasing as the valley base width increases.

The studies indicate that the change in core stiffness has practically no effect on the stresses in the pervious zones of the dam while the stresses in the core increase as the core stiffness increases. With increase in core stiffness, the displacements in the dam decrease, the reduction increasing from the dam faces upto the core centre line. With the change in material properties the performance of the dam with respect to valley shape is not affected.

NOTATIONS

$a, c, d,$	Material parameters
b	Material parameter, valley base width
$\langle b \rangle$	Body force vector
b_x, b_y, b_z	Body forces in x, y and z directions
$[B]$	Strain displacement matrix
$[B_i]$	B - matrix corresponding to node, i
c	Unit cohesion
C_f	Convergence factor
C_R	Convergence ratio
D	Compression modulus
$[D]$	Stress strain matrix
E	Young's modulus of elasticity
E_i	Initial Young's modulus
E_{oed}	Young's modulus obtained from oedometric tests
E_t	Tangent modulus of elasticity
F, K_b, n	Material parameters
$\langle F \rangle$	Load vector
$\langle F \rangle^e$	Element load vector
$\langle f \rangle$	Displacement vector
G	Material parameter, shear modulus
G_i	Initial shear modulus
G_t	Tangent shear modulus
i	Iteration/node number
$[I]$	Identity matrix
$[J]$	Jacobian matrix
K	Bulk modulus, modulus number
K_0	Coefficient of lateral earth pressure at rest
K_t	Tangent bulk modulus

$[K]$	Assembled stiffness matrix
$[K]^e$	Element Stiffness matrix
M_b	Bulk modulus
M_d	Distortional modulus
m	Mobilisation factor, material parameter
$[N]$	Shape function matrix
$\langle p \rangle$	Vector of pressure forces
P_x, P_y, P_z	Pressures in x, y and z directions
N_i	Shape function for ith node
P_a	Atmospheric pressure
R_f	Failure ratio
S_f	Shear ratio
u, v, w	Displacement along x, y and z axes
$\langle u \rangle, \langle v \rangle, \langle w \rangle$	Vectors of nodal displacements in x, y and z-directions
V	Volume
x, y, z	Co-ordinate along x, y and z axes
$\langle x \rangle, \langle y \rangle, \langle z \rangle$	Vectors of nodal coordinates in x, y and z directions
γ, γ_t	Unit weight
γ_{oct}	Octahedral shear strain
Δ	Increment
δ	Displacement
$\langle \delta \rangle$	Nodal displacement vector
δ_i	Displacement for ith node
ϵ_a	Axial strain
ϵ_r	Radial strain
ϵ_d	Resultant deviatoric strain
ϵ_m	Mean normal strain

ϵ_{oct}	Octahedral strain
ϵ_v	Volumetric strain
$\langle \epsilon \rangle$	Vector of strains
$\langle \epsilon_0 \rangle$	Initial strain vector
ν	Poisson's Ratio
ν_i	Initial Poisson's Ratio
ν_t	Tangent Poisson's Ratio
$\sigma_x, \sigma_y, \sigma_z$	Horizontal Normal Stress in x-direction
$\sigma_1, \sigma_2, \sigma_3$	Major, intermediate and minor principal stress
$(\sigma_1 - \sigma_3)$	Deviator stress
$(\sigma_1 - \sigma_3)_f$	Deviatoric stress at failure
$(\sigma_1 - \sigma_3)_{ult}$	Ultimate deviatoric stress
$\langle \sigma \rangle$	Vector of stresses
τ	Shear stress
$\tau_{xy}, \tau_{yz}, \tau_{zx}$	Shear stresses in the x-y, y-z and z-x planes respectively
τ_{oct}	Octahedral shear stress
τ_f	Octahedral shear stress at failure
τ_m	Mean shear stress
τ_{max}	Maximum shear stress
σ_1 / σ_3	Principal stress ratio
β	Valley width factor
μ	Accelerator
ϕ	Angle of internal friction
$\langle \psi \rangle$	Residual force vector
ξ, η, ζ	Natural coordinates
ξ_i, η_i, ζ_i	Natural coordinates of the i th node
$\frac{\partial}{\partial x}, \frac{\partial}{\partial y}, \frac{\partial}{\partial z}$	Partial derivatives with respect to cartesian coordinates

$$\frac{\partial}{\partial x}, \frac{\partial}{\partial y}, \frac{\partial}{\partial z}$$

Partial derivatives w.r.t. natural coordinates



CONTENTS

	Page No.
CERTIFICATE	i
ACKNOWLEDGEMENT	ii
SYNOPSIS	iii
NOTATIONS	vi
CONTENTS	x
LIST OF TABLES	xiv
LIST OF FIGURES	xvii
CHAPTER 1 : INTRODUCTION	1-10
1.1 GENERAL	1
1.2 LIMIT EQUILIBRIUM METHODS	2
1.3 FINITE ELEMENT METHOD FOR DAM ANALYSIS	3
1.4 3-D ANALYSIS VERSUS 2-D ANALYSIS	4
1.5 SCOPE OF THE STUDY	6
1.6 CONCLUSIONS OF THE STUDY	9
CHAPTER 2 : REVIEW OF LITERATURE	11-20
2.1 PALMERTON'S WORK	.
2.2 WORK BY EISENSTEIN et al	.
2.3 ANALYSIS OF DUNCAN DAM	14
2.4 ANALYSIS BY LEFEBVERE et al	16
2.5 ANALYSIS OF MICA DAM	18
2.6 ANALYSIS OF CHICOASEU DAM	21
2.7 ANALYSIS OF INFIERNILLO DAM	23
2.8 ANALYSIS OF OROVILLE DAM	26
2.9 ANALYSIS OF TEHRI DAM	27
CHAPTER 3 : METHOD OF ANALYSIS	33-59
3.1 DESCRIPTION OF THE METHOD	33
3.1.1 Displacement Function	33

3.1.2	Shape Functions	34
3.1.3	Strains	35
3.1.4	Stresses	38
3.1.5	Stiffness Matrix	39
3.2	NON LINEAR ANALYSIS	40
3.2.1	Techniques for Incorporating NonLinearity	41
3.2.1.1	Incremental procedures	41
3.2.1.2	Iterative procedures	43
3.2.1.3	Mixed Procedures	45
3.2.2	Approach used in the Studies	46
3.3	CONSTITUTIVE LAWS	51
3.3.1	Linear Elastic Analysis	51
3.3.2	Non-Linear Stress-Strain Behaviour	53
3.3.2.1	Bilinear Models	53
3.3.2.2	Multilinear or Piecewise Linear Models	53
	Tabular Form	53
	Functional Form	54
	Other Forms	57
CHAPTER 4 :	SALIENT FEATURES OF DIGITAL COMPUTER PROGRAM	60-74
4.1	FENA3D	60
4.2	GP3DPT	65
4.3	CONVERGENCE RATE	67
4.4	CPU TIME	69
CHAPTER 5 :	ANALYSIS TO STUDY THE EFFECT OF VALLEY WIDTH	75-146
5.1	ANALYSIS PERFORMED	76
5.2	NUMERICAL DATA	77
5.3	SIGN CONVENTION	77
5.4	PARAMETERS STUDIED	78
5.5	RESULTS AND DISCUSSIONS	79

5.5.1 Displacements	79
5.5.1.1 Horizontal Movement - u	79
5.5.1.2 Vertical Movement - w	81
5.5.1.3 Cross Valley Movement - v	84
5.5.2 Stresses	85
5.5.2.1 Transverse Normal Stress σ_x	85
5.5.2.2 Longitudinal Normal Stress σ_y	89
5.5.2.3 Vertical Normal Stress σ_z	90
5.5.3 Mobilisation Factor	94
5.5.4 Principal Stress Ratio (σ_1/σ_3)	97
5.5.5 Horizontal Stress Ratio (σ_x/σ_y)	100
5.5.6 Contact Pressure at Abutment Contact	103
5.6 CONCLUSIONS	104
CHAPTER 6 : EFFECT OF VALLEY SHAPE AND BASE WIDTH	147-192
6.1 CASES STUDIED	147
6.2 ANALYSES PERFORMED	148
6.3 RESULTS AND DISCUSSIONS	149
6.3.1 Displacements	149
6.3.1.1 Transverse Horizontal Movement (u)	149
6.3.1.2 Vertical Movement (w)	152
6.3.2 Stresses	154
6.3.2.1 Horizontal Normal Stress σ_x	154
6.3.2.2 Horizontal Normal Stress σ_y	157
6.3.2.3 Vertical Normal Stress σ_z	159
6.3.3 Stress Ratio	162
6.3.3.1 Horizontal Stress Ratio σ_x/σ_y	162
6.3.3.2 Principal Stress Ratio σ_1/σ_3	163
6.3.4 Mobilisation Factors	165
6.4 EFFECT OF VALLEY WALL SLOPE VARIATION AT CONSTANT BASE WIDTHS	168
6.4.1 Displacements	168
6.4.1.1 Horizontal Movements - u	168
6.4.1.2 Vertical Movements - w	170

6.4.2 Stresses	172
6.4.2.1 Horizontal Stress σ_x	172
6.4.2.2 Horizontal Longitudinal Stress σ_y	174
6.4.2.3 Vertical Normal Stress σ_z	176
6.5 CONCLUSIONS	178
CHAPTER 7 : EFFECT OF MATERIAL PROPERTIES ON DAM BEHAVIOUR	193-216
7.1 INTRODUCTION	193
7.2 CASES STUDIED	194
7.3 RESULTS	194
7.3.1 Different Values of K at Constant Valley Width, Case (1)	194
7.3.1.1 Stresses	194
7.3.1.2 Mobilisation Factors	197
7.3.1.3 Displacements	199
7.3.2 Effect of Valley Shape at Different Core Stiffness, Case (2)	202
7.3.2.1 Stresses	202
7.3.2.2 Displacements	204
7.4 CONCLUSIONS	206
CHAPTER 8 : CONCLUSIONS	217-221
EFFECT OF VALLEY WIDTH FACTOR	217
EFFECT OF VALLEY BASE WIDTH AND WALL SLOPES	218
EFFECT OF MATERIAL PROPERTIES	220
REFERENCES	222-227

LIST OF TABLES

TITLE	Page No.
2.1 Material Properties	12
2.2 Material Properties for Linear Analysis of Mica Dam	19
2.3 Material Properties Chicoasen Dam	22
2.4 Modified Mechanical Properties of Chicoasen Dam	22
2.5 Material Properties of Infiernillo Dam	24
4.1 Convergence Factors in Different Iterations	67
4.2 CPU time for a 3-D Analysis	69
5.1 Details of Valley Shapes Analysed	76
5.2 Material Properties	77
5.3 Cross Valley Displacements at Plane No. 2	84
5.4 Maximum - v Displacements on Plane no. 3	85
5.5 Maximum Values of Mobilisation Factors at Central Section	95
5.6 Maximum Values of σ_1/σ_3 along Verticals at Central Section	99
5.7 Maximum Values of Ratio σ_1/σ_3 at Plane No. 2	100
5.8 Normal Contact Pressure in Core at Abutment	103
6.1 Details of Cases Studied	147
6.2 Horizontal Movements (cms) On Plane No. 1	150
6.3 Horizontal Movement Values u(cms) on Plane No. 2	151
6.4 Vertical Settlements at Central Section	152
6.5 Vertical Settlement at Plane no. 2	153
6.6 Transverse Normal Stress σ_x at Central Section	155
6.7 Transverse Normal Stress σ_x on Plane No. 2	156
6.8 Longitudinal Normal Stress σ_y at Central Section	158

6.9 Longitudinal Normal Stress σ_y on Plane No. 2	158
6.10 Vertical Normal Stress σ_z at Central Section	160
6.11 Vertical Normal Stress σ_z on Plane No. 2	161
6.12 Typical Values of Stress Ratio σ_x/σ_y on Central Section	162
6.13 Typical Values of Stress Ratio σ_x/σ_y on Plane No. 2	163
6.14 Typical Values of Stress Ratio σ_1/σ_3 on Central Section	164
6.15 Typical Values of Stress Ratio σ_1/σ_3 on Plane No. 2	164
6.16 Mobilisation Factor m on Central Section	166
6.17 Mobilisation Factor m on Plane No. 2	166
6.18 Incremental Horizontal Transverse Displacements - u on Central Section	169
6.19 Incremental Horizontal Transverse Displacement - u on Plane No.2	170
6.20 Incremental Vertical Displacements - w On Central Section	171
6.21 Incremental Vertical Displacement - w on Plane No. 2	172
6.22 Incremental Transverse Normal Stress σ_x on Central Section	173
6.23 Incremental Transverse Normal Stress On Plane No. 2	174
6.24 Incremental Longitudinal Normal Stress σ_y on Central Section	175
6.25 Incremental Longitudinal Normal Stress σ_y on Plane no. 2	176
6.26 Incremental Vertical Normal Stress σ_z on Central Section	177
6.27 Incremental Vertical Normal Stress σ_z on Plane No. 2	178
6.28 Mobilisation Factors and Principal Stress Ratio	180
7.1 Horizontal Normal Stress σ_x Over Central Section	195
7.2 Horizontal Normal Stress σ_y Over Central Section	195
7.3 Vertical Normal Stress σ_z Over Central Section	196

7.4	Typical Maximum Values of Mobilisation Factors	197
7.5	Horizontal Movement - u (cms) Over Central Section	200
7.6	Vertical Movement - w (cms) Over Central Section	200
7.7	Cross Valley Movement - v (cms) at Plane no. 2	201
7.8	Horizontal Normal Stress σ_x (t/m^2) over Central Section	203
7.9	Horizontal Normal Stress σ_y (t/m^2) over Central Section	203
7.10	Vertical Normal Stress σ_z (t/m^2) over Central Section	204
7.11	Horizontal Movement - u (cms) Over Central Section	205
7.12	Vertical Movement - w (cms) Over Central Section	205



List of Figures

No.	Title	Page No.
2.1	(a) Typical Cross Section of Duncan Dam (b) Longitudinal Section of Duncan Dam and Foundation showing Construction Sequence and Location of Cracks	29
2.2	(a) Plan View of Mica Dam (showing also location of MV gauges) (b) Main Transverse Section of Mica Dam (showing also material distribution)	30
2.3	Major Principal Stresses along Vertical Columns of Core	31
2.4	(a) Maximum Transverse Section of Chicoasen Dam (b) Maximum Longitudinal Section of Chicoasen Dam	32
3.1	3-D Finite Element showing Node Numbers	58
3.2	Non Linear Curves	58
3.3	Basic Incremental Procedure	58
3.4	Iterative Procedures (a) Tangent Stiffness Procedure (b) Modified Procedure	59
3.5	Step Iterative Procedures	59
3.6	Mixed Procedure	59
4.1	Flow Chart for FENA3D Program	70-74
5.1.	Section of 260 m High Rockfill Dam	109
5.2.	Finite Element Idealisation of Dam (a) Longitudinal Section along Upstream Face of Core (b) Maximum Transverse Section of Dam	110
5.3.	Horizontal Movements u -along Height At Different Locations over Central Section	111
5.4.	(a) Maximum Horizontal Displacements at Central Section (b) Maximum Horizontal Displacements over Plane No. 2	112
5.5.	Sequential Variation of Horizontal Displacement u for 3-D Analysis at Central Section ($\beta=1.12$)	113

5.6.	Contours of Horizontal Movement - u at Central Section	114
	(a) Plane Strain and 3-D Analysis with $\beta = 1.12$	
	(b) 3-D Analysis with $\beta = 9$	
5.7.	Contours of Horizontal Movement-u at Longitudinal Section along Upstream Face of Core	115
	(a) Valley Width Factor $\beta=1.12$	
	(b) Valley Width Factor $\beta=9$	
5.8.	Vertical Movement w along Height at Different Locations over Central Section	116
5.9	(a) Maximum Vertical Displacements at Central Section	
	(b) Maximum Vertical Displacements over Plane No. 2	117
5.10.	Sequential Variation of Vertical Displacement-w for 3-D Analysis at Central Section ($\beta=1.12$)	118
5.11.	Vertical Movements w at Constant Elevation over Central Section	119
5.12.	Vertical Movement-w at Constant Elevations over Longitudinal Section	120
	(a) Along Upstream Face of Core	
	(b) Along Centre Line of Core	
5.13.	Contours of Vertical Movement-w at Central Section	121
	(a) Plain Strain and 3-D Analysis with $\beta = 1.12$	
	(b) 3-D Analysis with $\beta=9$	
5.14.	Horizontal Normal Stress σ_x along Height at Different Locations over Central Section	122
5.15.	Horizontal Normal Stress σ_x along Verticals over Plane No. 2	123
5.16	(a) Maximum σ_x Stress at Central Section	
	(b) Maximum σ_x Stress over Plane No. 2	124
5.17.	Sequential Variation of σ_x for 3-D Analysis $\beta=1.12$	125
5.18.	Horizontal Normal Stress σ_x at Constant Elevations	126
	(a) Central Section	
	(b) Plane No. 2	
5.19.	(a) Stress σ_x along Centre Line of Core	
	(b) Stress σ_x on Upstream Face of Core	127
5.20.	Contours of Stress σ_x at Central Section	128
	(a) Plane Strain and 3-D Analysis with $\beta=2.25$	
	(b) 3-D Analysis with $\beta=9$	

5.21.	Contours of Stress σ_x at Longitudinal Section ($\beta=2.25$)	129
	(a) Along the Upstream Face of Core	
	(b) Along Centre Line of Core	
5.22	(a) Maximum σ_y Stress at Central Section	130
	(b) Maximum σ_y Stress over Plane No. 2	
5.23.	Sequential Variation of σ_y for 3-D Analysis ($\beta=1.12$)	131
5.24.	Horizontal Normal Stress σ_y at Constant Elevations	132
	(a) Central Section	
	(b) Plane No. 2	
5.25.	Vertical Normal Stress σ_z along Height over Central Section	133
5.26	(a) Maximum σ_z at Central Section	134
	(b) Maximum σ_z Stress over Plane No. 2	
5.27.	Sequential Variation of σ_z for 3-D Analysis ($\beta=1.12$)	135
5.28.	Vertical Normal Stress σ_z at Constant Elevations	136
	(a) Central Section	
	(b) Plane No. 2	
5.29.	Contours of Stress σ_z at Longitudinal Section ($\beta=2.25$)	137
	(a) Along the Upstream Face of Core	
	(b) Along Centre Line of Core	
5.30	Contours of Stress σ_z at Central Section	138
	(a) Plane Strain and 3-D Analysis with $\beta=2.25$	
	(b) 3-D Analysis with $\beta = 9$	
5.31.	Contours of Stress σ_z over Plane No. 2	139
	(a) 3-D Analysis with $\beta=2.25$	
	(b) 3-D Analysis with $\beta=9.00$	
5.32.	Mobilisation Factor m along Height at Central Section	140
5.33.	Contours of Mobilisation Factor over Central Section	141
	(a) 3-D Analysis with $\beta=2.25$	
	(b) 3-D Analysis with $\beta=9.00$	
5.34.	Contours of Mobilisation Factor over Plane No. 2	142
	(a) 3-D Analysis with $\beta=2.25$	
	(b) 3-D Analysis with $\beta=9.00$	

5.35.	Principal Stress Ratio σ_1/σ_3 along Height at Central Section	143
5.36.	Contours of Ratio σ_1/σ_3 over Central Section (a) 3-D Analysis with $\beta=2.25$ (b) 3-D Analysis with $\beta=9.00$	144
5.37.	Contours of Ratio σ_1/σ_3 over Longitudinal Section (a) Along Centre Line of Core (b) Along Upstream Face of Core	145
5.38.	Horizontal Stress Ratio σ_x/σ_y along Height at Central Section	146
6.1	Finite Element Idealisation of the Dam (a) Longitudinal Section along Upstream Face of Core (b) Maximum Transverse Section of Dam	182
6.2.	Horizontal Movement-u along Height over Central Section	183
6.3.	Horizontal Movement-u along Height over Plane No. 2	184
6.4.	Vertical Movement-w along Height over Central Section	185
6.5.	Vertical Movement-w along Height over Plane No. 2	186
6.6.	Transverse Stress σ_x along Height over Central Section	187
6.7.	Transverse Stress σ_x along Height over Plane No. 2	188
6.8.	Longitudinal Stress σ_y along Height over Central Section	189
6.9.	Longitudinal Stress σ_y along Height over Plane No. 2	190
6.10.	Vertical Stress σ_z along Height over Central Section	191
6.11.	Vertical Stress σ_z along Height over Plane No. 2	192
7.1	Transverse Stress over Central Section (Effect of K)	207
7.2	Longitudinal Stress over Central Section (Effect of K)	208
7.3	Vertical Stress over Central Section (Effect of K)	209

7.4	Horizontal Movement - u over Central Section (Effect of K)	210
7.5	Vertical Movement - w over Central Section (Effect of K)	211
7.6	Transverse Stress over Central Section (Effect of K and β)	212
7.7	Longitudinal Stress over Central Section (Effect of K and β)	213
7.8	Vertical Stress over Central Section (Effect of K and β)	214
7.9	Horizontal Movement - u over Central Section (Effect of K and β)	215
7.10	Vertical Movement - w over Central Section (Effect of K and β)	216



CHAPTER 1

INTRODUCTION

1.1 GENERAL

With the increasing tempo of water resources development all over the world, there has been rapid increase in the number of dams constructed for irrigation, power generation, water supply and other purposes. Dams of all kinds and types have been built depending on the topographical and geological conditions obtaining at individual sites and the availability of construction materials. Earth and rockfill dams are being increasingly opted for by the designers. Majority of the dams which have been built during the last three decades belong to this category. A number of factors are responsible for the popularity of such types of dams. These include advancement in design methodology, adaptability to various types of foundations, use of naturally occurring earth materials and economy resulting from the use of new construction techniques and development of efficient earth moving equipment. A safe embankment dam can now be built on any type of foundation - hard, compressible or permeable. Practically all types of soils including weathered rock can be utilised for constructing such dams.

The failure of a dam is a calamity at par with such natural catastrophes as earthquakes, volcanic eruptions, land slides and the like, and this places a tremendous responsibility on the designer. Safety of a dam is a prime requisite, an indispensable must. Extreme caution and accuracy are required at the design stage, as well as continuous vigilance is required in monitoring the performance of the dam

after completion. The importance of this vigilance is steadily growing. Due to the ever increasing boldness of dam designer, there is a tendency towards higher dams and larger reservoir volumes. Dams are being built on more difficult and less favourable foundations, and reservoir capacities are now in thousands of millions of cubic metres.

1.2 LIMIT EQUILIBRIUM METHODS

The stability of an earth dam during construction or normal operation is conventionally examined using the limit equilibrium methods of stability analysis. In these methods, a sliding surface is assumed and a quantitative estimate of the factor of safety is obtained by examining the equilibrium conditions at the time of incipient failure and comparing the strength necessary to maintain limiting equilibrium with the available strength of the fill material on the entire surface. The basic assumption made is that the vertical load acting on an element of the slice equals the load of the fill above it. The common methods assuming a circular sliding surface are Fellenius method (24, 61) and Bishop Method (4). The methods enabling assumption of non circular sliding surface are the Morgenstern and Price method (43), wedge method (54, 57) and Janbu's general procedure of slices, GPS (29). This approach finds out the average factor of safety along the sliding surface and any local overstressing leading to redistribution of stress will not be accounted for. An assumption has also to be made regarding the point of application and direction of the interslice forces. These procedures indicate the factor of safety of the dam with respect to instability, but they provide

no information regarding the deformations of the dam. Equilibrium analyses are relatively simple compared to finite element analysis. Because there is a considerable amount of experience in their use, they provide a reasonably sound basis for establishing the stability of earth dams during construction and normal operation.

1.3 FINITE ELEMENT METHOD FOR DAM ANALYSIS

In recent years, however, there has been a growing realization of the need to determine the stress distribution and deformations inside a dam section which can best be done by the finite element method. The deformations may be of interest for a number of reasons (59).

1. Excessive settlements can lead to loss of freeboard and danger of overtopping. Duncan Dam, in Canada, settled about 4.2 m during and after construction.
2. Excessive spreading of an embankment may lead to the formation of longitudinal cracks which adversely affect its stability. Such cracks have been observed in many embankments built on clay foundations.
3. Differential settlements between sections along the crest of a dam may lead to development of transverse cracks through the embankment which could allow passage of water, and progressive failure by erosion and piping. Duncan Dam suffered many cracks which had to be repaired to ensure the integrity of the dam.
4. Differential compressibility of the core and shell of a zoned embankment can lead to reduction in stresses in the core, and may result in hydraulic fracturing, if the

stresses in the core at any elevation are reduced to values less than the pressure of the water in the reservoir at the same elevation, by transfer of part of the load to less compressible shells.

1.4 3-D ANALYSIS VERSUS 2-D ANALYSIS

One of the common assumptions frequently made in the analysis of earth embankments is that plane strain conditions are presumed so that instead of studying the full geometry of the dam, one or two main sections are analysed as a two dimensional problem. While the advantages of this step are obvious, the degree of error associated with it would not be negligible near abutments for high dams in narrow valleys. An earth dam, unless it is long relative to its height and built on fairly uniform foundations, is a three dimensional structure (23).

Until recently the use of the two dimensional simplifications has been dictated by necessity caused by the lack of analytical procedures and techniques powerful enough to handle the problem in three dimensions. Although the spatial effects in earth dams (e.g., cross - valley arching) have been recognised for some time, their quantitative evaluation has been largely a matter of speculation. The development of isoparametric finite elements by Clough (6) and Zienkiewicz et al (66) made it possible in practical terms to perform three - dimensional analyses of real structures with the present generation of computers.

Even when 3-D finite element analysis can be done on a regular basis, however, it will still be desirable to perform 2-D analysis for those conditions for which it is sufficiently

accurate, because 2-D analysis will always require much less man hours and computer time than 3-D analysis (8). Thus it is of considerable interest to determine those conditions for which 2-D analysis can be effectively used. For example, in the case of embankment dams, 2-D (plane strain) analysis provides an accurate representation of conditions in centrally located transverse sections of long dams of uniform cross section, and there is no reason to use 3-D analyses to study the stresses or movements under such conditions. However, plane strain analysis may not provide a suitable representation of the transverse section for dams in steep walled valleys, because of the effects of cross valley stress transfer. Similarly there is doubt concerning the accuracy of either plane stress or plane strain analysis of the longitudinal section of dams, as the thickness of a dam perpendicular to the longitudinal section (i.e., measured from u/s to d/s) varies from the top of the dam to the bottom.

Although the 3-D finite element programs can be utilised for practical problems, there is still a considerable difference in their application when compared with two dimensional analyses. The difference is mainly in the logistic and economic spheres, and approximately amounts to one order of magnitude in price, both in terms of computer expenses and in the cost of data preparation and handling. In view of this, it is quite improbable that three dimensional analysis will ever become a matter of routine use. The important question then is to assess the degree of error associated with the 2-D analysis and to delineate those classes of problems where a 3-D analysis

should be used (23).

1.5 SCOPE OF THE STUDY

Very few studies regarding comparisons between two-dimensional and three-dimensional analyses of earth dams have been reported in literature. Comparisons of two-dimensional and three-dimensional behaviour of zoned dams sections have been made by Palmerton (47), Mejia and Seed (42) by using nonlinear stress strain relationship for the materials of dams. Palmerton analysed a dam in a trapezoidal valley with 1H:1V wall slope while Mejia and Seed used two V-shaped valleys with valley width to height ratio of 2 and 6. Lefebvre et al (39) studied the three dimensional behaviour of homogenous dams with valley wall slopes of 1H:1V, 3H:1V and 6H:1V. However, they used linear elastic constant for the material. Eisenstien et al (21) and Singh et al (59) also used linear material properties to study the three dimensional effects on the response of dam located in V-shaped valleys with valley wall sloping at approximately 1H:1V.

Three dimensional analyses of completed dams or under construction at that time have been reported by Eisenstein et al (22) for Duncan dam, Marsal et al (41) for Chicoasen dam, Eisenstein and Simmons (23) for Mica dam and Justo and Saura (52) for Infiernillo dam. Nonlinear material properties have been used in the analysis of Duncan dam which is situated in a flat and wide valley. All other case studies in respect of Chicoasen, Mica and Infiernillo dams have used linear material properties and these dams are located in narrow valleys. It is thus clear that no comprehensive study has been made so far to study the three dimensional behaviour of embankment

dams using nonlinear material properties and simulating sequential construction. A study has, therefore, been carried out to assess the effect of valley shape on stresses and displacements in high embankment dams with zoned sections. Three dimensional incremental non-linear analyses simulating construction sequence of the dam, have been done for end of construction stage, for dams situated in valleys of different shapes. Attempt has been made to determine the limiting valley width where a plane strain analysis will be adequate to predict the response of the dam. Even though simple gravity loading has been used in this study, the pattern of variation in stresses and displacements in the dam with valley shape or soil parameters is expected to be similar with other loading conditions taking water forces into account, and the findings will remain valid for these conditions as well.

A 260 m high rockfill dam with an inclined core in the interior has been selected for the study. The valley walls are inclined at approximately 1H:1V giving a valley width factor (crest length to height ratio), of 2.25. Three other valley shapes have been obtained by scaling this valley by scale factors of 0.5, 2 and 4 in the cross valley direction(y) giving valley width factors of 1.12, 4.5 and 9 respectively. For comparison a plane strain analysis of the maximum transverse section of dam with the same mesh as used for 3-D analysis has also been carried out. The load of the dam is applied in 6 stages and non-linear hyperbolic stress-strain relationship has been used for all the dam materials. The results of all the four analyses have been plotted along vertical and horizontal

planes in the dam and the plane strain analysis results superimposed, wherever necessary. This study is reported in Chapter 5.

In order to distinguish between the effect of valley base width and valley wall slopes, three dimensional analyses have been carried out by varying valley base width at constant valley wall slope and by varying valley wall slope at constant valley base width. In all, six cases have been studied, as detailed below :

- (a) Valley wall slope $0.5H:1V$; base widths 20m, 40m and 80m
- (b) Valley wall slope $1H:1V$; base widths 40m and 80m
- (c) Valley wall slope $2H:1V$; base width 80m

The results of these analyses are presented in Chapter 6.

The influence of material properties on the three dimensional behaviour of embankment dams has been studied in Chapter 7. Three dimensional analysis results of the dam section used in Chapter 5, with a valley width factor β of 2.25, with four different values of core stiffness, keeping properties of other materials the same in all analyses, have been reported. The modulus constant K , describing the initial elasticity of material, of the core has been varied and the four values used are 100, 250, 400 and 1000 respectively. Study of the effect of valley width factor on the dam behaviour has been made at two more values of core modulus constant, K , namely $K=400$ and 1000. Three dimensional analyses with $\beta = 2.25$ and 4.5 respectively at each of the two sets of material properties have been made and the relative increase in stresses and displacements by widening the valley at two different material properties studied. These results too are given in

Chapter 7.

Three dimensional analyses reported in the literature have been briefly reported in Chapter 2. Brief description of the finite element method and element relationships used have been presented in Chapter 3. The various methods incorporating non-linearity of stress-strain relationship have been briefly described and the residual force approach used in this study has been explained in detail in this chapter. Non-linear stress strain models used in the analysis by various researchers have been discussed in brief and the hyperbolic stress-strain model has been described in detail in Chapter 3. Brief descriptions of the FENA3D program developed for performing 3-D nonlinear sequential analysis of the dam and program GP3DPT for plotting the results of various 3-D analyses have been given in Chapter 4. A flow chart of the program FENA3D has also been given in this chapter.

1.6 CONCLUSIONS OF THE STUDY

The studies show that for dams, situated in valleys with valley width factor B greater than or equal to 4.5, a plane strain analysis of the maximum transverse section is adequate to accurately predict the stresses in the dam section. For displacements, however, the limiting valley width factor beyond which a 3-D analysis will not be required is 9. For narrow valleys, significant differences in stresses and displacements are observed, with 3-D stresses and displacements substantially lower than those given by plane strain analysis. The contribution of valley base width to the effect due to simultaneous increase of both the valley base width and wall

slope is substantially higher than that of valley wall slope. For the valley shapes studied, flattening of valley wall beyond 1H:1V at a constant valley base width does not affect the stresses in the dam and the displacements are not affected beyond 2H:1V slope. The effect of valley wall slope goes on decreasing as the valley base width increases.

The studies indicate that for a given geometry the change in core stiffness has practically no effect on stresses in the pervious zones of the dam, while the stresses in the core increase as the core stiffness increases. With increase in core stiffness, the displacements in the dam decrease. The performance of the dam due to change in valley shape remains qualitatively unaffected by the change in material properties.

CHAPTER - 2

REVIEW OF LITERATURE

In view of the high costs involved in three dimensional finite element analysis of structures, the three dimensional analysis has not yet been very popular with dam engineers. Only a few cases are reported in literature where three dimensional analyses of earth dams by finite element method have been performed. The same are reported here in. These cases fall in all the three categories namely academic studies, case studies regarding performance of existing structures and design studies for design of earth dams prior to construction.

2.1 PALMERTON'S WORK

Palmerton (47) performed three dimensional analysis by finite element method using eight noded brick elements, of a 122 m high central core zoned earth fill dam, symmetrical about its centre line. The dam is located in a symmetrical trapezoidal (1H:1V side slopes) valley. Due to symmetry only one-fourth of the dam has been analysed. The dam has been constructed in 15 m thick layers. The abutments and foundations have been assumed to be rigid. The hyperbolic stress-strain model used by Duncan and Chang(16) has been used to simulate the stress-strain behaviour of dam materials. The properties of materials used in the analysis are given in Table 2.1. Plane strain analysis of the maximum transverse section has also been performed and the results of the two analyses have been compared.

In the lower portion of dam the three dimensional analysis gives lower values of stresses as compared to a plane

strain analysis. In the upper portion the two analyses give almost similar values. The reduction in stresses is more in core than in shells. The reduction in stresses for a 3-D analysis in terms of plane strain stresses is 40 % and 59 % in core and 7 and 22 % in shell in case of major and minor principal stresses respectively.

TABLE 2.1 Material Properties

Property	Shell	Core
$Y_t - t/cu\ m$	2.13	2.13
$C - t/sq\ m$	0.0	19.0
R_f	0.70	0.95
K	1000.0	550.0
n	0.50	0.35
d	6.0	0.50
G	0.32	0.44
F	0.14	0.02
K_o	0.50	0.50

Both the analyses give nearly same values of the displacements, with 3-D analysis giving slightly lower values. The location of maximum displacement is same for horizontal displacement, while for vertical displacement the 3-D analysis gives a slightly lower location as compared to a plane strain analysis. The displacements in the softer core are higher than those in shells, while the stresses are higher in the shells. Towards the abutment, the major principal stresses increase, while the minor principal stresses decrease. The points of maximum mobilisation factor also occur near the abutments. The maximum horizontal movement away from the abutment occurs

within the core material approximately midway between the centre line of the dam and the abutment. The maximum horizontal movement (outward) perpendicular to the dam axis is also observed midway between the longitudinal centre line and the faces of the dam. The vertical movements are maximum in the core at the centre line of the dam.

It is concluded that for dams located in narrow steep valleys, plane strain assumptions along the transverse section can lead to rather large errors in predicting behaviour since the action of arching is aided by the valley walls. While the predicted displacements from both plane strain and 3-D analysis are more or less similar, significant differences in stress conditions are observed.

2.2 WORK BY EISENSTEIN et al

Eisenstein et al (21) have studied the effect of three dimensional behaviour on the presence of tensile zones in a dam. The effect of incremental loading and zoning of the dam section on the cracking potential of a dam has also been studied by using different ratios of core and shell elasticity. They have studied a 100 m high zoned earth dam with a centrally located core situated in a symmetrical V-shaped valley (1H:1V side slopes). Due to the symmetry in both longitudinal and transverse directions only a fourth of dam has been analysed. Abutments and foundations have been assumed to be rough and rigid. The finite element analysis program uses 8 noded hexahedran elements. Linear material properties have been used in the analysis. The effects of incremental loading have been studied by comparing the results from construction in a single

lift to those from construction in five lifts. The study leads to the following conclusions :

- For longitudinal sections of symmetrical valley shapes, located along the centre line of a homogeneous embankment loaded by gravity alone, the differences between two and three dimensional analysis are small and, therefore, a plane strain analysis is adequate. For a non-homogeneous embankment constructed of two or more materials the differences between two and three dimensional analysis are appreciable.

- For a section with core stiffer than shell, a plane strain analysis gives lower values of tension and a smaller tension zone than a 3-D analysis while for section with softer core the opposite is the case. Thus, where cracking is imminent, a 3-D analysis will yield more realistic results.

- Incremental analysis reduces the value of tensile stresses as well as the tensile zones.

- By controlling the compaction of shell and moisture content of core and improving placement conditions, crack resistant embankment can be designed.

2.3 ANALYSIS OF DUNCAN DAM

Eisenstein, Krishnaya and Morgenstern (22) are the first to test the results of 3-D finite element analysis on a well documented case history of cracking sequence at Duncan Dam in Canada. Duncan Dam, built in 1964-67 on the Duncan river in British Columbia, Canada, is an earthfill dam of about 36 m height and 762 m length with an upstream sloping core. The dam has been built across a valley underlain by a buried canyon about 378 m deep which is filled with sediments. The stratigraphy of the foundation is rather irregular with the

upper layers possessing considerable compressibility. A typical cross section of the dam and longitudinal section are shown in Fig. 2.1.

Large amount of settlements anticipated in the dam had been accounted for in the design. While the predicted and observed settlements agreed in their magnitudes, the observed distribution pattern differed from the predicted one. Because of differential settlements along the longitudinal direction, transverse cracks appeared in an area located at the upstream side of the dam close to the left abutment.

The dam has been analysed by a 3-D finite element program using hexahedral isoparametric elements with 8 nodes. The analysis has been performed incrementally and follows the actual sequence of filling. The elastic parameters have been derived from stress-strain relationships obtained from triaxial compression tests on the core and shell materials. The curves were introduced directly into the computer point by point and the tangent material stiffness parameters were interpolated from them according to the particular level of deviator and minor principal stresses. The volumetric strain data were truncated to preclude any dilatancy. A poisson's ratio of 0.49 was used beyond the range covered by the curves.

The study concludes that the area computed in tension on the basis of a three-dimensional analysis, agrees well with the position of cracks observed on the dam. The results from the incremental analysis incorporating the nonlinear stress-strain relations and non-homogeneity of section, have been found to be consistent with both the location of the cracks and their

propagation during construction. Hence, finite element analysis can provide substantial information regarding the location and extent of cracks in earth structures and thus, can be of considerable assistance in design.

2.4 ANALYSIS BY LEFEBVRE et al

Lefebvre et al (39) made studies to show the accuracy with which 2-D analysis might be used to study the behaviour of dams in V-shaped valleys. Results from plane strain analysis of the transverse section and of both plane strain and plane stress analysis of the longitudinal sections of the dams in a number of valleys have been compared with those of the 3-D analyses. The valley walls used in the analysis are 1H:1V, 3H:1V and 6H:1V. Each of the dams analysed is 48 m high and is represented by 8 layers of elements of uniform thickness.

A quadrilateral element of arbitrary geometry has been used for the two-dimensional analyses while an eight node isoparametric element has been used for the three dimensional analyses.

Linear elastic material properties have been used in the analysis with Young's modulus $E=1090 \text{ t/m}^2$ and Poisson's ratio $=0.4$. Both the two dimensional and the three dimensional analyses have been performed using incremental procedure, in which placement of successive layers of the fill in the dam is simulated one at a time. The nodal points along the bottom of the dam are assumed to be fixed.

The study shows that the maximum values of stresses and displacements are generally smaller for dams in steeper valleys, indicating a significant degree of cross valley arching in dams located in such valleys. The horizontal

displacement attains the maximum value for the dam in the valley with a 3H:1V valley wall slope. It is believed that because of two counteracting effects of increasing valley wall slopes namely (i) greater tendency for horizontal movement and (ii) greater restraint against movement with steepness increasing, the magnitude of horizontal displacement first increases and then decreases as the valley wall slopes become steeper.

A plane strain analysis of the transverse section gives higher values of major principal stress (σ_1), maximum shear stress τ_{max} and displacements but lower values of minor principal stress σ_3 as compared to a 3-D analysis of the dam. The difference in the two sets of the results is quite small for dams in valley with slopes of 6H:1V and is large for dam in valley with slopes at 1H:1V. It is, therefore, concluded that for valley wall slopes at 3H:1V or flatter, a plane strain analysis of the maximum transverse section provides reasonable accurate results, while for valleys as steep as 1H:1V the results are not accurate due to the effect of cross valley arching.

Plane strain analysis of the maximum longitudinal sections provides fairly accurate results for all the valley slopes analysed. However, plane stress analyses of these sections provide inaccurate results and the inaccuracies are quite large and of the same order for all the slopes analysed.

2.5 ANALYSIS OF MICA DAM

Eisenstein and Simmons (23) performed both two and three

dimensional finite element analyses of the 243 m high earthfill Mica dam in British Columbia, Canada for the end of construction stage. The dam, built in a skewed, irregular and steep valley has been extensively instrumented and readings taken regularly. The program employed eight noded isoparametric hexahedral elements. Economic restrictions on mesh size limited the number of increments of loading to five, one modelling the river overburden excavation and the four for embankment construction (one each season). The program had options for linear or non-linear stress-strain relationship for incremental analysis and for criteria of failure due to tension or shear. The mesh consisted of 254 elements and 276 nodal points. The sections of the dam are given in Fig. 2.2.

Nonlinear stress strain relationships were inferred with judgement from oedometer laboratory tests and field data. The nonlinearity was modelled by allowing the moduli to vary with expected stress-levels in the elements. The selection of deformation modulus was made using Poisson's ratio and the one dimensional compression modulus D defined below, as the two required elastic parameters.

$$D = \frac{\Delta \sigma_z}{\Delta \epsilon_z} \quad (2.1)$$

where $\Delta \sigma_z$ = increment in vertical stress

$\Delta \epsilon_z$ = increment in vertical strain

The Poisson's ratio was chosen as a reasonably constant value given by $\nu = K_0/(1+K_0)$, where K_0 = coefficient of earth pressure at rest. The properties used in linear analysis are given in Table 2.2

Table 2.2: Material Properties for Linear Analysis of Mica Dam

Material	Unit wt. (t/m ³)	D (t/m ²)	ν
Core zone M1 (69 season)	2.30	17900	0.35
Core zone M1 (70-72 season)	2.40	36700	0.33
Shell zone M2 (69 season)	2.52	87700	0.28
Shell zone M2 (70-72 season)	2.43	87700	0.28
Shell zone M2DI (69 season)	2.50	75200	0.29
Shell zone M2DI (70-71 season)	2.43	65800	0.29
River overburden	2.43	98500	0.31

As the study was comparative in nature, following types of analyses were performed :

- i) Two-dimensional linear analysis
- ii) Three-dimensional linear analysis
- iii) Three-dimensional linear analysis with bedrock movement
- iv) Three dimensional multilinear analysis with bed rock movements.

The analyses with bedrock movements were made because the excavation of river overburden material for the core trench caused substantial heave of bedrock (a maximum of about 15 cms) and the heaved zone, when subsequently loaded by the fill experienced settlements larger than elsewhere. The measured vertical movements were used as known displacements at appropriate boundary nodes. Since the bedrock movements were related to the weight of the fill, the boundary displacements

were applied incrementally with corresponding lifts of the dam.

The computed displacements of Mice dam showed good agreement with field measurement. The plane strain settlements were for most points somewhat larger than the corresponding 3-D results, the maximum difference amounting to less than 20%. However, since the difference was not constant within the profile investigated it could be due to the coarse mesh. Horizontal movements were very small and no meaningful comparison could be made with the computed values. Maximum horizontal movements were 4 cm against 82 cm for maximum vertical settlement. The 3-D and 2-D plane strain stresses for the main transverse section in the zoned dam were very similar indicating that cross valley arching did not play an important role in the stress transfer.

In order to separate the effect of non-homogeneity of the zoned profile and of the arching across the narrow valley, a 3-D analysis of an equivalent homogeneous embankment was performed. For this type of analysis a modulus was sought which would yield overall displacement results matching approximately an overall behaviour. The major principal stress along a vertical in the core is shown in Fig. 2.3. for different analyses. It is seen that for the homogeneous dam, there is a stress transfer of about 30% from the core portion to the shell portion, while for the zoned dam the stress transfer is of the order of about 70% near the base. At higher elevations where the geometric effects would be minimal, the stress transfer was constant at about 10% and 40% respectively for the homogeneous and zoned embankments.

The study concluded that

- The 3-D finite element analysis despite the coarseness of the mesh successfully reproduces aspects of the field behaviour of Mica dam.

- Even with a structure so markedly three dimensional as Mica dam, the main transverse section can be studied using the plane strain model without a significant loss of accuracy. Thus increased detail and the sophistication of stress-strain response which can be incorporated into 2-D analyses appears to be more rewarding than efforts spent on 3-D modelling.

While studying the cracking potential of a dam, a 3-D analysis is needed, as such potential is highest near abutments where a 2-D analysis can shed no light at all.

Considerable but thoughtful simplification of material behaviour can be made and still produce adequate information for design and monitoring purposes.

2.6 ANALYSIS OF CHICOASEN DAM

Marsal and Moreno (41) carried out a 3-D analysis of Chicoasen dam in Mexico. This is the only case reported in literature where the 3-D analysis of dam has been done during design stage. Chicoasen dam is an earth and rockfill embankment, 210 m high over river bed with a maximum height over the bed rock of 264 m. The profile along the dam axis and the final cross-section adopted are shown in Fig. 2.4.

The three-dimensional finite element analysis was undertaken assuming linear elastic behaviour of the embankment materials using the properties given in Table 2.3. The analysis showed that the core stresses substantially decreased towards the abutments. To improve upon it, the zoning in the dam was

changed and the material properties were modified as given in Table 2.4. This analysis also showed some pockets prone to hydraulic fracturing and also a principal stress ratio of greater than 3 in the upper central zone of core, thus indicating large deformations therein.

Table 2.3 Material Properties Chicoasen Dam

Zone	E (t/m ²)	ν	unit wt (t/m ³)
Core	7000	0.45	1.9
Transition	7500	0.35	1.7
Compacted rockfill	6000	0.20	1.7
Dumped rockfill near the abutment 4m to 6m soft layer	4300	0.20	1.7

Table 2.4 : Modified Material Properties of Chicoasen Dam

Material	E(t/m ²)	ν	Unit wt(t/m ³)
Core	6000	0.45	2.0
Transition	6000	0.30	1.9
Dumped rockfill	3000	0.20	1.7
Compacted rockfill	5000	0.25	1.8

Additional computations were made for a curved embankment (radius of crest equal to 800m). Comparison of the stress states developed in this case with those of the straight crest structure did not reveal any significant influence of the curvature, except in the upper 30 to 40 m of the dam. The analysis was repeated considering a nonlinear elastic behaviour of the embankment materials. The distribution of the total

stresses within the dam was very similar to that given by linear elastic analysis. Important differences, however, were detected in the magnitude of the deformations calculated with the two above mentioned assumptions (linearity and nonlinearity). The dam section was changed by modifying gradation and placement conditions in different zones of the dam.

2.7 ANALYSIS OF INFIERNILLO DAM

Justo and Saura (32) carried out a 3-D finite element analysis of the Infiernillo dam in Mexico for end of construction and filling of reservoir. The Infiernillo dam is a rockfill dam with a thin, central, compacted clay core, with a height approaching 150 m. The dam site is narrow, with abutments next to 1/1, formed by silicified conglomerate, crossed by several basalt dykes.

The behaviour of materials is assumed to be linear elastic, although the no-tension strength of granular materials is taken into account by redistributing the tensile stresses appearing in the calculation with the method proposed by Zienkiewicz et al (67). Another feature of the program is the possibility of simulating the collapse of the upstream shell of a dam when the reservoir is filled, by a simple criterion such as the decrease of the Young's modulus of the soaked granular material. The technique employed is based on the method of Nobari and Duncan (46) but simplified to assume a linear elastic behaviour of materials.

The parameters E and ν have been derived from the behaviour during construction and checked with the results of oedometer tests at the laboratory. The relationship between

Young's modulus and oedometric modulus, E_{oed} is given by :

$$E = E_{oed} \frac{1-\nu-2\nu^2}{1-\nu} \quad (2.2)$$

For rockfill, ν has been estimated by the relationship used by Simmons et al(23) and an average value of 0.25 has been taken. For clay samples compacted to 3.7% on wet side, ν values ranging between 0.45 and 0.49 have been assumed. For transition material, ν has been taken as 0.25.

When the different combinations of ν for core were adopted, it was found that ν values in the core had a major influence on the longitudinal strain appearing in it and a small influence on settlements. E values for shells had a major influence on settlements in the core but displacements in the rockfill were little affected when core characteristics were changed concluding that the adjustment for shell displacements must be made by changing their own parameters. By adjusting the parameters of shell and core, the analysis was finally done with the parameters given in Table 2.5.

Table 2.5 : Material properties of Infiernillo Dam

Material	Parameters		
	E (MN/m ²)	ν	(kN/m ³)
Core	5	0.475	18.8
Transition	40	0.20	19.7
Compacted rockfill	30	0.20	18.1
Dumped rockfill	10	0.20	17.2

Only a quarter of the dam was analysed for end of construction stage but half of the dam was analysed for the

reservoir full condition. The construction was simulated in ten steps. The weight of each layer was introduced in every step as a load on the structure, and at the same time, the layer was integrated into the structure. The resulting displacements in the upper layer were set equal to zero before proceeding with the placement of the next one. The reservoir load was applied in two stages. The following effects of reservoir load were applied.

- 1) Water load over the core
- 2) Collapse in the shell

For the first stage of reservoir water elevation a decrease of 20% and for the second stage a decrease of 30% in modulus of elasticity gave acceptable agreement with the observed values.

The conclusions drawn from the analysis are -

- The three-dimensional, linear-elastic finite element method may give, in general terms, a good estimate of displacements and strains in the body of a dam with a central earth core, using parameters obtained from the settlements measured during construction. The agreement with measured movements is, in many cases, better than that obtained with nonlinear analysis based on data derived from triaxial tests. This may be due to the fact that the loading conditions are such that the structure considered here essentially behaves as if the relationship between stresses and strains were linear.

-A method has been indicated to study the behaviour of the dam during filling of the reservoir. A good qualitative prediction has been obtained, and, as far as the core is concerned, a good quantitative prediction for most of the

movements is found.

- Although the parameters used in calculations have been obtained from the movements measured during construction, the laboratory tests on compacted rockfill carried out in large oedometers give values of Young's modulus which agree with field values. The values of Poisson's ratio estimated from laboratory tests do not disagree with the values that fit the measured deformation. In design practice, laboratory tests might allow a first estimate of parameters, which may be corrected based on field tests carried out in the early stages of construction.

2.8 ANALYSIS OF OROVILLE DAM

Mejia and Seed (42) presented a comparison between the results of three dimensional and two dimensional dynamic analyses of two dams located in triangular canyons with widely different valley wall slopes. The two dams correspond to the Oroville dam and a hypothetical dam with the same main section as Oroville, but in a narrower canyon. Oroville dam situated in a triangular canyon with a crest length to height ratio of about 7, is representative of dams with moderate valley wall slopes. The second dam has a crest length to height ratio of 2 and is representative of dams with steep canyon walls.

It was found that a plane strain analysis of the maximum section of Oroville dam gave values for the shear stresses that were within 20% of those computed from a three dimensional analysis of dam. Slight effects of canyon geometry were observed, particularly near the vertex of the canyon. For dams in steeper canyons than that of Oroville Dam, the results indicated that plane strain analysis of the maximum section of

the dam could not simulate correctly the behaviour of the embankment and that it was necessary in those cases to perform three dimensional analysis to obtain satisfactory results for design purposes.

2.9 ANALYSIS OF TEHRI DAM

Singh, Gupta and Saini (59) studied the effect of providing curvature to the axis of Tehri Dam in U.P. state of India. The 260.5 m high earth and rockfill dam at Tehri has a moderately sloping core encased by shells on both sides. The gorge at the dam site is narrow with valley walls sloping at approximately 1.1H:1V.

A three-dimensional analysis of the dam has been carried out using linear material behaviour for end of construction and reservoir full condition for both cases, with the straight and curved axis (radius equal to 800 m). Linear elastic properties of the material have been used. The program uses 20 noded isoparametric brick elements. The construction and reservoir load have been applied in one stage. The abutments and foundations are considered rigid and the valley is simplified to a V-shaped one.

The water load has been accounted for as below :

1. Water load on the core
2. Buoyancy effect in the shell
3. Additional weight of core zone due to saturation.

The results show that there is no significant change in the stresses and displacements in the dam with straight and curved axis for both loading combinations.

It is observed that at the central section with the reservoir filling, the vertical normal compressive stresses get

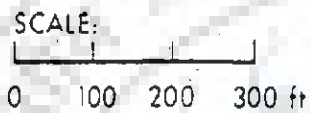
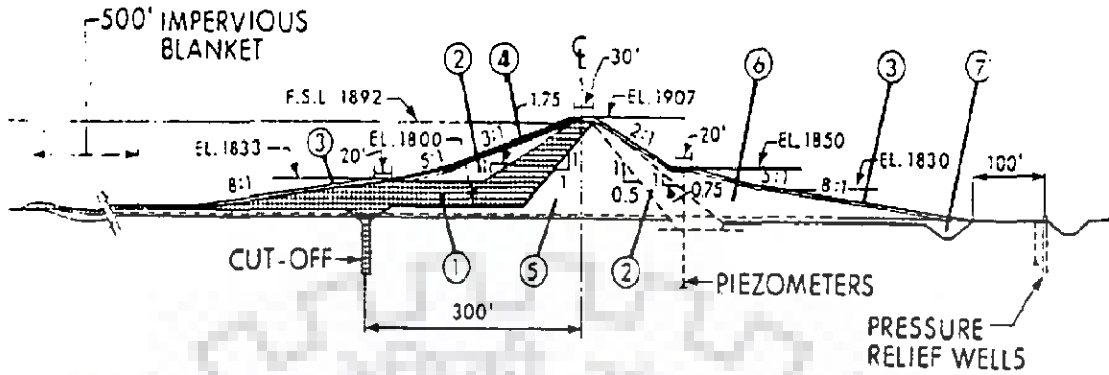
reduced in most part of the upstream shell and increased in the downstream shell. The horizontal stress σ_x (along the river) decreases over the entire central section. The distribution pattern even though not affected in the downstream shell is affected in the rest of the section.

The study has led to the following conclusions :

1. The gorge at dam site being narrow, the dam behaves as a three dimensional structure. There is ample arching action and a large portion of the load is transferred to the abutments through beam action.

2. The provision of curvature to the dam axis has no appreciable effect on the stresses and displacements in the dam body. Therefore, the idea of providing convexity to the dam axis offers no structural advantage.

3. There is indication of the occurrence of hydraulic fracturing in the dam. To study this phenomenon, a detailed 3-D analysis using sequential analysis and non-linear material properties is called for.



- ① IMPERVIOUS ZONE
- ② SELECT PERVIOUS ZONE
- ③ SELECT COARSE PERVIOUS ZONE
- ④ RIP-RAP
- ⑤ SEMI PERVIOUS ZONE
- ⑥ COMMON PERVIOUS ZONE
- ⑦ PROCESSED FILTER

FIG 2.1(a): -TYPICAL CROSS SECTION OF DUNCAN DAM .

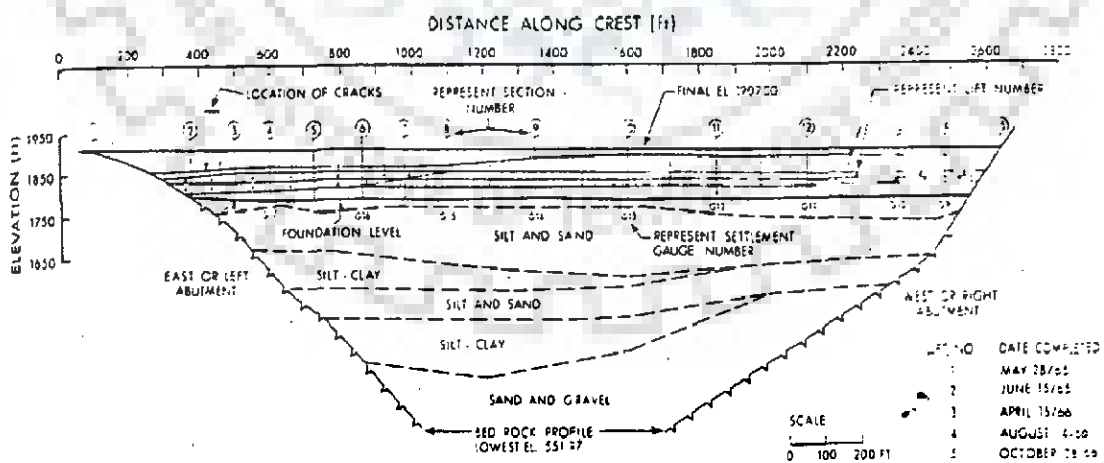


FIG 2.1(b): -LONGITUDINAL SECTION OF DUNCAN DAM AND FOUNDATION SHOWING CONSTRUCTION SEQUENCE AND LOCATION OF CRACKS

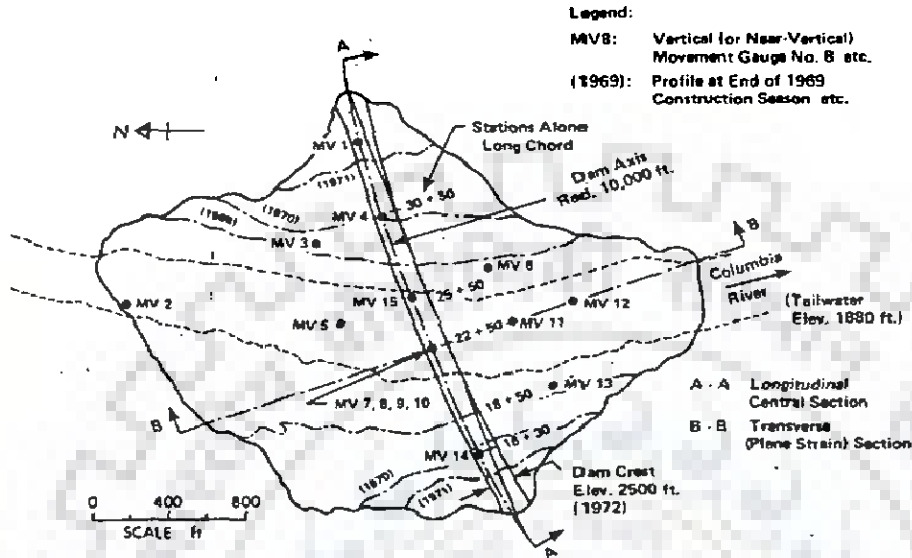
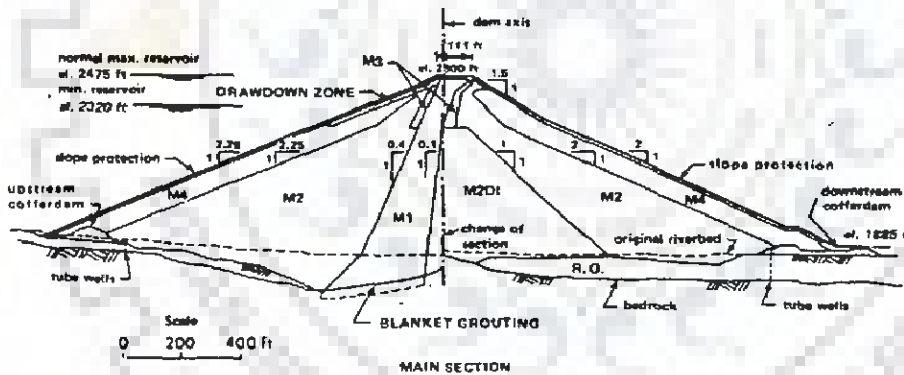


FIG. 2.2(a): PLAN VIEW OF MICA DAM (SHOWING ALSO LOCATION OF MV GAUGES)



ZONE	DESCRIPTION
M1	Core, glacial till in 25 cm (10") layers
M2	Main shell, sand and gravel in 30 cm (12") layers, changed during construction to 45 cm (18") layers
M2DI	Inner zone of poorer M2 materials
M3	Core support zone, sand and gravel or rock in 15 cm (6") layers
M4	Outer shell, sand and gravel or rock in 60 cm (24") layers
Drawdown Zone	Gravel, cobbles and boulders or rock in 60 cm (24") layers
R.O.	Original River Overburden

FIG. 2.2(b): MAIN TRANSVERSE SECTION OF MICA DAM (SHOWING ALSO MATERIAL DISTRIBUTION)

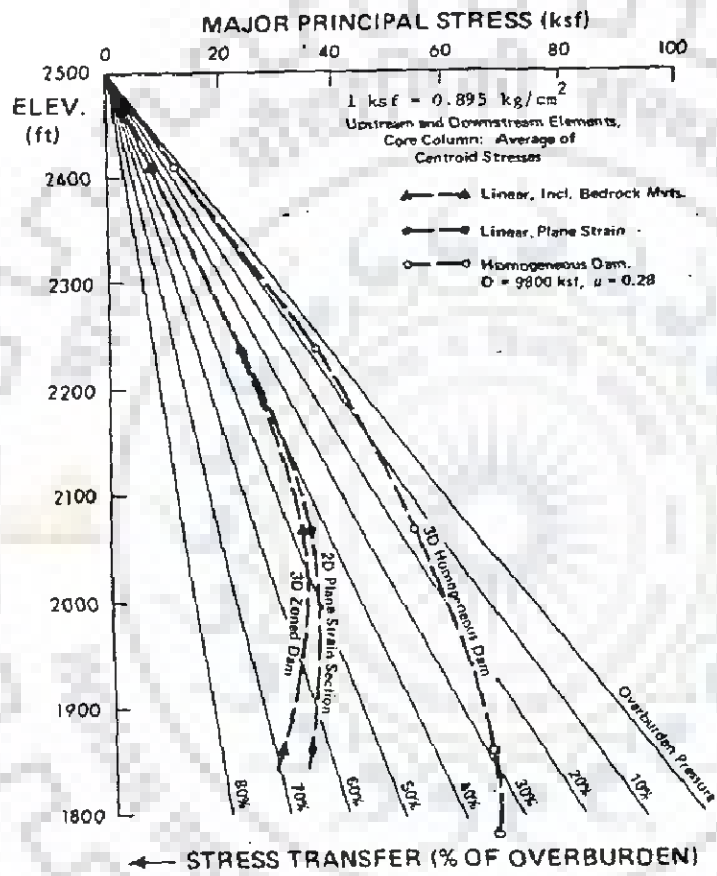


FIG. 2.3: MAJOR PRINCIPAL STRESSES ALONG VERTICAL COLUMN OF CORE

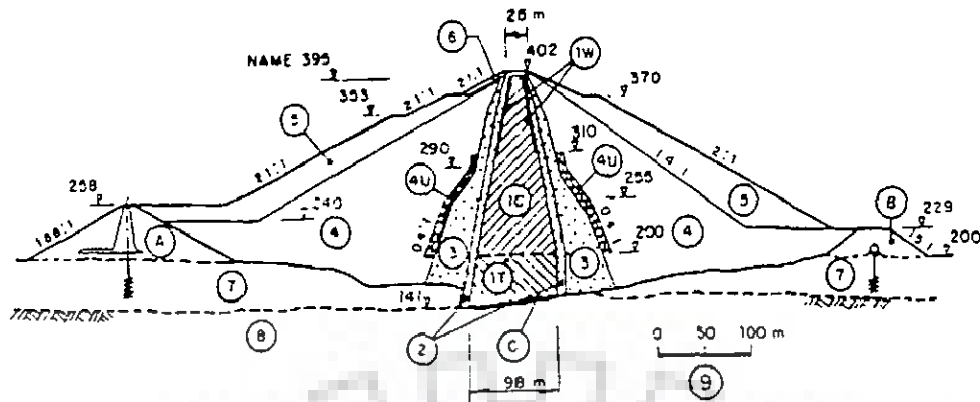


FIG 2.4(a): MAXIMUM TRANSVERSE SECTION OF CHICOASEN DAM

- | | |
|---------------------------------------|---|
| (A) Upstream cofferdam. | (B) Downstream cofferdam. |
| (1) Impervious core. | (1 T) Tejería material |
| (2) Filter. | (1 W) La Costilla material, wet of optimum. |
| (3) Transition zone. | NAME Maximum extraordinary water level. |
| (4) Compacted rockfill (well graded). | (8) Limestone (U-3). |
| (4 U) Uniform rockfill. | (9) Scale, in m. |
| (5) Dumped rockfill. | (C) Concrete. |
| (6) Selected rockfill. | (1 C) La Costilla material. |
| (7) Alluvium. | |

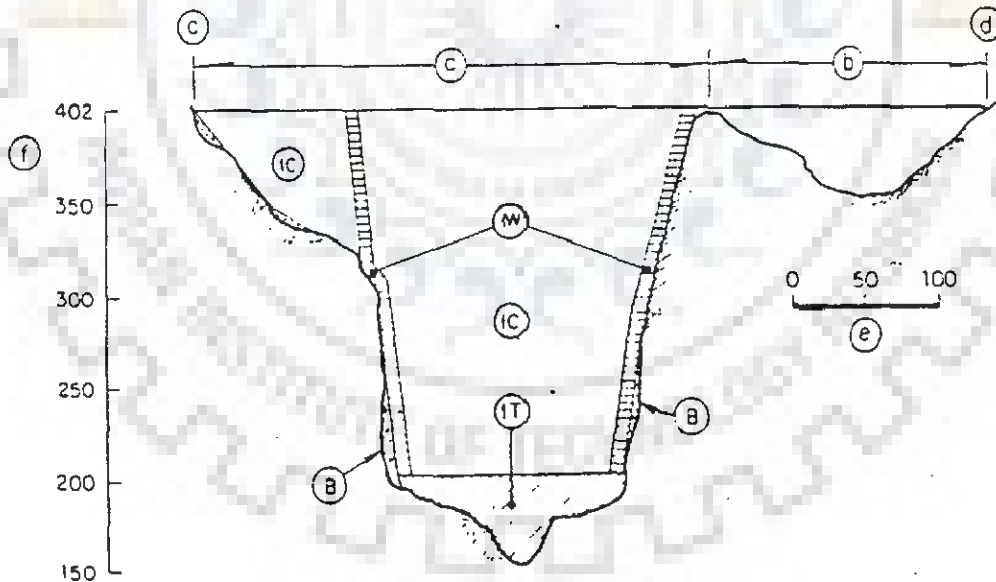


FIG 2.4(b): MAXIMUM LONGITUDINAL SECTION OF CHICOASEN DAM

- | | |
|---|-----------------------|
| (1 T) Tejería material (at optimum). | (a) Main dam. |
| (1 C) La Costilla material (0.8 % dry of optimum). | (b) Dike. |
| (1 W) La Costilla material (2 to 3 % wet of optimum). | (c) Left bank. |
| (B) Concrete. | (d) Right bank. |
| | (e) Scale, in m. |
| | (f) Elevations, in m. |

CHAPTER 3

METHOD OF ANALYSIS

For displacement and stress analysis of an embankment dam, the conventional methods of analysis are inadequate. With the availability of digital computers, the finite element method can provide the solution to any desired accuracy. The method can take into account irregular geometry, complex boundary conditions and material nonlinearity. The method has, therefore, been used for analysis in this study.

3.1 DESCRIPTION OF THE METHOD

The analysis of elastic structures by the finite element method has been described in the texts (12,65). However, for completeness, a brief description of the method is given below.

The various steps involved in the finite element analysis, are as follows :

- (i) Subdivision of the continuum into finite elements of suitable configuration.
- (ii) Evaluation of element properties.
- (iii) Assembly of element properties to obtain the global (structure) stiffness matrix and load vector.
- (iv) Solution of resulting linear simultaneous equations for the primary unknowns after introducing the boundary conditions.
- (v) Determination of secondary unknown quantities such as stresses and strains.

The mathematical equations for evaluating the finite element properties of three dimensional elements are presented here :

3.1.1 Displacement Function

A 20 - noded isoparametric finite element is shown in Fig.

3.1. For a typical finite element 'e', defined by nodes 1, j, m etc, the displacements $\langle f \rangle$ within the element are expressed as:

$$\langle f \rangle = [N] \langle \delta \rangle^e \quad \dots\dots(3.1)$$

where $[N] = [N_1 \ N_j \ N_m \ \dots]$

and $\langle \delta \rangle^e = \langle \delta_1 \ \delta_j \ \delta_m \ \dots \rangle^T \quad \dots\dots(3.2)$

The components of $[N]$ are in general functions of position and $\langle \delta \rangle^e$ represents a listing of nodal displacements for a particular element.

For the three dimensional element

$$\langle f \rangle = \begin{Bmatrix} u \\ v \\ w \end{Bmatrix} \quad \dots\dots(3.3)$$

represent the displacements in x, y and z directions at a point within the element and

$$\langle \delta_1 \rangle = \begin{Bmatrix} u_1 \\ v_1 \\ w_1 \end{Bmatrix} \quad \dots\dots(3.4)$$

are the corresponding displacements of node 1.

$[N_1]$ is equal to $[IN_1']$ where N_1' is the shape function of node 1 and I is an identity matrix

3.1.2 Shape Functions

The Shape functions for a 20-noded isoparametric(6,66) hexa-hedral element used in this study are given by the following.

At corner nodes (node nos. 1, 3, 5, 7, 13, 15, 17, 19)

$$N_1' = \frac{1}{8} (1 + \xi_0) (1 + \eta_0) (1 + \zeta_0) (\xi_0 + \eta_0 + \zeta_0 - 2) \quad \dots\dots(3.5 a)$$

For mid-side nodes:

$$(1) \quad \xi_1 = 0, \eta_1 = \pm 1 \quad \text{and} \quad \zeta_1 = \pm 1$$

(node nos 2, 6, 14, 18)

$$N_1' = \frac{1}{4} (1 - \xi^2) (1 + \eta_0) (1 + \zeta_0) \dots (3.5b)$$

$$(11) \quad \eta_1 = 0, \quad \xi_1 = \pm 1, \quad \zeta_1 = \pm 1$$

(node nos 4, 8, 16, 20)

$$N_1' = \frac{1}{4} (1 - \eta^2) (1 + \xi_0) (1 + \zeta_0) \dots (3.5c)$$

$$(111) \quad \zeta_1 = 0, \quad \xi_1 = \pm 1 \quad \text{and} \quad \eta_1 = \pm 1$$

(node nos 9, 10, 11, 12)

$$N_1' = \frac{1}{4} (1 - \zeta^2) (1 + \xi_0) (1 + \eta_0) \dots (3.5d)$$

$$\text{where } \left. \begin{array}{l} \xi_0 = \xi \xi_1 \\ \eta_0 = \eta \eta_1 \\ \zeta_0 = \zeta \zeta_1 \end{array} \right\} \dots (3.6)$$

ξ_1, η_1, ζ_1 are the local coordinates of the i^{th} node and ξ, η and ζ are the local coordinates of the point concerned.

3.1.3 Strains

With displacements known at all points within the element, the strains at any point can be determined. Six strain components are relevant in three dimensional analysis and the strain vector can be expressed as :

$$(e) = \begin{Bmatrix} \epsilon_x \\ \epsilon_y \\ \epsilon_z \\ \gamma_{xy} \\ \gamma_{yz} \\ \gamma_{zx} \end{Bmatrix} = \begin{Bmatrix} \frac{\partial u}{\partial x} \\ \frac{\partial v}{\partial y} \\ \frac{\partial w}{\partial z} \\ \frac{\partial u}{\partial y} + \frac{\partial v}{\partial x} \\ \frac{\partial v}{\partial z} + \frac{\partial w}{\partial y} \\ \frac{\partial w}{\partial x} + \frac{\partial u}{\partial z} \end{Bmatrix} \dots (3.7)$$

which can be further written as :

$$\{\epsilon\} = [B] \{\delta\}^e = [B_1 \ B_j \ B_m \ \dots] \{\delta\}^e \quad \dots (3.8)$$

in which [B] is the strain displacement matrix.

[B₁] is given by

$$[B_1] = \begin{bmatrix} \frac{\partial N_1'}{\partial x} & 0 & 0 \\ 0 & \frac{\partial N_1'}{\partial y} & 0 \\ 0 & 0 & \frac{\partial N_1'}{\partial z} \\ \frac{\partial N_1'}{\partial y} & \frac{\partial N_1'}{\partial x} & 0 \\ 0 & \frac{\partial x_1'}{\partial N_1'} & \frac{\partial N_1'}{\partial z} \\ \frac{\partial N_1'}{\partial z} & 0 & \frac{\partial y_1'}{\partial N_1'} \\ 0 & 0 & \frac{\partial N_1'}{\partial x} \end{bmatrix} \quad \dots (3.9)$$

with other submatrices obtained in a similar manner simply by interchange of subscripts.

For isoparametric elements

$$\left. \begin{aligned} x &= \sum N_1' x_1, \quad y = \sum N_1' y_1, \quad z = \sum N_1' z_1 \\ u &= \sum N_1' u_1, \quad v = \sum N_1' v_1, \quad w = \sum N_1' w_1 \end{aligned} \right\} \quad \dots (3.10)$$

the summation being over total number of nodes in an element.

Because the displacement model is formulated in terms of the natural coordinates ξ , η and ζ , it is necessary to relate Eq.(3.9) to the derivatives with respect to these local coordinates.

The natural coordinates ξ , η , ζ are functions of global coordinates x , y , z . Using the chain rule of partial

differentiation, we can write :

$$\frac{\partial N_1'}{\partial \xi} = \frac{\partial N_1'}{\partial x} \frac{\partial x}{\partial \xi} + \frac{\partial N_1'}{\partial y} \frac{\partial y}{\partial \xi} + \frac{\partial N_1'}{\partial z} \frac{\partial z}{\partial \xi} \quad (3.11)$$

Performing the same differentiation w.r.t. the other two coordinates and writing in matrix form

$$\begin{Bmatrix} \frac{\partial N_1'}{\partial \xi} \\ \frac{\partial N_1'}{\partial \eta} \\ \frac{\partial N_1'}{\partial \zeta} \end{Bmatrix} = [J] \begin{Bmatrix} \frac{\partial N_1'}{\partial x} \\ \frac{\partial N_1'}{\partial y} \\ \frac{\partial N_1'}{\partial z} \end{Bmatrix} \quad \dots (3.12)$$

where [J] is given by

$$[J] = \begin{bmatrix} \frac{\partial x}{\partial \xi} & \frac{\partial y}{\partial \xi} & \frac{\partial z}{\partial \xi} \\ \frac{\partial x}{\partial \eta} & \frac{\partial y}{\partial \eta} & \frac{\partial z}{\partial \eta} \\ \frac{\partial x}{\partial \zeta} & \frac{\partial y}{\partial \zeta} & \frac{\partial z}{\partial \zeta} \end{bmatrix} \quad \dots (3.13)$$

The matrix [J] is called the Jacobian matrix. The global derivatives can be found by inverting [J] as follows :

$$\begin{Bmatrix} \frac{\partial}{\partial x} \\ \frac{\partial}{\partial y} \\ \frac{\partial}{\partial z} \end{Bmatrix} = [J]^{-1} \begin{Bmatrix} \frac{\partial}{\partial \xi} \\ \frac{\partial}{\partial \eta} \\ \frac{\partial}{\partial \zeta} \end{Bmatrix} \quad \dots (3.14)$$

Substituting Eq. (3.10) into Eq. (3.13), the Jacobian is given by

$$[J] = \begin{bmatrix} \sum x_1 \frac{\partial N_1'}{\partial \xi} & \sum y_1 \frac{\partial N_1'}{\partial \xi} & \sum z_1 \frac{\partial N_1'}{\partial \xi} \\ \sum x_1 \frac{\partial N_1'}{\partial \eta} & \sum y_1 \frac{\partial N_1'}{\partial \eta} & \sum z_1 \frac{\partial N_1'}{\partial \eta} \\ \sum x_1 \frac{\partial N_1'}{\partial \zeta} & \sum y_1 \frac{\partial N_1'}{\partial \zeta} & \sum z_1 \frac{\partial N_1'}{\partial \zeta} \end{bmatrix} \quad (3.15a)$$

$$\text{or } [J] = \begin{bmatrix} \frac{\partial N_1'}{\partial \xi} & \frac{\partial N_2'}{\partial \xi} & \frac{\partial N_3'}{\partial \xi} & \dots \\ \frac{\partial N_1'}{\partial \eta} & \frac{\partial N_2'}{\partial \eta} & \frac{\partial N_3'}{\partial \eta} & \dots \\ \frac{\partial N_1'}{\partial \zeta} & \frac{\partial N_2'}{\partial \zeta} & \frac{\partial N_3'}{\partial \zeta} & \dots \end{bmatrix} \begin{bmatrix} x_1 & y_1 & z_1 \\ x_2 & y_2 & z_2 \\ x_3 & y_3 & z_3 \\ \dots & \dots & \dots \\ \dots & \dots & \dots \end{bmatrix} \quad (3.15b)$$

3.1.4 Stresses

The stresses are related to the strains as:

$$\langle \sigma \rangle = [D] (\langle \epsilon \rangle - \langle \epsilon_0 \rangle) + \langle \sigma_0 \rangle \quad \dots (3.16)$$

where $[D]$ is an elasticity matrix containing the appropriate material properties, $\langle \epsilon_0 \rangle$ is the initial strain vector, $\langle \sigma \rangle$ is the stress vector $\langle \sigma_x, \sigma_y, \sigma_z, \tau_{xy}, \tau_{yz}, \tau_{xz} \rangle^T$ and $\langle \sigma_0 \rangle$ is the initial stress vector.

For an elastic, isotropic material the elasticity matrix is given by:

$$[D] = \frac{E}{(1+\nu)(1-2\nu)} \begin{bmatrix} 1-\nu & \nu & \nu & 0 & 0 & 0 \\ & 1-\nu & \nu & 0 & 0 & 0 \\ & & 1-\nu & 0 & 0 & 0 \\ & & & (1-2\nu)/2 & 0 & 0 \\ \text{Symmetric} & & & & (1-2\nu)/2 & 0 \\ & & & & & (1-2\nu)/2 \end{bmatrix} \quad (3.17)$$

where E is the Young's modulus of elasticity and ν the Poisson's ratio of the material of the element.

3.1.5 Stiffness Matrix

The stiffness matrix of the element is given by the following relation

$$\langle F \rangle^e = [K]^e \langle \delta \rangle^e \quad \dots (3.18)$$

where $\langle F \rangle^e$ is the element nodal load vector and $[K]^e$, the element stiffness matrix given by :

$$[K]^e = \int_V [B]^T [D] [B] dV \quad \dots (3.19)$$

where V refers to the volume of the element.

The equivalent nodal forces are obtained as :

(i) Forces due to body forces $\langle b_x \ b_y \ b_z \rangle^T$ per unit volume are given by :

$$\langle F^e \rangle_b = \int_V [N]^T \langle b \rangle dV \quad \dots (3.20a)$$

(ii) Forces due to pressure distribution $\langle p_x \ p_y \ p_z \rangle^T$ per unit area are given by :

$$\langle F^e \rangle_p = \int_A [N]^T \langle p \rangle dA \quad \dots (3.20b)$$

For the complete structure, relation of the form given below is obtained

$$[K] \langle \delta \rangle = \langle F \rangle \quad (3.21)$$

where $\langle \delta \rangle$ is the vector of global displacements, $\langle F \rangle$ the load vector and $[K]$ the stiffness matrix.

The global stiffness matrix $[K]$ is obtained by directly adding the individual stiffness coefficients in the global

stiffness matrix. Similarly the global load vector for the system is also obtained by adding individual element loads at the appropriate locations in the global vector.

The mathematical statement of the assembly procedure is :

$$\left. \begin{aligned} [K] &= \sum_{e=1}^E [K]^e \\ [F] &= \sum_{e=1}^E \{F\}^e \end{aligned} \right\} \dots (3.22)$$

where E is the total number of elements.

To transform the variable and the region with respect to which the integration is made, the relationship

$$dx \, dy \, dz = \det [J] \, d\xi \, d\eta \, d\zeta \quad \text{is used.}$$

Writing explicitly

$$\int dx \, dy \, dz = \int_{-1}^1 \int_{-1}^1 \int_{-1}^1 \det[J] \, d\xi \, d\eta \, d\zeta \quad \dots (3.23)$$

A 2x2x2 integration has been used for the three dimensional analysis. Similar relationships can be derived for 2-D parabolic isoparametric elements (12,65).

3.2 NON LINEAR ANALYSIS

The stress strain relationship in case of soils is generally non-linear. The values of elastic constants E and ν depend upon the stress level. Therefore, the calculation of stresses gets complicated and the problem becomes non-linear in nature. Furthermore, most embankments are constructed by incremental processes and the loading is accumulated gradually during the construction stage and later on during reservoir filling. Therefore, for a realistic assessment of the dam behaviour, the analysis should provide for not only non-linear

stress strain behaviour but also the load being applied in increments rather than being applied in one stage.

Since the matrix $[D]$ containing E and ν depends upon the stresses and thus displacements, it follows that matrix $[K]$ is a function of $\langle \delta \rangle$ and $\langle F \rangle$, as $\langle \delta \rangle$ depends upon $\langle F \rangle$. $[K]$, therefore, can be represented by

$$[K] = [K(\langle \delta \rangle, \langle F \rangle)] \quad \dots (3.24)$$

The symbolic non-linear relationship between $\langle F \rangle$ and $\langle \delta \rangle$ is shown in Fig. 3.2(a). Figure 3.2(b) shows the non-linear stress-strain curve corresponding to the load $\langle F \rangle$ and displacements. It is on the basis of this stress-strain or constitutive law that the variable matrix $[D(\langle \delta \rangle)]$ for the non-linear analysis is determined.

3.2.1 Techniques For Incorporating Nonlinearity

The solution of non-linear problem by the finite element method is usually attempted by one of the three basic techniques viz. (a) incremental or step wise procedures (b) iterative or Newton methods and (c) step-iterative or mixed procedures.

3.2.1.1 Incremental Procedures

The basis of the incremental or stepwise procedure is the subdivision of the load into many small partial loads or increments. Usually these load increments are of equal magnitude, but in general they need not be equal. The load is applied one increment at a time and during the application of each increment the equations are assumed to be linear. A fixed value of $[K]$ is thus assumed throughout each load increment but $[K]$ may take different values during different increments.

The solution for each step of loading is obtained as an increment of the displacement $\langle \Delta \delta \rangle$, which is added up to

give the total displacement at any stage of the loading , and the incremental process is repeated until the total load has been reached.

Essentially, the incremental procedure approximates the non-linear problem as a series of linear problems, that is, the non-linearity is treated as piecewise linear.

The total load $\langle F \rangle$ is given by

$$\langle F \rangle = \langle F_0 \rangle + \sum_{i=1}^M \langle \Delta F_i \rangle \quad \dots (3.25)$$

where $\langle F_0 \rangle$ is the initial load vector and M is the total number of increments and $\langle \Delta F_i \rangle$ is the incremental load vector in the i th increment. Hence after the application of the i th increment, the load is given by

$$\langle F_i \rangle = \langle F_0 \rangle + \sum_{j=1}^i \langle \Delta F_j \rangle \quad \dots (3.26)$$

Similarly after the i^{th} iteration, the displacement is given by

$$\langle \delta_i \rangle = \langle \delta_0 \rangle + \sum_{j=1}^i \langle \Delta \delta_j \rangle \quad \dots (3.27)$$

where $\langle \delta_0 \rangle$ represents initial displacement.

Usually $\langle F_0 \rangle$ and $\langle \delta_0 \rangle$ are null vectors because the solution is started from the undeformed state of the body. However, any initial equilibrium state of $\langle F_0 \rangle$ and $\langle \delta_0 \rangle$ can be specified.

To compute the increment of displacements, a fixed value of the stiffness is used which is evaluated at the end of the previous increment. Therefore,

$$[K_{i-1}] \langle \Delta \delta_i \rangle = \langle \Delta F_i \rangle \quad \text{for } i=1,2,3,\dots,M \quad (3.28)$$

where the subscripts refer to the incremental stage and

$[K_0]$ is the initial value of the stiffness. $[K_0]$ is computed from material constants derived from the given stress-strain curves at the start of the loading.

The incremental procedure is schematically indicated in Fig. 3.3. Usually, in the incremental procedure the tangent moduli (E_t) are used to formulate $[D(o)]$ and to compute the stiffness $[K]$. The matrix $[K]$ is often referred to as the tangent stiffness matrix.

The accuracy of the incremental procedure can be improved by taking smaller increments of the load, say by adopting half of the load increment. However, since a new incremental stiffness matrix $[K_{i-1}]$ must be computed for each step, the accuracy, it is evident, is purchased at the cost of additional computational effort.

The procedure has the advantage that non-zero initial stresses pose no additional difficulties. The disadvantage is that strain softening behaviour (stress decreasing after peak) can not be modelled, since this would require use of a negative modulus value to represent the post peak behaviour. This method fits in very well with the step wise construction.

3.2.1.2 Iterative Procedures

The iterative procedure involves a sequence of calculations in which the structure is fully loaded in each iteration. Because some approximate, constant value of the stiffness is used in each step, the equilibrium is not necessarily satisfied. After each iteration, the portion of the total load that is not balanced is calculated and used in the next step to compute an additional increment of the displacements. The process is repeated until equilibrium is

approximated to some acceptable degree. Essentially, the iterative procedure consists of successive corrections to a solution until equilibrium under the load $\langle F \rangle$ is satisfied.

For the i th cycle of iteration process, the necessary load is determined by

$$\langle F_i \rangle = \langle F \rangle - \langle F_{e,i-1} \rangle \quad \dots (3.29)$$

where $\langle F_{e,i-1} \rangle$ is the load equilibrated after the previous step. An increment to the displacements is computed during the i th step by using the relation.

$$\langle K_{i-1} \rangle \langle \Delta \delta_i \rangle = \langle F_i \rangle \quad \dots (3.30)$$

where the subscript, i , denotes a cycle of iteration. The total displacement after the i^{th} iteration is computed using the relationship of Eq. (3.27).

Finally, $\langle F_{e,i} \rangle$ is calculated as the load necessary to maintain the displacement $\langle \delta_i \rangle$. The procedure is repeated until the increments of displacement or the unbalanced forces become zero, that is, $\langle \Delta \delta_i \rangle$ or $\langle F_i \rangle$ become null according to some preselected criterion.

Instead of computing a different stiffness for each iteration, a modified iterative technique is also employed which utilizes only the initial stiffness $\langle K_0 \rangle$. Obviously, the modified procedure necessitates a greater number of iterations. However, there is a substantial saving of computation because it is not necessary to invert a new stiffness at each cycle. The iterative procedures are illustrated schematically in Fig. 3.4.

3.2.1.3 Mixed Procedures

The step iteration or mixed procedure utilizes a combination of the incremental and iterative schemes. In this method, the load is applied incrementally, but after each increment successive iterations are performed. This method yields higher accuracy at the price of more computational effort. The scheme of procedure is illustrated in Fig. 3.5

Because the mixed method combines the advantages of both the incremental and iterative procedures and tends to minimize the disadvantages of each, step iteration is being utilized increasingly. The additional computational effort is justified by the fact that the iterative part of the procedure permits one to assess the quality of the approximate equilibrium at each stage.

Another version of the mixed method known as the procedure of successive approximations has also been reported by Resendiz and Romo (52), Alberro (1), Sharma (55) and Desai (13). The method is schematically represented in Fig 3.6. The problem is analysed repeatedly, adjusting the modulus values assigned to each element each time, until the calculated values of stress and strain are consistent with the desired non-linear relationship. The total load is applied in each iteration.

Since at each iteration a new value of $[K]$ has to be calculated and the number of iterations may be, in some cases large, the number of iterations are specified not to exceed a given number. The criteria used by Resendiz and Romo (52) to stop iteration was that the change in modulus of deformation between two consecutive cycles was smaller than 10 percent.

Two iterations per load increment were specified by Valera and Chan. The average value of stress was used to calculate the values of E_t and ν_t . Alberro (1) specified 3 iterations for the analysis of Infiernillo dam. When a new stage of construction was begun the values for the Young's moduli and Poisson's ratios of different elements were taken as those corresponding to the mean values of the two previous iterations. Sharma (55) specified a maximum of 3 iterations or the stage when the difference between E_t values from two consecutive iterations was less than 10% to stop further trials. Tanaka et al (60) and Eisenstein et al (22) used two iterations per layer. Palmerton (47) did not specify the maximum iterations but the number of iterations required was generally one.

3.2.2 Approach Used in the Studies

Sharma (56) used a modified form of the residual force approach presented by Nayak and Zienkiewicz (44). The same approach has been used in this study also and is described in the following paragraphs.

The total equilibrium of the assembled structure, at any stage of the construction is considered at every stage of iteration along with the assumption that the constitutive law allows incremental stresses at a point, to be determined uniquely in terms of the incremental nodal displacements, $\langle \Delta \delta \rangle$ or in turn incremental strain $\langle \Delta \epsilon \rangle$ defined by

$$\langle \Delta \epsilon \rangle = [B] \langle \Delta \delta \rangle \quad \dots \dots (3.31)$$

where $[B]$ is the strain displacement matrix. The incremental stress given by

$$\langle \Delta \sigma \rangle = [D] \langle \Delta \epsilon \rangle \quad \dots \dots (3.32)$$

and incremental displacements $\langle \Delta \delta \rangle$ at any stage of iteration, i , are additive. Thus

$$\left. \begin{aligned} \langle \delta_i \rangle &= \langle \delta_{i-1} \rangle + \langle \Delta \delta_i \rangle \\ \langle \sigma_i \rangle &= \langle \sigma_{i-1} \rangle + \langle \Delta \sigma_i \rangle \end{aligned} \right\} \dots (3.33)$$

The equilibrated load at the end of i^{th} iteration is given by

$$\langle F_{e,i} \rangle = \int_V [B^T] \langle \sigma_i \rangle dV \dots (3.34)$$

The residual load at the end of i^{th} iteration is given by

$$\langle \psi_i \rangle = \langle F \rangle - \langle F_{e,i} \rangle \dots (3.35)$$

In the $(i+1)^{\text{th}}$ iteration $\langle \psi_i \rangle$ would be the load and, therefore, the incremental displacement would be given by

$$\langle \Delta \delta_{i+1} \rangle = [K_i]^{-1} \langle \psi_i \rangle \dots (3.36)$$

where $[K_i]$ is the tangent stiffness matrix at the end of i^{th} iteration. The E_t and ν_t used in formulation of $[D]$ matrix are obtained for the $\langle \sigma \rangle$ values of the i^{th} iteration.

The iterations would continue till a suitable convergence criteria is achieved. The criteria chosen for convergence is the norm of forces. The iteration will stop when the ratio of the norm of residuals to the norm of applied loads is less than a specified value. In the analysis, the ratio is specified as 4 percent. In the earlier stages of the analysis the ratio of norm of residuals to that of the applied load $\langle F \rangle$ was specified to be less than 2%. However, a comparison of the displacements and stresses, with the norm of residuals at 2% and 4%, showed that the two results were not significantly different and, therefore, the limiting ratio was specified to

be 4 percent later on.

The norm of residuals at the end of i th iteration and that of the total loads would be

$$\left. \begin{aligned} |\langle \psi_1 \rangle| &= (\langle \psi_1 \rangle^T \langle \psi_1 \rangle)^{1/2} \\ |\langle F \rangle| &= (\langle F \rangle^T \langle F \rangle)^{1/2} \end{aligned} \right\} \dots (3.37)$$

The convergence factor $(C_f)_i$, at the end of i^{th} iteration is expressed as

$$(C_f)_i = \frac{|\langle \psi_1 \rangle|}{|\langle F_1 \rangle|} \times 100 \quad \dots (3.38)$$

The convergence factor $(C_f)_i$ is compared with $(C_f)_{i-1}$, at the end of the previous iteration, to calculate the convergence ratio, C_R , given by

$$C_R = \frac{(C_f)_i}{(C_f)_{i-1}} \quad \dots (3.39)$$

The value of the convergence ratio C_R governs the stiffness matrix in the next iteration. If the ratio is more than a specified value, convergence is assumed to be fast and the stiffness matrix is not recalculated and the old one is used. If however, C_R is smaller than the specified value, the convergence is considered slow and the stiffness matrix needs to be recalculated. Then

$$[K_1] = \int_V [B^T] [D(\langle \sigma_1 \rangle, \langle \delta_1 \rangle)] [B] dV \quad \dots (3.40)$$

The C_R value in the study is specified to be 1.2 for determining whether the stiffness matrix needs to be recalculated.

The various steps in the solution algorithm of the residual force approach used in the study are:

1. The embankment is assumed to be constructed in 6 layers

2. Initially the elastic constants in the current layer, are assumed on the basis of anticipated values of stresses, $\sigma_1 = \sigma_2 = \gamma h$ and $\sigma_3 = K_0 \sigma_1$, where h is the average height of the fill in the layer, γ is the bulk density, which is taken 2.0 for all materials for this purpose and K_0 is the coefficient of earth pressure at rest. An initial value of 0.8 for K_0 is adopted in the analysis for all materials.
3. In the completed layers, the elastic constants are calculated on the basis of anticipated stress values which are obtained by adding γh to the major principal stress and $K_0 \gamma h$ to the minor principal stress values obtaining at the end of the previous construction stage.
4. The gravity loads of the new layer only (ΔF^i), are calculated. These are added to the loads of the previous layer to get the total loads $\langle F^i \rangle = \langle F^{i-1} \rangle + \langle \Delta F^i \rangle$
5. The stiffness matrix $[K]$ of the structure upto the end of current layer is calculated.
6. The incremental displacements $\langle \Delta \delta \rangle$, the incremental strains $\langle \Delta \epsilon \rangle$ and incremental stresses $\langle \Delta \sigma \rangle$ are calculated

$$\langle \Delta \delta \rangle = [K]^{-1} \langle \Delta F^i \rangle$$

$$\langle \Delta \epsilon \rangle = [B]^T \langle \Delta \delta \rangle$$

$$\langle \Delta \sigma \rangle = [D] \langle \Delta \epsilon \rangle$$

The $[D]$ matrix used here is calculated according to the proposed stress-strain model at the existing stress

level, prior to this iteration.

7. The stress-strain matrix is found out at the stress state obtained by adding the incremental stresses in step 6 to those at the beginning of the iteration.
8. Incremental stresses $\langle \Delta \sigma \rangle$ are recalculated with the new value of $[D]$
9. The total stresses are found out by adding the incremental stresses of step 8 to the stresses at the beginning of the iteration.

10. The equilibrated load vector is calculated by

$$\langle F_e \rangle = \int_V [B]^T \langle \sigma \rangle dV$$

and residual load vector $\langle \psi \rangle$ by

$$\langle \psi \rangle = \langle F^{(1)} \rangle - \langle F_e \rangle$$

11. $\langle \Delta F_j \rangle$ is set equal to $\langle \psi \rangle$, where j is the iteration number and the superscript refers to the layer number.
12. The norm of residuals and the convergence factor $(C_f)_j$ are calculated as per Eqs. (3.37) and (3.38).
13. If the convergence factor $(C_f)_j$ is within the specified limit, the iterations are terminated and results saved and the next step is skipped. Otherwise the next step is followed.
14. The convergence ratio C_R is calculated as per Eq. (3.39).
If C_R is less than the specified value 1.2, go to step 5. If C_R is more than 1.2, the old stiffness matrix is used and proceed to step 6.
15. Take next layer, if left and proceed from step 2, otherwise stop the computations.

610976.



3.3 CONSTITUTIVE LAWS

A constitutive law (stress-strain relationship) is dependent upon many factors viz, (i) constitutional factors - which include the characteristics of the soil and (ii) environmental factors - which include the loading characteristics such as confining pressures (17). The constitutive laws can be broadly classified as follows.

3.3.1 Linear Elastic Analysis

In this analysis the stress-strain relationship is taken as linear so that the elastic modulus is constant at all stress levels. Since the soils and rocks exhibit non-linear stress-strain relationship, taking a constant value of elastic modulus will, thus, not be realistic.

Linear analysis has been used by Clough and Woodward(7) , Lefebvre and Duncan(39) , Eisenstein et al (21) , Singh et al (58) , Marsal et al (41) , Lee and Idriss (40).

Penman et al (49) used a linear stress strain relationship for the analysis of Llyn Brianne dam by working out equivalent values of Young's modulus based on equivalent compressibility approach for rockfill using the results of one-dimensional compression tests on the embankment material.

Clough and Woodward (7) suggested the use of bulk modulus M_b and distortional modulus M_d defined as follows, to be used in place of E and ν .

$$\left. \begin{aligned} \sigma_b &= (\sigma_1 + \sigma_3)/2 = M_b(\epsilon_1 + \epsilon_3) \\ \text{and } \sigma_d &= (\sigma_1 - \sigma_3)/2 = M_d(\epsilon_1 - \epsilon_3) \end{aligned} \right\} \dots (3.41)$$

$$\left. \begin{aligned}
 M_b = \text{bulk modulus} &= \frac{E}{2(1+\nu)(1-2\nu)} \\
 M_d = \text{distortional modulus} &= \frac{E}{2(1+\nu)}
 \end{aligned} \right\} \dots (3.42)$$

Where σ_1 and σ_3 are the major and minor principal stresses and ϵ_1 and ϵ_3 are the major and minor principal strains, E is the Young's modulus and ν , the Poisson's ratio.

Cole and Burland (9) used the linear analysis for prediction of movements and strut loads in London clay. Eisenstein and Simmons (23) used linear stress strain relationship for three dimensional analysis of Mica dam. Instead of E , one dimensional compression modulus D defined in Eq. (2.1) was used to calculate the stiffness matrix.

Justo and Saura (32) carried out a 3-D linear analysis of El-Infiernillo dam wherein the parameters E and ν used in the analysis were derived from the behaviour during construction. The value of Young's modulus E was found out from Oedometric modulus as described in Eq. (2.2) and the Poisson's ratio ν was estimated by the method used by Simmons (23).

Knight, Naylar and Davis (33) used an approach similar to that used by Penman et al (49) for analysing a 85 m high embankment dam. For rockfill, constant values of Young's moduli and Poisson's ratio were used. For core a constant value of $\nu = 0.4$ was used in conjunction with different values of E so as to give good agreement between the observed and computed values. The Young's moduli were related to the overburden pressure by a trial and error approach and a straight line relationship was obtained for E and σ_2 .

3.3.2 Non-Linear Stress-Strain Behaviour

The relationship between stress and strain in soils are more complicated than the simple, linearly elastic ones described in previous section. The non-linear model can be further subdivided as follows :

3.3.2.1 Bilinear Models

This is the simplest type of non-linear relation where the material has initially modulus $[D_1]$ until the stresses reach a yield value σ_{yield} after which the modulus is changed to $[D_y]$

Bilinear stress-strain relationships have been used in finite element analysis by Dunlop et al (9), Dunlop and Duncan (20), Holmberg (28), Andersen (3), D'Appolonia and Lambe (10). Experience has shown that the computed values of stresses are seldom exactly equal to the strength and the stresses in some elements invariably are found to exceed the assigned strength values before the modulus value is reduced.

3.3.2.2 Multilinear or Piecewise Linear Models

Instead of the stress-strain relation being represented by two lines, it is represented by a number of lines. Two general forms which are available for this purpose are tabular forms and functional forms.

Tabular Form:

The stress-strain results obtained from laboratory tests can be used directly in tabular form for finite element analysis as was done in case of Infiernillo Dam by Alberro(1), and Duncan Dam by Eisenstein et al (22). For this, several

points of the stress-strain curves are fed as input to the computer in the form of number pairs denoting stress and strain at these points. The material parameters E and ν are interpolated for the desired level of stress or strain by a suitable interpolation method, if it is on a single curve. If instead, there are more than one curve, as will be the case for materials whose stress-strain relationship is a function of the confining pressure, interpolation is done for the different curves as well. The tabular form is cumbersome as it occupies a relatively large storage space in the computer.

Functional Form:

An obvious advantage of the use of the mathematical functions is that, in contrast to the tabular form in which a number of data points are input, only a few parameters are needed to describe the curves.

The most widely used function for simulation of stress strain curves in finite element analyses was formulated by Duncan and Chang (16) using Kondner's (34) finding that the plot of stress v/s strain in a triaxial compression test is very nearly a hyperbola. The procedure uses Mohr Coulomb failure criterion and develops relationships for the tangent modulus and Poisson's ratio which may be expressed in terms of total or effective stresses. This model has been widely used (5,36,37, 46,48,50,51,64) and is being briefly described below.

The tangent modulus E_t at a particular stress level is given by

$$E_t = (1-mR_f)^2 E_1 \quad \dots (3.43)$$

where, R_f is the failure ratio defined as the ratio of the deviatoric stress at failure to the ultimate deviatoric stress

given by

$$(\sigma_1 - \sigma_3)_f = R_f (\sigma_1 - \sigma_3)_{ult} \quad \dots (3.44)$$

where σ_1 and σ_3 denote the major and minor principal stresses respectively.

$m = (\sigma_1 - \sigma_3) / (\sigma_1 - \sigma_3)_f$ known as the mobilisation factor and is defined as the ratio of the deviatoric stress $(\sigma_1 - \sigma_3)$ acting at any element to the failure deviatoric stress $(\sigma_1 - \sigma_3)_f$.

E_1 is the initial modulus of elasticity for a particular confining pressure.

The value of E_1 is defined by Janbu (30) as follows :

$$E_1 = K P_a \left(\frac{\sigma_3}{P_a} \right)^n \quad \dots (3.45)$$

in which σ_3 is the confining pressure, P_a is the atmospheric pressure expressed in the same units as E_1 , K is a dimensionless number termed the modulus number, and n is a dimensionless exponent.

Expressing the compressive strength and confining pressure in terms of Mohr-Coulomb failure criterion and using c and ϕ as strength parameters, the value of tangent modulus of elasticity can be expressed as :

$$E_t = \left[1 - \frac{R_f (1 - \sin \phi) (\sigma_1 - \sigma_3)}{2c \cos \phi + 2\sigma_3 \sin \phi} \right]^2 K P_a \left(\frac{\sigma_3}{P_a} \right)^n \quad \dots (3.46)$$

in which c is the unit cohesion and ϕ is the angle of shearing resistance for the material.

The expression for tangent Poisson's ratio has been given by Kulhawy and Duncan (35) as follows :

$$\nu_t = \frac{G - F \log(\sigma_3 / P_a)}{(1 - d e_a)^2} \quad \dots (3.47)$$

$$\text{in which } \epsilon_a = (\sigma_1 - \sigma_3) / (E_1(1 - mR_f)) \quad (3.48)$$

- G = value of initial Poisson's ratio v_1 , at one atmospheric pressure
- F = reduction in initial Poisson's ratio for a ten fold increase in confining pressure
- d = dimensionless parameter expressing the rate of change of v_1 with strain.

More complicated forms of Kondner's hyperbolic functions have been suggested by Hansen(25) as follows :

$$\left. \begin{aligned} (\sigma_1 - \sigma_3) &= \sqrt{\epsilon_a / (a + b\epsilon_a)} \quad \text{and} \\ (\sigma_1 - \sigma_3) &= \frac{\sqrt{\epsilon_a}}{a + b\epsilon_a} \end{aligned} \right\} \quad (3.49)$$

where a and b are constants analogous to a and b used in Kondner's equation.

Al-Hussaini and Radhakrishanan (2) have extended the Kondner's hyperbolic form to develop non-linear octahedral stress-strain model in the form

$$\tau_{\text{oct}} = \frac{\gamma_{\text{oct}}}{a + b\gamma_{\text{oct}}} \quad (3.50)$$

where a and b are analogous but not identical to a and b in the Kondner's relationship. τ_{oct} and γ_{oct} are octahedral shear stress and octahedral shear strain defined by

$$\left. \begin{aligned} \tau_{\text{oct}}^2 &= 1/9[(\sigma_1 - \sigma_2)^2 + (\sigma_2 - \sigma_3)^2 + (\sigma_3 - \sigma_1)^2] \\ \gamma_{\text{oct}}^2 &= 2/3[(\epsilon_1 - \epsilon_2)^2 + (\epsilon_2 - \epsilon_3)^2 + (\epsilon_3 - \epsilon_1)^2] \end{aligned} \right\} \quad (3.51)$$

Relationships similar to those of Kulhawy and Duncan(35) were developed as follows :

$$G_t = (1 - S_f \tau_{\text{oct}} / \tau_f)^2 G_1 \quad (3.52)$$

where G_t is the tangent shear modulus, S_f is the shear ratio similar to the failure ratio defined by Kondner(29) and is given by :

$$S_f = \tau_f / \tau_{ult} \quad \dots (3.53)$$

G_1 is the initial value of the tangent shear modulus given by :

$$G_1 = C P_a (\sigma_3 / P_a)^m \quad \dots (3.54)$$

where C and m are pure numbers.

Other Forms:

Besides hyperbolic form, other forms of stress/strain relationship have also been used by different researchers. A parabolic form of the stress-strain relationship has been used by Wong (63). Desai (11) proposed a functional form based on spline functions as an alternative form and improvement on hyperbolic form of representation. Jawarski (31) used a polynomial relation successfully to study the behaviour of braced excavations.

As an alternative to E_t and ν_t , Duncan et al (18) have proposed that hyperbolic models expressed in terms of E_t and K_t can be more conveniently utilised for a better representation of soil behaviour near and after failure. The expression of K_t is given as a function of the confining pressure σ_3 .

$$K_t = K_b P_a (\sigma_3 / P_a)^m \quad \dots (3.55)$$

in which both K_b and m are dimensionless material constants.

Other models in use are the $K - G$ models used by Damaschuk and Wade (14) and Damaschuk and Valliappan (15); $K_t - G_t$ models employed by Izumi et al (28) and the hypoelastic model used by Vagnernon et al (62).

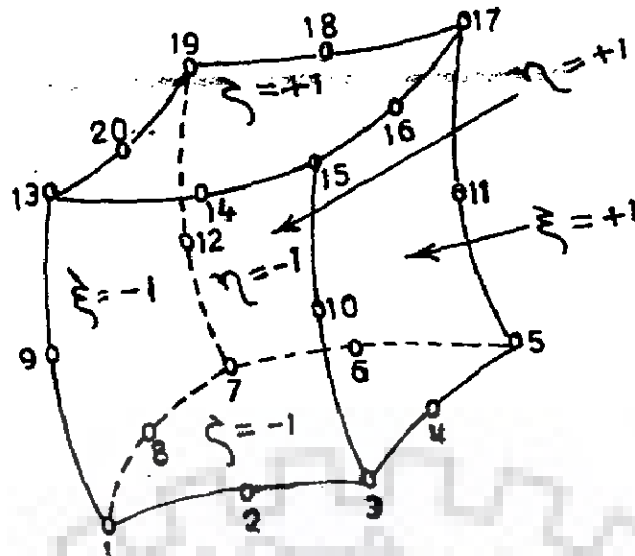


FIG.3.1 3-D FINITE ELEMENT SHOWING NODE NUMBERS

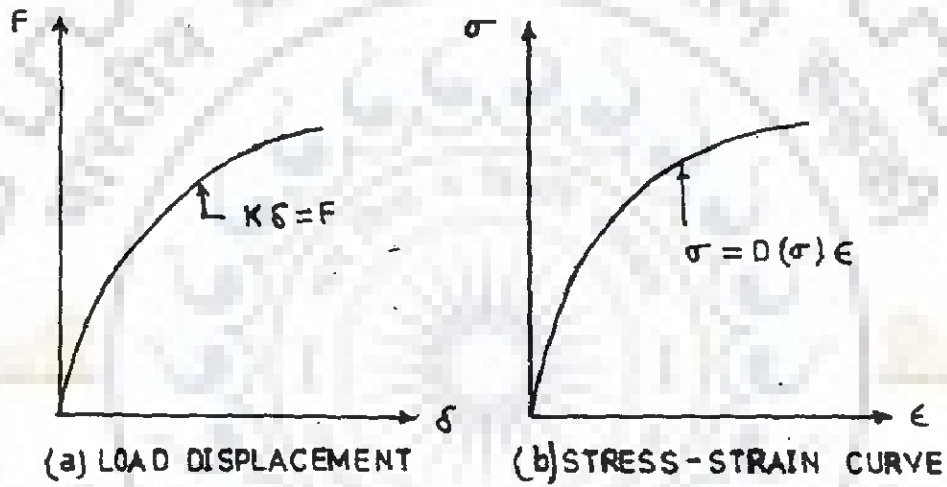


FIG. 3.2 NON LINEAR CURVES

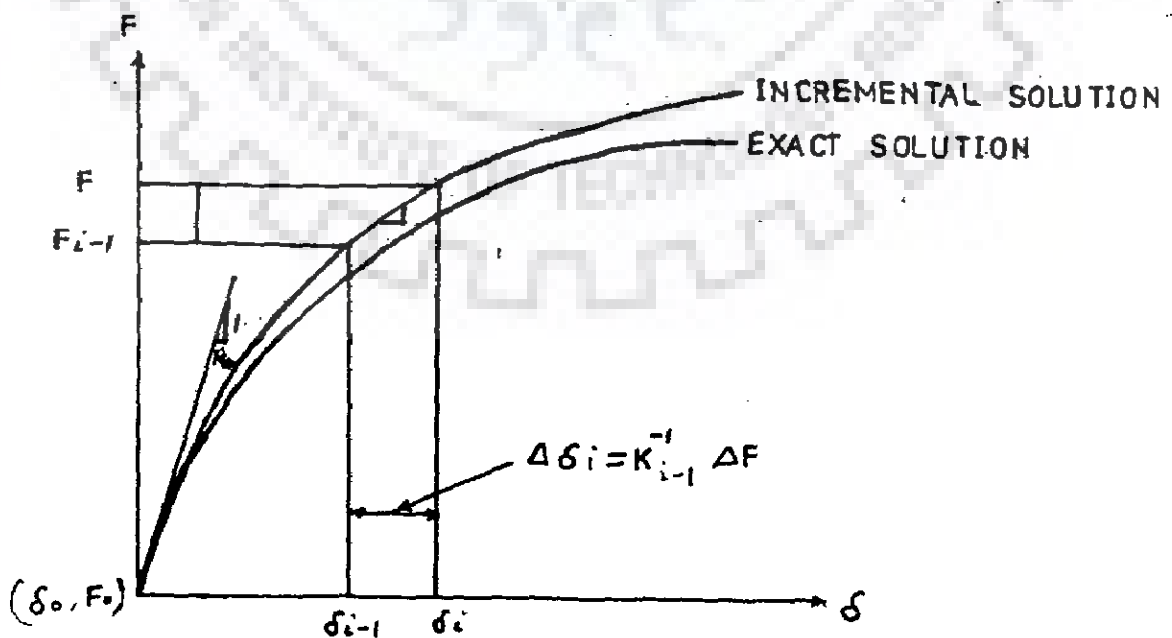
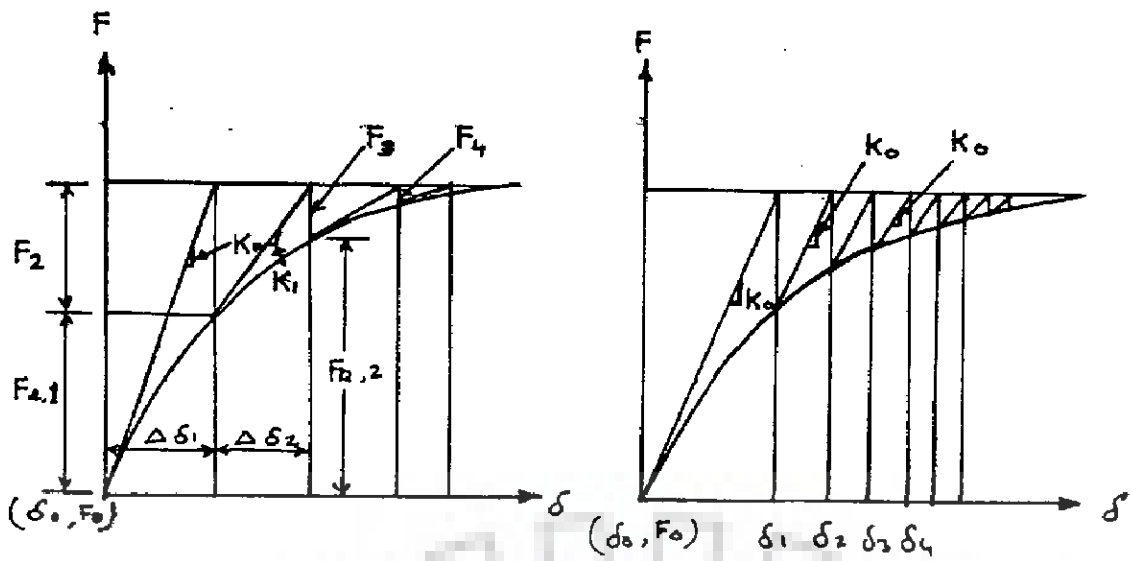


FIG.3.3 BASIC INCREMENTAL PROCEDURE



(a) TANGENT STIFFNESS PROCEDURE (b) MODIFIED PROCEDURE
 FIG. 3.4 ITERATIVE PROCEDURE

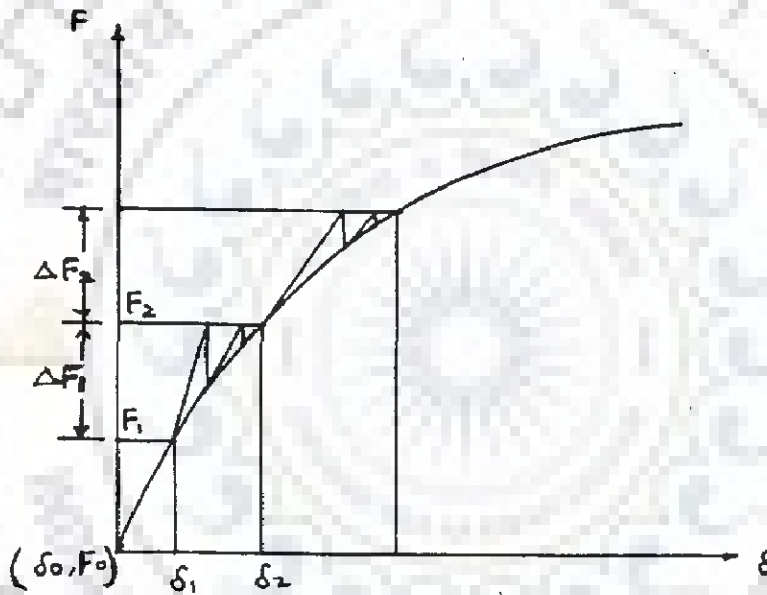


FIG. 3.5 STEP ITERATIVE PROCEDURE

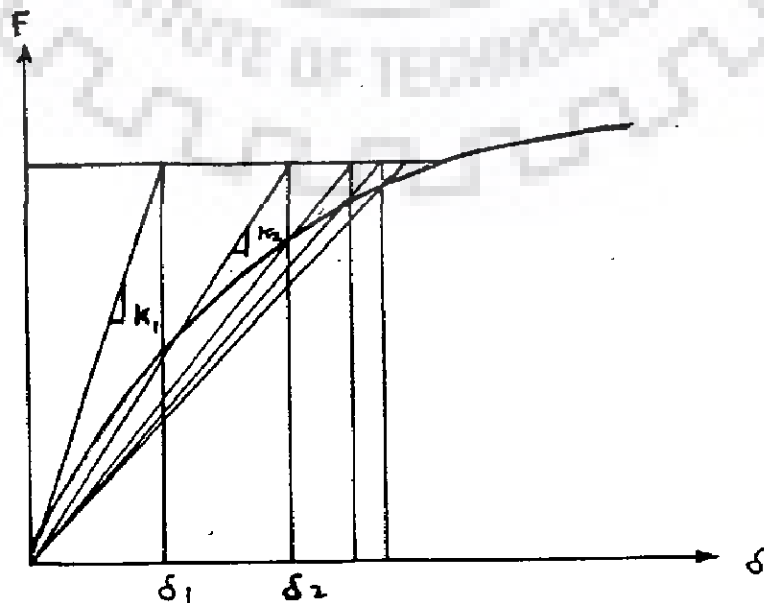


FIG. 3.6 MIXED PROCEDURE

CHAPTER 4

SALIENT FEATURES OF DIGITAL COMPUTER PROGRAM

For 3-D analysis of dam simulating sequential construction and using non-linear material properties, a program FENA3D has been developed. The program uses 20-noded isoparametric hexahedral elements. To solve the set of simultaneous linear equations, frontal solver (27) has been used. For plotting of results on a CALCOMP plotter a program GP3DPT has been developed.

4.1 FENA3D

The program in its present form can handle upto 100 elements and 800 nodes. The maximum front width of the problem is restricted to 105. For larger sized problems, the dimensions of the variables have to be modified. The programme has been executed on DEC-2050 system at University of Roorkee, Roorkee.

The program has the option of performing linear or non-linear analysis. It also has provision of having some materials with constant elastic moduli and others with stress-dependent elastic moduli. Hyperbolic stress strain relationship has been used to model the non-linear behaviour of the dam materials' stress strain relationship. The residual force approach has been used to achieve convergence.

The CPU time for a complete analysis of dam system is more than two hours. Since the computers, these days, are mostly time sharing ones, the total connect up time required for the job is more than 10 to 12 hours and, therefore, it is not feasible to get the entire dam analysed in one run, owing to

the frequent system crashes due to voltage fluctuation. The program, therefore, has the provision of analysing the dam in parts. The results of the part analysed dam are stored in a file, which are used for subsequent analysis. The program also stores the interim results after each iteration and thus, has the option of terminating the execution midway and resuming thereafter or from some earlier iteration stage to get better convergence. The assembled equations' coefficients are also stored in a file and the same can be used at any desired iteration stage. The temporary file having coefficients of assembled equations requires a huge disc storage. Option is available to store this file on magnetic tape to save on hard disc space.

The program FENA3D, in addition to the main program uses the following subroutines

- | | | | |
|----------|------------|------------|------------|
| 1. INPUT | 2. GAUSS | 3. PFRONT | 4. ELCORD |
| 5. STIFM | 6. SOLVE | 7. RESOLV | 8. BSUB |
| 9. ELRHS | 10. RESULT | 11. SFR | 12. JACOBI |
| 13. DMAT | 14. STRESS | 15. NODOUT | 16. PRINCS |
| 17. DISP | | | |

A brief description about the functions of various subroutines follows :

- (1) **INPUT** : This routine reads all the input data required.
- (2) **GAUSS** : The routine calculates the position of all the Gaussian points for integration and also the weightages associated with each Gaussian point.
- (3) **PFRONT** : This routine calculates the maximum front width, the destination array of each element nodes in the front and also the last appearance of each element node. When a node is

making its last appearance, it is assigned a negative number.

(4) **ELCORD** : The routine ELCORD is called for each element every time the coordinates of the element nodes are required; unlike the previous three routines which are called only once in the beginning. This routine calculates the coordinates of mid side nodes and also the local coordinates array of the element.

(5) **STIFM** : This subroutine is also called once for each element. It calculates the stiffness matrix for each element and since the stiffness matrix is symmetric, only half of it is stored in the memory.

The subroutine calls the following routines for each Gaussian point :

(a) **SFR** (b) **JACOBI** (c) **DMAT**

(6) **SOLVE** : This routine is called once for each element. The stiffness matrix of each element calculated by STIFM, is taken to its appropriate location in the global stiffness matrix. The equations corresponding to the nodes making their last appearance are modified for boundary conditions. To reduce the memory requirement, the modified equations (which are no longer active) are written in a file (unit 1) and after rewinding it are read again during resolution and back substitution stage. This routine also calls subroutine DISP.

(7) **ELRHS** : This routine calculates the element load vector due to gravity forces. It calls ELCORD, SFR & JACOBI routines.

(8) **RESOLV** : The routine RESOLV places the load vector of the element to its appropriate locations in the global load vector depending upon its destination in the front. The right hand

side of the equations is modified as per boundary conditions. It reads the coefficients of equations from the file on unit 1 and stores the modified right hand side corresponding to the nodes no longer active in a file on unit 2. The element load data is taken either from unit 4 or calculated from residual load vector evaluated just before this routine is called element wise.

(9) **BSUB** : This routine is called element wise starting backward from last element to the first element. The relevant data required is read backwards from unit 1 and 2. It calculates the element displacement vector which is written element wise on a file (unit 4) to be used later on for calculating strains and stresses.

(10) **RESULT** : This routine calculates incremental stresses and strains at Gaussian points for each element. It also calculates the final stresses, strains and displacements at the end of each iteration. It finds out the residual load vector, convergence factor and convergence ratio. Depending upon this ratio it sets the value of **ITEST** variable which determines whether convergence has been achieved. It stores the result of the iteration in a file, if convergence has not been achieved. If convergence has been achieved, the final results of the stage are stored in a separate file and the file containing results of each iteration is deleted. The stresses at Gaussian points and nodal displacements are printed.

This subroutine calls in addition to **SFR**, **JACOBI** and **DMAT**, the following routines.

1. **STRESS** 2. **NODOUT** 3. **PRINCS**

(11). **SFR** : The subroutine **SFR** calculates the shape functions

and their partial derivatives w.r.t. the three normalised coordinates.

(12). **JACOBI** : The subroutine **JACOBI** calculates the inverse of Jacobian matrix and its determinant. It also calculates the partial derivatives of the shape functions w.r.t. the cartesian coordinates x, y and z .

(13). **DMAT** : The routine **DMAT** calculates E_t and ν_t at each point from nonlinear hyperbolic stress-strain relationship. If the material is linear or the analysis itself is linear, there is provision for taking constant values of E and ν . The elements of $[D]$ matrix are also calculated here itself.

Subroutines **SFR**, **JACOBI** and **DMAT** are always called for each of the gaussian points of integration.

(14). **STRESS** : The routine **STRESS** calculates the six strain and six stress components at each of the Gaussian points. It uses the displacements calculated in **BSUB** and stored on unit 4. It is called for each of the elements.

(15). **NODOUT** : The routine **NODOUT** finds by extrapolation the six stresses at the nodal points. This is called for each element. To calculate the principal stresses at the nodal points, it calls upon routine **PRINCS** to do this job.

(16). **PRINCS** : The routine **PRINCS** is called to calculate the principal stresses and their directions at Gaussian points. It is called for each node by the routine **NODOUT** to calculate the nodal principal stresses and their directions.

(17). **DISP** : This routine applies boundary conditions to the set of assembled equations.

A flow-chart for the program is given in figure 4.1

4.2 GP3DPT

The plotting work has been done with the help of a general purpose plotting program GP3DPT.

The program can accomplish the following plots

1. Mesh plotting over any designated section on transverse (x-z), longitudinal (y-z) or horizontal (x-y) planes.
2. Deformed shape of a given section, with deformations magnified.
3. Sequential variation of horizontal and vertical displacements and normal stresses along designated sections over a transverse section of the dam for an analysis.
4. The variation with height of the displacements, stresses, strains, stress ratios and mobilisation factor along designated sections for a combination of analyses.
5. The variation of the variables listed at s.no 4 along horizontal planes on a transverse section of the dam for different analyses.
6. Plot the variation of the above variables along horizontal planes on a longitudinal section of the dam for different cases of analysis.

The program has also the option of superimposing the results of 2-D analysis for comparison for plots mentioned at S.No. 4 and 5. All the above plots can be had in one go or a combination of these at one go.

The program GP3DPT in addition to the main program uses the following subroutines.

1. **INPUT** :- It reads all geometric data of the dam.
2. **PLCORD**:- It calculates and stores in memory the x and y coordinates for plotting the variables along horizontal or

vertical planes.

This subroutine is called separately for plotting along horizontal and vertical planes.

3. **VVPLOT** :- This subroutine plots the variation of the different variables, namely displacements and stresses etc, one after other. The values for different analyses are superimposed over each other in the same plot.
4. **MESH** :- This subroutine plots the mesh of the dam used in the analysis in either or all of x-z, y-z or x-y planes.
5. **DOTLIN** :- It draws a dotted line between two given points.
6. **VHPLT** :- This subroutine plots on the dam section the variation of different variables along horizontal planes for various analyses.
7. **LEGEND** :- It draws the legend used for different cases.

Besides these subroutines the following library routines are also called.

1. **PLOT** :- Moves the pen from the current pen position to the given point. It has the option to move the pen in up or down position.
2. **AXIS** :- It draws the axis line of desired length at a given point. The annotations are also written by this subroutine.
3. **SYMBOL** :- It makes a centered symbol at a desired location. From the current pen position to the desired location, the pen can be in up or down position as desired.
4. **NUMBER** :- It writes at a given location the numerical value of a floating point variable.
5. **PLOTS** :- It initialises the plotter.

4.3 CONVERGENCE RATE

It is observed that the number of iterations required decreases as the dam nears completion i.e., the number of stage increases. Since in the first iteration the stiffness matrix is based on anticipated stress levels, the stiffness matrix is recalculated in the second iteration. In subsequent iterations the same matrix is used if the convergence ratio C_r is less than 1.2. It has been observed that generally there was no occasion to necessitate recalculation of the stiffness matrix, beyond the second iteration.

Table 4.1 shows the values of convergence factors in different iterations for different layers for a typical run.

Table 4.1: Convergence Factors in Different Iterations

Iteration No.	Convergence factor C_r for layer no.					
	1	2	3	4	5	6
1	87.25	35.49	22.84	21.17	16.84	11.68
2	47.45	16.26	10.21	8.88	8.55	6.56
3	27.92	8.31	5.25	4.71	4.12	3.77
4	17.50	4.74	3.90	3.08	2.59	
5	11.44	2.92				
6	7.70					
7	5.20					
8	3.60					

It is seen from the table that the number of iterations required are 8,5,4,4,4 and 3 respectively in stages (layers) 1 through 6. It is also seen that as the completed height increases the convergence factor goes on reducing as compared to that in previous stages, pertaining to the corresponding

iterations.

The iterations have been terminated when the convergence factor is less than 4%. In the early stages of analyses, the convergence factor was specified to be 2%. A comparison of the results with 4% and 2% accuracies showed that the stress values were practically unaffected. The displacement values at some of the nodes showed marginal variations (less than 2%) and therefore, for further analyses the accuracy was specified to be 4%.

The incremental load in iterations other than the first one is to be the residual load (Ψ_j) given by

$$\{\Psi_j\} = \{F\} - \int_V [B]^T \{\sigma_{j-1}\} dV$$

Where j refers to the iteration number, $\{F\}$ is the global load vector, $[B]$ the strain displacement matrix and $\{\sigma\}$ is the stress vector.

It has been observed that the rate of convergence is affected if the incremental load is taken as $\mu\{\Psi_j\}$ in place of $\{\Psi_j\}$ only, where μ is a scalar termed as accelerator (45). The accelerator value is found to be generally varying from 0.6 to 0.8. A value of more than 1 for μ as suggested by Naylor and Pande (45) has not led to convergence in these analyses. No rationale could be established to determine the value of μ for faster convergence. It depends upon many factors, namely the stage of analysis, the valley shape and the material properties. However, a higher value of μ is generally required for analyses of lower layers and a lower value leads to faster convergence when the dam has been raised higher.

It is found that convergence rate depends on the value of

accelerator and is slower with a low value of μ . A value of μ between 0.6 and 0.8 generally gave good convergence.

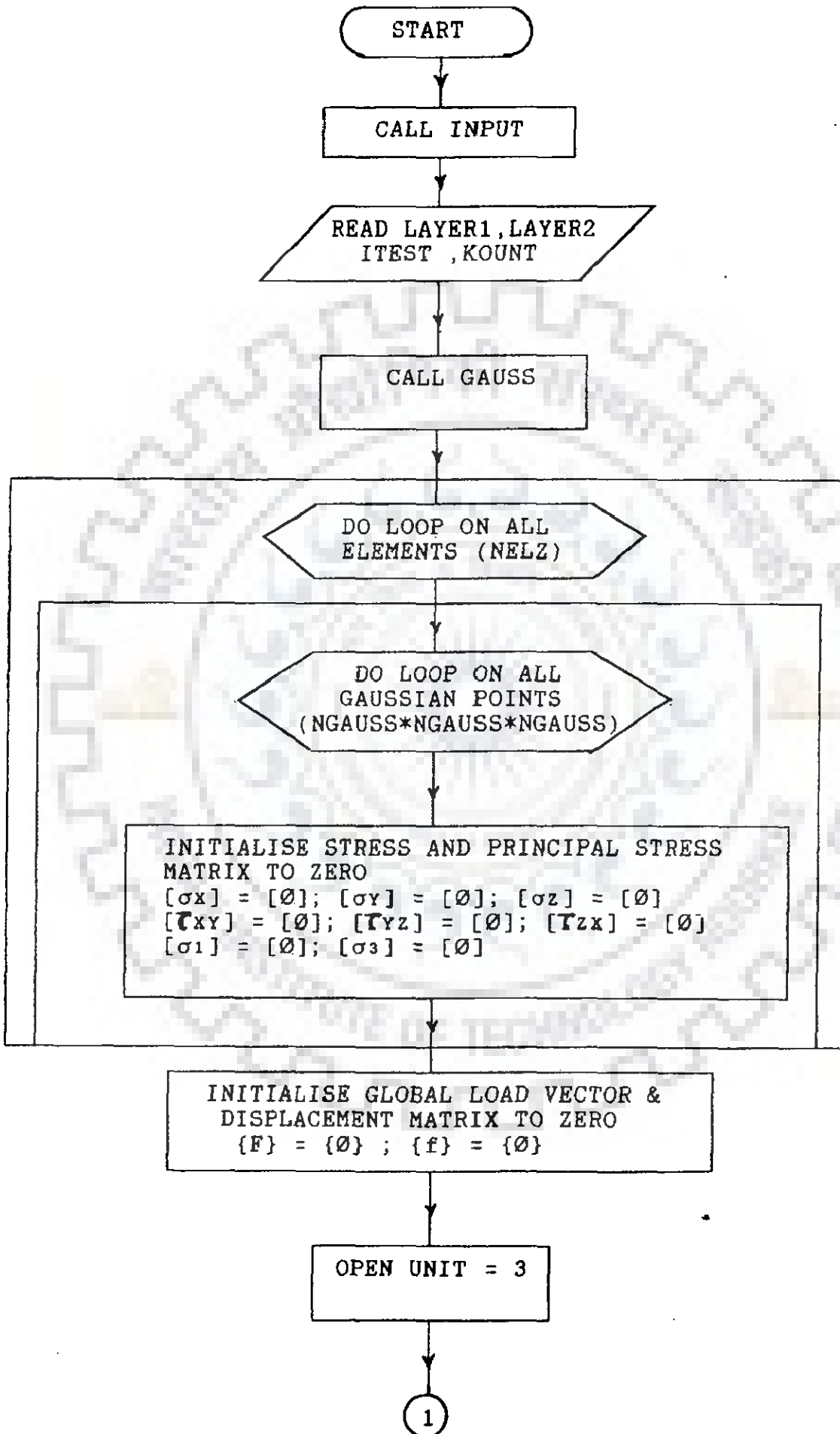
4.4 CPU TIME

The CPU time required for a typical run along with the number of iterations required are given in Table 4.2. The number of times, the stiffness matrix is required to be calculated is also shown in Table 4.2.

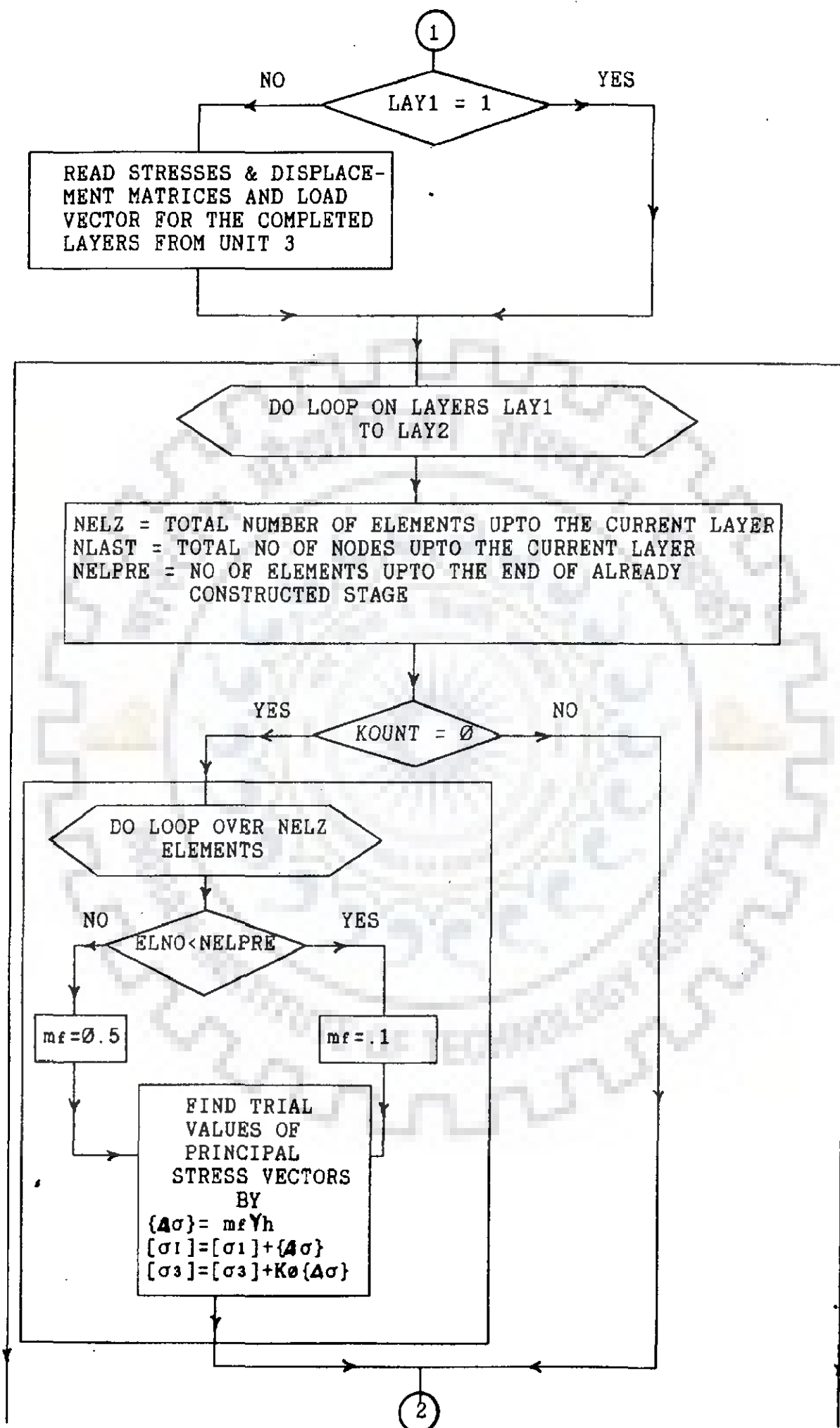
Table 4.2: CPU Time for a 3-D Analysis

Layer No.	No. of times [K] is to be Calculated	Total iterations required	CPU Time Min: seconds
1	2	8	30:57.47
2	2	5	
3	2	4	
4	2	4	20:46.58
5	2	4	32:47.54
6	2	3	40:01.28
		Tctal	----- 2:04:33.87

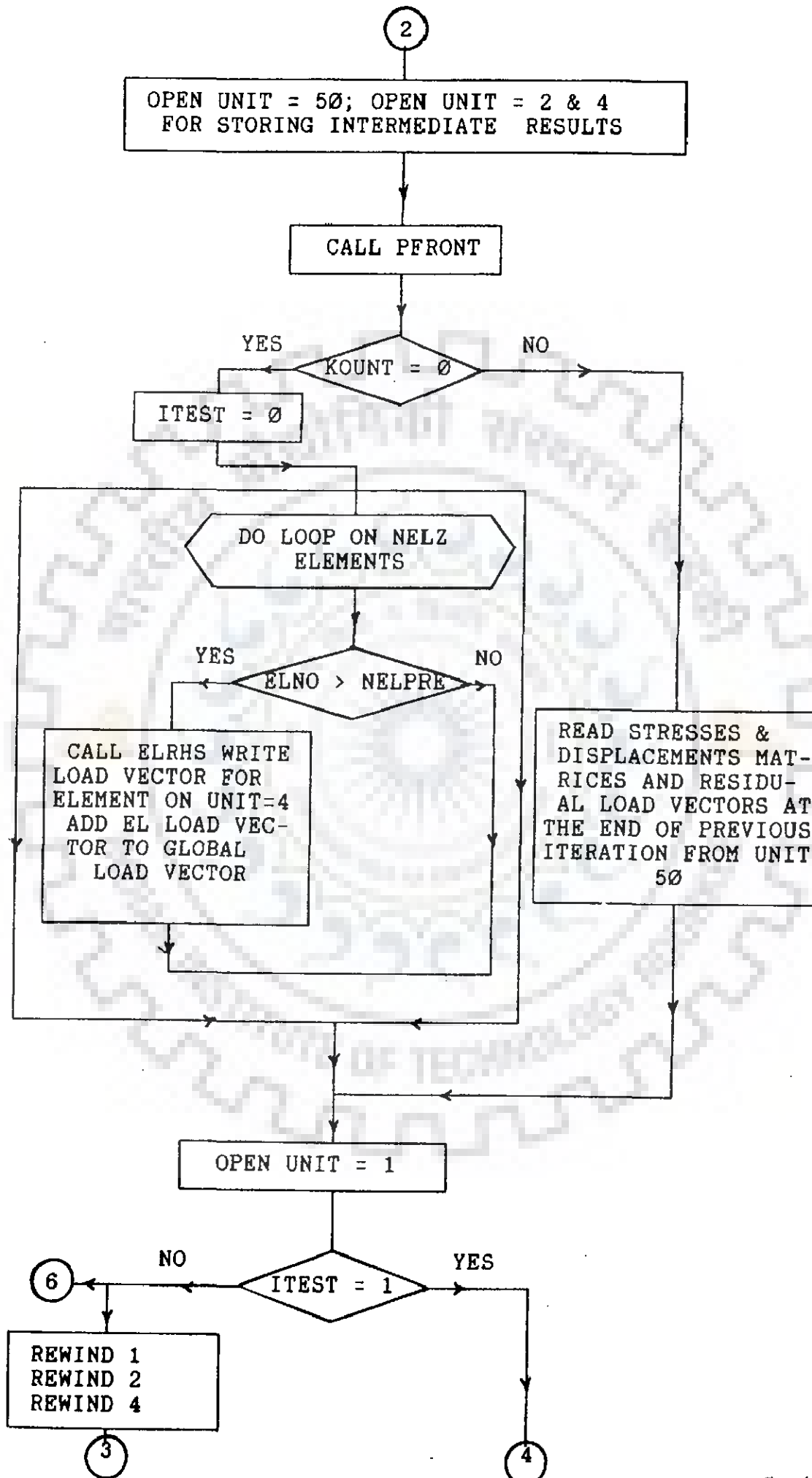
Fig 4.1 FLOW CHART FOR PROGRAM FENA3D



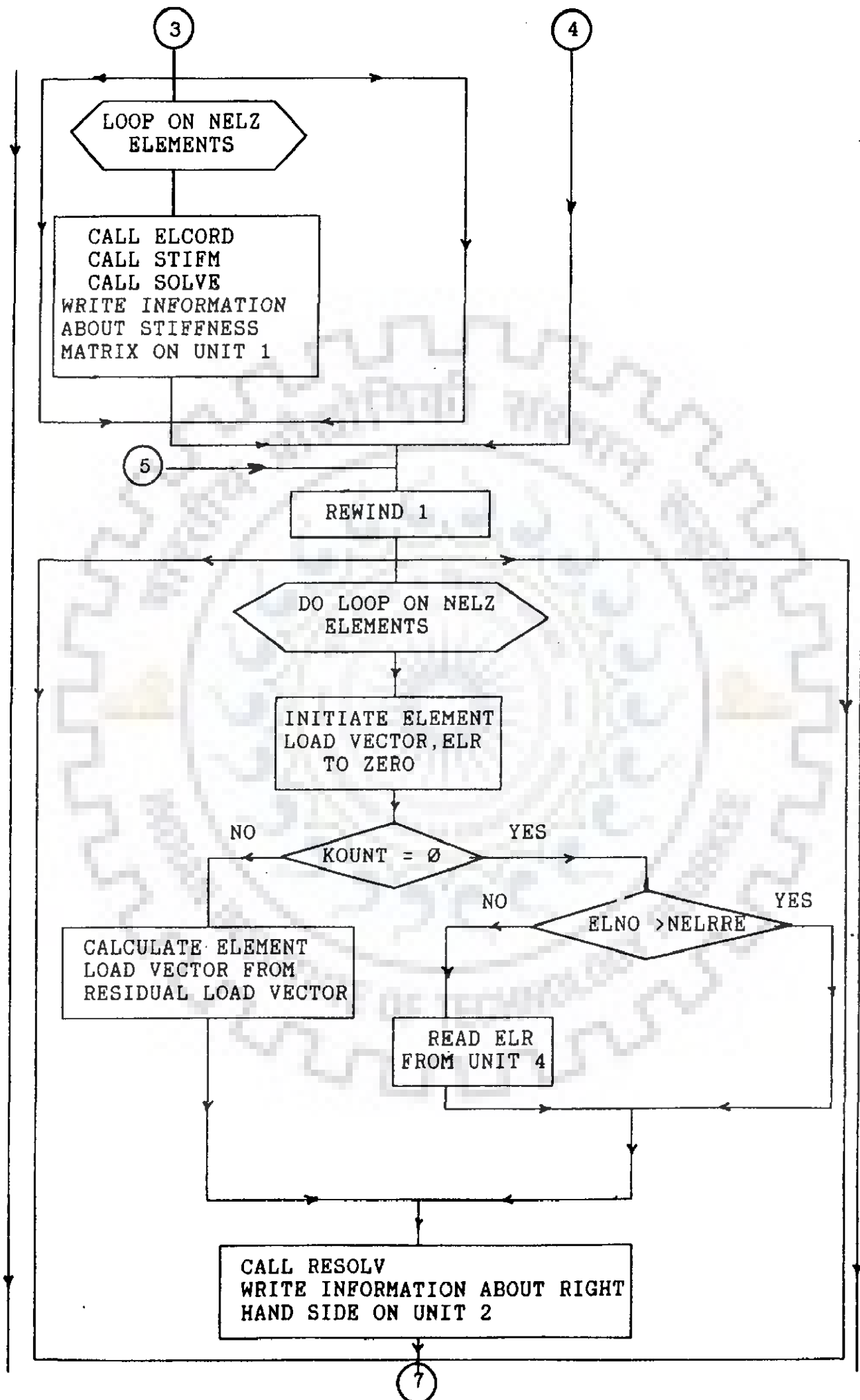
Contd.....



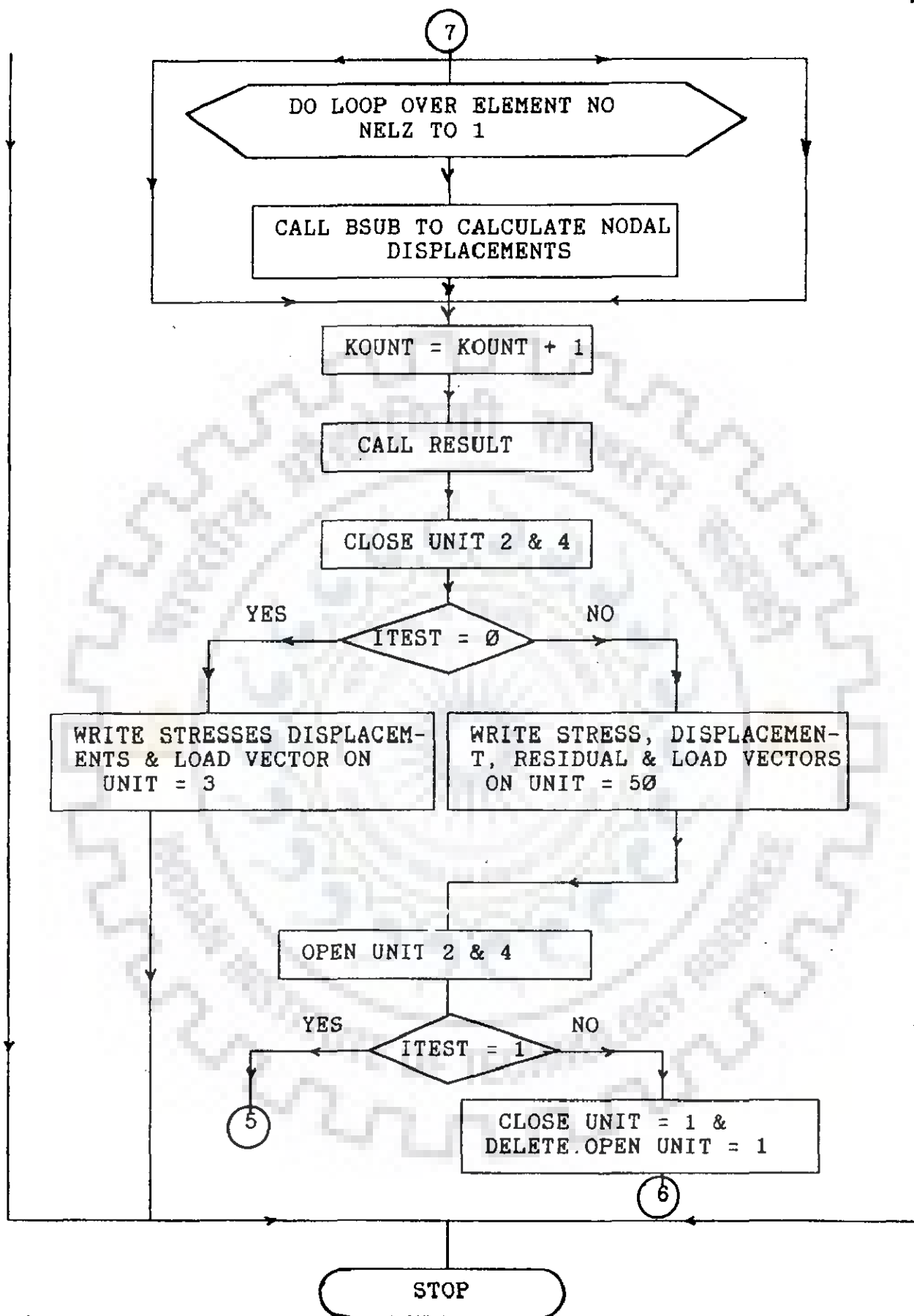
Contd.



Contd.....



Contd.....



CHAPTER 5

ANALYSIS TO STUDY THE EFFECT OF VALLEY WIDTH

A 260 m high proposed rockfill dam section has been chosen for this study and is shown in Fig. 5.1. The dam has a moderately inclined core supported by shells on both sides. In between the core and shells thin zones of filter/transition lie on both sides. The slopes of upstream and downstream core faces are $0.5H:1V$ and $0.2H:1V$ respectively, both inclined upstream. The upstream and downstream slopes of the dam are $2.5H:1V$ and $2H:1V$ respectively. The core width at the foundation contact is to be equal to the hydraulic head to give a unit hydraulic gradient. This is achieved by flattening the slope of the upstream face of core to $1H:1V$ near the foundation contact. The dam core extends upto fresh rock.

The dam is situated in a narrow, nearly symmetrical valley with valley walls at an average slope of $1.1H:1V$, as shown in Fig. 5.1. To reduce the size of the problem, the valley profile has been assumed symmetrical about the centre line of the valley and, therefore, only one half of the dam has been considered in the analysis.

The rocks at the dam site are phyllites of different grades. The deformation modulus of the phyllites is quite high relative to the dam material and, therefore, the foundation has been considered as rigid.

The dam has been idealized into 98 number of 20 noded brick elements, each node having 3 degrees of freedom. The mesh consists of 724 nodes, thus having a total of 2172 degrees of freedom. Since the valley is symmetrical in the y -direction

all the nodes on the central section have been assigned zero movement values in that direction. The number of elements in the 6 stages of construction are 14, 26, 38, 58, 76 and 98 respectively. The finite element idealisation of the dam at the maximum transverse section (called central section hereafter) and at the longitudinal section in the y-z plane along the upstream face of core is shown in Fig. 5.2. To simulate sequential construction, the dam is assumed to be raised in 6 layers, each of 40 m height.

5.1 ANALYSES PERFORMED

To study the effect of valley width, four different valley shapes, with the same transverse section of the dam, have been analysed by 3-D analysis. The first valley shape is the idealized valley shape of the proposed dam. The valley has a valley width factor (Ratio of Valley width to height) of 2.25. Three other valley shapes have been obtained by multiplying the y-coordinate along the dam axis by scaling factors of 0.5, 2 and 4 giving valley width factors of 1.12, 4.5 and 9.0 respectively. The details of these four shapes are given in Table 5.1. These four valley shapes represent the general range of valley shapes for rockfill dams.

Table 5.1 : Details of Valley Shapes Analysed

S.NO	Base width of valley	Average wall slope	Valley width factor β
1	14 m	0.55H:1V	1.12
2	28 m	1.1H:1V	2.25
3	56 m	2.2H:1V	4.50
4	112 m	4.4H:1V	9.00

5.2 NUMERICAL DATA

The properties of the material used in the analysis are given in Table 5.2. These properties are the same as used by Sharma(56) for analysis of Tehri dam. In the absence of test results on dam materials, these properties were adopted on the basis of values given by Kulhawy et al (35).

TABLE 5.2 : Material Properties

Sl.No.	Parameters	Shell	Transition	Core
1.	Unit wt.in tonnes/m ³	1.80	1.99	1.96
2.	Cohesion C,tonnes/m ²	-	-	1.00
3.	Friction angle ϕ (°)	38.00	32.00	27.00
4.	Modulus number K	2500.00	3000.00	500.00
5.	Modulus exponent n	0.25	0.30	0.60
6.	Failure ratio R _f	0.76	0.76	0.90
7.	Poisson's ratio parameters :			
	G	0.43	0.43	0.48
	F	0.19	0.19	0.0
	d	14.80	14.80	0.0

5.3 SIGN CONVENTION

The following sign convention has been followed throughout in this study.

The positive x - direction is from upstream to downstream along the river, positive y-direction from the central section to the abutment along the dam axis and the positive z-direction is upwards as indicated in Fig. 5.2.

The displacements u, v and w are positive in the positive x,y and z directions respectively.

The normal stresses, σ_x in the transverse direction, σ_y in the longitudinal direction and σ_z in the vertical direction and the three principal stresses σ_1 , σ_2 and σ_3 are positive

if tensile and negative if compressive.

5.4 PARAMETERS STUDIED

The following parameters have been studied:

1. Displacements u , v and w in x , y and z directions
2. Normal stresses σ_x , σ_y and σ_z in x, y and z directions
3. Mobilisation factors
4. Principal stress ratio (σ_1/σ_3)
5. Horizontal stress ratio (σ_x/σ_y)
6. Contact pressure at abutments

The variation of these parameters has been studied for various analyses along the height and at constant elevations over the central section and plane no. 2. (shown in Fig. 5.2(a)).

The study at central section enables comparison of 3-D analyses with the plane strain analysis. The study at plane no.2 is representative of the behaviour on sections towards the abutments.

For studying the variation of different parameters along the height, following typical locations have been chosen on the two cross sections:

1. Two locations in shell, one in upstream and the other in downstream shell.
2. The shell/transition interfaces on both sides of core.
3. Three locations in core i.e., along the upstream face of core, centre line and the downstream face of core.

Since these locations are on inclined planes and the variation has been analyzed with respect to height, henceforth

these locations have been called verticals. Verticals numbering 1 through 7 (from upstream to downstream) are on central section and the verticals number 8 through 14 are on plane No.2. For the central section, the locations are marked in Fig. 5.2.

The distribution pattern along horizontal planes, has been studied at ground level and at elevations 40m, 80m, 120m, 160m and 200m above ground level. For studying the behaviour of parameters at constant elevations on longitudinal sections through the upstream face and centre line of core, the elevations chosen are 40m, 80m, 120m, 160m, 200m and 240m respectively. The y-dimension in plots for all the four cases has been kept the same, as for the normal valley shape with side slopes of 1.1H:1V, to facilitate comparisons on a common base.

The stresses, strains and other stress dependent parameters have been calculated at the gaussian points. The results of these parameters presented here pertain to the gaussian points adjacent to the locations under consideration.

5.5 RESULTS AND DISCUSSIONS

5.5.1 Displacements

5.5.1.1 Horizontal Movement-u

Figure 5.3 shows the variation of horizontal movements - u along the verticals over central section of the dam. It is noted from the figure that the movements in the upstream portion of the dam are towards upstream and those in the downstream portion are towards downstream i.e., the dam expands laterally. The distribution indicates small movements at the

top and maxima occurring at about mid height above base in shells and at about one-third height above base in core and transitions. The upstream movements are more than the corresponding downstream movements. A similar distribution pattern in core and transitions is also found at plane no. 2 as well.

The maximum values of horizontal movement - u at different verticals over central section and plane no. 2 are plotted in Fig. 5.4 against the valley width factor. It is observed that the movement increases with increase in the valley width factor. Over the central section the maximum movements are seen in the shells. Beyond $\beta = 9$, the curves tend to be flat. A comparison of the 3-D analysis values at the central section with those of plain strain values shows that the 3-D values are about 25-40 %, 55-80 % and 75-100 % of the plain strain values for valleys with valley width factors β equal to 1.12, 2.25 and 4.5 or above respectively.

On plane no. 2 the maximum movement values are about one-third of those at the central section. In the upstream portion of the section, the maximum movements are nearly of the same order at all locations. In the downstream portion, however, the maximum movements increase from the centre towards the faces. The effect of valley width at this section is small beyond β equal to 4.5.

The sequential variation of horizontal movement- u along height, as the dam is raised in different stages, is shown in Fig. 5.5 at different locations at the central section for a dam with valley width factor $\beta = 1.12$. It is seen that at all

locations the horizontal displacements at different stages of construction follow the same pattern as for the final displacements. In the shells, at verticals no 1 and 7, where the dam height is only 200 m, the horizontal movements increase considerably even during the placement of last layer.

The contours of horizontal movements u over central section for a narrow valley with $\beta = 1.12$, a wide valley with $\beta = 9$ and plain strain analysis are shown in Fig. 5.6. It is seen from the figure that for the wide valley the contour lines are almost horizontal in shells, while for the narrow valley this is not so. It means that in a wide valley the horizontal movements in shell remain unchanged at constant elevation. It is also seen that near dam top, the movements are towards downstream. This zone is smaller in size for narrow valleys and increases with the valley width factor. The plain strain analysis contours are almost identical to those for a wide valley with $\beta = 9$.

The contours of horizontal movement on the longitudinal ($y-z$) plane along the upstream face of core are shown in Fig. 5.7 for valleys with valley width factors β equal to 1.12 and 9 respectively. It is observed from the figure that for both valley shapes, the maximum movements take place near the centre line of the valley. The contours are parallel to valley profile in the lower half height and tend to be flat in the upper half height.

5.5.1.2 Vertical Movement- w

The variation of vertical settlement $-w$ along different verticals over central section of the dam is shown in Fig. 5.8. It is seen from the figure that the vertical movements

increase with height above base to attain maximum values at about two-third the dam height and then decrease towards top. In the top portion of the dam, the reduction in settlement values is sharp. The effect of valley width is more pronounced for vertical movements than for horizontal movements and the settlements gradually increase with valley width factor. For 3-D analysis with $\beta = 1.12, 2.25, 4.5$ and 9 the settlement values are approximately 35-45%, 50-60%, 60-75% and 90-98% respectively of plane strain values.

The maximum settlement values over the two transverse sections for all the 3-D analyses are plotted in Fig. 5.9 against the valley width factor. It is seen that at central section, the settlement at all locations gradually increases with the valley width. The rate of increase is maximum from $\beta=1.12$ to $\beta = 2.25$ and, thereafter, the rate decreases. For both the transverse sections, the maximum settlements are observed at the core centre line and least in shells. The maximum settlements at the centre line are 48, 68, 91 and 125 cms at the central section and 37, 50, 50 and 51 cms at plane no. 2 for valleys with $\beta =1.12, 2.25, 4.5$ and 9 respectively. The maximum settlement for plain strain analysis is 142 cms. The settlements at plane no. 2 are about 70 %, for a narrow valley with $\beta = 1.12$ and about 40 %, for a wide valley with $\beta = 9$, of the corresponding values at the central section.

The sequential variation of vertical movement-w with height is shown in Fig. 5.10 at different locations at the central section of the dam with a valley width factor $\beta= 1.12$. It is noted from the figure that at all locations, the

displacements along the height follow the same pattern as for the final stage. The maximum settlements occur in the core at about two-third height from the base.

The distribution of settlement- w along horizontal planes at central section is shown in Fig. 5.11. It is seen that at all elevations the settlement increases from the dam face, towards the interior. This increase continues at almost uniform rate in shells upto close to transition zones whereafter the rate of change of settlement with distance changes. At lower elevations the settlement values decrease towards the transition and then in core as well, such that the maximum settlements are observed in shell. In the top half portion the gradients, however, increase sharply in core. It is also observed that the settlements in downstream shell are more than the corresponding settlements in the upstream shell all through the height. The settlement curves for plane strain analysis are almost coincident with those for 3-D analysis with $\beta = 9$.

The settlements at constant elevations over the y - z plane along the upstream face and centre line of core for different cases are shown in Fig. 5.12. It is seen that the settlement magnitudes decrease towards the abutments and remain unaffected by the valley shape in this reach. The maximum settlements occur at the central section and are of the order of 1.2 m.

The contours of vertical settlement over the central section are shown in Fig. 5.13 for valley width factors of 1.12 and 9 and for plane strain analysis. It is noted that with $\beta = 9$, the contours for 3-D analysis and for plane strain

analysis are similar except for minor differences in values at about two-third height from base. For all the analyses the contours are spreading in the downstream shell, thereby indicating that the downstream shell settles more than the upstream shell. The horizontal alignment of contours in the downstream shell for about three quarters of the shell zone indicates that the settlements remain constant at a given elevation in a major part of the downstream shell.

5.5.1.3 Cross Valley Movement - v

The cross valley displacements - v are small in magnitude as compared to the transverse and vertical movements u and w. Because of the symmetry, the cross-valley movements are not present at the central section and, therefore, these are discussed at plane no. 2 and another section still nearer to the abutments named as plane no. 3.

The maximum movements at different locations at plane no. 2 are given in Table 5.3.

Table 5.3 : Cross-Valley Displacements at Plane No. 2

Verticals No.	Magnitude of displacements - v (cm)			
	$\beta=1.12$	$\beta=2.25$	$\beta=4.50$	$\beta=9.00$
8	-3.9	-7.2	-7.3	-7.7
9	-6.3	-12.6	-14.9	-11.7
10	-5.7	-19.0	-14.0	-11.5
11	-6.7	-19.3	-15.6	-11.9
12	-8.1	-15.0	-20.0	-11.5
13	-12.3	-12.6	-14.6	-11.0
14	-5.4	-9.3	-11.0	-7.4

It is noted that the movements are negative, i.e., towards the centre of valley for all cases. Largest movements are observed in the core followed by those in transitions. As the valley width increases, the displacements increase upto $\beta = 2.25$ and then decrease further. The maximum displacement is of the order of 20 cms.

Table 5.4 gives the maximum displacements on plane no. 3. It is noted from the table that the cross valley movements are substantially smaller at this section as compared to those at plane no. 2. The maximum displacements are observed for $\beta=2.25$ and decrease for narrow as well as wide valleys. The movements in the core interior are maximum as compared to other locations. The maximum movements are about one third of those at plane no. 2.

Table 5.4: Maximum v - Displacements on Plane No. 3

Locations	v (cms) for 3-D analyses			
	$\beta=1.12$	$\beta=2.25$	$\beta=4.50$	$\beta=9.00$
Transition U/S	-2.5	-7.8	-4.0	-1.7
Core U/S face	-3.0	-6.6	-3.9	-1.7
Core Centre line	-4.2	-6.8	-4.5	-1.9
Core D/S face	-3.8	-6.8	-3.2	-1.6
Transition D/S	-4.4	-7.5	-2.7	-1.4

5.5.2 Stresses

5.5.2.1 Transverse Normal Stress σ_x

The variation of horizontal normal stress σ_x with height

at different locations on central section of the dam is shown in Fig. 5.14. It is seen that the variation of σ_x is nonlinear. The distribution in the core is of concave shape while that in shells and transitions varies from slightly convex to near linear. It is also noted from the figure that in the upper two third height of the dam, the stresses for different cases are approximately of the same magnitude. In the lower one-third portion the stresses increase with the valley width factor. The height in which the stress σ_x is unaffected by valley width factor is maximum in upstream transition and downstream shell and least in upstream shell and downstream transition. At plane no. 2, the effect of valley width is seen to exist over larger heights than at central section, as shown in Fig. 5.15.

The maximum values of stress at different verticals over central section and plane no. 2 are plotted against valley width factor in Fig. 5.16. It is seen that the stresses increase with valley width factor upto β equal to 4.5, beyond which the curves are nearly flat. The maximum magnitude of horizontal normal stress is observed at the core centre line on central section and on the upstream face of core at plane no. 2. Lowest values of σ_x are observed in upstream shell. On central section, stresses obtained from 3-D analyses for $\beta=1.12$, 2.25 and 4.50 are about 51%, 72% and 95% of the corresponding plane strain values. The effect of valley width on stresses is maximum in core and least in pervious zones of the dam. The stresses at plane no. 2 are lower in pervious zones and higher in core than the corresponding values at central section.

The variation of σ_x along height for different stages of construction is shown in Fig. 5.17 for different locations over

the central section, for a narrow valley with $\beta = 1.12$. It is seen that right from the first stage, the stress distribution is almost of the same shape as the final stress distribution curve. During the last layer, the increase in core stresses is smaller in comparison to the increase during earlier stages.

The variation of σ_x at constant elevations over central section and plane no. 2 are shown in Fig. 5.18. It is seen that starting from the dam face where the σ_x stress values are low, the stresses increase towards the interior. The effect of valley width is not evident in the upper half height. In the lower half height, the effect of valley width is small beyond $\beta = 4.5$. The stresses in the core are higher than the stresses in the adjoining shells and are caused due to the presence of core trench at the base.

The distribution of σ_x at constant elevations over the longitudinal section of the valley is shown in Fig. 5.19, along the upstream face and the centre line of core. It is seen that over the upstream face of core, σ_x increases towards the abutments in the lower half height. In this portion, the stress values drop sharply in the core trench to increase sharply at the bottom of core trench. In the upper half height the stresses remain constant in the central one-third length. In the one third length near the abutments the stresses follow the same pattern as in the lower half portion near the abutments.

At the longitudinal section along the core centre line the σ_x values increase gradually towards the abutments. In the

core trench the σ_x values again increase sharply, to decrease partially at the base of core trench. Maximum σ_x values at the same elevation are observed in the middle of the core trench all over the height. The effect of valley shape is appreciable in the lower two third height and is more on sections nearer the abutments.

The contours of horizontal normal stress σ_x over the central section, for valley with $\beta = 2.25$, $\beta = 9$ and for plain strain analysis, are shown in Fig. 5.20. It is seen that the stress contours in the shells are almost parallel to the dam faces and the contours get depressed at the core faces, recovering at the centre of the core. In the interior of the dam the stress contours are steeper than at the dam faces. The stress contours in the core near the base are densely populated indicating high stress gradients. A comparison of the two analyses indicates that in the upper portion, a narrow valley gives higher stresses than a wider one, while in the lower reaches, a wider valley gives higher stresses. The contours from a plane strain analysis are almost identical to those from a 3-D analysis with $\beta = 9$.

The stress contours on the longitudinal sections along the upstream face and the centre line of core are shown in Fig. 5.21 for a valley with $\beta = 2.25$. It is noted that the stresses in dam portion away from the central-section, are more than those at the central section. The stresses in the core trench are of the same order as those on the central section.

5.5.2.2 Longitudinal Normal Stress σ_y

The maximum values of horizontal normal stress σ_y are plotted against valley width factor in Fig. 5.22 for both central section and plane no. 2. It is seen, that the stresses are of the same order at all locations for valleys with $\beta=4.50$ or more. The minimum stress values occur in upstream shell. The maximum stresses on the upstream face of the core are 220, 310, 379 and 390 t/m² (compressive) at central section for $\beta=1.12, 2.25, 4.5$ and 9 respectively. The corresponding plane strain value is 408 t/m². The 3-D analysis values are about 75% and 94% for $\beta = 1.12$ and 2.25 respectively and 98 to 100 % for $\beta = 4.5$ or more, of the corresponding plane strain analysis values.

The variation of σ_y at different verticals of central section for different stages of dam construction is shown in Fig. 5.23 for 3-D analysis with $\beta = 1.12$. It is seen that, the distribution along height for different stages is similar to the final distribution obtained on the completion of dam construction.

The variation of horizontal normal stress σ_y at constant elevations on central section is shown in Fig. 5.24(a). It is seen that the stresses increase linearly in the shells from dam faces towards the interior. The distribution at ground level indicates a sharp increase at the core faces accompanied by a drop in the core interior. At other elevations, the stresses sharply increase from core faces towards the core centre line. This increase goes on smoothing with the height. The σ_y stresses in core are thus more than those in the adjoining transitions. The stresses increase with increasing valley

width factor upto $\beta = 4.5$ beyond which the increase is small. At plane no. 2, the distribution at constant elevations is similar to that at the central section and is shown in Fig. 5.24(b).

5.5.2.3 Vertical Normal Stress σ_z

The distribution of σ_z along height at the central section of the dam is shown in Fig. 5.25. The overburden pressures are also superimposed for comparison.

It is noted from the figure that in the upper one third height, the 3-D stress values are close to the plane strain values. The effect of valley width factor is visible in the lower two third height and the stress values increase with increasing valley width factor. The effect is more prominent in shells and transitions than in core. The presence of the core trench affects the stress distribution in the core at the base significantly.

The over-burden pressure on the central section is generally more than the vertical stress indicating stress transfer to the adjoining regions. It is seen that the stress transfer is more on the downstream face of the core than from the rest of the core. The stress transfer is more for narrow valleys and decreases with increase in valley width factor.

The maximum values of σ_z are plotted against the valley width factor in Fig. 5.26. It is seen that the stress values sharply increase with valley width factor upto a valley width factor of 4.5, beyond which the increase is small. It is also seen that the stresses on the downstream side are more than those on the corresponding locations on the upstream side for

all cases. The maximum stresses are, however, obtained on the downstream face of core at central section but on the upstream face of core at plane no. 2.

The maximum vertical stress values on the upstream face of core over central section are 231, 329, 409 and 421 t/m² (compressive) for 3-D analyses with $\beta = 1.12, 2.25, 4.5$ and 9.0 respectively, in comparison to the plane strain value of 440 t/m². These are about 50 to 60%, 70 to 80% and 90 to 100% of the corresponding plane strain values. For $\beta = 9$ the stress values are quite close to those from plane strain analysis.

The variation of σ_z with height as the dam height is raised in layers, is shown in Fig. 5.27 over the central section for 3-D analysis with $\beta = 1.12$. It is seen that the stress variation along height for all stages is similar to the final stress distribution. The stress increase from stage 1 to stage 5 is almost uniform but is small for the last stage.

The variation of σ_z at constant elevations over the central section is shown in Fig. 5.28(a). It is seen that the stresses are very low at the dam faces and increase gradually towards the interior in the shells at nearly constant gradients. At ground level where the stresses are maximum of all elevations, the peak stresses are observed at or near the core faces with reduction in the core interior. At other elevations the maximum stresses occur in the transition, and the core stresses are lower than the transition stresses. It is also seen that in the upper half height the stresses are not significantly affected by the valley width. The effect of valley width is maximum at the ground level where the stresses increase with the valley width factor. Beyond

$\beta=4.5$ the stresses are not affected much by valley width factor and the stresses are close to those obtained from plane strain analysis.

It is found that over plane no. 2 (Fig. 5.28(b)) at a constant elevation the core stresses are greater than the transition stresses in the lower one-third height. In the upper two third height the stresses in core are less than the transition stresses. The effect of β is more visible in shells than in core. The effect of valley width factor on this section is insignificant in the upper two-third height while in the lower one-third height it is more than that at the central section.

The contours of stress σ_z on longitudinal sections along upstream face and centre line of core are shown in Fig. 5.29, for a valley width factor $\beta = 2.25$. It is seen that along the core face, near the base the contours are moving downwards, then remain horizontal and finally in the upper two third height the contours are going upwards indicating that the stresses are increasing towards the abutments. Near the abutments the contours are moving downwards along the valley profile to rise back in the core trench. It, therefore, means that in the core trench the stresses get reduced but again increase gradually at the core trench base.

At longitudinal section along the centre line of core, in the lower one third height the stress contours follow upward trend towards the abutments, but move downwards near the abutments, to rise again in the core trench. It means that the stress σ_z increases towards the abutments, but drops at

the abutment contact to increase sharply in the core trench in the lower one third portion. In the middle -third height, the contours remain horizontal over the entire width. In the core trench the contours rise along the valley profile and then remain horizontal in the core trench. It means that in this portion the stress is constant at a given elevation but rises sharply near the abutments into the core trench. In the upper reaches of dam the stress remains constant all over the valley width.

The σ_z contours over the central section are shown in Fig. 5.30 for 3-D analyses with $\beta = 2.25, 9.0$ and for plane strain analysis. The contours are almost parallel to the dam faces except in the interior where the contours are steeper than the dam face slopes. The contours get depressed in the core indicating the load transfer from the core to the adjoining shells. The load transfer is maximum in the middle third height and minimum in the upper third height. The contour shape and magnitude for plane strain analysis and for 3-D analysis with $\beta = 9$, are almost similar indicating that for this valley, a plain strain analysis will be adequate.

The contours of σ_z over plane no 2 are given in Fig. 5.31 for 3-D analyses with $\beta = 2.25$ and $\beta = 9$. Comparison of these with the respective plots at central section indicates that the shells and transitions have lower stresses in general, and in the lower half in particular. The reduction in core stresses is not that sharp but is confined only to the interior of core. The reduction is more for $\beta = 9$ than that for $\beta = 2.25$. The zone of lower stresses in core goes on shifting upstream as

the valley width increases. In the upper half the reduction is confined to the upstream face only. The difference in shape and magnitude of the contours for the two cases is more pronounced on this section than at the central section.

5.5.3 Mobilisation Factor

The mobilisation factor m is a measure of the mobilised strength of the material. It is thus a measure of the factor of safety, along a plane, as given by :

$$F = \frac{\sum l}{\sum m l} \quad (5.1)$$

where, F = Factor of safety against sliding

m = Mobilisation factor along the failure plane over a length l

$\sum l$ = Total length of the failure plane

The variation of mobilisation factors with height at different verticals of the central section is shown in Fig. 5.32. It is noted that the values of mobilisation factors increase with valley width factor at all verticals. However, the effect of valley width is minimum in shells and upstream transition and maximum in core and the downstream transition.

The maximum values of mobilisation factors on the central section for various valley width factors are given in Table 5.5. A perusal of the table along with Fig. 5.32 indicates that the mobilisation factors in the downstream shell and transition are more than the corresponding values in the upstream, and in core are almost same for all the three locations. The maximum values of mobilisation factors are found on the downstream transition/shell interface followed by

those in core.

Table 5.5: Maximum Values of Mobilisation Factors at Central Section

Vertical No.	Maximum m for 3-D analyses			
	$\beta = 1.12$	$\beta = 2.25$	$\beta = 4.5$	$\beta = 9$
1.	0.33	0.36	0.37	0.37
2.	0.25	0.28	0.31	0.35
3.	0.31	0.43	0.47	0.55
4.	0.34	0.43	0.47	0.56
5.	0.28	0.36	0.44	0.54
6.	0.4	0.42	0.51	0.62
7.	0.35	0.43	0.44	0.45

The variation of mobilisation factors with height at plane No.2 is also found to be similar to the one at central section. The values of mobilisation factors increase with valley width factor. The effect of valley width however, is not as marked as on the central section. The maximum values of mobilisation factors vary from 0.42-0.50 and 0.49-0.57 in the upstream and downstream shells, from 0.45-0.54 and 0.5-0.65 in the upstream and downstream transitions. In core the maximum values of mobilisation factors vary from 0.37-0.52 in the upstream half and from 0.33-0.50 on the downstream face. Downstream shells and transitions exhibit higher mobilisation factors than the corresponding upstream locations. In core the mobilisation factors are almost same at all three locations in it with slightly lower values on the downstream face. For a narrow valley with valley width factor β equal to 1.12, the mobilisation factors all over the sections at plane No.2 are

more than the corresponding values at central section. For other valley shapes i.e., $\beta = 2.25, 4.5$ and 9 the mobilisation factors in core are lower, whereas, elsewhere over the section the mobilisation factors are higher than those on the central section. This indicates that the factor of safety against sliding is lower at sections towards the abutments and, therefore, a plane strain analysis of the central section may give a false sense of security and, therefore, a 3-D analysis is essential.

Over both the central section and plane No.2, the mobilisation factors in the downstream shell are greater than those in the upstream shell, indicating a lower factor of safety against sliding for the downstream slope as compared to that for upstream slope for all analyses. This is expected since the analysis is for gravitational forces and the downstream slope is steeper. Also narrow valleys exhibit higher factors of safety than wider valleys.

The contours of mobilisation factors over the central section for the 3-D analyses with $\beta = 2.25$ and 9 are shown in Fig. 5.33. It is seen that in shells, the contours of highest mobilisation factors lie along the dam base and the transition/shell interfaces which indicates that the minimum factor of safety would be along these wedges. The critical failure planes on both faces are wedge shaped and not circular ones. In the upstream shell the mobilisation factors are almost same for all cases except in a smaller height near the base, where wider valleys have higher mobilised strength i.e., lower factors of safety. In the downstream shell, however, wider valleys have higher mobilised

strength. It is also seen that at the dam faces local zones of higher mobilised strength are found for all valley shapes indicating local slope failure. These local zones of higher mobilised strength are larger in size and magnitudes for narrower valleys and decrease in size and magnitudes with increase in valley width. This means that the local failure zones are more prevalent in narrower valleys but a narrower valley is more safe against a mass slide failure.

The mobilisation factor contours on plane No.2 are shown in Fig. 5.34 for 3-D analyses with $\beta = 2.25$ and 9. It is seen that the mobilised strength at this plane is higher than that at the central section. There is no clear cut deep sliding wedge at this section as at central section. The critical surface is circular in shape and is confined to the top half height. The factor of safety of the two dam faces are of the same order at this plane. However for a failure encompassing the entire slope the upstream slope exhibits higher factor of safety against sliding than the downstream face.

5.5.4 Principal Stress Ratio (σ_1/σ_3)

The principal stress ratio, a measure of the resistance against shear failure and hydraulic fracturing is plotted along the height at different locations over the central section in Fig. 5.35. It is seen that the magnitudes of principal stress ratio (psr) increase from top towards bottom in shells and are more or less constant for the shell/transition interfaces. The variation in core is non-linear with maximum values near mid height on the upstream

face of core and in the upper third height on core centre line and downstream face.

In a major part of height from top in upstream shell and in the upper one third height in the downstream shell, the principal stress ratio is higher for narrow valleys. In rest of the section the principal stress ratio increases with increasing valley width factor. It is also worth noting that for all valley shapes, at core trench base the principal stress ratios are low, of the order of 1.10. At top of the verticals in core the principal stress ratios are again same for all analyses, 1.55, 1.40 and 1.68 respectively at the upstream face, centre line and downstream face respectively.

Near top of the verticals the psr values decrease from 1.60 to 1.32 in upstream shell and from 1.96 to 1.65 in downstream shell, as the valley width factor increases from 1.12 to 9. Near base of the verticals the psr values increase from 2.05 to 2.45 in upstream shell and from 2.06 to 2.49 in downstream shell for valley width factor increase from 1.12 to 2.25. In transitions the corresponding values vary from 1.8 to 2.24 on upstream side and from 1.87 to 2.35 on the downstream side.

The variation of principal stress ratio σ_1/σ_3 along height over verticals of plane no 2 is also found to be similar to that at central section. Here variation is non-linear in shells and transitions with the maxima at about one third the height above base. The effect of valley shape here is not as pronounced as on central section.

The maximum values of ratio σ_1/σ_3 at different verticals are shown in Tables 5.6 and 5.7. It is observed that ratio

σ_1/σ_3 in downstream shell is higher than that at the corresponding locations on the upstream side. At central section, the downstream transition shows higher values and at plane no. 2 the upstream transition shows higher values than the corresponding locations on the opposite side of core. In core the values on all the three locations are of the same order with the core interior exhibiting slightly higher values than at faces at central section, and the faces showing slightly higher values than the core interior at plane no. 2. As expected the variation of σ_1/σ_3 along height is similar to that for mobilisation factors.

The principal stress ratios are in general more than 2 for shells and transitions and vary from 1.1 to 1.9 in core. The stress ratios σ_1/σ_3 on plane no.2 are more than the corresponding magnitudes at central section.

Table 5.6 : Maximum Values of σ_1/σ_3 along Verticals at Central Section

Vertical No.	σ_1/σ_3 for 3-D analyses			
	$\beta = 1.12$	$\beta = 2.25$	$\beta = 4.5$	$\beta = 9$
1	2.05	2.15	2.34	2.45
2	1.95	2.24	2.44	2.44
3	1.53	1.74	1.82	1.95
4	1.58	1.75	1.81	1.98
5	1.68	1.68	1.76	1.95
6	2.03	2.14	2.21	2.48
7	2.24	2.39	2.45	2.49

Table 5.7: Maximum Values of Ratio σ_1/σ_3 at Plane No. 2

Vertical No.	σ_1/σ_3 for 3-D analyses			
	$\beta = 1.12$	$\beta = 2.25$	$\beta = 4.5$	$\beta = 9$
8	2.38	2.60	2.52	2.36
9	2.45	2.72	2.60	2.46
10	1.64	1.79	1.84	1.87
11	1.57	1.65	1.74	1.80
12	1.69	1.77	1.76	1.87
13	2.41	2.49	2.37	2.39
14	2.58	2.83	2.68	2.51

The contours of principal stress ratio σ_1/σ_3 over central section are shown for two valley shapes with $\beta = 2.25$ and $\beta = 9$ in Fig. 5.36. The contours over longitudinal sections through the upstream face and the centre line of core are shown in Fig. 5.37 for a valley with $\beta = 2.25$. It is seen that the stress ratio contours rise towards the abutment following valley profile indicating higher stress ratios in regions near the abutments than the corresponding values at the central section. The upstream face shows higher stress ratios as compared to the ones along the centre line.

5.5.5 The Horizontal Stress Ratio σ_x/σ_y

The ratios of stress σ_x to σ_y are plotted against height along different verticals at the central section for the four cases of 3-D analyses in Fig. 5.38. It is seen that the distribution is of concave shape in transitions and core with the minima lying at about two third the height above base, except at the upstream face of core where it is at about mid

height above base. In shells the ratio remains almost constant with height. The ratio decreases with increasing valley width factor. It is also seen that the ratio decreases from a valley with $\beta = 1.12$ to $\beta = 2.25$ and, thereafter, the effect of valley width is only marginal. The effect is more in transitions and shells than in core. In about 40 m height near top the ratio σ_x/σ_y is higher for the wider valleys. The maximum values of ratio increase from 0.9 to 1.15 in upstream shell and decrease from 1.0 to 0.96 in downstream shell. The maximum values of ratio in transition decrease from 1.54 to 1.23 and from 1.27 to 1.14 in upstream and downstream portions respectively. The maximum values of ratio in core vary from 1.05 to 1.31 on upstream face and 0.85 to 0.99 on downstream face. For all locations the first value pertains to the narrowest valley and the second value to the widest valley.

In a major portion of core height the ratio σ_x/σ_y varies between 0.65 to 0.50. It is also seen that at the base of dam, the ratio increases from dam faces towards interior upto the transition/core interfaces and then decreases in core. The upstream values are more than the corresponding downstream values for all zones, and the shell values are higher than those in the core. At other elevations, i.e., at 40 m, 80 m, 120 m and 160 m the ratios are highest at faces and reduce gradually upto the core centre line from both sides. At elevation 200 m the variation at constant elevation is same as at base but the ratios σ_x/σ_y in shells are less than those in core.

It is found that on plane no. 2, except above elevation

200 m the variation of ratio σ_x/σ_y along height is a linear increase towards base in core. In shells the variation along height is insignificant and in transitions it is bilinear, the ratios increasing with height in the top portion and then decreasing towards base. In transitions and shells the ratios increase with valley width factor, while in core the ratios are higher for a narrow valley. In shells the σ_x/σ_y ratios are nearly equal to unity and in transitions the ratios vary from a minimum of 0.5 at top to a maximum of 1.5 at the upstream face and from a minimum of 0.64 at top to a maximum of 1.35 on the downstream face. In core the ratios vary from a minimum of 0.6 to a maximum of 1.10. The ratios are lower in shells and transitions and higher in core than the corresponding values at the central section. The effect of valley width is more evident on this plane as compared to that at the central section and the ratios vary with valley width factor gradually.

It is also seen that a narrow valley exhibits conditions more nearer to the triaxial state as compared to a wider valley and also sections towards the abutments are more nearer to the triaxial state as compared to the central section. Therefore, for doing a realistic evaluation of soil characteristics, a plane strain test with varying values of σ_x/σ_y is needed, specially for the core material. For purposes of hydraulic fracturing, the least principal stress would be σ_x , and vertical planes normal to it i.e., parallel to dam axis are most prone to hydraulic fracturing. Greater safety is available on the more critical vertical planes normal to σ_y , i.e., in the upstream-downstream direction.

5.5.6 Contact Pressure at Abutment

It is found that the normal contact pressures are more in the interior of the core than on faces. Moreover, the contact pressures on the upstream face are more than those on the downstream face. On both upstream and downstream core faces the contact pressures increase with valley width factor in the lower one-fourth height. In the upper three fourth height the contact pressures decrease with valley width factor upto a valley with $\beta = 4.5$ and then again start increasing. In the interior of the core, however, the contact pressures generally increase with valley width factor.

Table 5.8: Normal Contact Pressure in Core at Abutment

Location	Contact pressure for valley width factor (t/m^2)							
	$\beta=1.12$		$\beta=2.25$		$\beta=4.5$		$\beta=9$	
	(i)	(ii)	(i)	(ii)	(i)	(ii)	(i)	(ii)
U/S face	202	139	289	108	352	92	355	99
Interior	265	106	324	143	344	135	345	144
D/s Face	196	139	253	115	294	106	294	107

Note : The columns (i) and (ii) refer to the values near ground level and mid height respectively.

The typical values of contact pressure near ground level and at about mid height are given in Table 5.8. It is seen that there is no appreciable change in the contact pressure when the valley widens beyond a valley width factor $\beta = 4.5$. The contact pressures are throughout compressive, contrary to some of the earlier results, using 2-D analysis and neglecting sequential construction, which indicated tensile contact

stresses near the top. Higher contact stresses for narrower valleys at mid-height are also contrary to earlier results. However, it may be noted that near the base the contact pressures would be less than the hydrostatic pressure (≈ 260 t/m²) for $\beta = 1.12$, while they are marginally equal at mid height (hydrostatic pressure ≈ 130 t/m²) for $\beta = 1.12$, and lower for larger valley width factors. Thus the dam section would not be safe against hydraulic fracturing in these cases, and it would be necessary to increase the contact pressures. This can be done by using softer core material towards the abutments.

5.6 CONCLUSIONS

The following conclusions can be drawn from the study described in this chapter :

(A) Displacements

1. Variation of horizontal movement u is non-linear along the height, the maximum values occurring at about one third the height above ground level in the interior of the dam and at about mid height in shells.
2. Shells exhibit higher horizontal movements than the core and transition and the upstream portion moves more than the corresponding downstream locations.
3. The horizontal movement of the dam is away from the axis i.e., the dam expands laterally.
4. The horizontal movement values increase with valley width factor, approaching plane strain values for wide valleys with $\beta \geq 9$. The 3-D movement values on the central section are about 25-40 %, 40-60 %, 55-80 % and 75-100 % of the plane strain values for valleys with valley width factors $\beta = 1.12, 2.25, 4.5$ and 9 respectively.

5. The horizontal movement values decrease sharply towards the abutments, the magnitudes at plane no. 2 being about 30 % of those on central section.
6. The variation of settlement - w along height is of a convex shape with maximum settlement occurring at about two-third the height above base.
7. At a given elevation the settlements increase from the dam's faces towards the interior, with the core centre exhibiting maximum settlements.
8. The settlements increase with valley width factor β . Over central section the settlement values for $\beta = 9$ almost match with the plane strain values. The settlement values for 3-D analyses with $\beta = 1.12, 2.25, 4.5$ and 9 are about 35-45 %, 50- 60 % and 90 - 98 % of the corresponding plane strain values.
9. The effect of valley width at plane no. 2 is significant only in narrow valleys. The settlement increases for valleys with $\beta = 1.12$ to $\beta = 2.25$. There is no significant increase of settlements by further widening the valley.
10. For a partially built dam the variation of displacements along height is similar to the one for full height of dam.
11. The longitudinal movements of the dam are towards the central section, with core movements being larger than those in pervious zones. The movements increase with valley width factor upto $\beta = 4.5$, beyond which the movements start decreasing. The reduction is more for sections nearer the abutments.

(B) Stresses

1. The distribution of normal stresses along the height is either slightly convex or near linear in pervious zones and of concave shape in the core.
2. In the top one-third to two-third height, the stress magnitudes from different 3-D analyses are practically of the same order. In the lower regions, the stress values increase with valley width factor, with valleys having β greater than or equal to 4.5 having the same stress values as those from a plane strain analysis. The stresses obtained from 3-D analyses with $\beta = 1.12, 2.25$ and 4.5 or more are about 50-60 %, 70-80 % and 90-100 % of the corresponding plane strain values.
3. At a constant elevation the stresses increase from dam faces towards the interior with adjustments in the core.
4. The stress magnitudes as well as the effect of valley width factor increase towards the abutments.
5. The σ_x/σ_y ratio is maximum in transition and least in core. A narrow valley exhibits conditions more nearer to the triaxial state as compared to a wider valley and also sections towards the abutments are more nearer to the triaxial state as compared to the central section.
6. The principal stress ratio is generally more than 2 in pervious zones and vary from 1.1 to 1.9 in core. Sections towards the abutments show higher principal stress ratios as compared to those at central section. The principal stress ratios increase with valley width factor at central section. On plane no. 2 the principal stress ratios increase with valley width factor upto $\beta = 2.25$,

whereafter, the ratios decrease with increasing valley width factor.

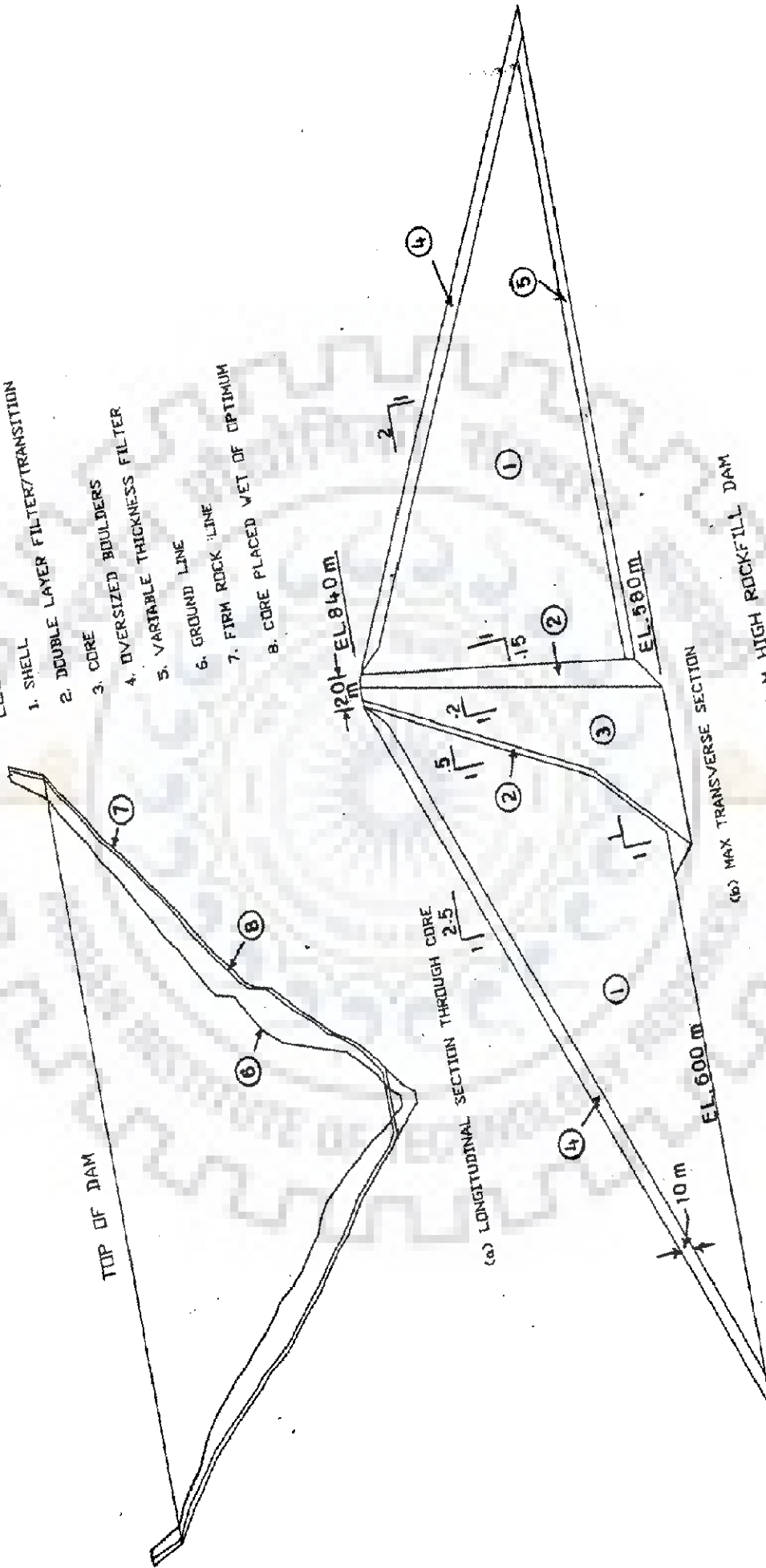
7. The mobilisation factors increase with valley width factor all over the dam. The effect of valley width on the magnitudes of mobilisation factor on central section is least in shells and upstream transition and maximum in core and downstream transition. The magnitudes of mobilisation factor on plane no. 2 are higher but the effect of valley shape is not as sharp as at central section. At central section the mobilisation factors for valleys with valley width factors equal to 1.12, 2.25 and 4.5 are approximately 70, 80 and 95 % in shells; 60, 65 and 85 % in transitions and 55, 75 and 85 % in core of the corresponding values for a wide valley with $\beta = 9$. At plane no. 2 the corresponding figures in core are 85, 80 and 65 % respectively.
8. The potential failure planes are wedge shaped on central section and circular at plane No. 2.
9. Local zones of high mobilised strength are observed on the dam faces. These zones are larger in size and magnitude for narrower valleys than for wider valleys.
10. The potential sliding wedge encompasses the entire shell zones on central section. On plane No.2, however, the circular failure plane involves slide only in the upper half, and the factor of safety is same for both faces. However a larger sliding mass involving the entire face has a higher factor of safety against sliding for the upstream face.

11. The normal contact pressure at lower levels at the core contact increases with valley width. For valleys with $\beta > 4.5$, there is no further effect of valley shape on the contact pressure. At higher elevations the contact pressure decreases with valley width factor. A narrow valley is thus comparatively more safe against hydraulic fracturing in comparison to a wide valley. However, for the assumed material properties, there is risk of hydraulic fracturing near ground level for $\beta=1.12$, and at mid height for $\beta=2.25$ or more.



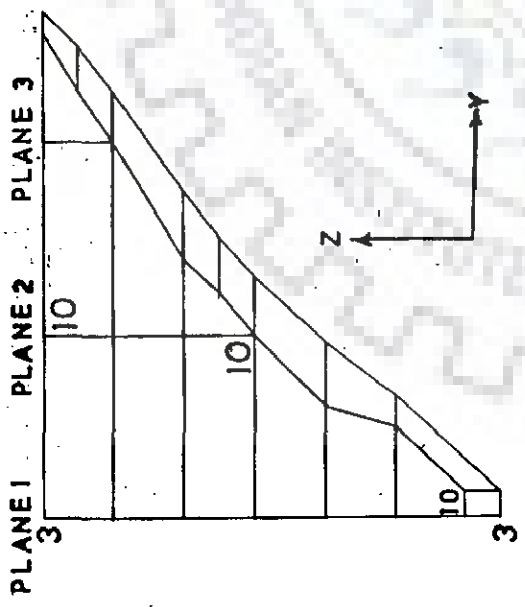
LEGEND

- 1. SHELL
- 2. DOUBLE LAYER FILTER/TRANSITION
- 3. CORE
- 4. OVERSIZED BOULDERS
- 5. VARIABLE THICKNESS FILTER
- 6. GROUND LINE
- 7. FIRM ROCK LINE
- 8. CORE PLACED WET OF OPTIMUM

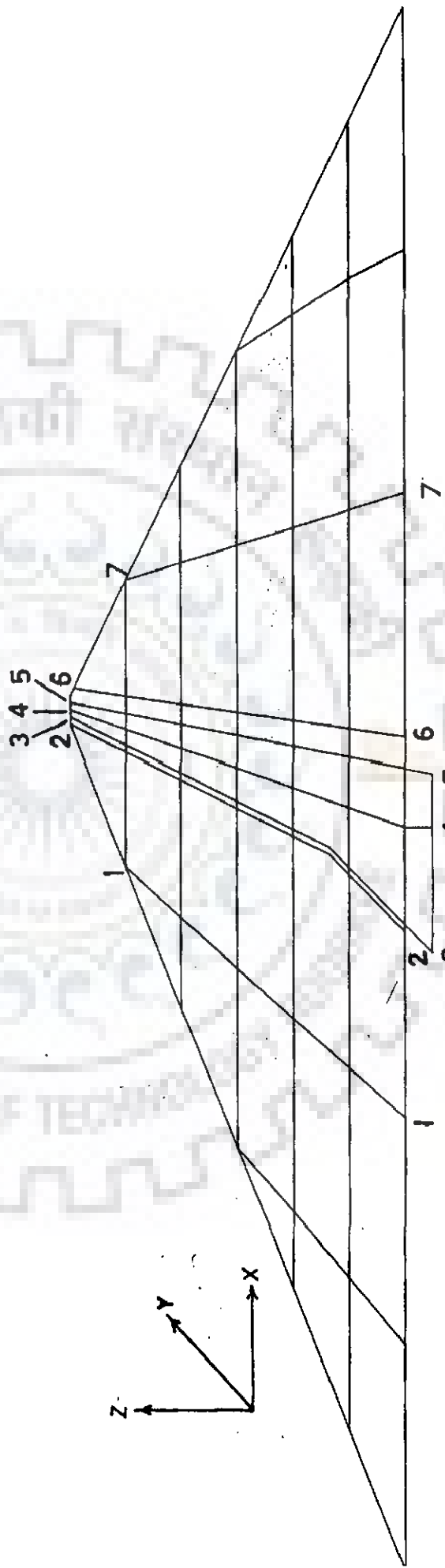


(b) MAX TRANSVERSE SECTION

FIG 5.1 SECTION OF 260 M HIGH ROCKFILL DAM



(a) LONGITUDINAL SECTION ALONG UPSTREAM FACE OF CORE

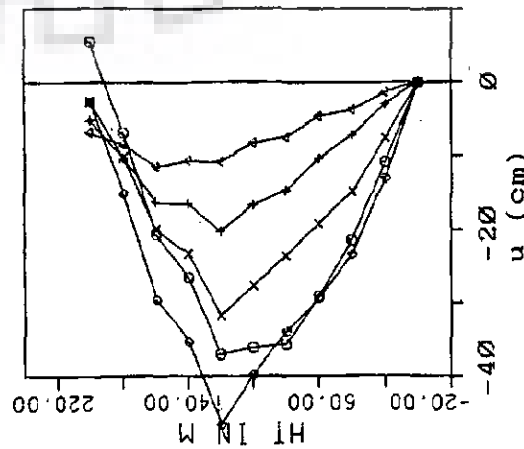
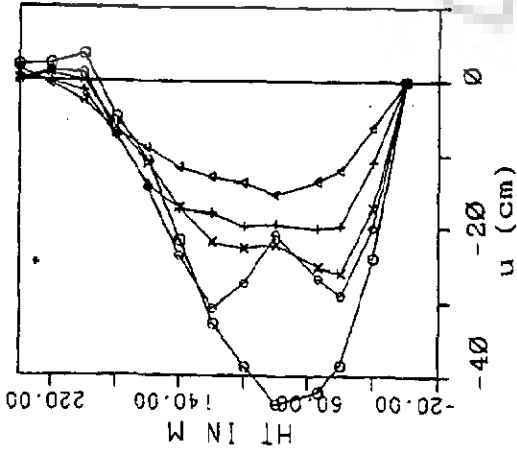
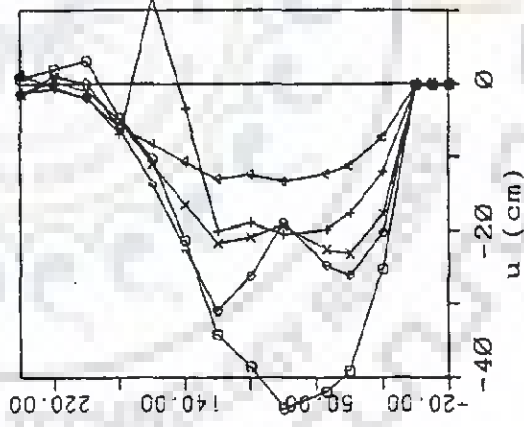
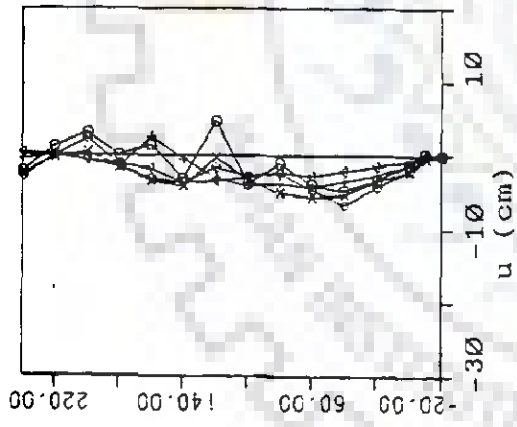
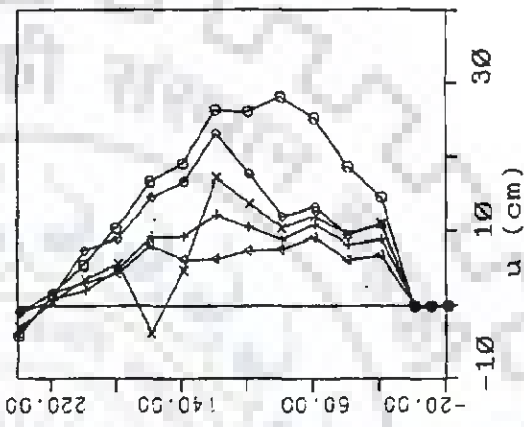
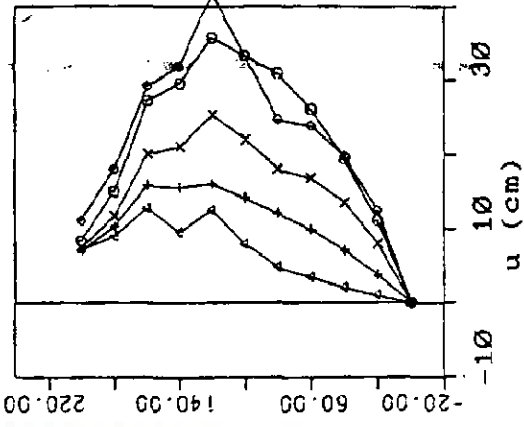
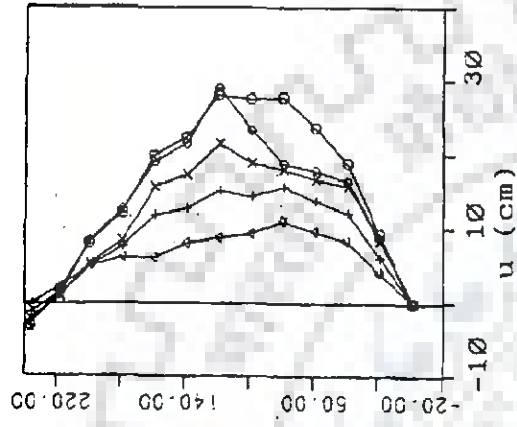


(b) MAXIMUM TRANSVERSE SECTION OF DAM

Fig 5.2: FINITE ELEMENT IDEALISATION OF THE DAM

LEGEND

- 2-D
- ◐ β = 1.125
- ◑ β = 2.25
- × β = 4.50
- ◒ β = 9.00



VERTICAL NO. 1
VERTICAL NO. 2
VERTICAL NO. 3
VERTICAL NO. 4
VERTICAL NO. 5
VERTICAL NO. 6
VERTICAL NO. 7

FIG. 5.3 HORIZONTAL MOVEMENTS u ALONG HEIGHT AT DIFFERENT LOCATIONS OVER CENTRAL SECTION

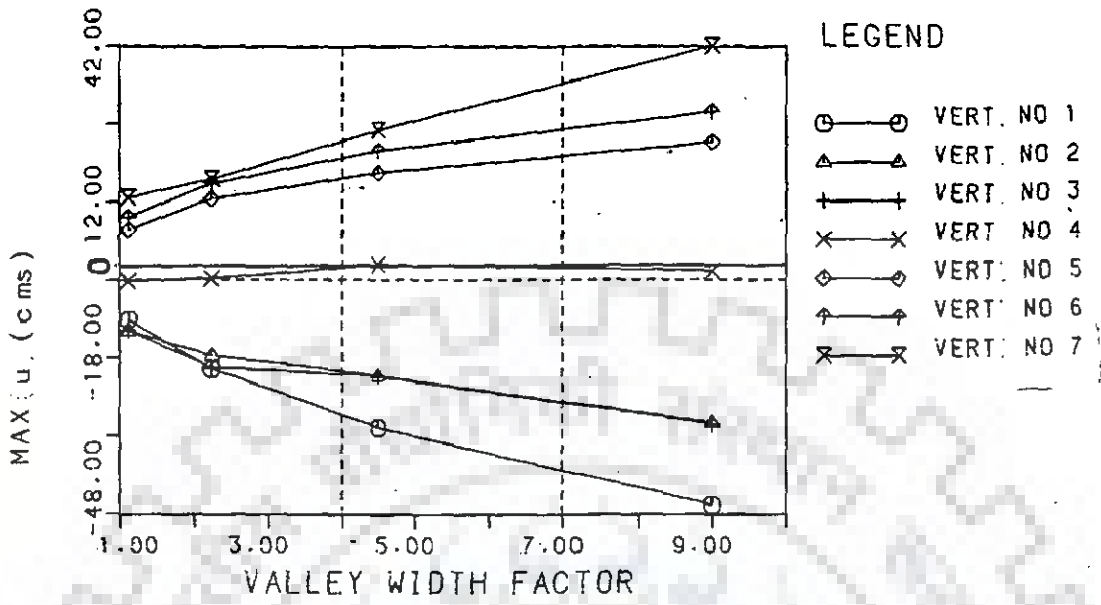


FIG 5.4(a) MAXIMUM HORIZONTAL DISPLACEMENTS AT CENTRAL SECTION

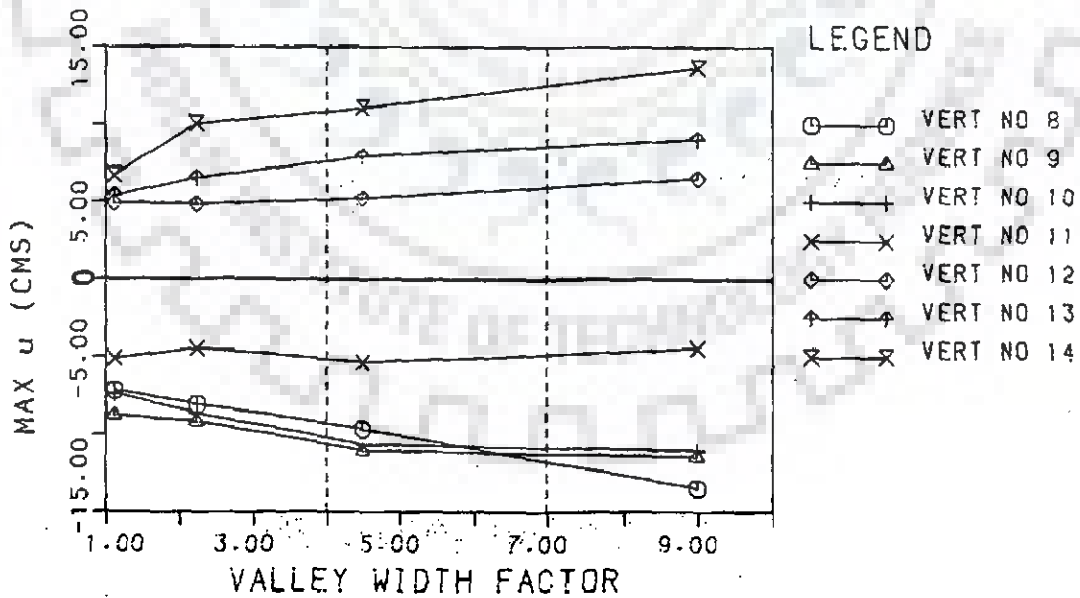


FIG 5.4(b) MAXIMUM HORIZONTAL DISPLACEMENTS OVER PLANE NO.2

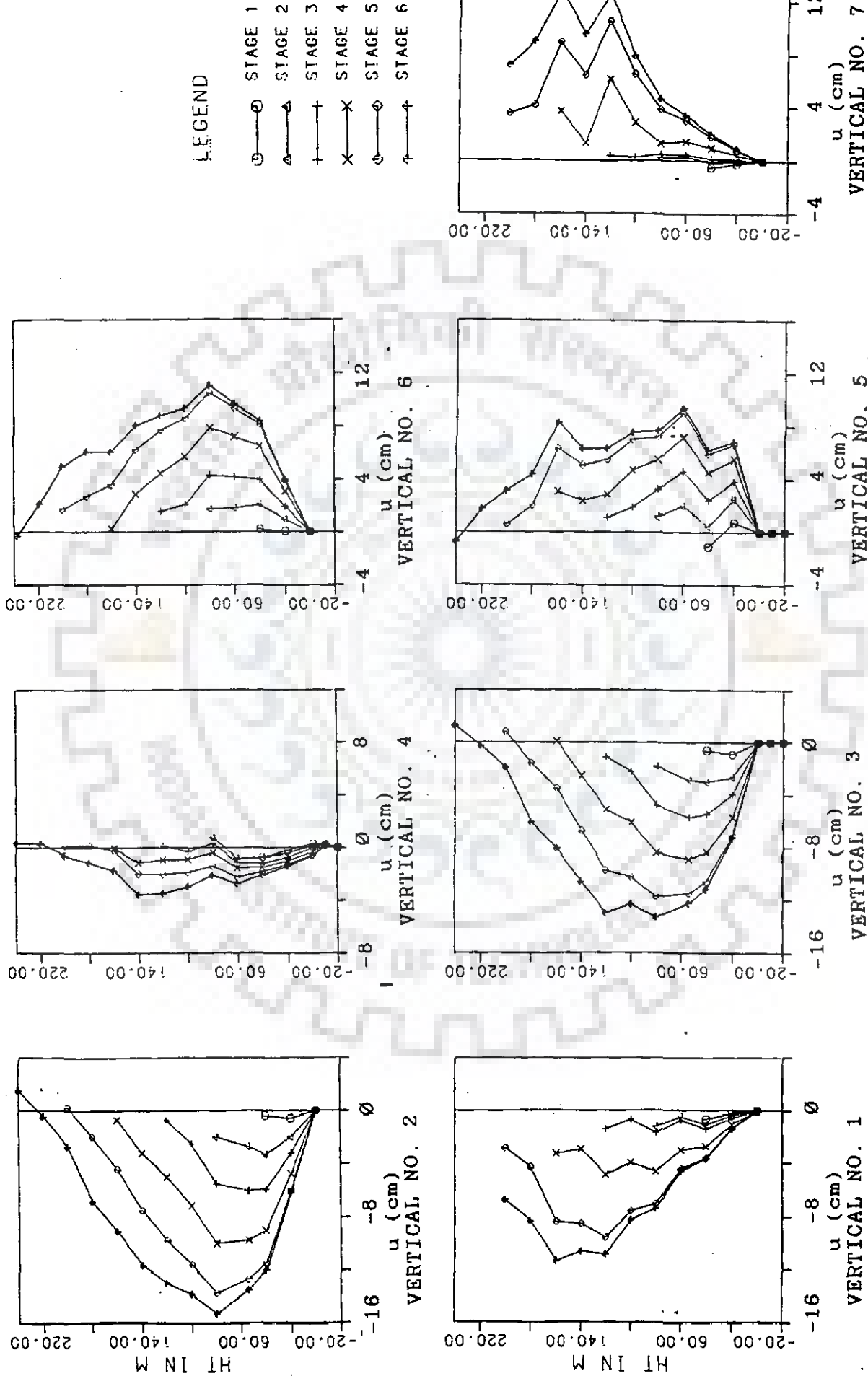
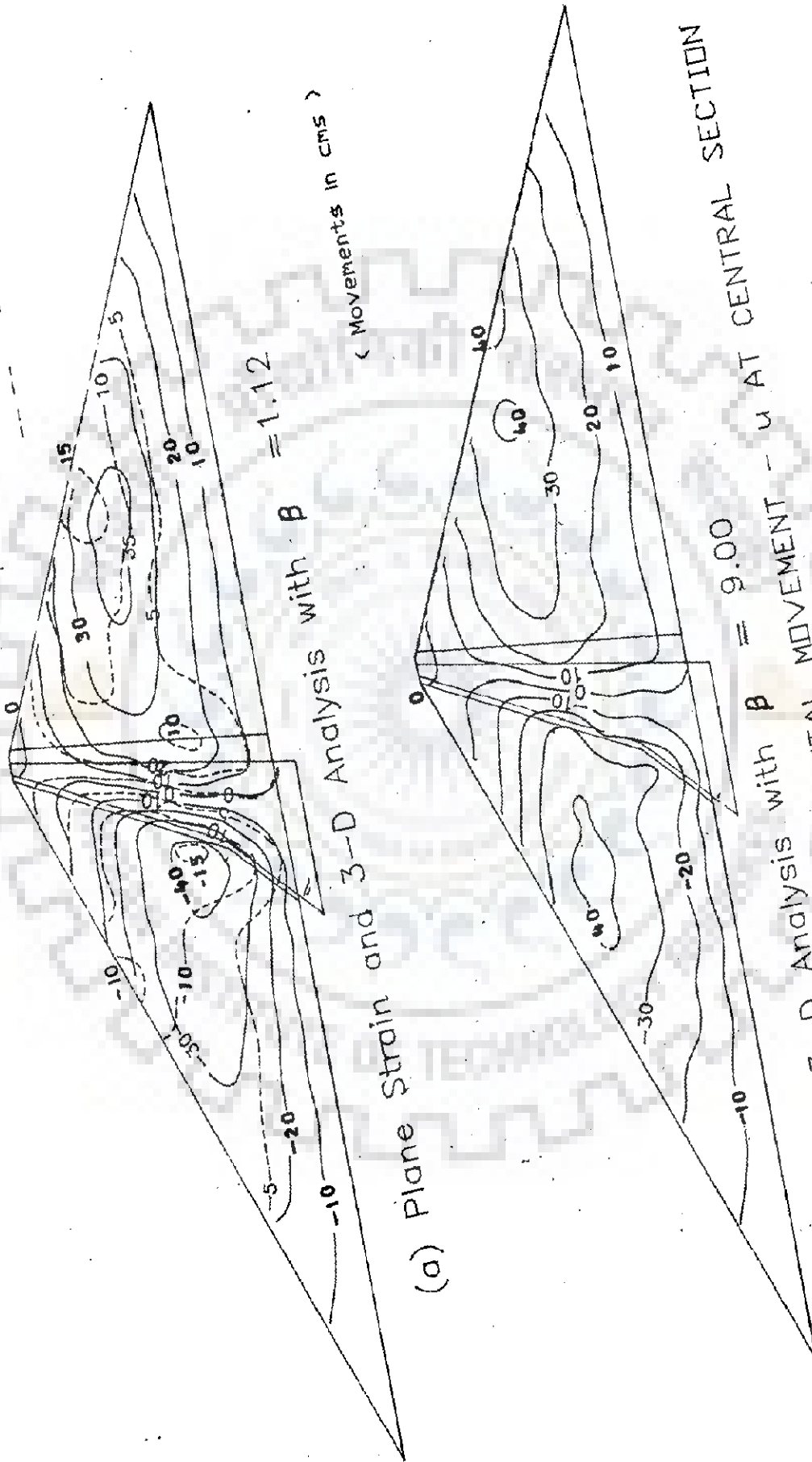


FIG. 5.5 : SEQUENTIAL VARIATION OF HORIZONTAL DISPLACEMENT -u FOR 3-D ANALYSIS AT CENTRAL SECTION ($\beta = 1.12$)

Plane Strain

3 - D



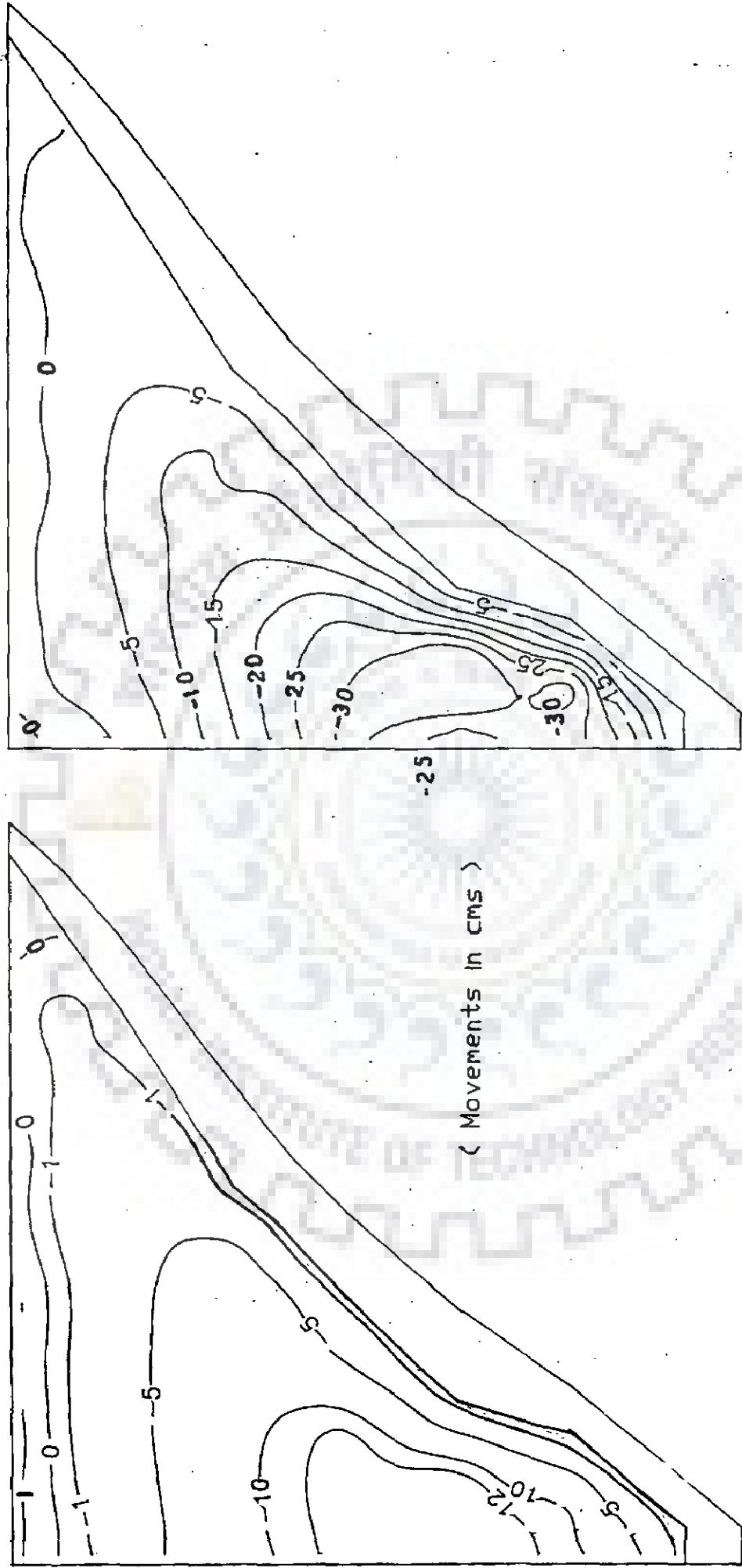
(a) Plane Strain and 3-D Analysis with $\beta = 1.12$

(b) 3-D Analysis with $\beta = 9.00$

u AT CENTRAL SECTION

CONTOURS OF HORIZONTAL MOVEMENT

FIG 5.6



(a) Valley Width Factor $\beta = 1.12$

(b) Valley Width Factor $\beta = 9$

FIG 5.7 : CONTOURS OF HORIZONTAL MOVEMENT - u AT LONGITUDINAL SECTION ALONG UPSTREAM FACE OF CORE

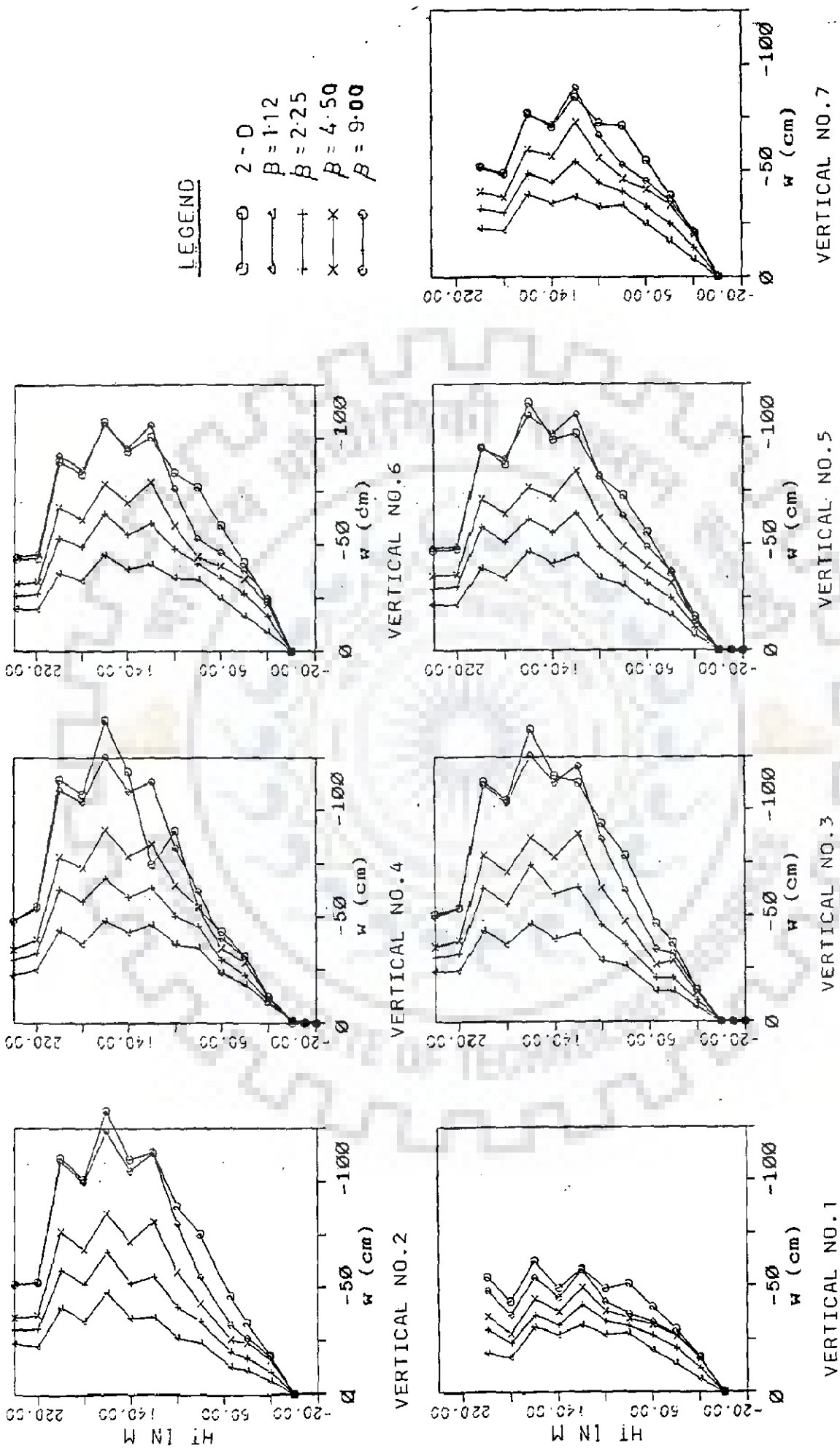


FIG. 5.8 : VERTICAL MOVEMENTS w ALONG HEIGHT AT DIFFERENT LOCATIONS OVER CENTRAL SECTION

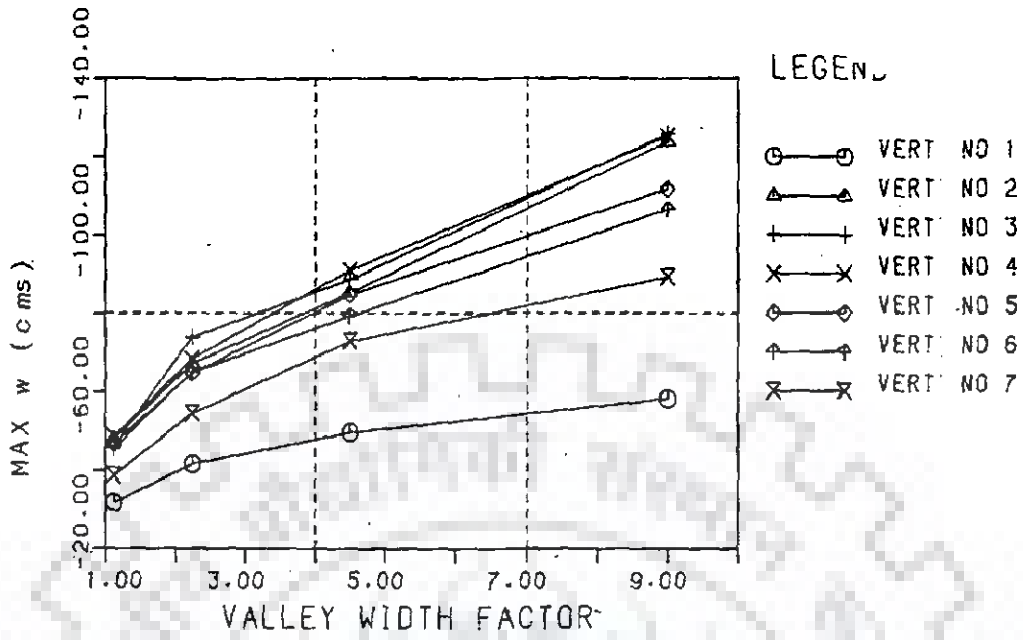


FIG 5.9(a) MAXIMUM VERTICAL DISPLACEMENTS AT CENTRAL SECTION

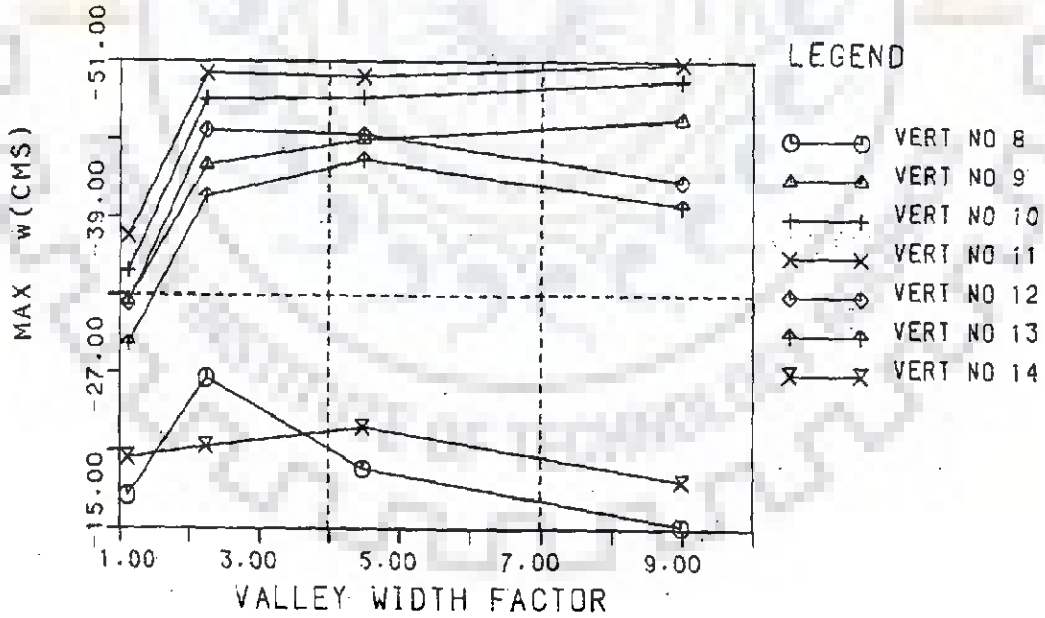


FIG 5.9(b) MAXIMUM VERTICAL DISPLACEMENTS OVER PLANE NO.2

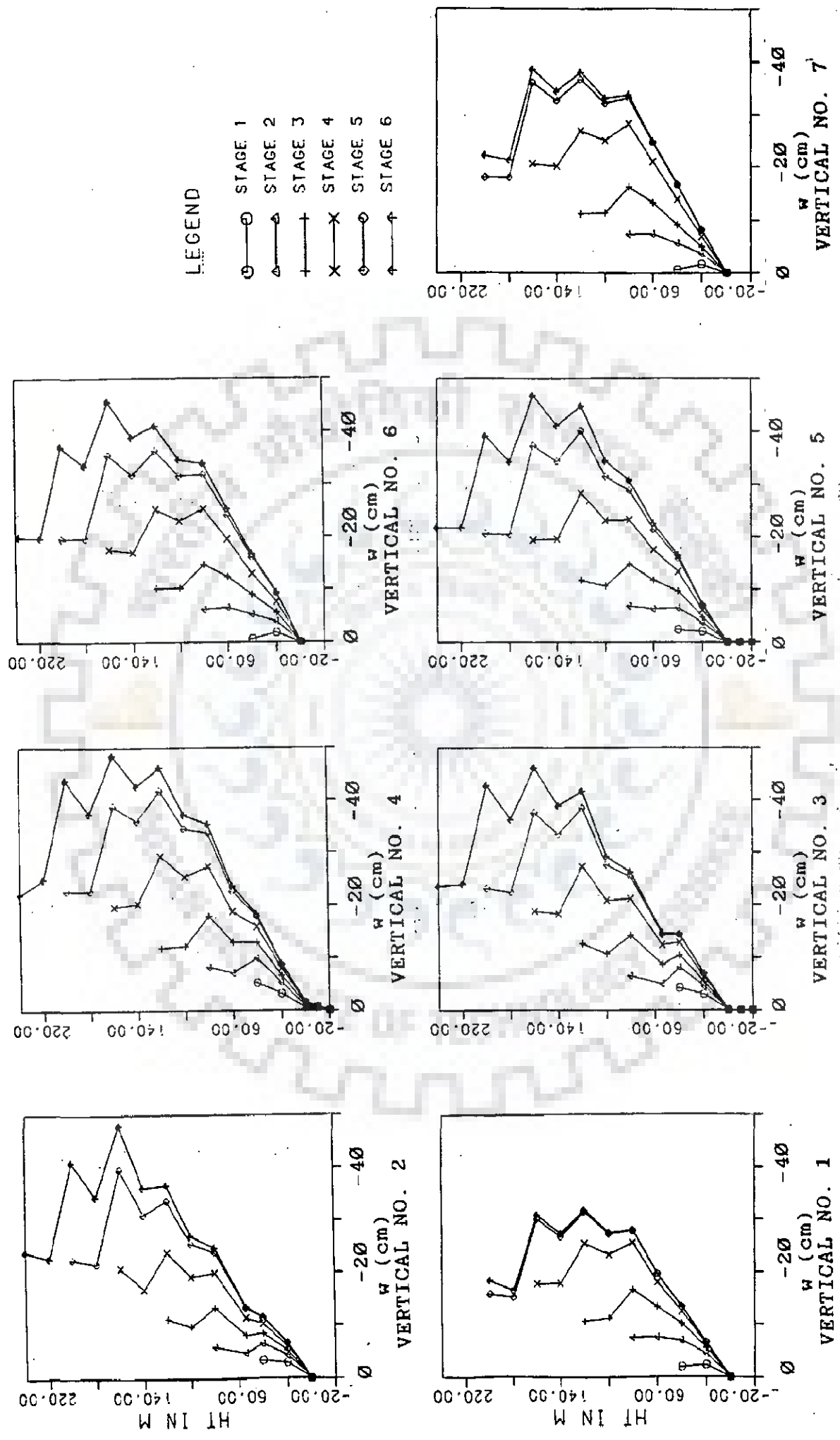


FIG.5.10: SEQUENTIAL VARIATION OF VERTICAL DISPLACEMENT - w FOR 3-D ANALYSIS AT CENTRAL SECTION ($\beta = 1.12$)

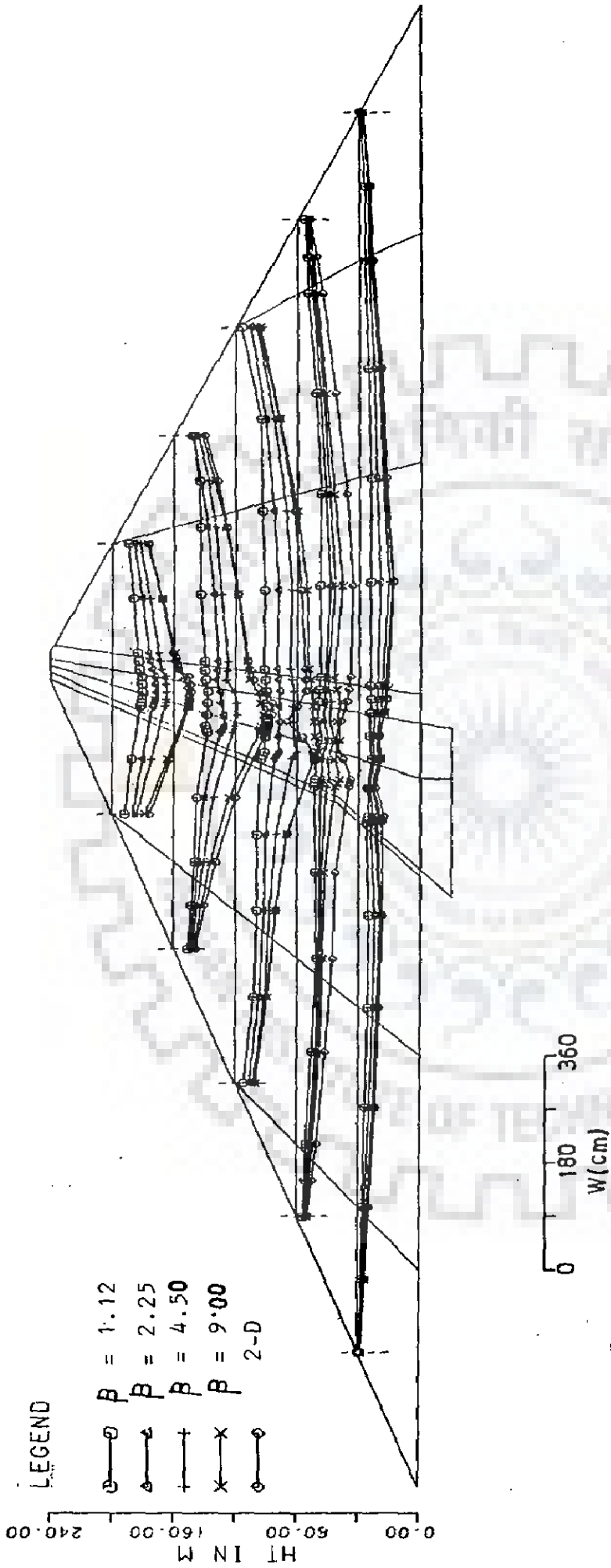
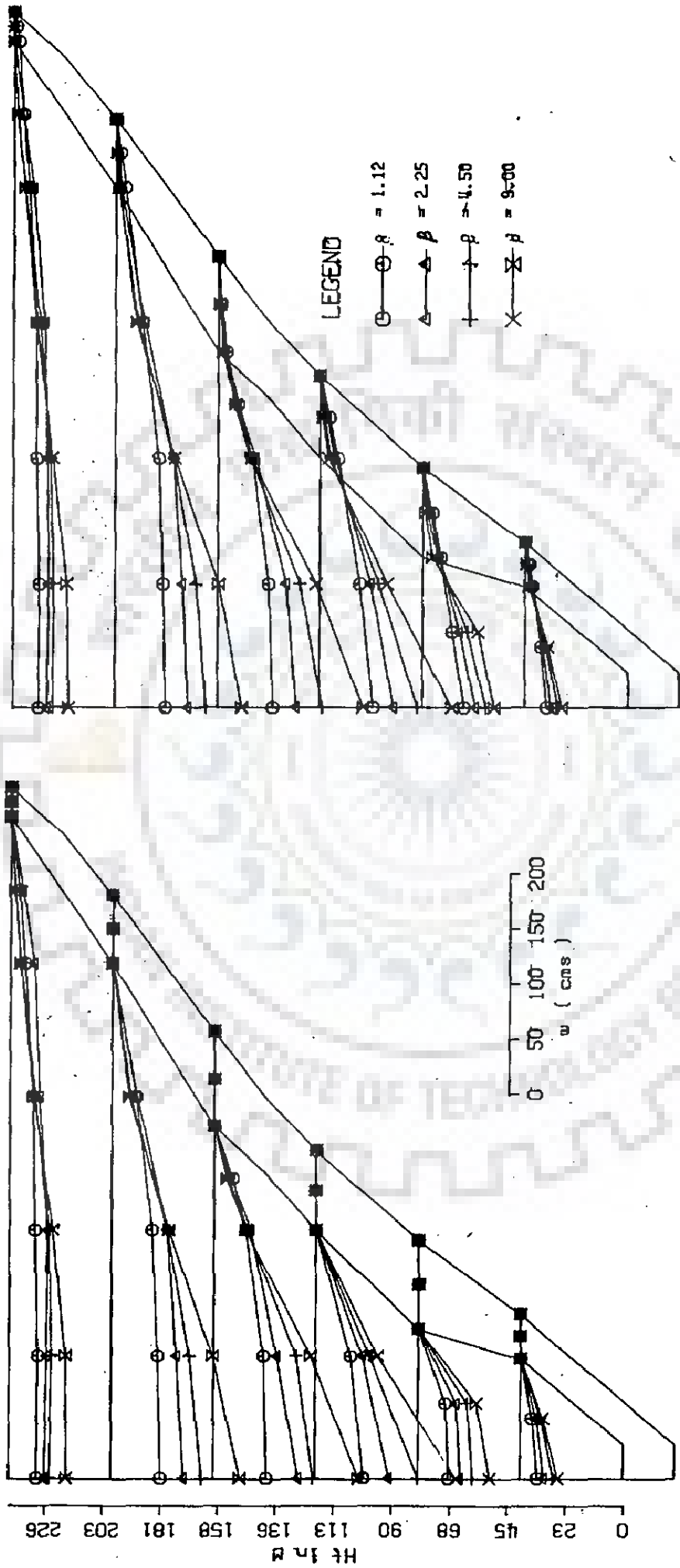


FIG 5.11. VERTICAL MOVEMENTS w AT CONSTANT ELEVATIONS OVER CENTRAL SECTION

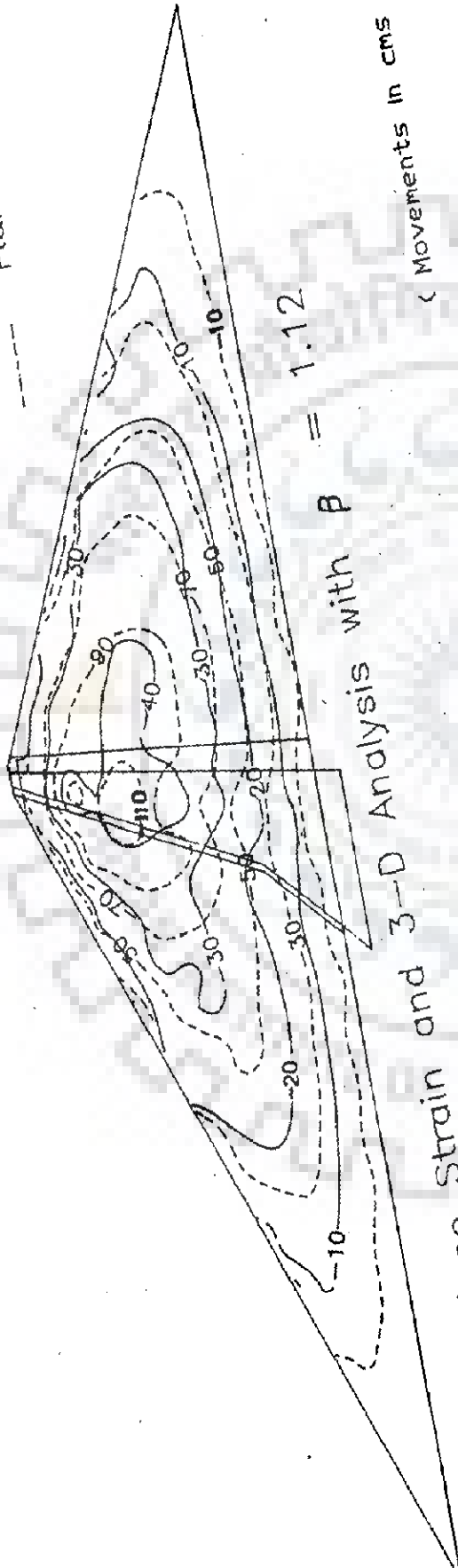


(a) Along Upstream Face of Core

(b) Along Centre Line of Core

Fig 5.12 : VERTICAL MOVEMENT- w AT CONSTANT ELEVATIONS OVER LONGITUDINAL SECTION

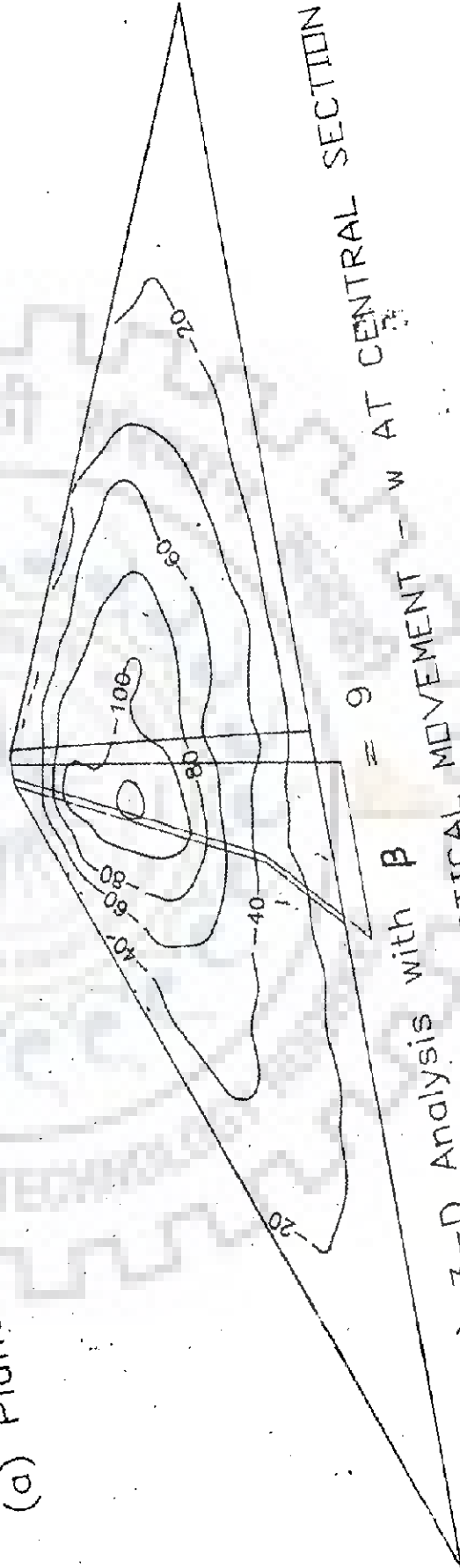
3 - D
Plane Strain



(Movements in cms)

$\beta = 1.12$

(a) Plane strain and 3-D Analysis with $\beta = 1.12$



$\beta = 9$

(b) 3-D Analysis with $\beta = 9$ AT CENTRAL SECTION

FIG 5.13: CONTOURS OF VERTICAL MOVEMENT

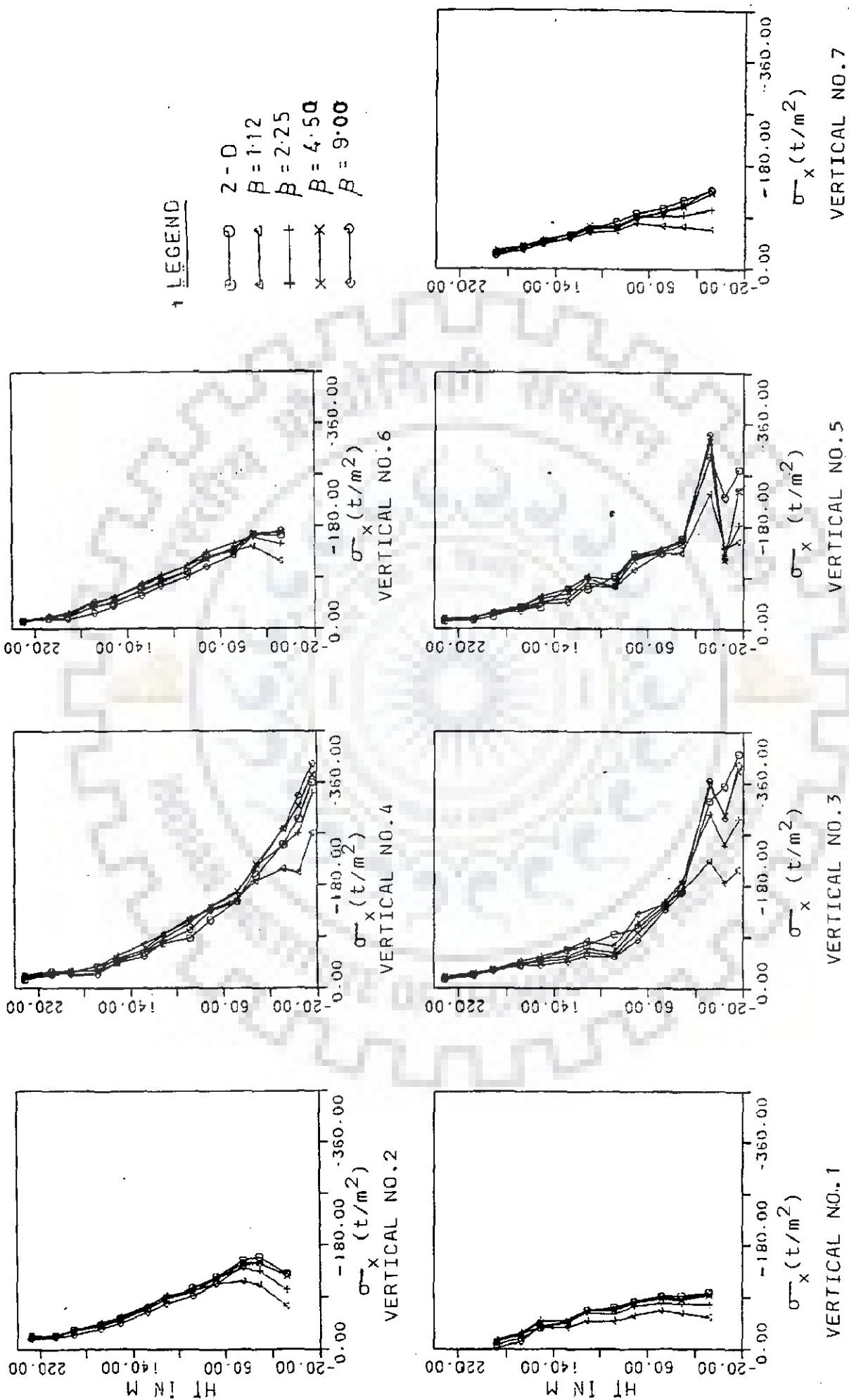


FIG. 5.14 HORIZONTAL NORMAL STRESS σ_x ALONG HEIGHT AT DIFFERENT LOCATIONS OVER CENTRAL SECTION

- LEGEND
- — $\beta = 1.12$
 - △ — $\beta = 2.25$
 - † — $\beta = 4.00$
 - × — $\beta = 9.00$

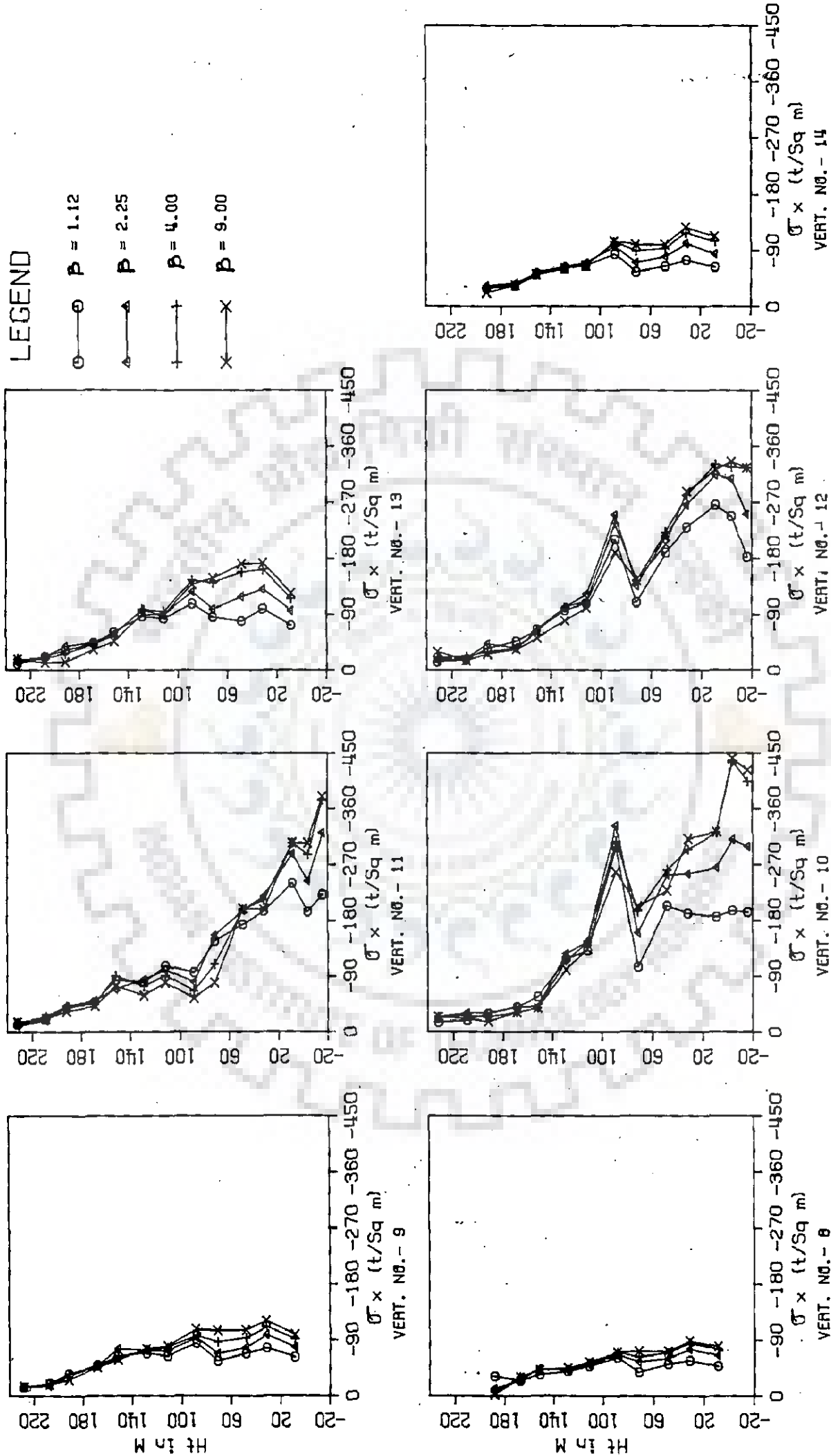


FIG 5.15 : HORIZONTAL NORMAL STRESS σ_x ALONG VERTICALS OVER PLANE NO. 2

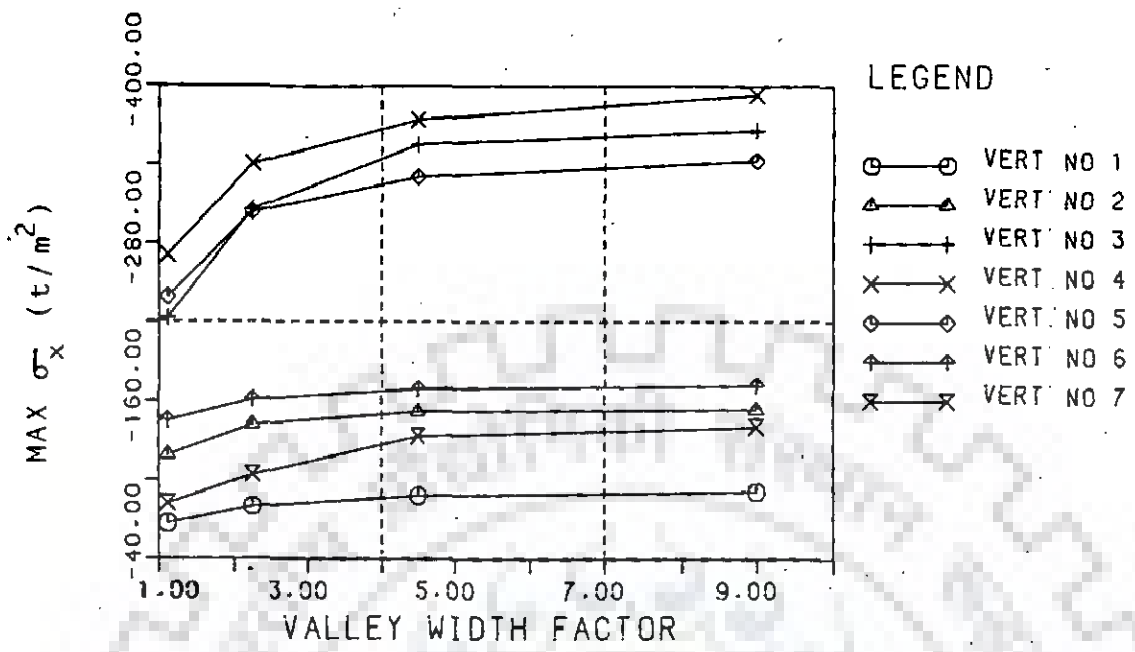


FIG 5.16(a) MAXIMUM σ_x STRESS AT CENTRAL SECTION

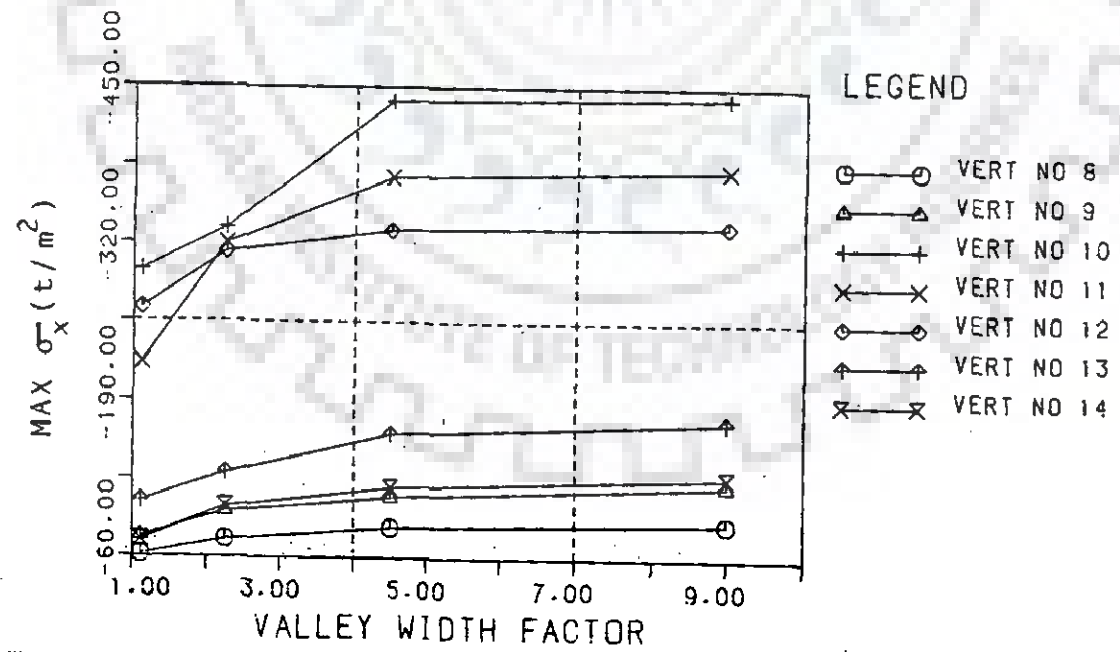
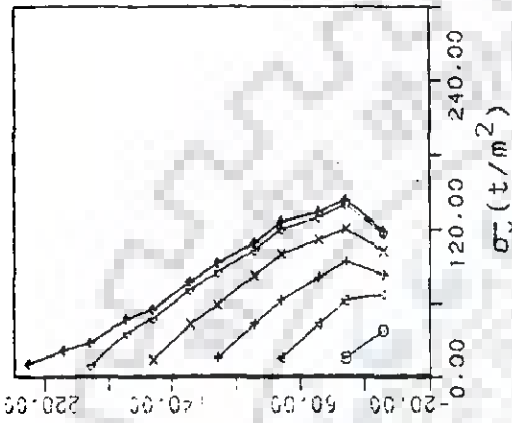


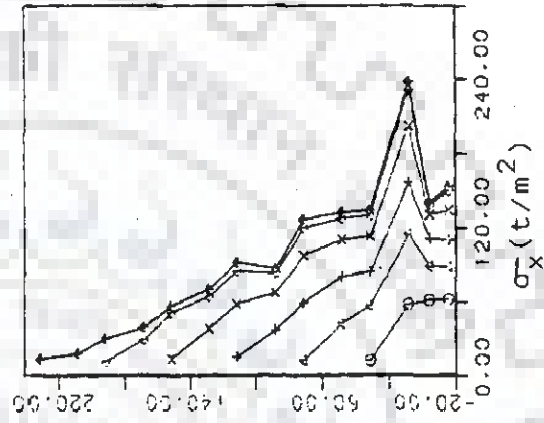
FIG 5.16(b) MAXIMUM σ_x STRESS OVER PLANE NO.2

LEGEND

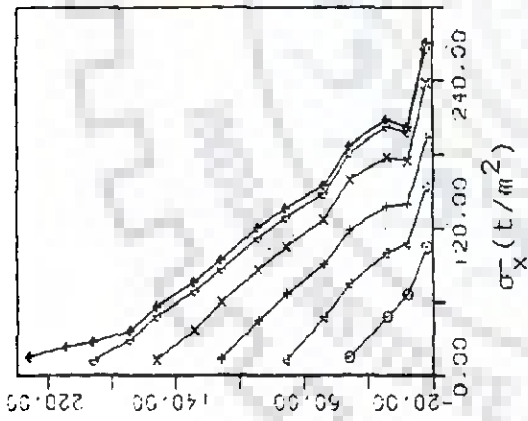
- STAGE 1
- △ STAGE 2
- + STAGE 3
- × STAGE 4
- ◇ STAGE 5
- STAGE 6



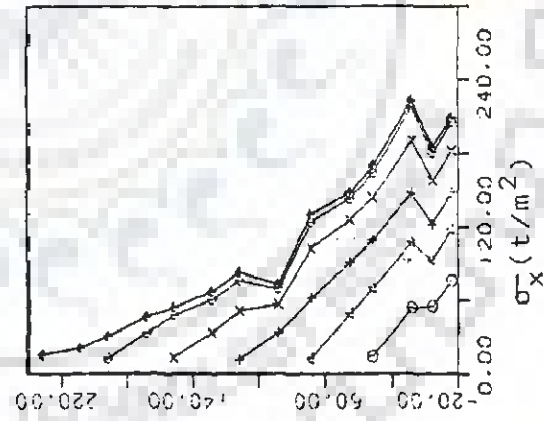
VERTICAL NO - 6



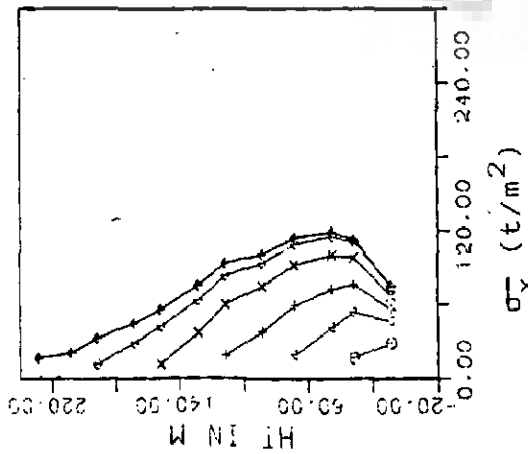
VERTICAL NO - 5



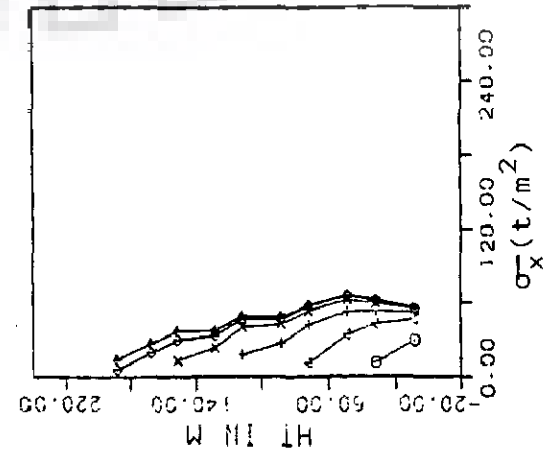
VERTICAL NO - 4



VERTICAL NO - 3



VERTICAL NO - 2



VERTICAL NO - 1

FIG. 5.17: SEQUENTIAL VARIATION OF σ_x FOR 3-D ANALYSIS: $\beta = 1.12$.

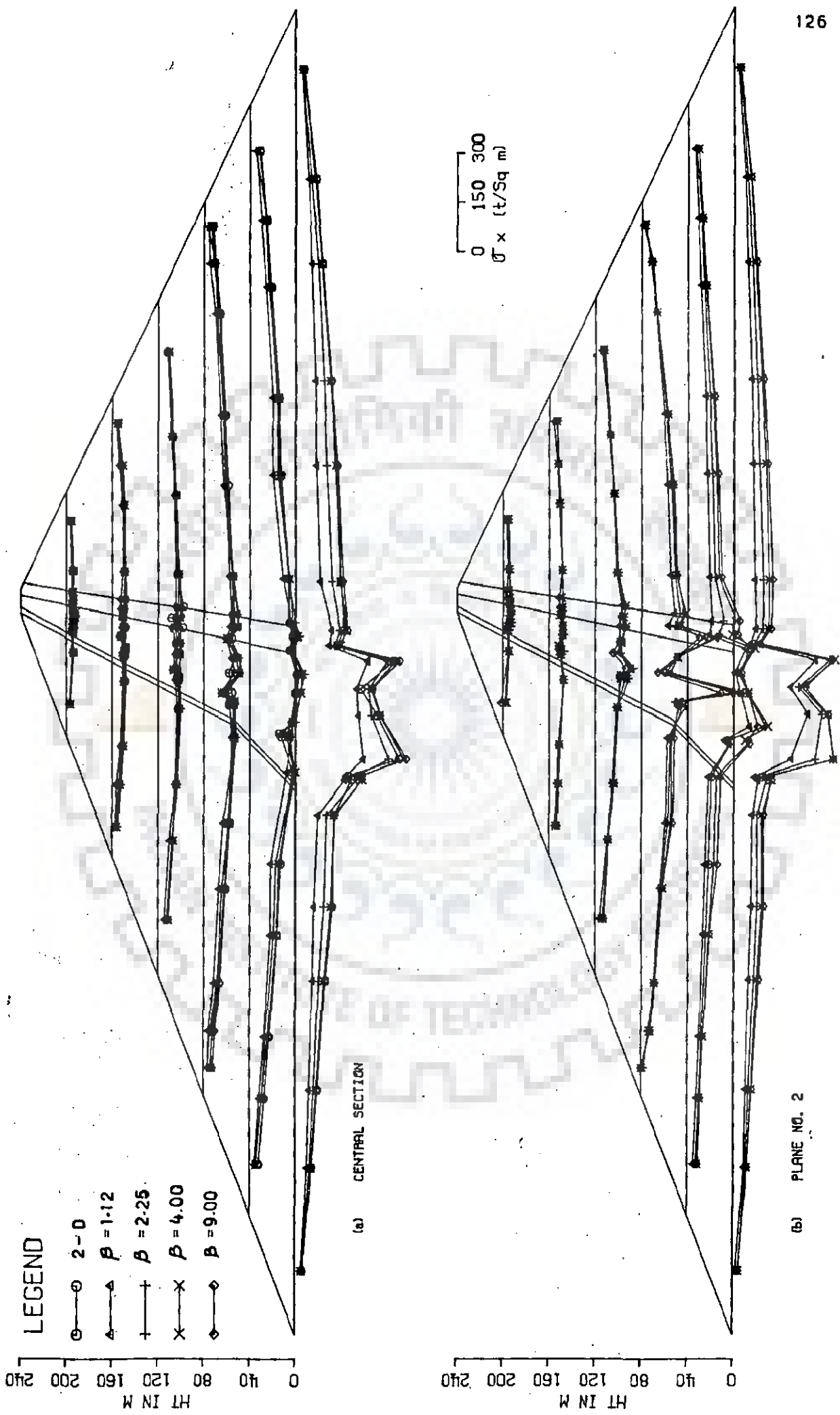


FIG 5.18 : HORIZONTAL NORMAL STRESS σ_x AT CONSTANT ELEVATIONS

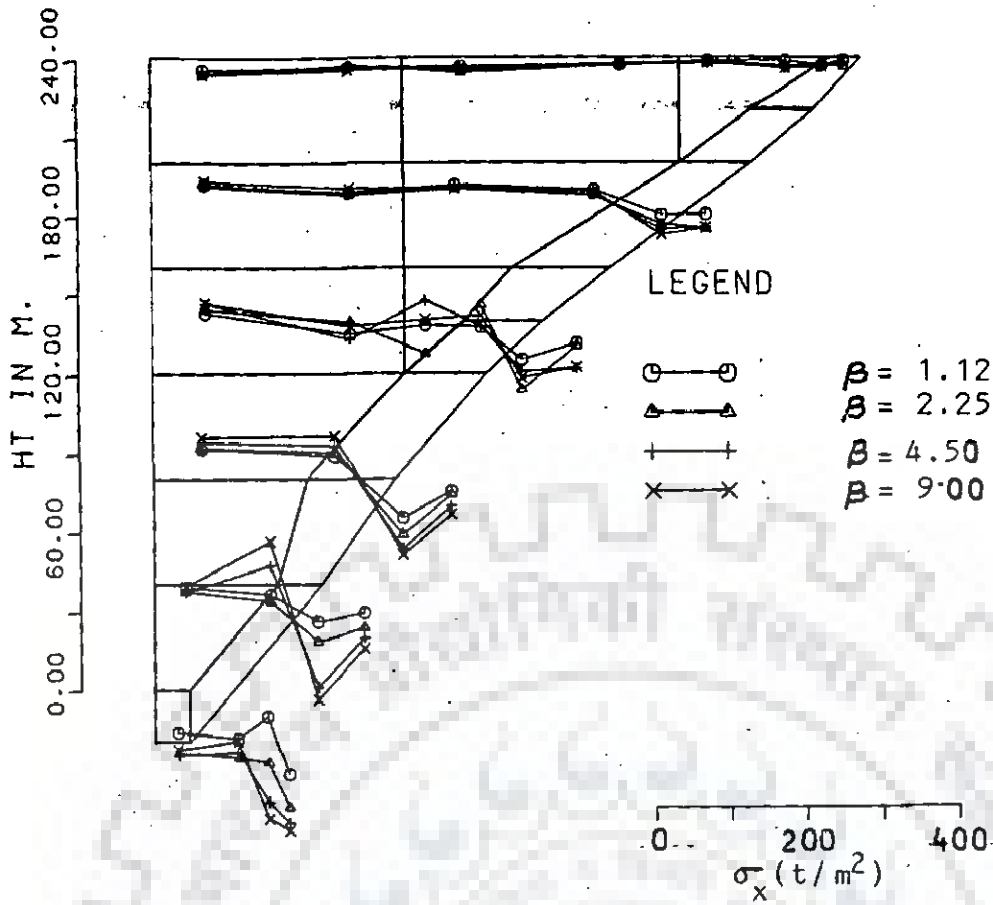


FIG 5.19(a) STRESS σ_x ALONG CENTRE LINE OF CORE

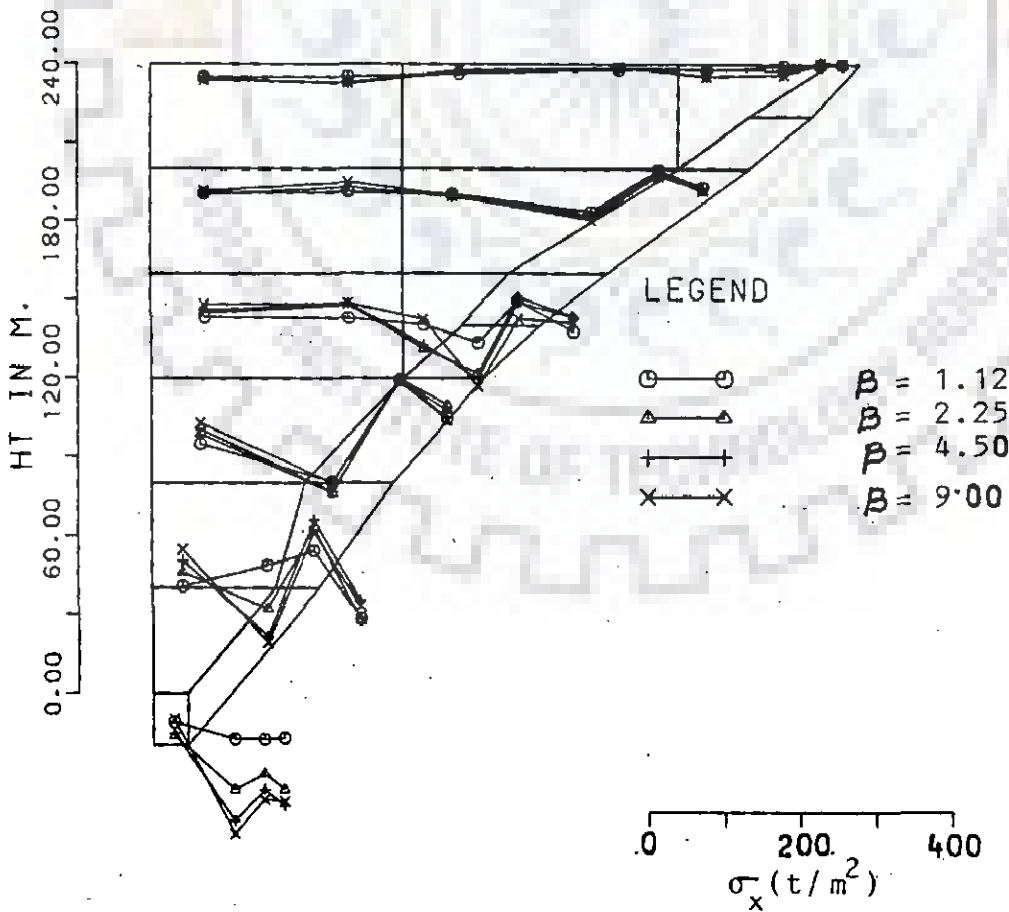
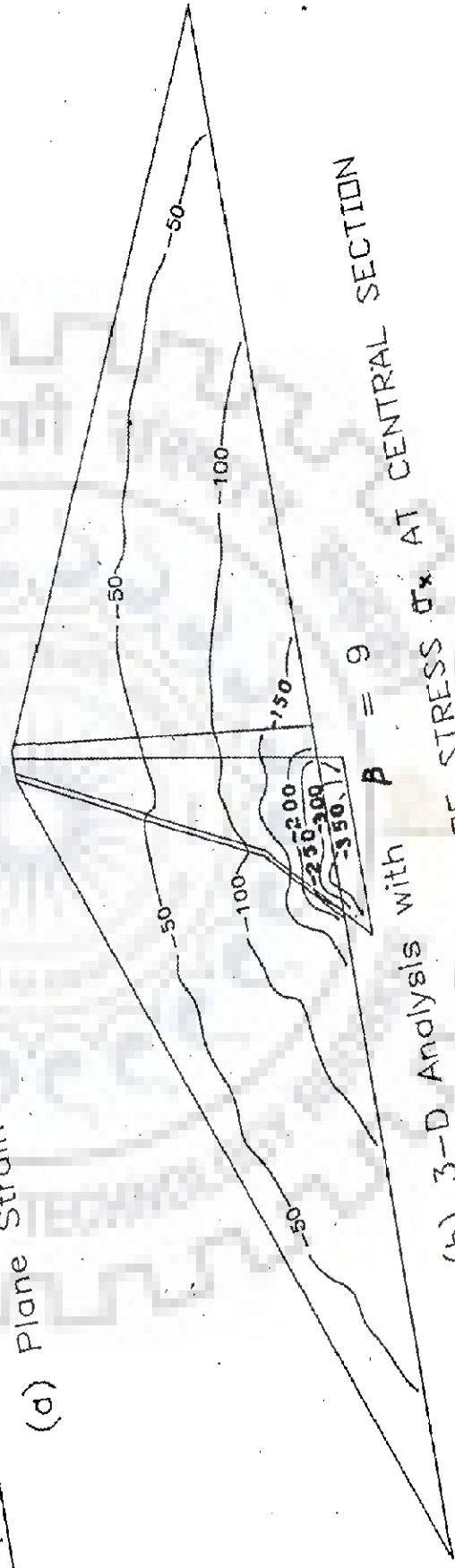
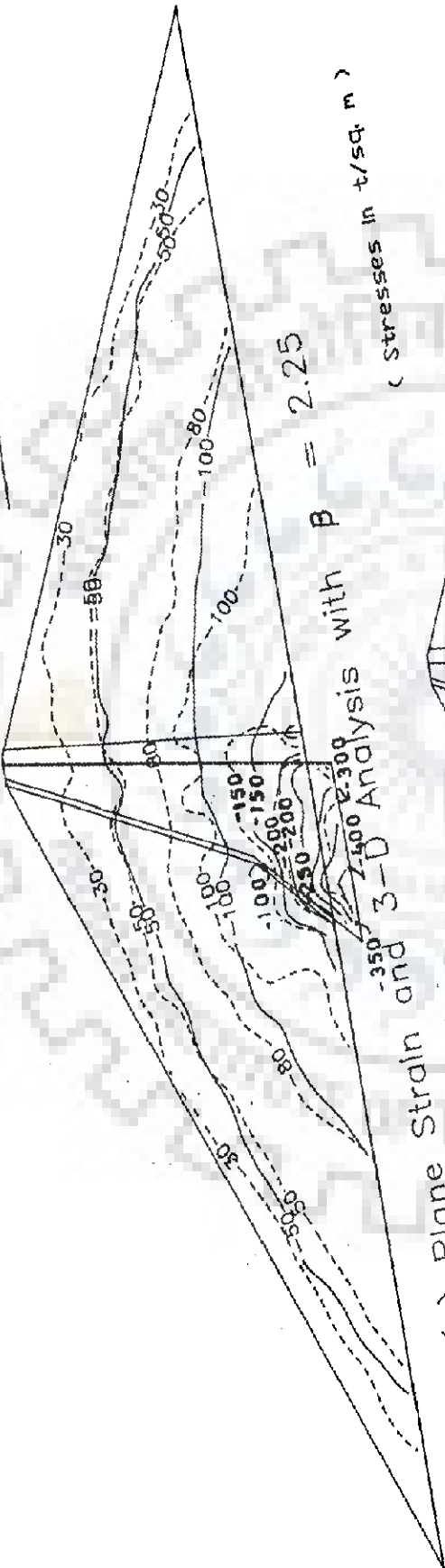


FIG 5.19(b) STRESS σ_x ON UPSTREAM FACE OF CORE

3 - D
Plane Strain



(b) 3-D Analysis with $\beta = 9$
FIG 5.20 : CONTOURS OF STRESS σ_x AT CENTRAL SECTION

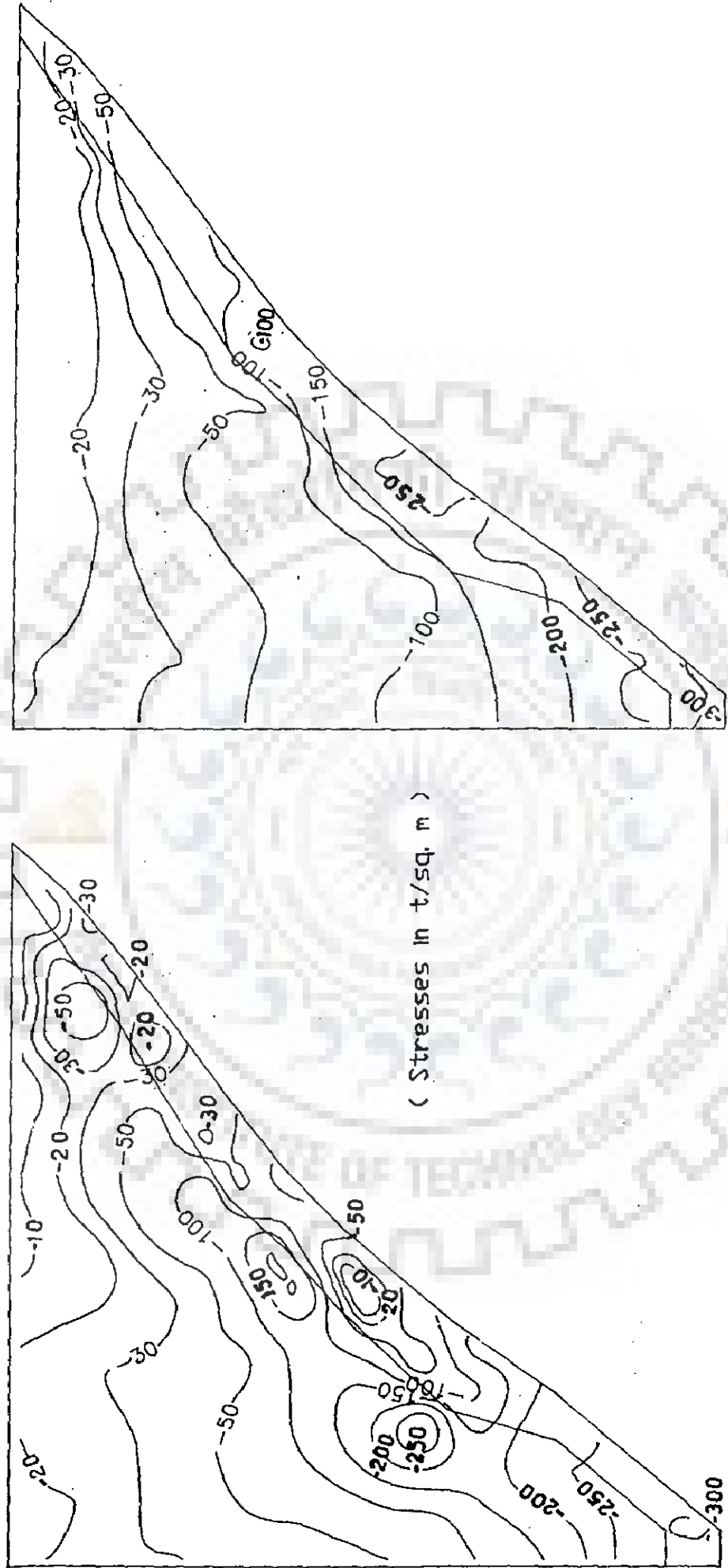


Fig 5.21 : CONTOURS OF STRESS σ_x AT LONGITUDINAL SECTION ($\beta = 2.25$)

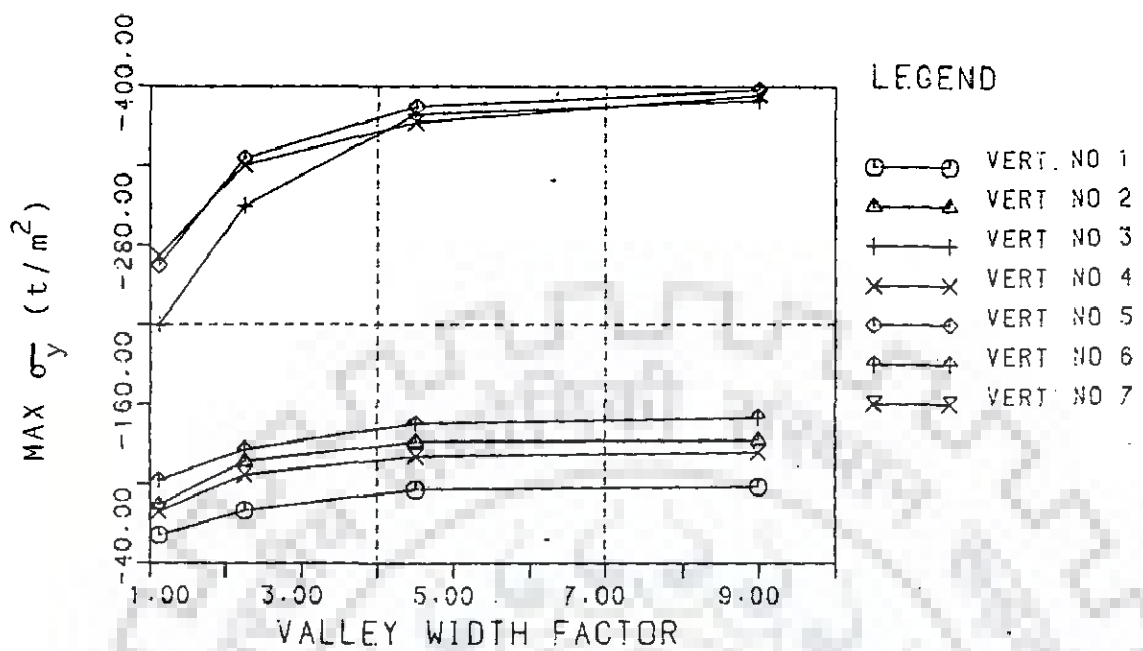


FIG 5.22(a) MAXIMUM σ_y STRESS AT CENTRAL SECTION

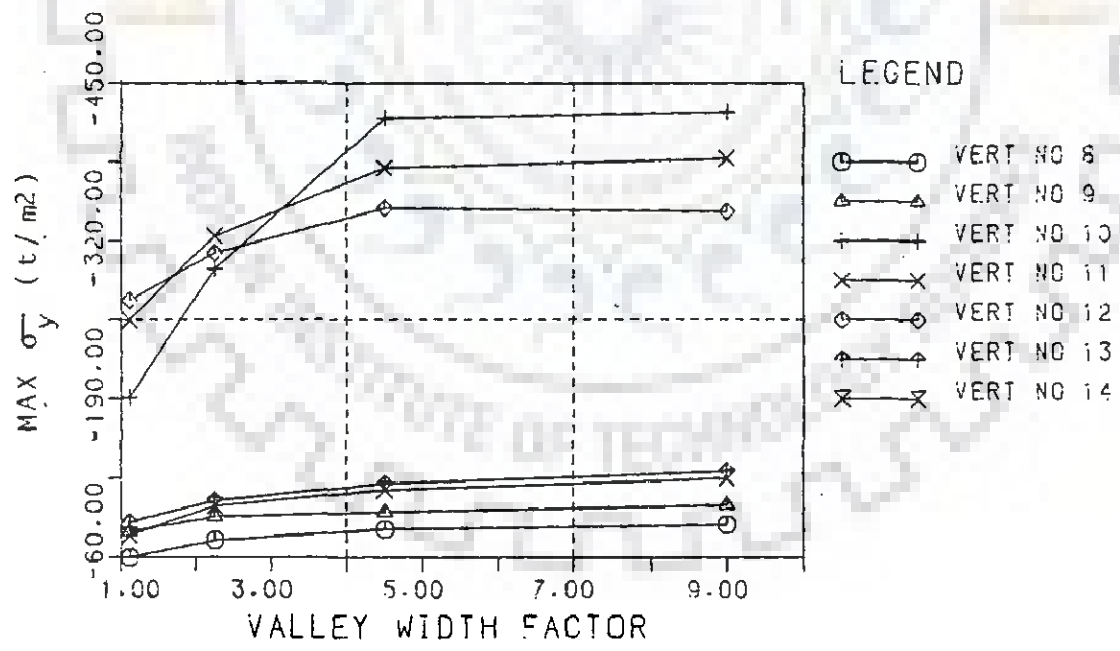


FIG 5.22(b) MAXIMUM σ_y STRESS OVER PLANE NO.2

LEGEND

- STAGE 1
- △ STAGE 2
- † STAGE 3
- × STAGE 4
- ⊙ STAGE 5
- ▲ STAGE 6

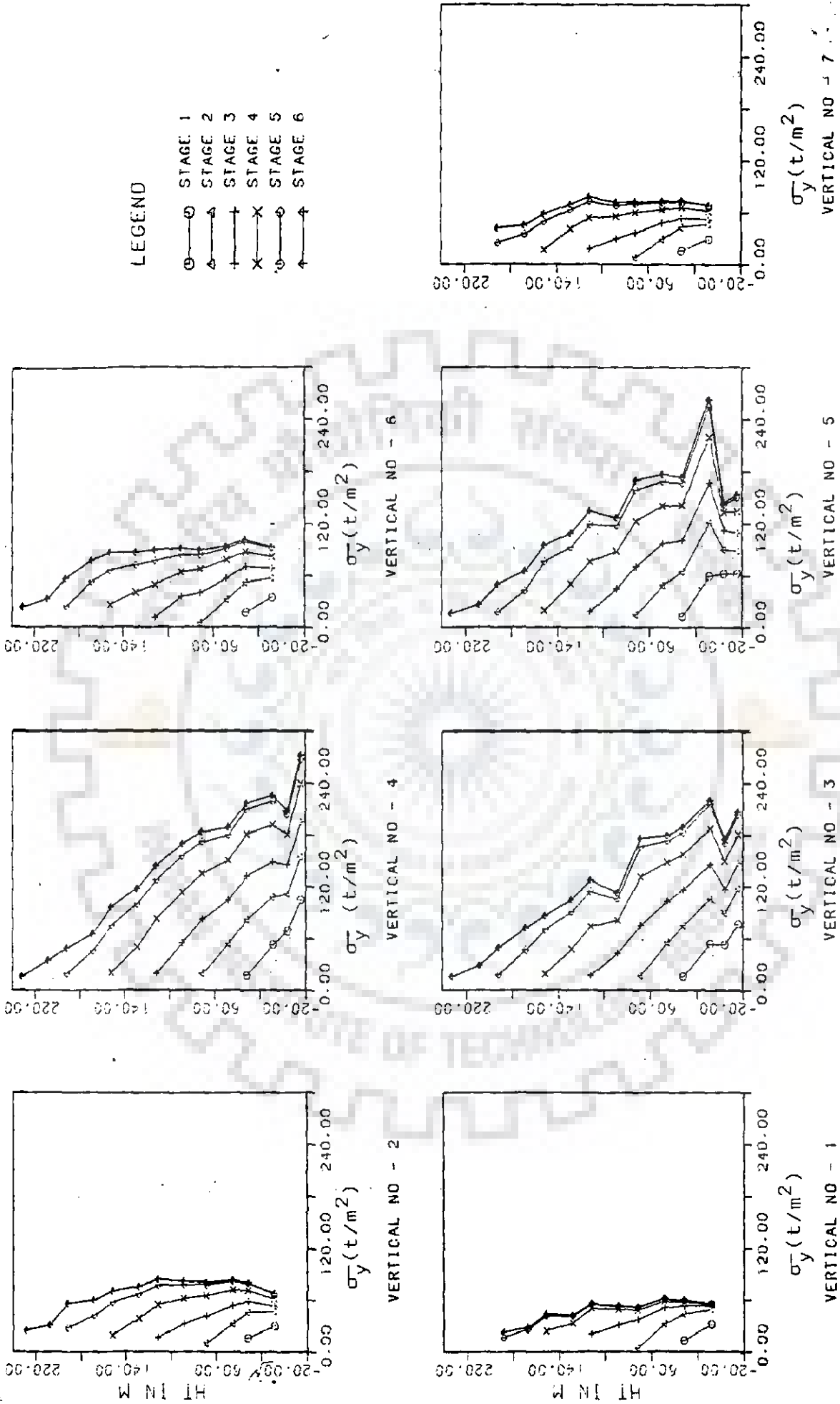


FIG. 5.23 : SEQUENTIAL VARIATION OF σ_y FOR 3-D ANALYSIS : $\beta = 1.12$

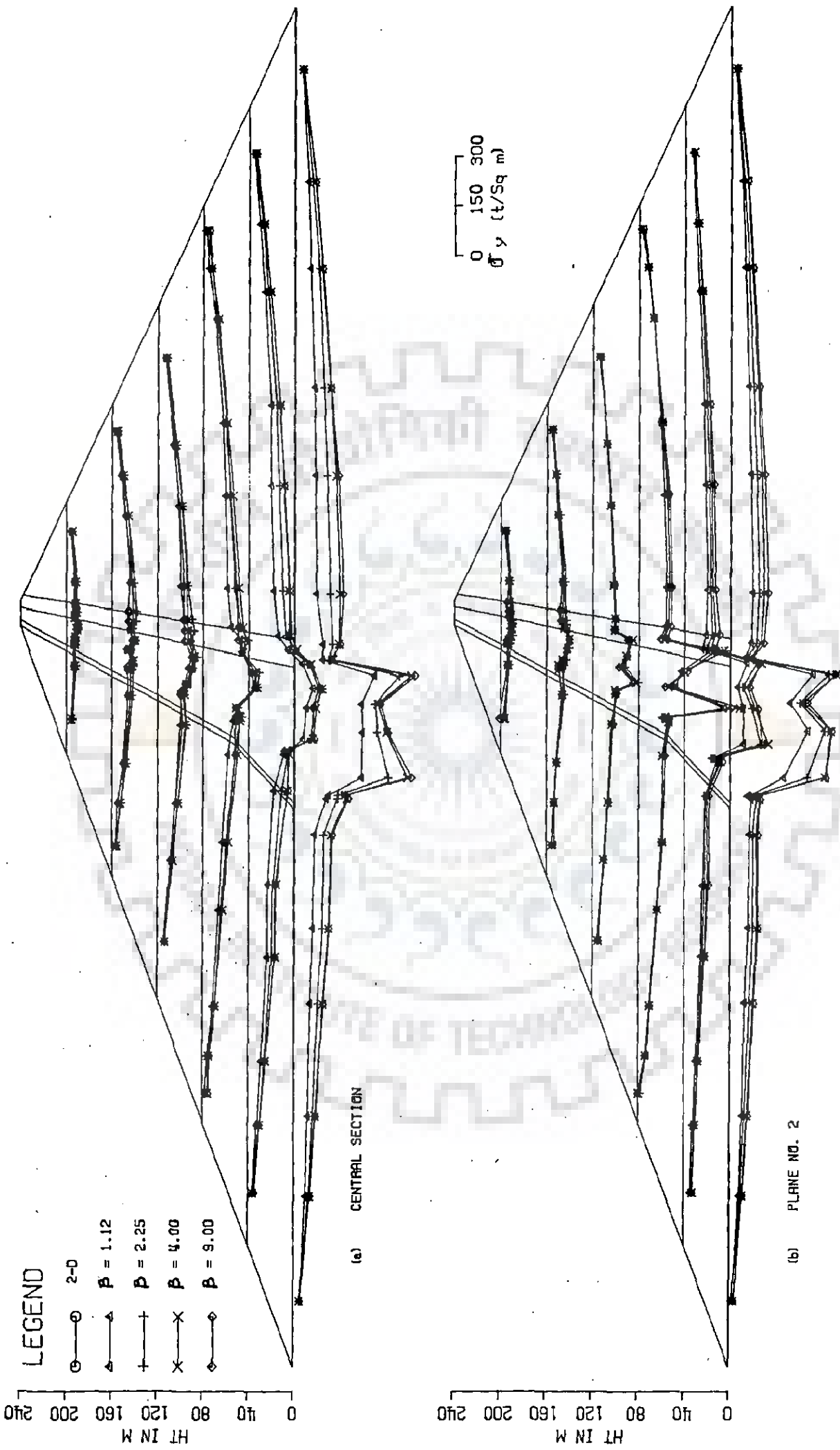
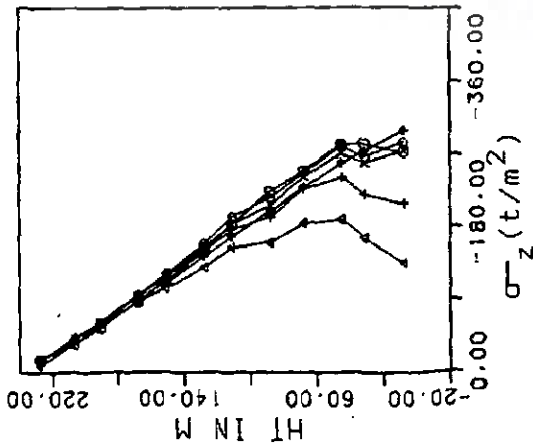


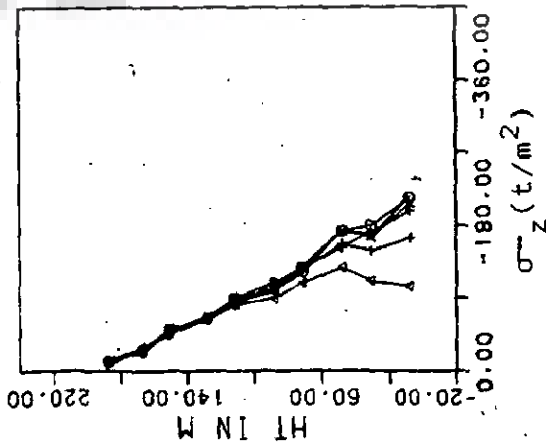
FIG 5.24 : HORIZONTAL NORMAL STRESS σ_y AT CONSTANT ELEVATIONS

LEGEND

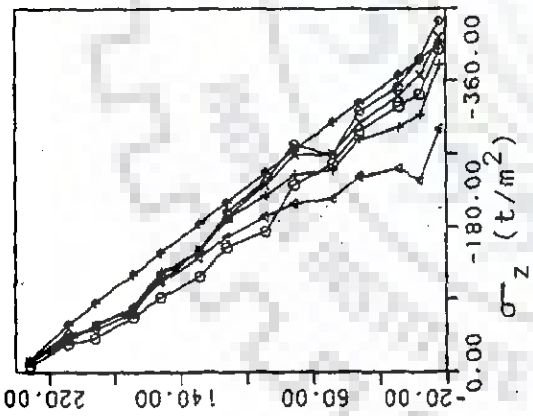
- 2-D
- △—△ $\beta = 1.12$
- †—† $\beta = 2.25$
- ×—× $\beta = 4.50$
- ◇—◇ $\beta = 9.00$
- ↑—↑ Over burden



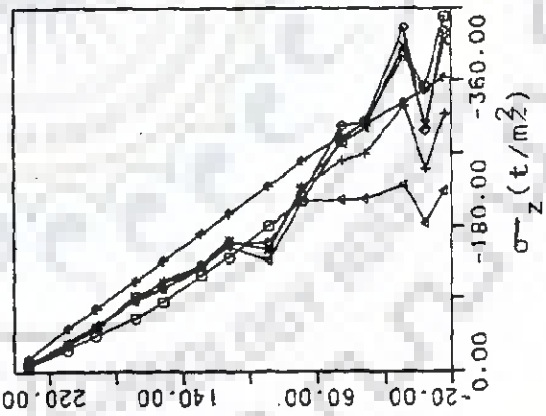
VERTICAL NO.1



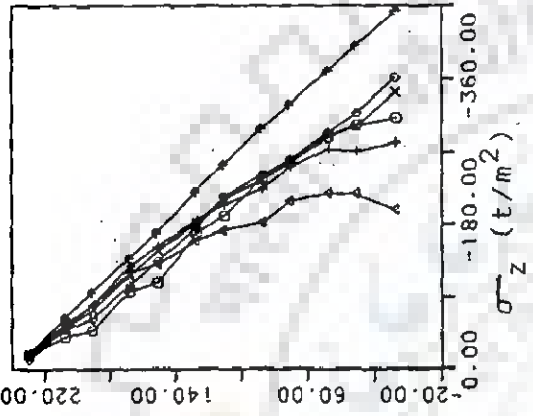
VERTICAL NO.2



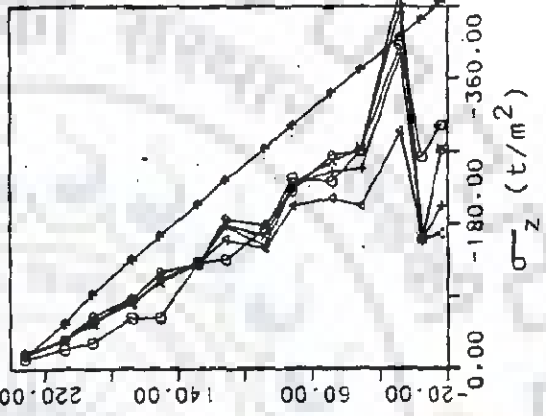
VERTICAL NO.3



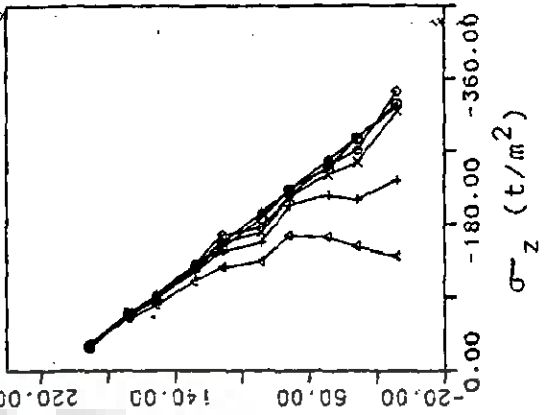
VERTICAL NO.4



VERTICAL NO.5



VERTICAL NO.6



VERTICAL NO.7

FIG. 15.25: VERTICAL NORMAL STRESS σ_z ALONG HEIGHT OVER CENTRAL SECTION

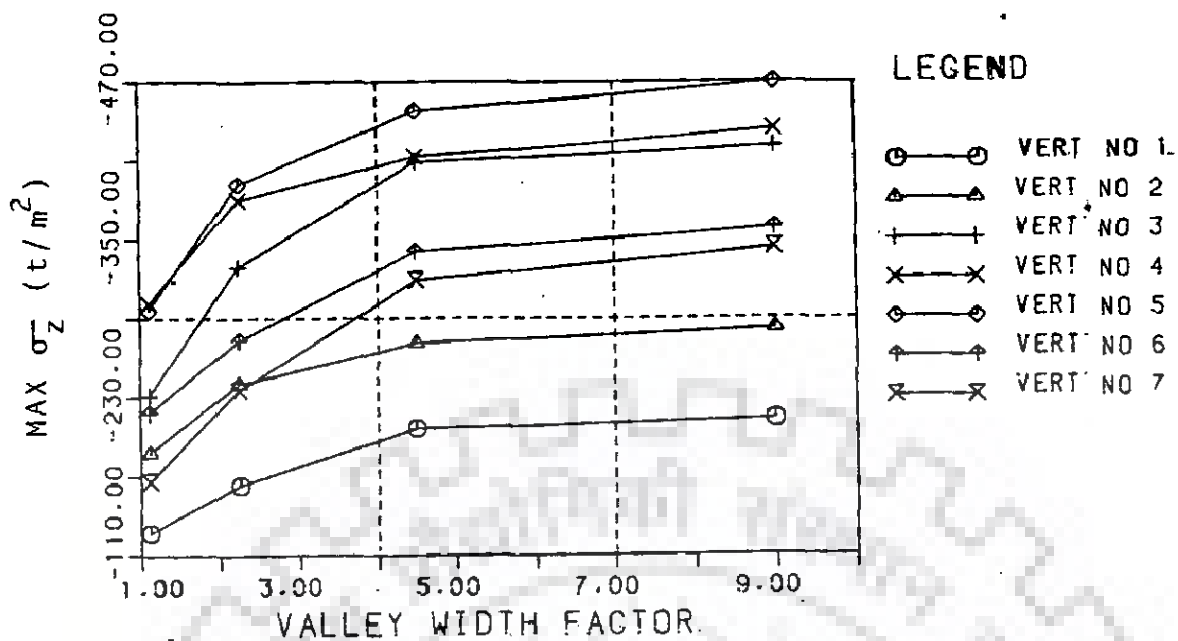


FIG 5.26(a) MAXIMUM σ_z AT CENTRAL SECTION

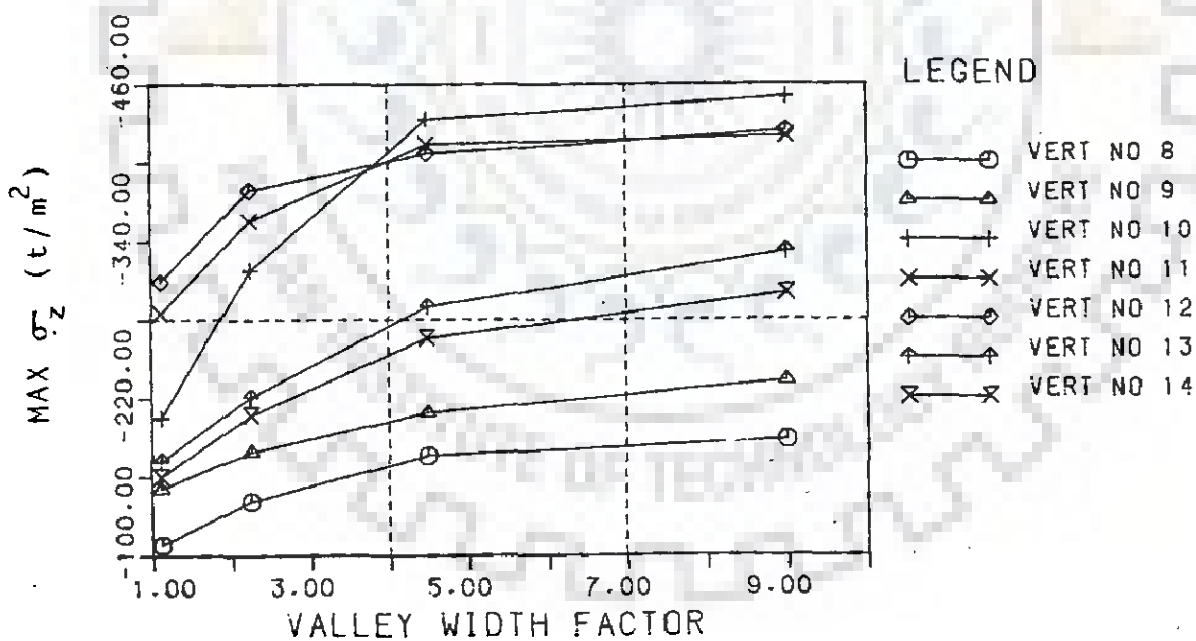


FIG 5.26(b) MAXIMUM σ_z STRESS OVER PLANE NO.2

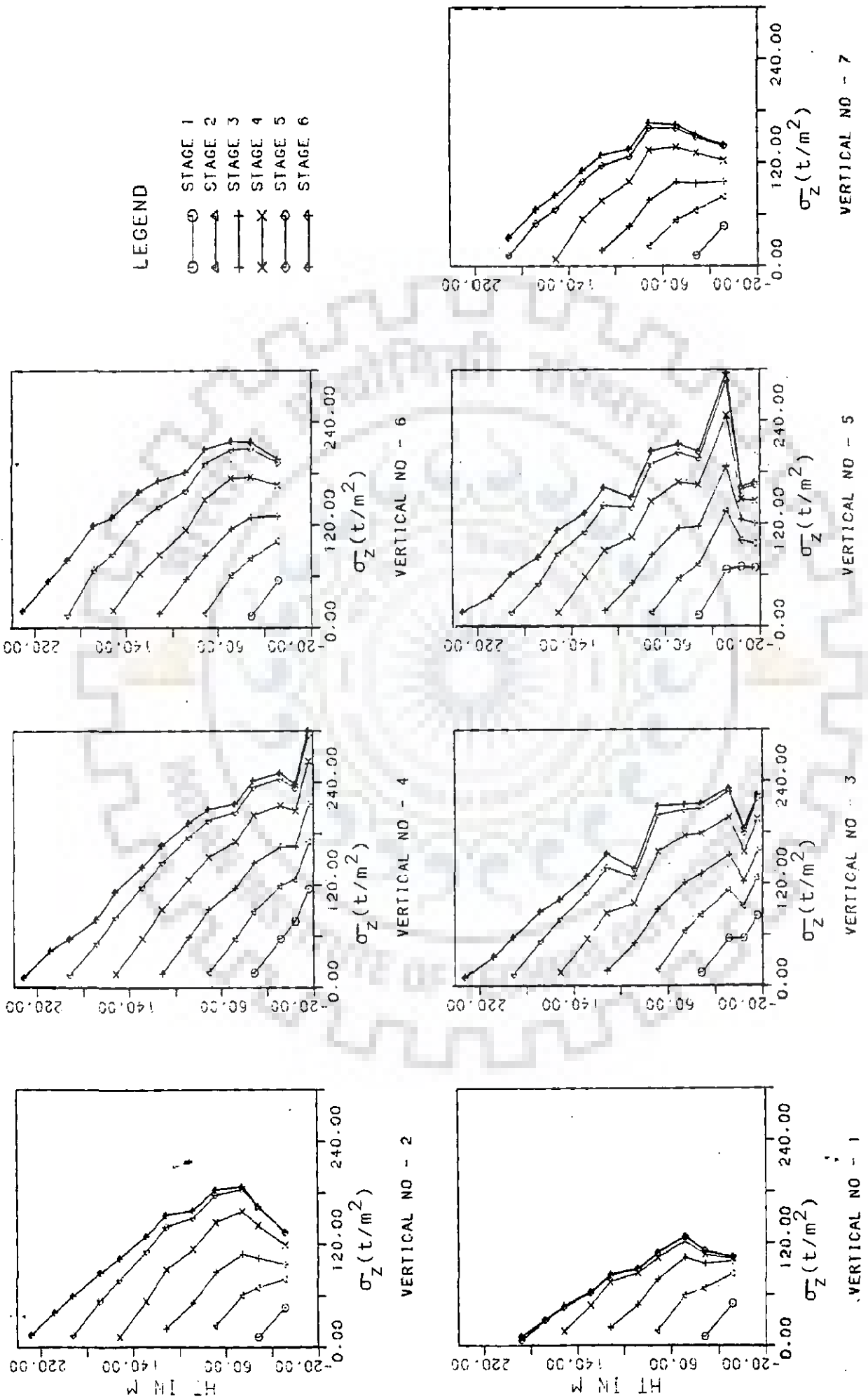


FIG. 5.27 : SEQUENTIAL VARIATION OF σ_z FOR 3-D ANALYSIS: $\beta = 1.12$

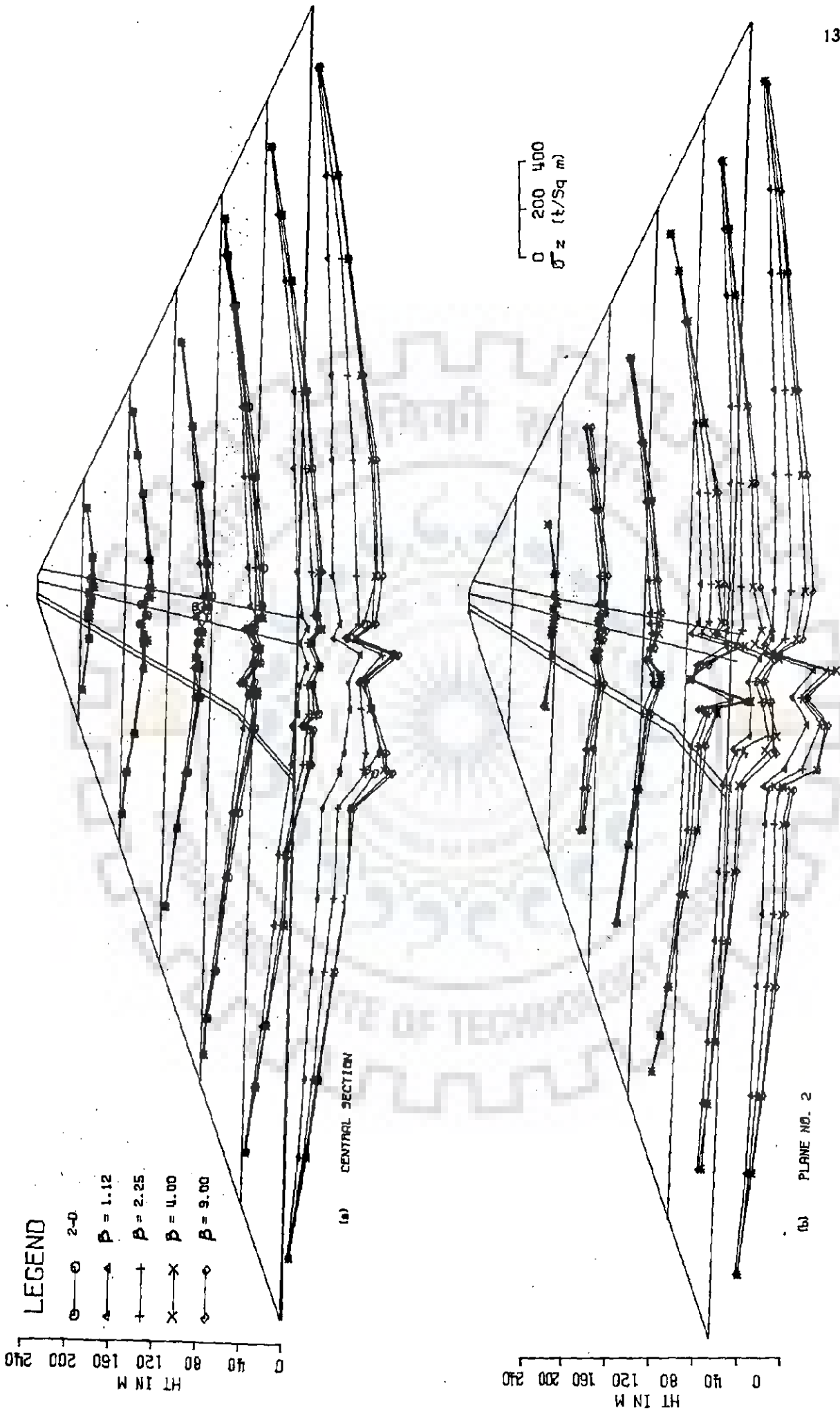


FIG 5.28 : VERTICAL NORMAL STRESS σ_z AT CONSTANT ELEVATIONS

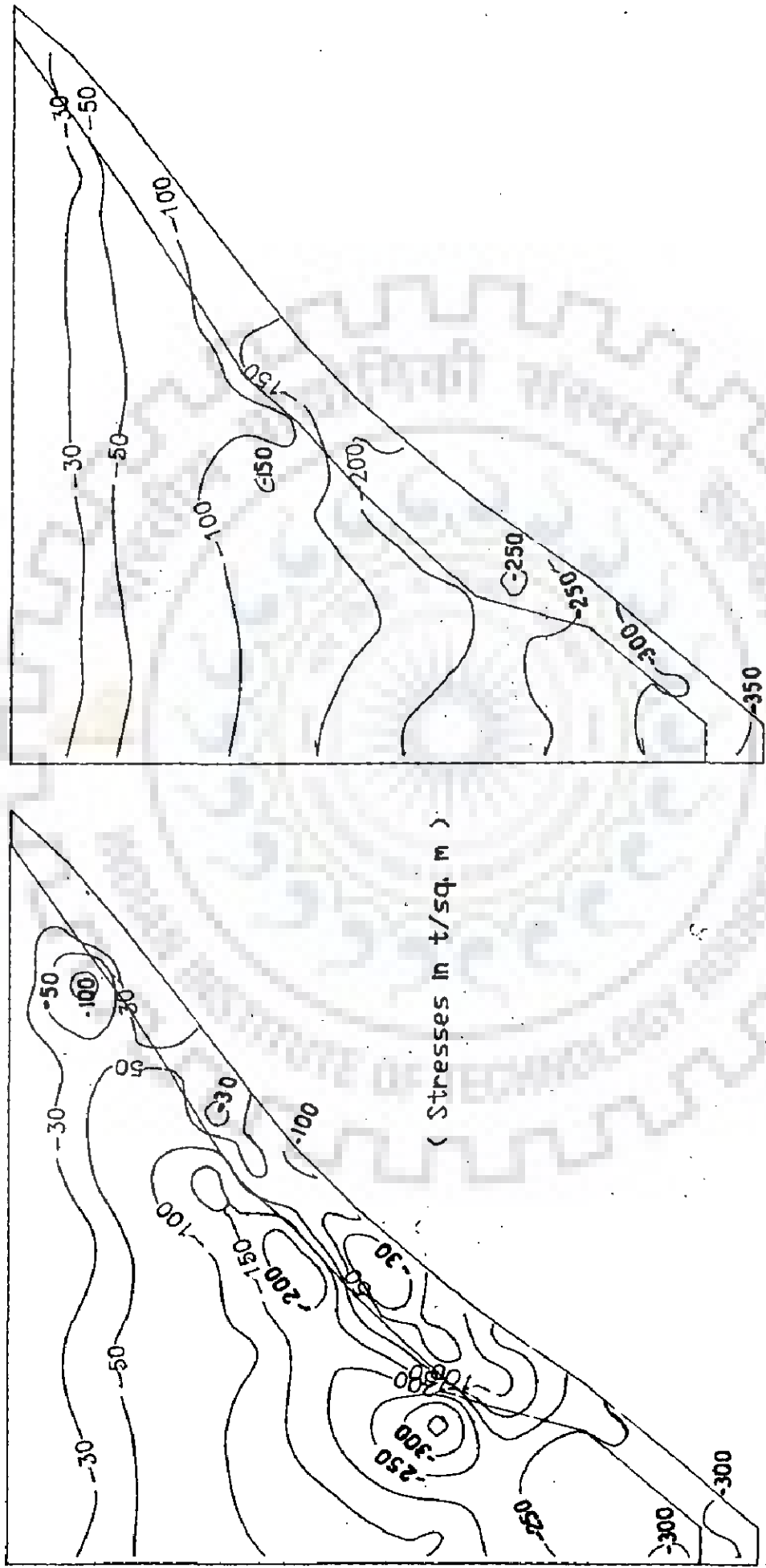


Fig 5.29 : CONTOURS OF STRESS σ_z AT LONGITUDINAL SECTION ($\beta = 2.25$)

3 - D
Plane Strain

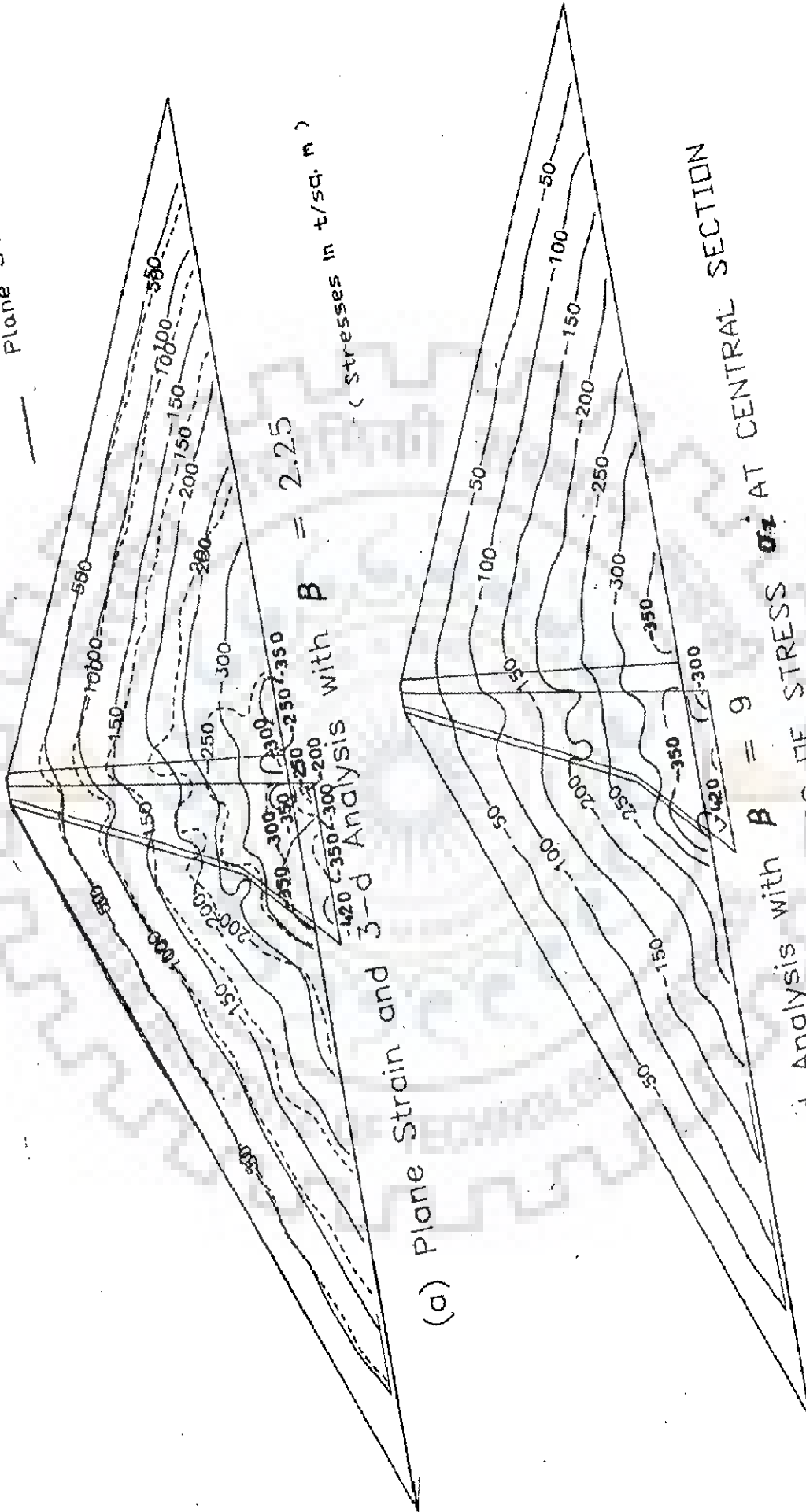


FIG 5.30 : CONTOURS OF STRESS σ_z AT CENTRAL SECTION

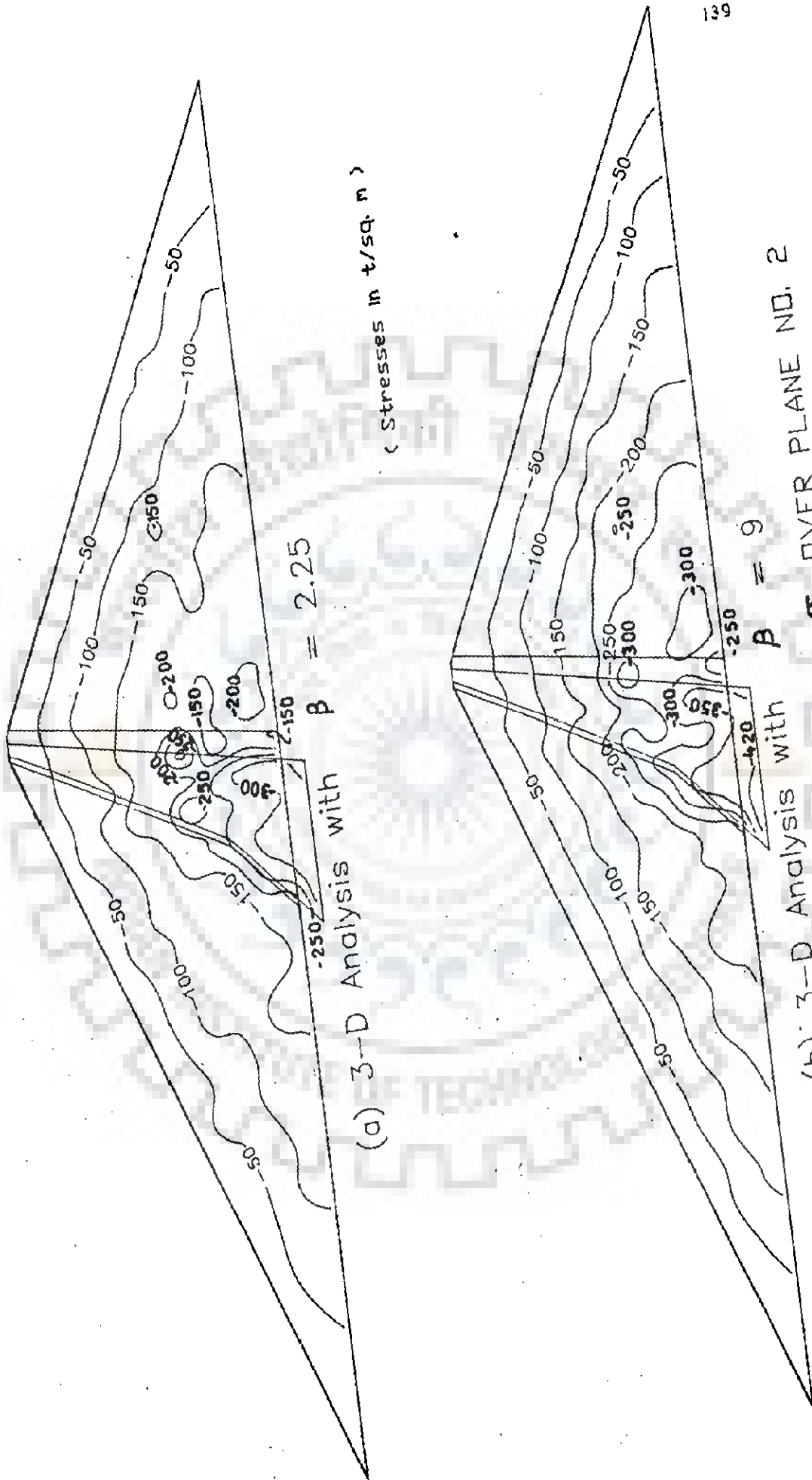
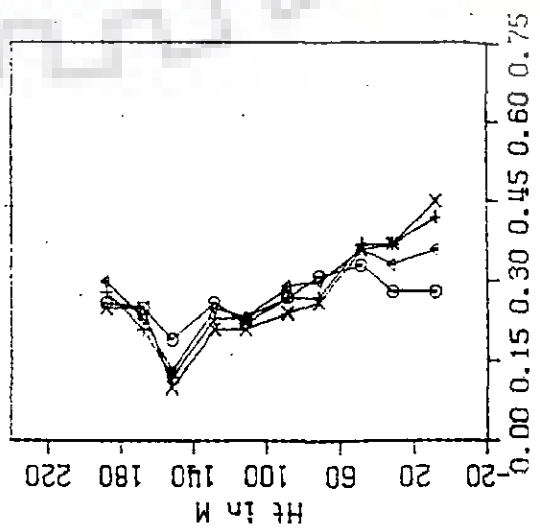
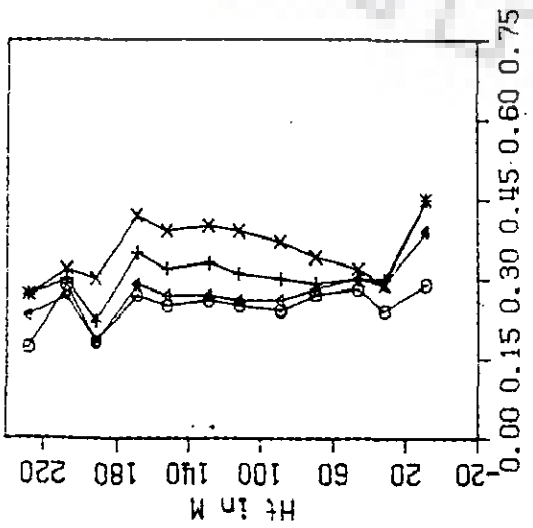
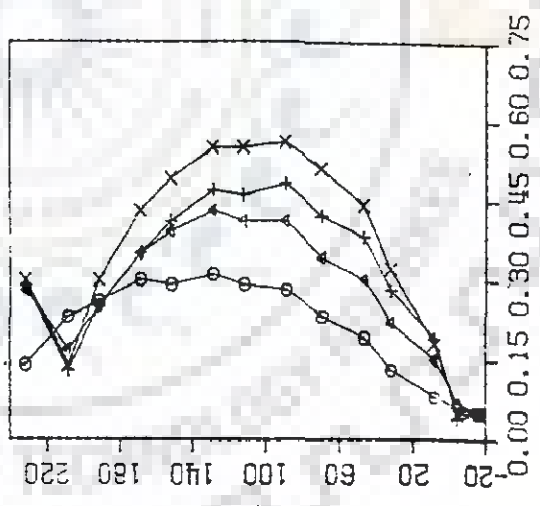
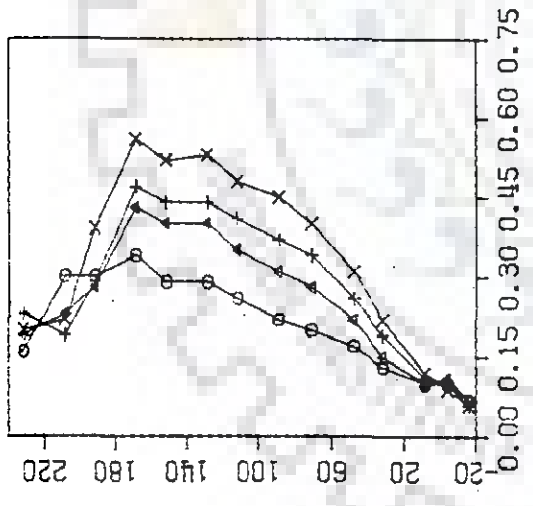
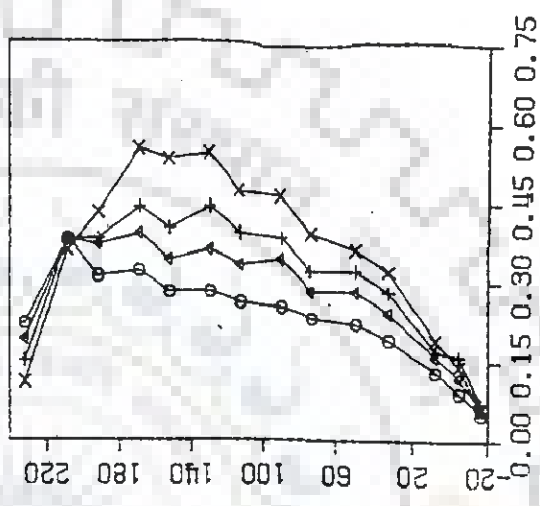
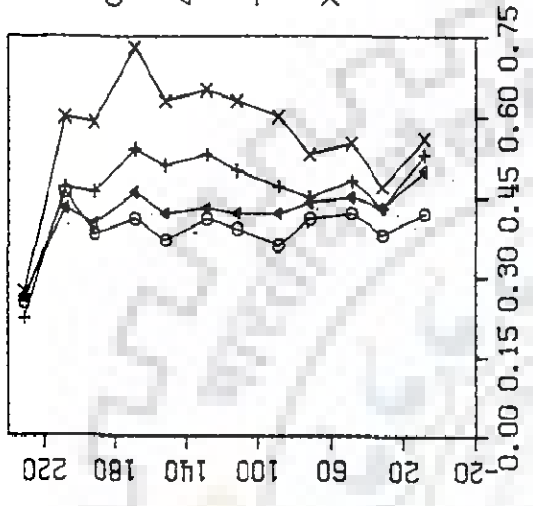
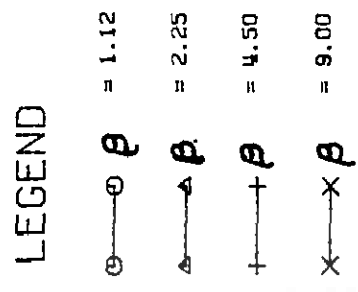


FIG 5.31 : CONTOURS OF STRESS σ_z OVER PLANE NO. 2



VERT. NO. - 7

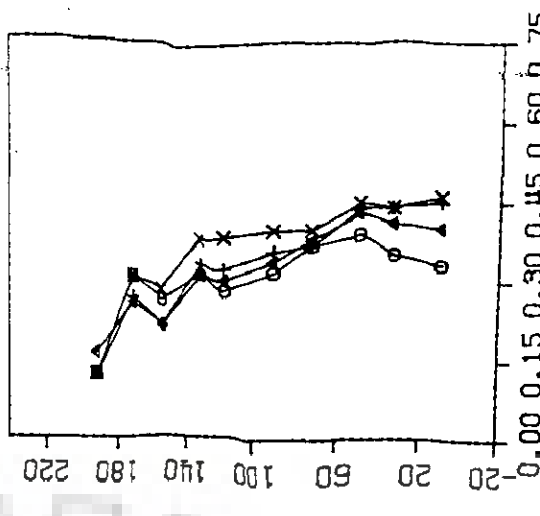
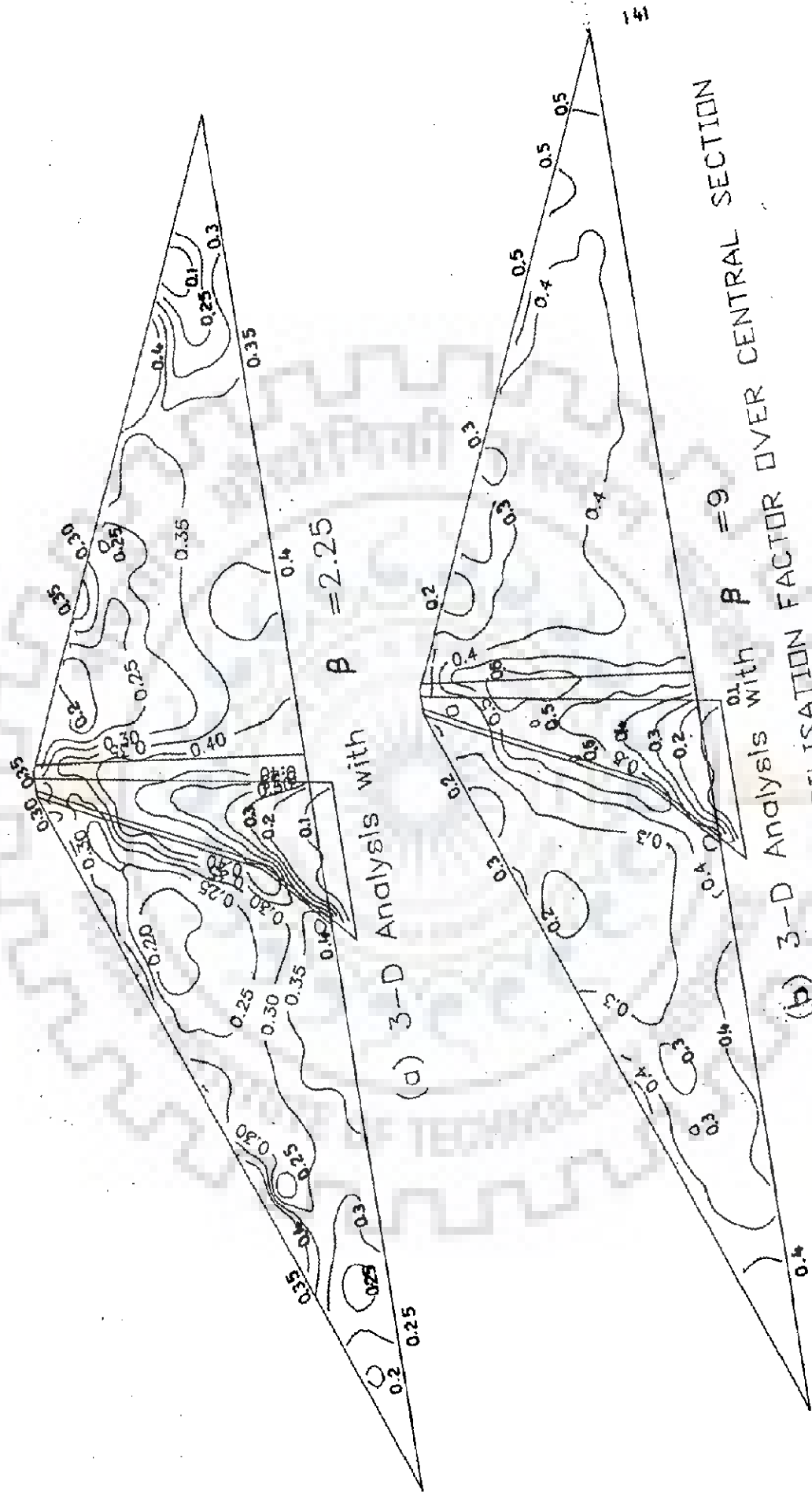


Fig 5.32: Mobilisation Factor m Along Height at Central Section



(b) 3-D Analysis of MOBILISATION FACTOR OVER CENTRAL SECTION

Fig 5.33 | CONTOURS OF MOBILISATION FACTOR

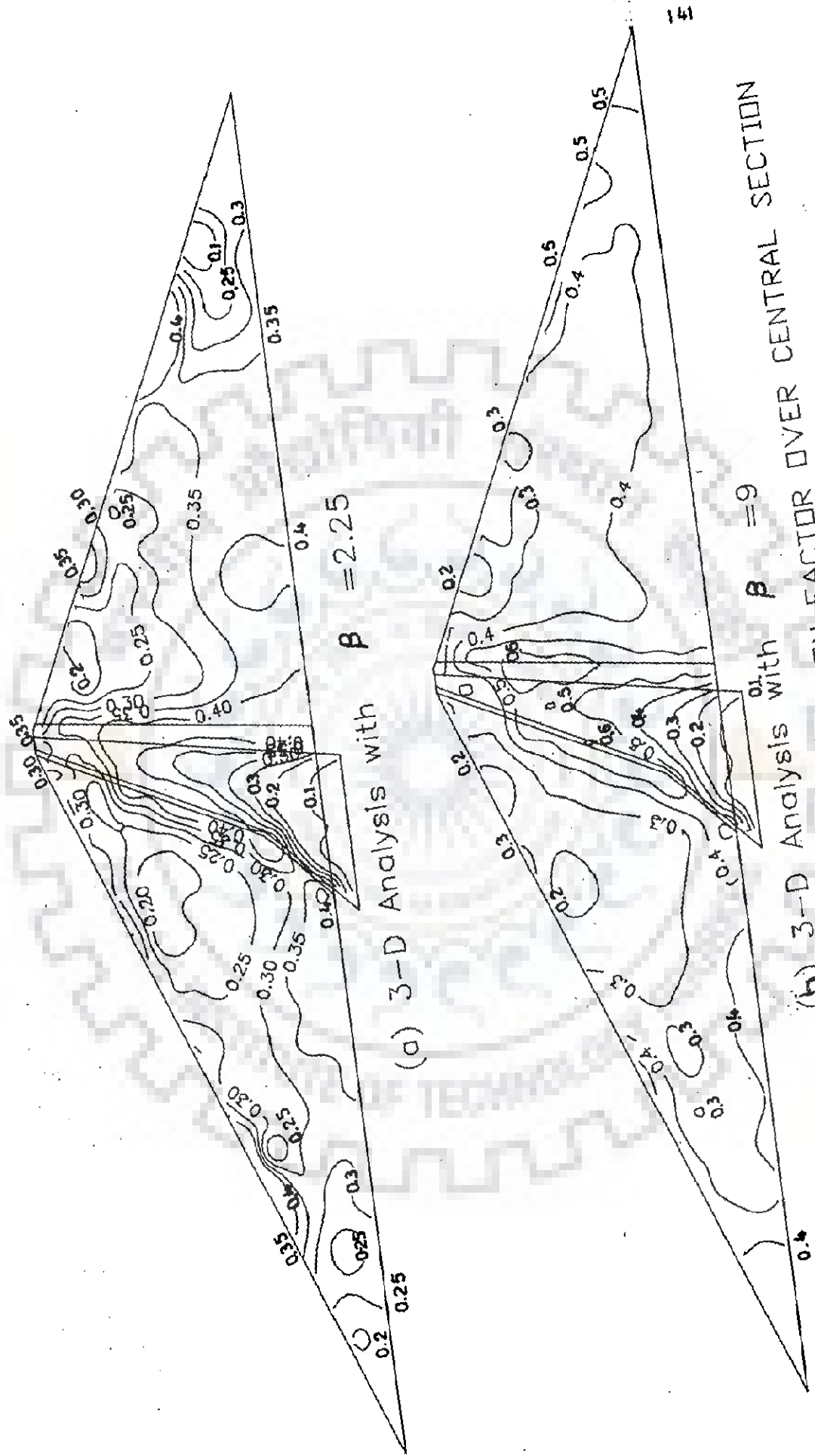
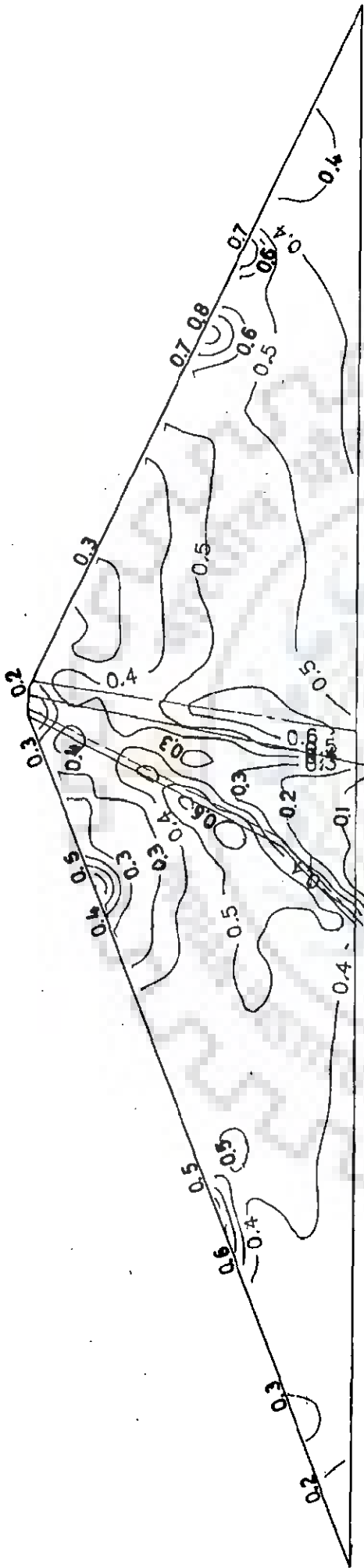
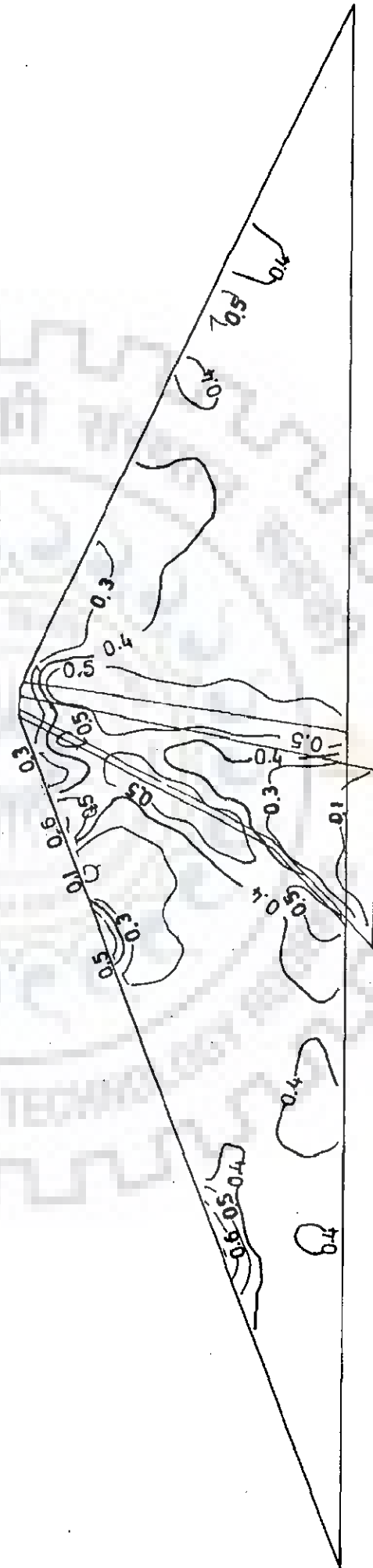


FIG 5.33 : CONTOURS OF MOBILISATION FACTOR OVER CENTRAL SECTION



(a) 3-D Analysis with $\beta = 2.25$



(b) 3-D Analysis with $\beta = 9$

Fig 5.34 : CONTOURS OF MOBILISATION FACTOR OVER PLANE NO. 2

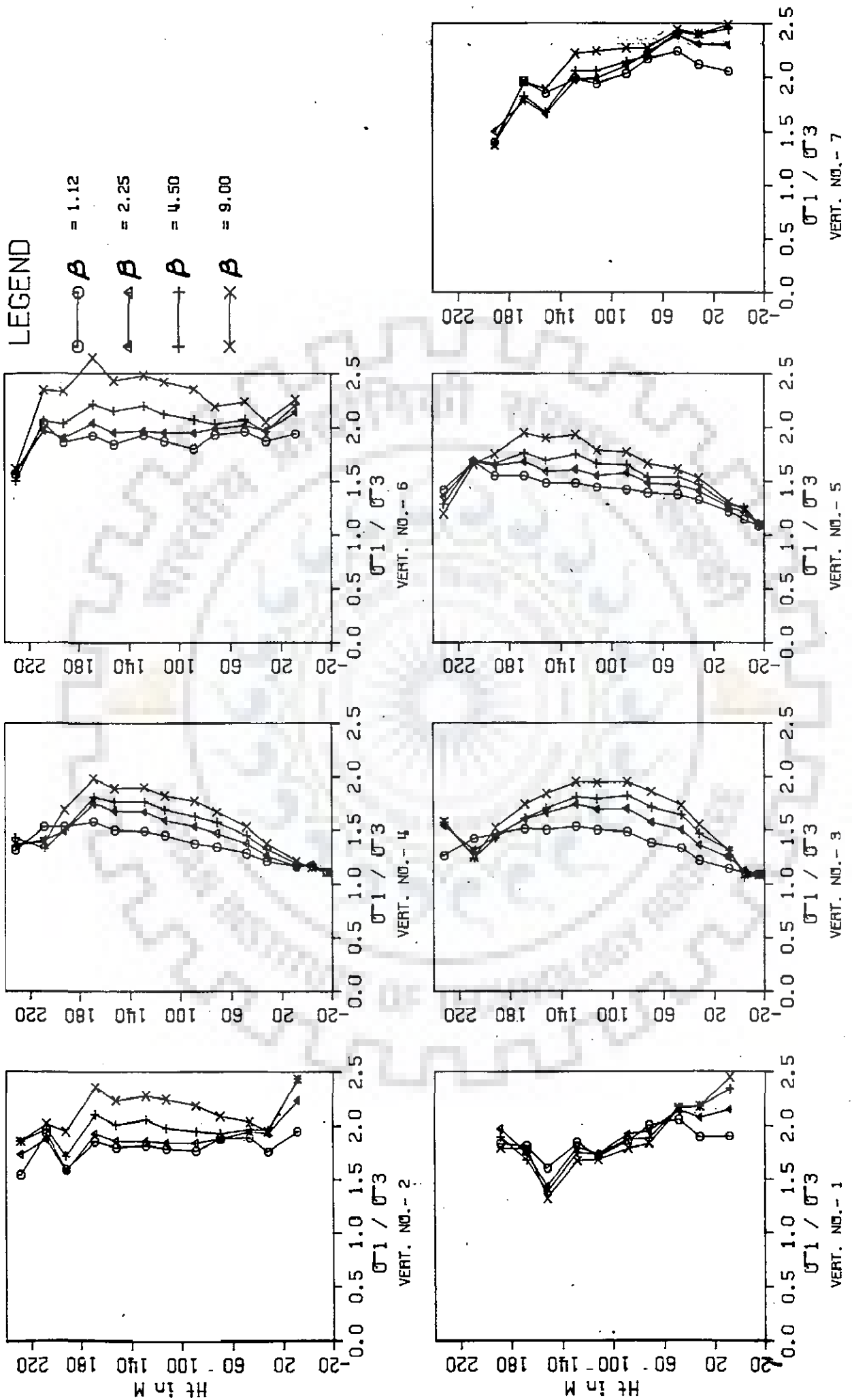
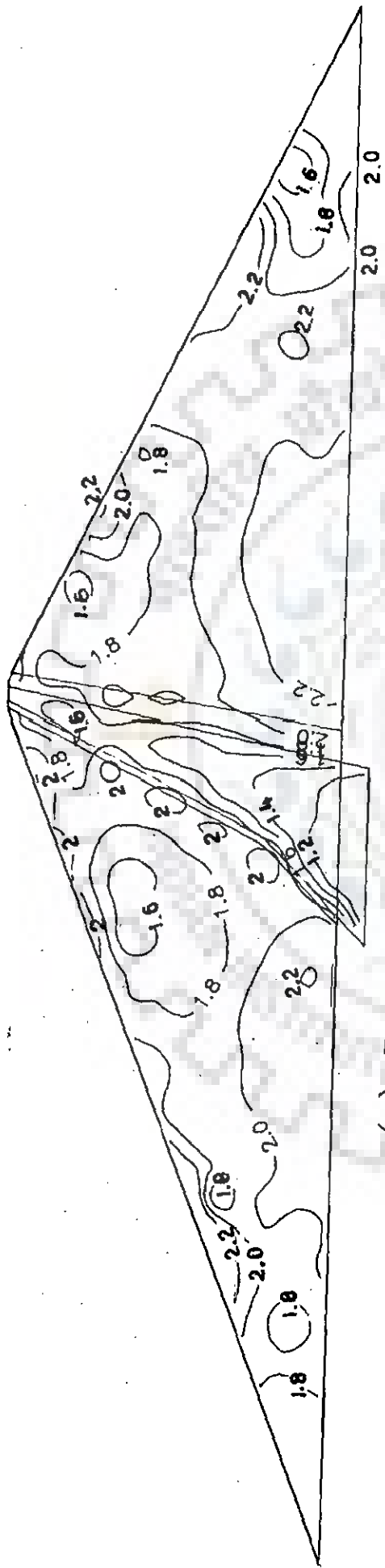
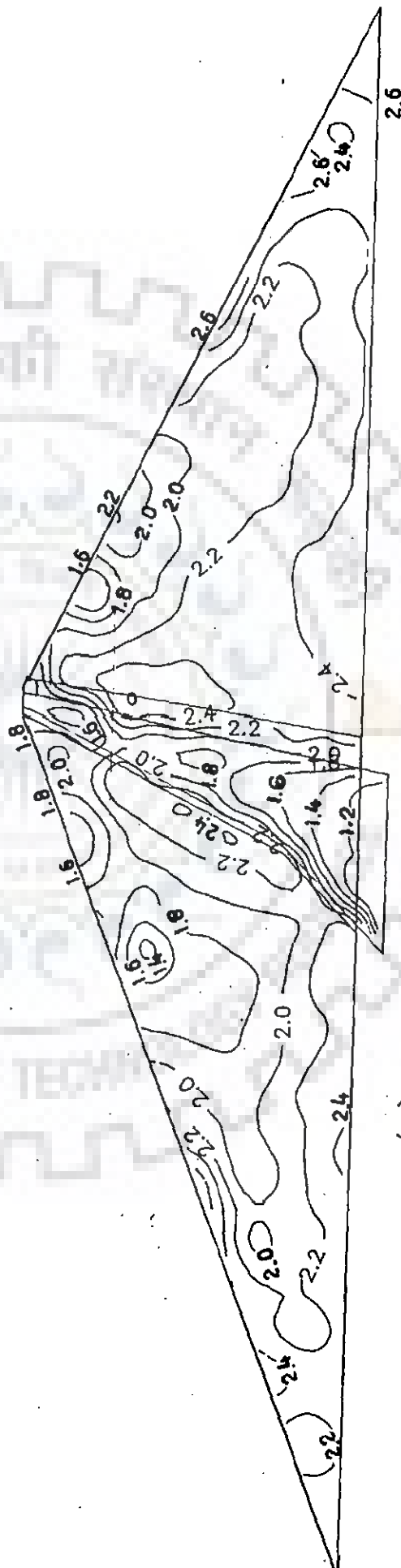


Fig 5.35: Principal Stress Ratio $\frac{\sigma_1}{\sigma_3}$ Along Height at Central Section

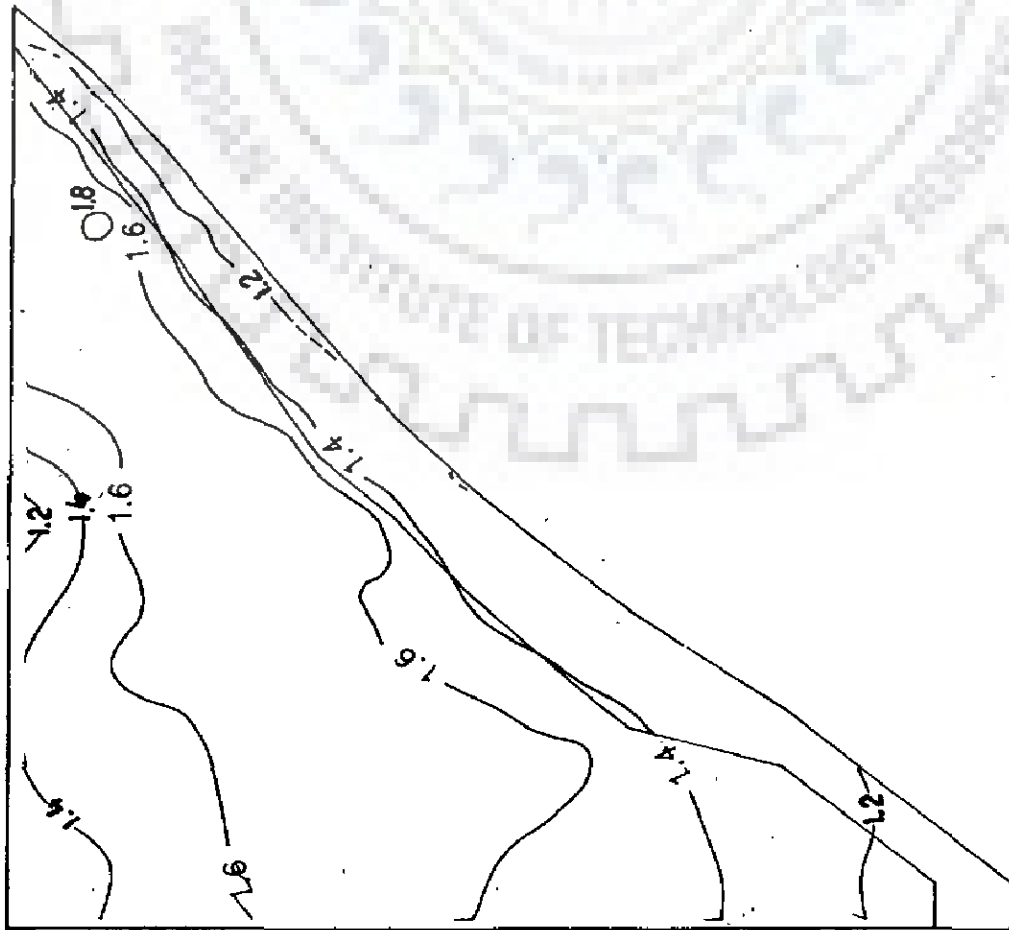


(a) 3-D Analysis with $\beta = 2.25$

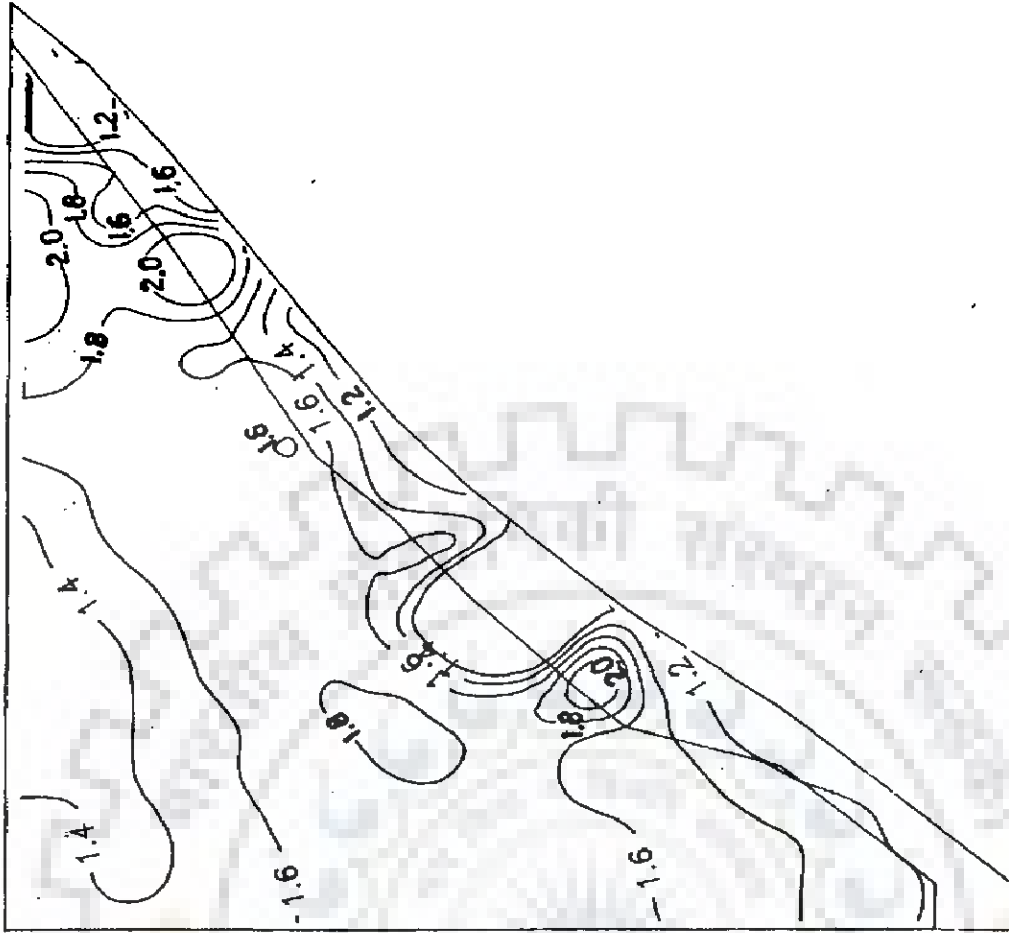


(b) 3-D Analysis with $\beta = 9$

FIG 5.36 : CONTOURS OF RATIO σ_1 / σ_3 OVER CENTRAL SECTION



(a) Along Centre Line of Core



(b) Along Upstream Face of Core

Fig 5.37 : CONTOURS OF RATIO σ_1 / σ_3 OVER LONGITUDINAL SECTION
($\beta = 2.25$)

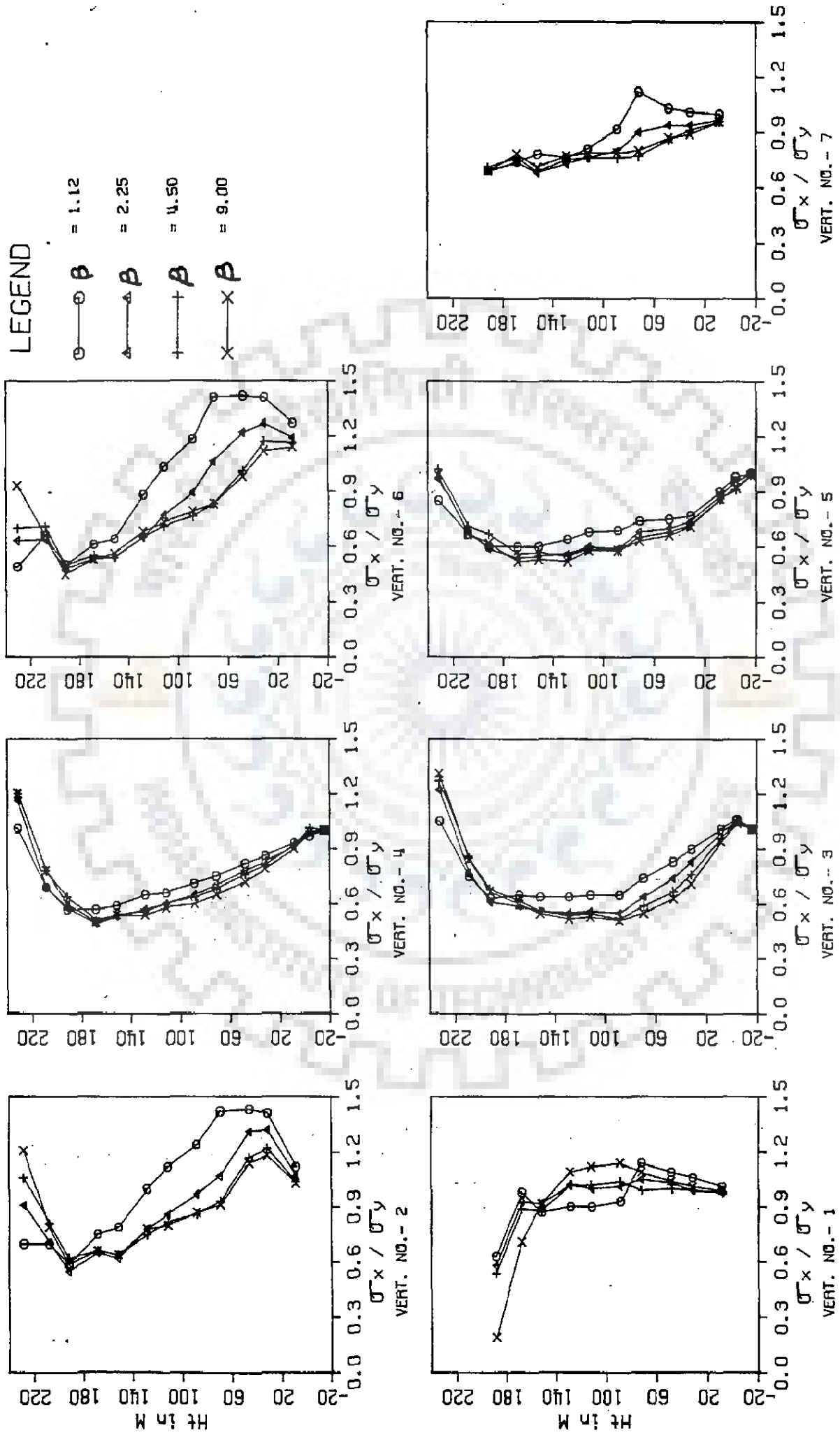


Fig 5.38: Horizontal Stress Ratio $\frac{\sigma_x}{\sigma_y}$ Along Height at Central Section

CHAPTER 6

EFFECT OF VALLEY SHAPE AND BASE WIDTH

The effect of valley width factor on the dam behaviour has been discussed in Chapter 5. The effect studied, combines the effects of change of valley base width as well as the valley wall slopes. From this study, it is not possible to ascertain separately the contribution of change in valley base width and that of change in valley wall slope. To determine this effect, another study has been carried out in which the effect of each parameter has been brought out separately. The results of this study are presented in this Chapter.

6.1 CASES STUDIED

Since both, the valley base width and the valley wall slopes are likely to affect the dam behaviour, two valley slopes have been chosen for studying the effect of valley base width, namely $0.5H:1V$ and $1H:1V$. To compare the results with those obtained by changing both together, the case with valley wall slopes of $2H:1V$ has also been analysed. The different cases analysed can thus be classified into 3 groups, as given in Table 6.1.

TABLE 6.1 :- Details of Cases Studied

S.No	Group	Case No.	Valley Shape	
			base width (m)	side slopes H:V
1	1]	1	20	$0.5:1$]
2		2	40	
3		6	80	
4	2]	3	40	$1:1$]
5		4	80	
6	3	5	80	$2:1$

Note : Valley wall slope wherever not specified shall be taken as H:V

The valley has been assumed symmetrical in the y -direction and a uniform valley wall slope from ground level to the top of dam has been used in this study. Unlike the core slopes used in Chapter 5, where the slope of the upstream face of core changes near the ground level, a uniform upstream core slope of $0.5H:1V$ has been taken in this study. The constant slopes from top to bottom for the valley and the upstream core face have been used so that the results are not affected by the variation in the slopes. The transverse and a longitudinal section of the dam along with the discretisation thereon for case 3 are shown in Fig. 6.1.

6.2 ANALYSES PERFORMED

The 6 cases under 3 groups have been analysed for end of construction condition.

The transverse horizontal movement - u , the vertical settlement - w and the three normal stresses σ_x , σ_y and σ_z have been studied. In addition, the horizontal stresses ratio σ_x/σ_y , the principal stresses ratio σ_1/σ_3 and also the mobilisation factor m have been studied.

These parameters have been compared on central section (plane no. 1) and plane no. 2, along the seven locations, one each in both zones of transition and shell and three in the core as shown in Fig. 6.1.

In the study described in the previous chapter, the y -coordinates were doubled, thus simultaneously doubling both the valley width and the slopes. Cases 1 and 3 of the present study, as also cases 3 and 5, conform to that pattern. Accordingly these two pairs of cases, indicated as category 1 and category

2 respectively, are taken as base of comparison, and percentage variations worked out with respect to these base cases. The maximum values of stresses and displacements pertain to cases 1, 2, 3, 6, 4 and 5 respectively unless specified otherwise.

6.3 RESULTS AND DISCUSSIONS

6.3.1 Displacements

6.3.1.1 Transverse Horizontal Movement (u)

The variation of horizontal movement-u with height at different locations is shown in Figs. 6.2 and 6.3 at central section and plane no. 2. It is seen that the distribution along the height is non-linear. At central section, the maximum values are observed at about half the height above base except in the upstream transition and upstream face of core, where it occurs at about one-third the height above base. At plane no. 2 the maximum occurs at elevation 160 m i.e., at two third of the height above base for all locations. The horizontal movements are away from the dam axis i.e., the dam expands. The upstream movements are more than the corresponding downstream movements. In the upstream half the maximum movements are observed at the shell/transition interface, while in the downstream half the shells exhibit higher movement than the transitions.

Table 6.2 shows the range of maximum horizontal movements in the dam at different locations over central section and also the percentage increase in each case at constant slopes, expressed as a percentage of the base cases defined above.

When the valley is stretched in y-direction, to change the slope from 0.5:1 to 1:1 and the width from 20m to 40m, the

movements increase by about 45 % on all locations, except in the upstream shell where the increase is about 78 %. Of this increase, the contribution of base width is about 25 % to 30 % only, except on upstream face of core (Vert 3, 45%). Further increase of base width to 80m increases this share to about 80 %. Though by increasing the base width, the overall valley width to height ratio is not increased much, the increase in displacements is significant.

With valley slopes at 1:1, stretching the y-dimension by 2 results in horizontal movement increase of about 25% in the interior of dam and 37% and 12% respectively in the upstream and downstream shells. Of this increase, the contribution of base width increase alone is about 50 to 60% in the interior of the dam and about 35 to 45% in the shells.

Table 6.2 : Horizontal Movements (cms)on Central Section

Vert No.	Range of maximum values (for six cases) (cms)	Category 1 (%)			Category 2 (%)	
		β based increase (case 1 to 3)	Share of base width		β based increase (case 3 to 5)	Share of base width (case 4)
			Case 2	Case 6		
1	-13.1 to -30.9	78	27	70	37	42
2	-17.1 to -31.0	44	30	70	16	50
3	-14.7 to -23.5	40	45	55	20	60
5	9.9 to 16.8	44	20	70	25	50
6	12.6 to 22.3	40	40	85	26	48
7	12.9 to 26.7	44	25	80	12	35

The maximum values of horizontal movement over plane no. 2 are shown in Table 6.3. It is seen from the table and Fig. 6.3 that the values of movement u are small as compared to that at central-section. The effect of valley slope is more for narrow valleys than for wide valleys. The increase in base width only, keeping the slopes constant, does not significantly affect the movement values for narrow valleys but the effect is quite pronounced for wider valleys. At constant base width, the horizontal movement - u increases with the increase in valley wall inclination from the vertical. However, at this section the effect of valley base width is smaller as compared to that at central section.

Table 6.3 : Horizontal Movement Values u (cms) on Plane No.2

Vert. No.	Displacement- u in Cms for Case No.					
	1	2	6	3	4	5
8.	-9.3	-9.2	-10.4	-11.5	-11.1	-12.5
9.	-10.3	-10.2	-10.4	-14.7	-15.7	-11.4
10.	-11.2	-12.0	-12.6	-9.2	-10.0	-12.4
12.	6.2	7.2	7.3	6.3	8.9	7.6
13.	7.0	7.4	8.2	10.4	10.2	10.1
14.	8.7	9.6	10.2	12.6	12.9	12.3

It can thus be said that on central section the base width influences the horizontal movements substantially, the effect being more predominant in wide and flatter valleys than in narrow and steep valleys. On plane no. 2, however, the influence of base width is negligible and only the side slopes govern the movements. The effect is more in core than in

pervious zones.

6.3.1.2 Vertical Movement (w)

The variation of vertical movement - w along height over central section and plane no. 2 at different verticals is shown in Figs. 6.4 and 6.5. It is seen that for all cases, at all locations the variation is non-linear with the maximum settlements occurring between the midheight and two third height from bottom on central section and between elevation 160 m and 200 m on plane no. 2. The settlements are maximum at the core centre line, decreasing gradually in both the upstream and downstream directions.

Tables 6.4 and 6.5 show the typical maximum values of settlements for cases 1 to 6 on central section and plane no. 2 respectively. It is seen that the settlements in the downstream shell are more than those in the upstream shell.

Table 6.4 : Vertical Settlements at Central Section

Vert No.	Range of maximum values (for six cases) (cms)	Category 1 (%)			Category 2 (%)	
		β based increase (case 1 to 3)	Share of base width		β based increase (case 3 to 5)	Share of base width (case 4)
			Case 2	Case 6		
1	35 to 52	25	55	95-100	20	60
2	54 to 88	32	30	-do-	22	47
3	57 to 95	40	30	-do-	25	47
4	59 to 95	32	45	-do-	22	55
5	57 to 85	30	45	-do-	25	50
6	58 to 82	26	35	-do-	15	55
7	44 to 72	35	40	-do-	25	55

Table 6.5 : Vertical Settlement at Plane No 2

Vert No.	Range of maximum values (for six cases) (cms)	Category 1 (%)			Category 2 (%)	
		β based increase (case 1 to 3)	Share of base width		β based increase (case 3 to 5)	Share of base width (case 4)
			Case 2	Case 6		
8	25 to 27	15	30	10	8	53
9	43 to 57	22	26	10	8	54
10	48 to 63	22	29	30	8	18
11	50 to 65	20	32	30	8	-11
12	44 to 58	23	21	20	7	50
13	41 to 55	19	35	30	12	38
14	29 to 32	10	50	55	5	60

When the valley is stretched by 2 in y-direction with valley wall slope changing from 0.5:1 to 1:1, there is an increase in settlement values of about 35% at central section. When the valley wall slope changes from 1:1 to 2:1, the increase in settlements is of the order of 25%. At plane no. 2, the corresponding figures are 15 to 20% for valley wall slope change from 0.5:1 to 1:1 and 8% for a change of valley wall slope from 1:1 to 2:1.

However, when only the base width is doubled, keeping the valley slope constant at 0.5:1 the increase in settlements is of the order of 30 to 45% of the increase when slopes too are changed. If the base width is further widened from 40 m to 80 m at valley wall slopes of 0.5:1, the increase in settlements is of the order of 95% to 100% on central section, which indicates that the effect of increase in valley base width is more pronounced than that of valley wall slope. On plane no. 2,

however, there is a slight decrease in settlements at this stage, which means that on plane no. 2 beyond a certain base width to top width ratio, the effect of valley width gets reversed i.e., the settlements decrease as the valley base width increases.

When the base width alone is doubled at valley wall slopes of 1:1, the increase in settlements for both planes is of the order of 47 to 55 % of the increase for the case when in addition, valley wall slopes too are changed.

Since the change of base width does not substantially affect the overall valley width to height ratio, it is inferred that the vertical settlements are more influenced by the base width than by the valley wall slope. A valley with a wall slope of 0.5:1 but with a base width of 80 m has almost the same settlements as a valley with valley wall slopes of 1:1, but with a base width of 40m. The contribution of base width is more at flatter valley wall slopes and is more in the shells than in interior of the dam.

6.3.2 Stresses

6.3.2.1 Horizontal Normal Stress σ_x

The distribution of transverse horizontal stress σ_x over height is shown in Figs. 6.6 and 6.7 for central section and plane no. 2 respectively. The typical maximum values of σ_x and the increase in stress values from one group to another and also the contribution of base width alone are shown in Tables 6.6 and 6.7 for the two planes.

It is noted that when the valley is flattened from a slope of 0.5:1 to 1:1, with both the valley slopes and base width

Table 6.6 : Transverse Normal stress σ_x (compression) at central section

Vert No.	Range of maximum values (for six cases) (t/sq m)	Category 1 (%)			Category 2 (%)	
		β based increase (case 1 to 3)	Share of base width		β based increase (case 3 to 5)	Share of base width (case 4)
			Case 2	Case 6		
1	77 to 95	17	40	85	5	72
2	111 to 133	20	49	90	5	95
3	275 to 412	39	35	70	8	48
4	309 to 454	42	29	55	11	17
5	280 to 370	25	30	61	6	41
6	138 to 159	20	65	>100	-8	45
7	86 to 133	27	45	95	6	90

being scaled by two, the increase in stress over that with valley slopes of 0.5 : 1 is of the order of 20 to 40 %, over central section. For plane no. 2, the increase is about 25 % in core and about 30 % in pervious zones. At central section, the increase in stress is more in the interiors than on the dam faces. Of this increase, the contribution of base width increase alone is about 30 to 50 % over central section and only about 30 % over plane no. 2. When the base width of the valley is further increased to 80 m keeping the valley slopes still at 0.5:1, at the central section the contribution of base width alone rises to about 85-95 % in pervious zones and to about 55 to 70 % in core, with the core centre line showing the least contribution. Over plane no. 2 the share of base width increase is of the order of 40 to 50 % all over the section.

Table 6.7: Transverse Normal Stress σ_x (compression) on Plane No.2

Vert No.	Range of maximum values (for six cases) (t/sq m)	Category 1 (%)			Category 2 (%)	
		β based increase (case 1 to 3)	Share of base width		β based increase (case 3 to 5)	Share of base width (case 4)
			Case 2	Case 6		
8	62 to 92	27	29	54	9	17
9	84 to 125	30	25	43	10	3
10	288 to 371	38	20	42	10	10
11	263 to 370	24	30	61	10	40
12	310 to 361	25	30	40	5	40
13	93 to 157	40	30	75	15	40
14	82 to 126	32	25	45	13	12

When the valley is scaled by 2 from a slope of 1:1 to 2:1, the stress increase in the vicinity of maximum stress values is of the order of 6% at central section in all zones, with slightly higher increments in the upstream half of core. On plane no. 2 the stress increase is of the order of 10% in the upstream half and about 15% in the downstream half. Of this increase, the contribution of base width alone at central section is 70 to 95% in pervious zones and only 40 to 50% on core faces. The contribution of the base width at the core centre line is as low as only 20%. On plane no. 2, the share of base width to the stress increase is of the order of 15% in shells and about 40% in the interior.

It, therefore, emerges that the percentage increase in stresses is more for narrow and steeper valleys than for wide and flatter valleys. The increase is more in the interior than in the exterior zones on central section, while it is more in

the exteriors over plane no. 2. Of the increase in stresses due to the increase of base width and the valley slopes flattening, the contribution of base width alone is significant. It increases with the inclination of the valley walls from the vertical.

The effect of base width is the greatest in shells and the least in core, over central section. On plane no. 2 the contribution of base width is of the same order in all zones at a slope of 0.5:1, while at valley walls slope of 1:1, the core exhibits higher influence of base width.

As compared to the behaviour at central section, the effect of valley width factor over plane no. 2 is slightly more but the contribution of base width to the increase in stresses is smaller at this section.

6.3.2.2 Horizontal Normal Stress σ_y

The distribution of the longitudinal horizontal normal stress σ_y along height is shown in Figs. 6.8 and 6.9 for central section and plane no. 2 respectively. Typical values of σ_y at different verticals near their bottom along with the percentage increase for different cases are given in Tables 6.8 and 6.9 for the two sections.

A perusal of the tables shows that, the increase in stress due to the valley being scaled by 2 in y-direction from a slope of 0.5:1 is of the order of 30 to 45 % at central section and 20 to 30 % at plane no. 2, with the core exhibiting relatively higher increments.

Table 6.8 : Longitudinal Normal Stress σ_y (compression) at Central Section

Vert No.	Range of maximum values (for six cases) (t/sq m)	Category 1 (%)			Category 2 (%)	
		β based increase (case 1 to 3)	Share of base width		β based increase (case 3 to 5)	Share of base width (case 4)
			Case 2	Case 6		
1	72 to 97	27	32	60	4	58
2	92 to 133	39	30	58	9	38
3	283 to 455	46	31	65	10	37
4	310 to 453	40	28	56	10	25
5	311 to 430	29	29	61	7	38
6	115 to 153	30	30	37	5	70
7	96 to 140	38	27	54	7	52

Table 6.9 Longitudinal Normal Stress σ_y (compression) at Plane No.2

Vert No.	Range of maximum values (for six cases) (t/sq m)	Category 1 (%)			Category 2 (%)	
		β based increase (case 1 to 3)	Share of base width		β based increase (case 3 to 5)	Share of base width (case 4)
			Case 2	Case 6		
8	63 to 86	20	43	85	11	35
9	86 to 113	20	41	71	7	10
10	280 to 366	39	20	44	10	40
11	277 to 392	28	28	61	10	35
12	318 to 381	27	30	50	5	30
13	88 to 123	25	40	95	13	45
14	84 to 119	25	50	75	12	19

To this increase, the contribution of base width alone is of the order of about 30 % of the total increase at central section. On plane no. 2 the contribution of base width is

about 40 to 50 % in pervious zones and about 20 to 30 % in the core. Further multiplication of valley base width by 2 at a constant slope of 0.5:1 raises this contribution to about 55-60 % at central section. On plane no. 2 this increase is about 45-60 % in core and about 75 to 85 % in pervious zones.

When the valley is scaled by 2 in y-direction from a valley slope of 1:1 to 2:1, the stress increase on central section is small, of the order of 5 to 10%, with core exhibiting higher increments than pervious zones. On plane no. 2, the corresponding stress increase is of the order of 10 to 12 %. The contribution of base width to the stress increment at central section is approximately 50 to 55 % in shells and reduces to about 25 % at the core centre line. On plane no. 2, this contribution is about 35 % in core and 20 to 35 % in pervious zones.

Even though the increase in stress due to increase of both valley slope and base width is greater as compared to that for σ_x , the contribution of base width to the increase is smaller for σ_y . The effect of valley width on the stress increase is more or less of the same magnitude at all locations, with the core showing slightly higher values.

6.3.2.3 Vertical Normal Stress σ_z

Figures 6.10 and 6.11 show the vertical normal stress σ_z plotted along height for all the six cases analysed over central section and plane no. 2 respectively. The typical values of σ_z in the regions of high stress and the incremental percentages are shown in Tables 6.10 and 6.11 for the two planes.

It is noted from the tables that over central section, the β based increase from 0.5:1 slopes to 1:1 slopes obtained by scaling the y-coordinates by 2, is about 25-30 % in pervious zones and about 30 to 50 % in core. On plane no. 2, the corresponding increments are 50 to 55 % in pervious zones and about 30 to 50 % in core. The percentage stress increase is thus more in the upstream portion as compared to those in downstream portion.

Table 6.10 : Vertical Normal Stress σ_z (compression) at Central Section

Vert No.	Range of maximum values (for six cases) (t/sq.m)	Category 1 (%)			Category 2 (%)	
		β based increase (case 1 to 3)	Share of base width		β based increase (case 3 to 5)	Share of base width (case 4)
			Case 2	Case 6		
1	132 to 206	28	53	115	7	99
2	182 to 299	35	50	106	8	95
3	311 to 514	48	35	75	12	51
4	342 to 501	39	34	65	10	35
5	351 to 503	32	38	81	9	61
6	238 to 347	20	45	93	3	100
7	185 to 321	28	40	102	7	95

Over central section, the contribution of base width to the increases in stresses due to increase of base width as well as valley slopes is about 45-50 % in pervious zones and 35 % in core. On plane no. 2, the corresponding contributions are 20 to 25 % in pervious zones and 25 to 30 % in core. The base width effect is least at the centre line of core over central section and on the upstream face of core over plane no. 2.

Table 6.11 Vertical Normal Stress σ_z (compression)
on Plane No.2

Vert No.	Range of maximum values (for six cases) (t/sq m)	Category 1 (%)			Category 2 (%)	
		β based increase (case 1 to 3)	Share of base width		β based increase (case 3 to 5)	Share of base width (case 4)
			Case 2	Case 6		
8	105 to 190	45	25	45	15	19
9	143 to 271	50	20	45	18	7
10	299 to 402	40	20	44	14	5
11	306 to 429	28	27	60	6	35
12	370 to 457	28	30	45	6	-5
13	154 to 321	56	22	55	28	26
14	150 to 294	55	20	45	15	15

Further increase of valley base width to 80 m with valley slopes still at 0.5:1 raises the contribution of base width at central section to about 100 percent in pervious zones, 70-80 % in core and over plane no. 2 to about 45-50 % at all locations.

From a 1H:1V valley slope to 2:1 valley slope, the stress increase over those for 1:1 slope analysis is relatively small over central section, about 3 to 8 percent in pervious zones and about 10 percent in core. On plane no. 2, the β based increases are 15-20 % in pervious zones and about 6 % in core. The contribution of base width increase alone to this increment over central section is quite large (about 95 to 100 %) in pervious zones. In core, this contribution is about 50 to 60 % on the faces and about 35 % in the centre of core. On plane no. 2, the contribution of base width is about 15-25 % in pervious zones and only 5 % in core,

with higher contribution at the core centre line.

6.3.3 Stress Ratio

6.3.3.1 Horizontal stress Ratio σ_x/σ_y

The magnitudes of ratio σ_x/σ_y at different verticals in the regions of high stress magnitudes are given in Tables 6.12 and 6.13 for central section and plane no. 2 respectively.

A perusal of the tables shows that the core exhibits lowest ratios of σ_x/σ_y , while transitions exhibit highest σ_x/σ_y ratios. The upstream face of core has higher ratios of σ_x/σ_y than the downstream face. The upstream shell exhibits higher ratios than the downstream shell. On central section, the upstream transition has highest σ_x/σ_y ratio, while on plane no. 2 the downstream transition exhibits highest σ_x/σ_y ratios. In core, the ratio is less than unity over a major part of height, while in transitions the σ_x/σ_y ratio is more than unity over most of the height.

Table 6.12: Typical Values of Stress Ratio σ_x/σ_y at Central Section

Vert. No.	Ratio σ_x/σ_y for Case No.					
	1	2	3	6	4	5
1	0.98	1.01	0.94	1.04	0.98	0.98
2	1.27	1.29	1.15	1.31	1.16	1.09
3	0.97	0.97	0.93	0.95	0.93	0.91
4	0.99	0.99	1.00	0.99	0.99	1.00
5	0.90	0.89	0.87	0.88	0.87	0.86
6	1.24	1.28	1.06	1.28	1.09	0.99
7	0.90	0.91	0.79	0.88	0.79	0.80

Table 6.13: Typical Values of Stress Ratio σ_x/σ_y at Plane No.2

Vert. No.	Ratio σ_x/σ_y for Case No.					
	1	2	3	6	4	5
8	1.06	1.06	1.12	1.05	1.12	1.14
9	1.05	1.06	1.16	1.08	1.17	1.21
10	0.93	0.91	0.89	0.89	0.87	0.84
11	0.86	0.85	0.79	0.81	0.78	0.76
12	0.88	0.86	0.85	0.84	0.83	0.80
13	1.18	1.19	1.37	1.24	1.38	1.38
14	1.03	1.05	1.10	1.03	1.10	1.09

At a constant valley slope, the ratio of σ_x to σ_y marginally increases with the increase in valley base width. Over central section the σ_x/σ_y ratio in core is not affected significantly by the increase in valley base width. However, over plane no. 2, the σ_x/σ_y ratios in core decrease marginally with increase in valley base width at a given valley slope.

At constant base width the ratio σ_x/σ_y decreases with flattening of valley slopes. However, over plane no. 2, the ratio σ_x/σ_y in pervious zones increases with the increase in inclination of valley walls from the vertical.

Plane no. 2 exhibits higher stress ratio of σ_x/σ_y as compared to that at the central section on all locations.

6.3.3.2 Principal stress ratio σ_1/σ_3

The principal stress ratio σ_1/σ_3 is an indication of the shearing stability of the material. Higher the ratio σ_1/σ_3 , smaller is the factor of safety against shearing failure.

The typical values of σ_1/σ_3 corresponding to the locations

of maximum stress values in each case are given in Tables 6.14 and 6.15 for central section and plane no. 2 respectively.

Table 6.14: Typical Values of Stress Ratio σ_1/σ_3 at Central Section

Vert. No.	Ratio σ_1/σ_3 for Case No.					
	1	2	3	6	4	5
1	1.93	2.03	2.02	2.17	2.12	2.12
2	1.94	2.02	1.99	2.14	2.06	2.03
3	1.24	1.30	1.32	1.37	1.37	1.36
4	1.17	1.22	1.21	1.28	1.27	1.25
5	1.20	1.22	1.26	1.24	1.26	1.28
6	2.07	2.10	2.05	2.20	2.11	2.07
7	2.24	2.30	2.28	2.43	2.36	2.36

Table 6.15: Typical Values of Stress Ratio σ_1/σ_3 at Plane No.2

Vert. No.	Ratio σ_1/σ_3 for Case No.					
	1	2	3	6	4	5
8	2.59	2.58	2.42	2.60	2.40	2.33
9	2.71	2.70	2.55	2.68	2.53	2.44
10	1.71	1.73	1.78	1.76	1.78	1.80
11	1.73	1.75	1.77	1.72	1.76	1.84
12	1.61	1.64	1.64	1.66	1.66	1.71
13	2.58	2.56	2.43	2.55	2.43	2.33
14	2.82	2.82	2.66	2.83	2.66	2.55

It is noted from the tables that on central section, the principal stress ratios are maximum in shells and decrease towards the core, with the lowest values occurring at the core

centre line. On plane no. 2, the least values of σ_1/σ_3 are observed on the downstream face of core. On central section, the principal stress ratio σ_1/σ_3 increases with the valley base width at constant valley slope. At constant base width, with the flattening of valley wall, the ratio decreases in pervious zones, but increases in core. However, flattening the valley walls beyond 1:1 does not have any influence on the principal stress ratio. On plane no. 2, ratios σ_1/σ_3 are not affected by valley base width at a given slope. At constant base width with the increase in valley wall slope, the σ_1/σ_3 ratios decrease continuously in pervious zones and increase in core. The effect is, however, very small, at about 4-5 % at all locations.

As compared to central section, the psr values are higher at plane no. 2. However, the relative change in magnitudes of the psr due to change in valley slope is roughly of the same order on both the planes.

It is found that along height, the variation in σ_1/σ_3 ratio is small in all cases.

6.3.4 Mobilisation Factors

The values of mobilisation factors along typical sliding planes are given in Tables 6.16 and 6.17 for all 6 cases over central section and plane no. 2 respectively.

It is seen from the tables that in core, the mobilisation factors increase with increase in either of the valley base width and the valley wall slope. The incremental values are more for wider and steeper valleys and decrease with either of the base width and valley wall slope. At a base width of 40 m, the contribution of base width to the increase in

mobilisation factor values is about 60 % while it is less than 50 % at a base width of 80 m. On plane no. 2, however, at constant base width, the valley slopes do not have any appreciable influence on the mobilisation factors in core.

Table 6.16 : Mobilisation Factor m on Central Section

Vert. No.	Mobilisation Factor m for Case No.					
	1	2	3	6	4	5
1	0.32	0.34	0.34	0.37	0.36	0.36
2	0.29	0.31	0.29	0.34	0.31	0.31
3	0.33	0.36	0.41	0.40	0.43	0.45
4	0.26	0.29	0.32	0.34	0.35	0.37
5	0.27	0.30	0.32	0.33	0.34	0.37
6	0.44	0.48	0.45	0.52	0.50	0.49
7	0.39	0.40	0.40	0.45	0.40	0.42

Table 6.17 : Mobilisation Factor m on Plane No. 2

Vert. No.	Mobilisation Factor m for Case No.					
	1	2	3	6	4	5
8	0.46	0.46	0.45	0.46	0.44	0.42
9	0.52	0.51	0.47	0.50	0.47	0.42
10	0.31	0.33	0.33	0.34	0.34	0.34
11	0.26	0.29	0.30	0.31	0.32	0.33
12	0.33	0.32	0.32	0.36	0.33	0.32
13	0.70	0.69	0.62	0.67	0.63	0.58
14	0.57	0.57	0.52	0.57	0.52	0.48

In shells, on central section the values of m increase with valley base width but remain unaffected by valley wall

slope at a constant base width, for narrow valleys. For wider valleys, the mobilisation factors, at constant base width decrease with valley slope. There is no further influence of valley slope flattening beyond 1:1 slope. On plane no. 2, at constant valley slope the base width does not affect the mobilisation factors. At constant base width, however, the magnitudes of mobilisation factor decrease with the flattening of the valley.

It, therefore, follows that on central section, for shallow failure surfaces, a narrow valley has a higher factor of safety against sliding. At constant base width of valley, the factor of safety is more for a flatter valley as compared to a steep walled valley.

For a deep failure surface involving the core, on central section, the factor of safety decreases with increase in either of the valley base width and the inclination of the sides with the vertical. Therefore, a narrow valley exhibits a higher factor of safety against wedge failure as compared to a wider and flatter valley. It is also seen that the downstream face shows a lower factor of safety against sliding in comparison to the upstream face of the dam.

On plane no. 2, for a shallow failure surface a wide valley with flatter slopes gives a higher factor of safety than a narrow and steep walled valley. The base width influence is small as compared to that of the valley wall slopes.

For a wedge shaped failure surface on plane no. 2 passing through core, a narrow valley has a higher factor of safety against sliding. The valley wall slopes have no significant influence on the sliding stability.

As compared to the central section the values of mobilisation factors over plane no. 2 are higher in pervious zones but smaller in core. Therefore, a circular sliding surface has a lower factor of safety at this section but a wedge shaped failure surface involving core in the slide has a higher factor of safety against sliding as compared to that on the central section.

6.4 EFFECT OF VALLEY WALL SLOPE AT CONSTANT BASE WIDTH

The results of the 6 cases analysed above are studied to evaluate the effect of change of valley wall slope at constant base width. This study has been classified into two categories.

Category 1--> Valley base width = 40 m

The slopes studied are two, namely 0.5H:1V and 1H:1V

Category 2--> Valley base width = 80 m

The slopes studied are three, namely 0.5H:1V, 1H:1V and, 2H:1V

The results of parameters u , w , σ_x , σ_y and σ_z are discussed in the following paragraphs. In each category the increase in parameters is expressed as a percentage of the values of the first case in the category i.e., the analysis with valley slope of 0.5:1 at each base width. The two categories are representative of a narrow gorge and a normal gorge for siting of earth dams.

6.4.1 Displacements

6.4.1.1 Horizontal Movements - u

The average percentage increases in horizontal movements over the height at constant base widths over central section

are shown in Table 6.18.

Table 6.18: Incremental Horizontal Transverse Movement-u at Central Section

Vert. No.	Percentage increase of -u above the case of 0.5:1 slope for :		
	Category 1 b = 40 m 1H : 1V	Category 2 (b = 80 m)	
		1H:1V	2H:1V
1	42	23	44
2	31	13	22
3	20	18	25
5	21	19	30
6	25	14	22
7	51	26	45

It is evident from the table that the incremental displacements in category 1 are, about 20 % in core , 25-30% in transitions and 40-50 % in shells; in category 2 for a 1:1 slope, 18 % in core , 14 % in transitions and 25 % in shells. For a 2:1 slope in category 2, the increment is about 25-30 % in core , 22% in transitions and about 45 % in shells.

It is also noted that for a 1:1 slope in category 1 the percentage incremental displacements are highest on dam faces and decrease towards the core. In category 2, the transitions exhibit lowest percentage of incremental displacements and shells exhibit the highest.

In category 2, for a slope of 2:1, the incremental displacements are roughly twice of those for a 1:1 valley slope, except in core, where these are approximately 1.5 times of those of incremental percentages for a 1:1 slope.

The percentage increase in the horizontal movements over

those for a valley with valley slopes of $0.5H:1V$ are shown in Table 6.19 for different verticals over plane no. 2. In core the movements are smaller in magnitudes and a trend is, therefore, not emerging.

Table 6.19: Incremental Horizontal Transverse Movement - u at Plane No. 2

Vert. No.	Percentage increase of -u above the case of $0.5:1$ slope for:		
	Category 1 b = 40 m 1H : 1V	Category 2 (b = 80 m)	
		1H:1V	2H:1V
8	25	11	24
9	30	28	10
13	30	26	28
14	30	27	25

At a base width of 40 m the percent increase of horizontal movement in pervious zones is about 30 % while at a base width of 80 m the percent increase for both 1:1 and 2:1 slopes is of the order of about 25 %. On this plane, the flattening of valley wall slopes beyond 1H:1V has practically no influence on the displacements and the increase in displacements due to flattening of valley wall slopes is slightly higher for valleys with narrow base width.

6.4.1.2 Vertical Movements - w

The average percentage increase of settlements over height for the three cases (one in category 1 and two in category 2) are given in Table 6.20 for all the 7 locations over central section.

**Table 6.20: Incremental Vertical Movement - w
at Central Section**

Vert. No.	Percentage increase of -w above the case of 0.5:1 slope for :		
	Category 1 b = 40 m 1H : 1V	Category 2 (b = 80 m)	
		1H:1V	2H:1V
1	13	5	12
2	18	9	20
3	20	10	21
4	17	8	17
5	15	10	20
6	13	5	13
7	17	6	13

A perusal of Table 6.20 shows that in category 1, at a base width of 40 m the increase in valley slope to 1:1 from 0.5:1 results in incremental settlements of 13 to 18 % in pervious zones and about 15-20 % in core.

In category 2, at a base width of 80 m, for a slope increase to 1:1 from 0.5:1 the incremental settlements are about 5-6 % in pervious zones and 8 to 10 % in core. For an increase in slope to 2:1 from 0.5:1 the incremental displacements are about 17-20 % in core and about 15 % in pervious zones. The incremental displacements for a slope of 2:1 are roughly twice of those for a valley slope of 1:1.

The percentage increase of vertical settlements at different base width over plane no. 2 are given in Table 6.21. It is noted from the table that at a base width of 40 m when the valley slopes are flattened from 0.5:1 to 1:1 the settlements increase by about 12 to 15 % at all locations with

slightly lower increase in downstream shell.

**Table 6.21: Incremental Vertical Displacement-w
On Plane No. 2**

Vert. No.	Percentage increase of -w above the case of 0.5:1 slope for :		
	Category 1 b = 40 m 1H : 1V	Category 2 (b = 80 m)	
		1H:1V	2H:1V
8	12	5	5
9	15	18	21
10	14	8	12
11	13	5	14
12	15	17	24
13	12	8	11
14	8	1	1

At base width of 80 m, the percentage increments in the values of settlements, for a slope increase to 1:1 from 0.5:1, are about 5 to 10 % every where, except in shells where it is almost negligible. For a slope increase to 2:1 from 0.5:1 the incremental settlements are about 15-20 % in transitions and core. In shells the increase in valley wall slope beyond 1:1 has no influence on settlements. The influence of slope flattening is thus more for a valley with narrow base width than for a valley with wide base and is lowest in shells.

6.4.2 Stresses

6.4.2.1 Horizontal stress σ_x

The incremental stresses in the regions of higher stress values over those for valleys with valley wall slope of 0.5:1, for two valley base widths are given in Table 6.22 for all

seven locations over central section.

Table 6.22: Incremental Transverse Normal Stress σ_x On Central Section

Vert. No.	Percentage increase of σ_x above the case of 0.5:1 slope for :		
	Category 1 b = 40 m 1H : 1V	Category 2 (b = 80 m)	
		1H:1V	2H:1V
1	12	6	6
2	10	5	5
3	22	14	19
4	26	17	28
5	16	11	15
6	9	4	1
7	17	10	11

From a perusal of the table it is noted that, the percentage increase in stress σ_x at a base width of 40 m is about 10-15 % in pervious zones and about 15-25 % in core. At base width of 80 m, the stress increase for a slope of 1:1 is of the order of about 15 % in core and about 5-7 % in pervious zones of the dam. When the slope is further increased to 2:1, there is no further increase of stress in pervious zones of the dam, In core, however, the incremental stress σ_x is between 15-25 % of the stresses with the analysis for slopes of 0.5:1.

The percent incremental stress values for σ_x are given in Table 6.23 at different locations over plane no. 2. It is noted from the table that at a base width of 40 m, when the valley slopes are changed from 0.5H:1V to 1H:1V the stresses increase by about 25 % in pervious zones of the dam and by 15 %

in core. At a base width of 80 m, for a slope change from 0.5:1 to 1:1 the stress increase in pervious zones is about 16 % and in core about 12 % for a slope change from 0.5:1 to 2:1, the stress increase is about 28 % in pervious zones and about 15 % in core.

Table 6.23: Incremental Transverse Normal Stress σ_x at Plane No. 2

Vert. No.	Percentage increase of σ_x above the case of 0.5:1 slope for :		
	Category 1 b = 40 m 1H : 1V	Category 2 (b = 80 m)	
		1H:1V	2H:1V
8	25	15	26
9	26	14	28
10	17	13	14
11	17	12	19
12	11	7	2
13	24	17	30
14	27	17	30

The incremental stresses are more in pervious zones than in core. In core, the downstream face of core exhibits the lowest incremental stress due to increase of valley slopes.

6.4.2.2 Horizontal longitudinal stress σ_y

The incremental stress values for σ_y are given in Table 6.24 for all the verticals over central section.

From a perusal of the table it is observed that at a base width of 40 m at a slope of 1:1, the incremental stress is approximately 25 % in core and about 15-24 % in pervious zones of the dam. At a base width of 80 m at a slope of 1:1,

the incremental stress is about 17 % in core and about 15 % in pervious zones. At base width of 80 m for a slope of 2:1, the incremental stress is about 25 % in core and about 20 % elsewhere. For a slope of 2:1 the incremental stress in pervious zones is substantially larger than that for a slope of 1:1.

Table 6.24 Incremental Longitudinal Normal Stress σ_y at Central Section

Vert. No.	Percentage increase of σ_y above the case of 0.5:1 slope for:		
	Category 1 b = 40 m 1H : 1V	Category 2 (b = 80 m)	
		1H:1V	2H:1V
1	15	8	9
2	20	13	17
3	27	17	24
4	26	18	27
5	19	13	17
6	24	20	26
7	23	14	17

The percent incremental stresses over plane no. 2 at different verticals in the region of high stresses are given in Table 6.25. It is observed from a perusal of table that at a basewidth of 40 m, when the valley slope increases to 1:1 from 0.5:1, the stresses σ_y increase by about 11-18 % . At a base width of 80 m, for a slope increase to 1:1 from 0.5:1, the stresses increase by about 7 % in pervious zones and by about 12 % in core; for a slope increase to 2:1 from 0.5:1, the stresses increase by about 15 % on all locations with a low value (3 %) on the downstream face of core.

Table 6.25: Incremental Longitudinal Normal Stress σ_y at Plane No. 2

Vert. No.	Percentage increase of σ_y above the case of $\emptyset.5:1$ slope for :		
	Category 1 b = 40 m 1H : 1V	Category 2 (b = 80 m)	
		1H:1V	2H:1V
8	18	7	15
9	16	5	13
10	17	12	13
11	18	13	21
12	11	7	3
13	12	6	13
14	18	7	16

The incremental stresses in case of σ_y are less than those for σ_x . Just as for σ_x the influence of valley slope change on σ_y is lowest on the downstream face of core. The upstream half of the core exhibits slightly higher influence of slope as compared to the pervious zones of the dam.

6.4.2.3 Vertical Normal Stress σ_z

The incremental stress in the regions of maximum values for σ_z are given in Table 6.26 for two base widths at different verticals over central section. A perusal of table makes it clear that with a base width of 40 m, when the slope is increased to 1:1 from $\emptyset.5:1$, the stresses σ_z increase by about 15-25 % in core and 15-20 % in pervious zones of the dam. At a base width of 80 m, when the slope is increased from $\emptyset.5H:1V$ to a slope of 1:1, the stress increase is about 10-15 % in core and about 5-10 % in pervious zones of the dam; for a

slope of 2:1, the stress increase is again of the same order as that for 1:1 in pervious zones and about 15-20 % in core, i.e., the valley walls slope has no influence in pervious zones for valleys flatter than 1:1 from vertical, and the influence of valley slope is restricted only to the core of the dam.

Table 6.26: Incremental Vertical Normal Stress σ_z at Central Section

Vert. No.	Percentage increase of σ_z above the case of 0.5:1 slope for :		
	Category 1 b = 40 m 1H : 1V	Category 2 (b = 80 m)	
		1H:1V	2H:1V
1	14	6	6
2	20	11	12
3	27	16	22
4	22	15	22
5	17	11	14
6	16	7	6
7	23	12	14

The percent incremental stress values for σ_z for plane no. 2 at different locations in dam are given in Table 6.27. It is noted from the table that at a base width of 40 m, for a valley slope increase from 0.5:1 to 1:1, the vertical normal stresses σ_z increase by about 45 % in pervious zones and by about 17 % in core. At a base width of 80 m, for a valley slope change from 0.5:1 to 1:1 the vertical normal stresses increase by about 30 % in pervious zones and by about 13 % in core; for a valley slope change from 0.5:1 to 2:1 the stresses increase by about 15-20 % in the upstream half of core. The stress increase on the downstream face is very low at 5 % i.e., there

is a fall in stress as compared to those for a 1:1 slope.

Table 6.27: Incremental Vertical Normal Stress σ_z at Plane No. 2

Vert. No.	Percentage increase of σ_z above the case of 0.5:1 slope for :		
	Category 1 b = 40 m 1H : 1V	Category 2 (b = 80 m)	
		1H:1V	2H:1V
8	41	27	48
9	45	30	57
10	19	14	15
11	17	13	20
12	14	9	5
13	43	33	60
14	48	32	58

6.5 CONCLUSIONS

Based upon the results presented in this chapter the following conclusions are arrived at.

1. When valley wall slope as well as valley base width is increased simultaneously, both the stresses and displacements increase. The contribution of base width to this increase is substantial even though it does not appreciably increase the valley width factor.
2. When the valley is widened by multiplying both the base width and wall slope of 0.5:1 by 2, the contribution of base width to the overall stress increase is about 30-50 % at central section and about 20-30 % over plane no. 2. Further multiplication of base width alone by 2 raises the share of base width to the overall stress increase in

shells to 80-100 % and 50-60 % at central section and plane no. 2 respectively. The corresponding contribution of base width to stress increase in core is about 50-60 % and 40-60 % respectively.

3. When the valley is widened by multiplying 1:1 slope and base width by 2, the contribution of base width alone to the overall stress increase is about 70-90 % in pervious zones and 40-50 % in core, at central section. At plane no. 2 the corresponding contribution of base width increase alone is 15-25 % in pervious zones and about 35 % in core.
4. Though the stress increase due to both valley wall slope flattening and valley base width increase is more at plane no. 2 as compared to that at central section, the base width contribution to the total stress increase at central section is more than that at plane no. 2.
5. At constant base width the effect of slope on stresses depends upon the base width of the valley and is more for narrower base widths.
6. The effect of slope flattening at constant base width is more on sections towards the abutments as compared to that on central section. At central section, flattening the valley slopes beyond 1:1 has practically no influence on the stresses in pervious zones and only marginal effect in core.

On plane no. 2 the stresses increase with increase in the flatness of the valley walls at a constant base width, the increment in pervious zones being more than that in core.

7. The principal stress ratios and the mobilisation factors

are influenced by the valley base width and slope as given below in Table 6.28.

Table 6.28: Mobilisation Factors and Principal Stress Ratio

Plane No.	Influence of width at constant slope	Influence of slope at constant width
1.	Increase in all Zones	Slight decrease in pervious Zones. Slight increase in core.
2.	No change in pervious zones Increase in core	Slight decrease in pervious Zones. Slight increase in core.

8. A sliding surface passing largely through pervious zones has a higher factor of safety in a narrow valley at central section and in a wider valley at sections towards the abutments. A valley with flatter wall slopes has a higher factor of safety against sliding as compared to that for a steep walled valley. The influence of base width is more at central section while at plane no.2 the slopes play a dominant role in the sliding stability.

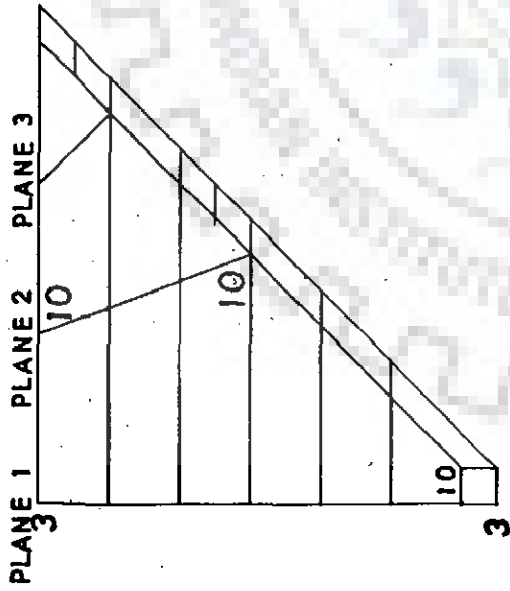
For a deep failure surface involving the core, a valley with narrow base width and steeper wall slopes is more safe against sliding as compared to a wider and flatter valley. The effect of valley wall slope on the safety factor against sliding is negligible on sections near the abutments but substantial on central section.

9. The increase in displacements when the valley slopes as well as base width are multiplied by 2 from 0.5:1 slope to 1:1, is of the order of 40 % for horizontal displacements and 30 % for vertical displacements on the central section. On plane no. 2, the percentage increase is

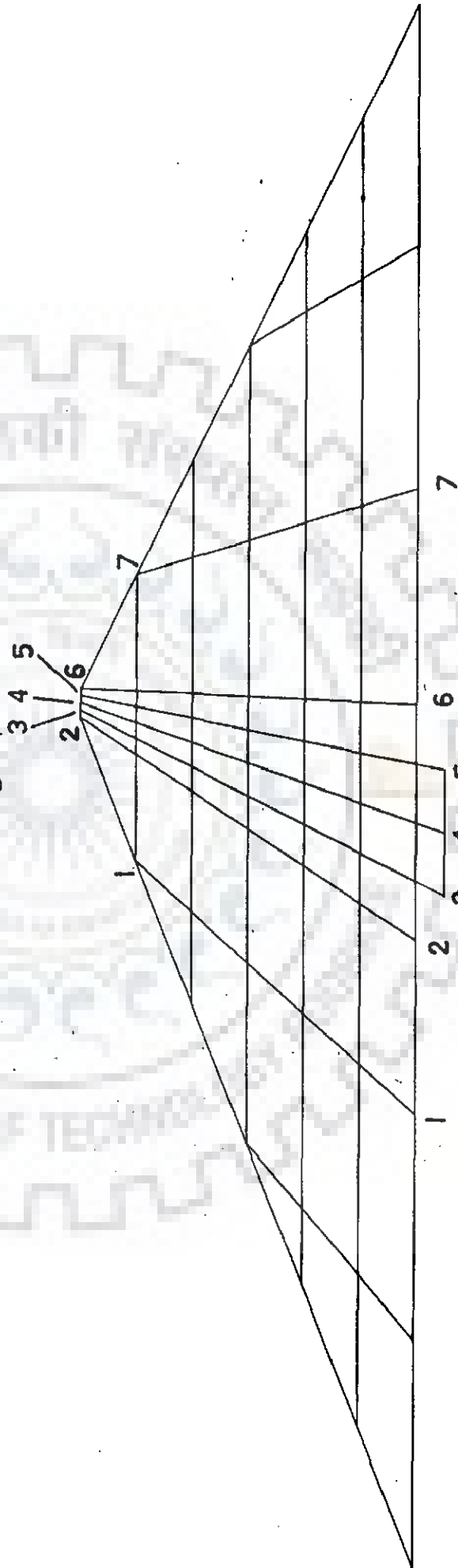
comparatively smaller. Of the total increase, about 30 to 40 % at central section and 20-30 % at plane no.2 is due to base width increase alone. A further increase in base width with slopes still at 0.5:1 raises the base width share to the incremental displacements to about 70-100 % at central section. It means that base width plays a far greater role than valley slopes in the displacements. The role of base width is far more pronounced at central section than at plane no. 2.

Scaling the y-coordinates of the valley by 2 from valley wall slopes of 1:1 to 2:1 results in about 25 % increase in displacement over central section and about 8-10 % at plane no. 2. The contribution of base width increase to these incremental displacements is about 50-55 %.

10. At a constant base width the displacements increase with the increasing flatness of the valley slopes on central section. On plane no. 2 , however, the displacements in the pervious zones of the dam are not affected by valley wall slopes increase beyond 1:1 slope.



(a) Longitudinal Section Along Upstream Face of Core



(b) Maximum Transverse Section of Dam

Fig 6.1 : FINITE ELEMENT IDEALISATION OF THE DAM

LEGEND
CASE 1 ○
CASE 2 △
CASE 3 +
CASE 4 ×
CASE 5 ◇
CASE 6 †

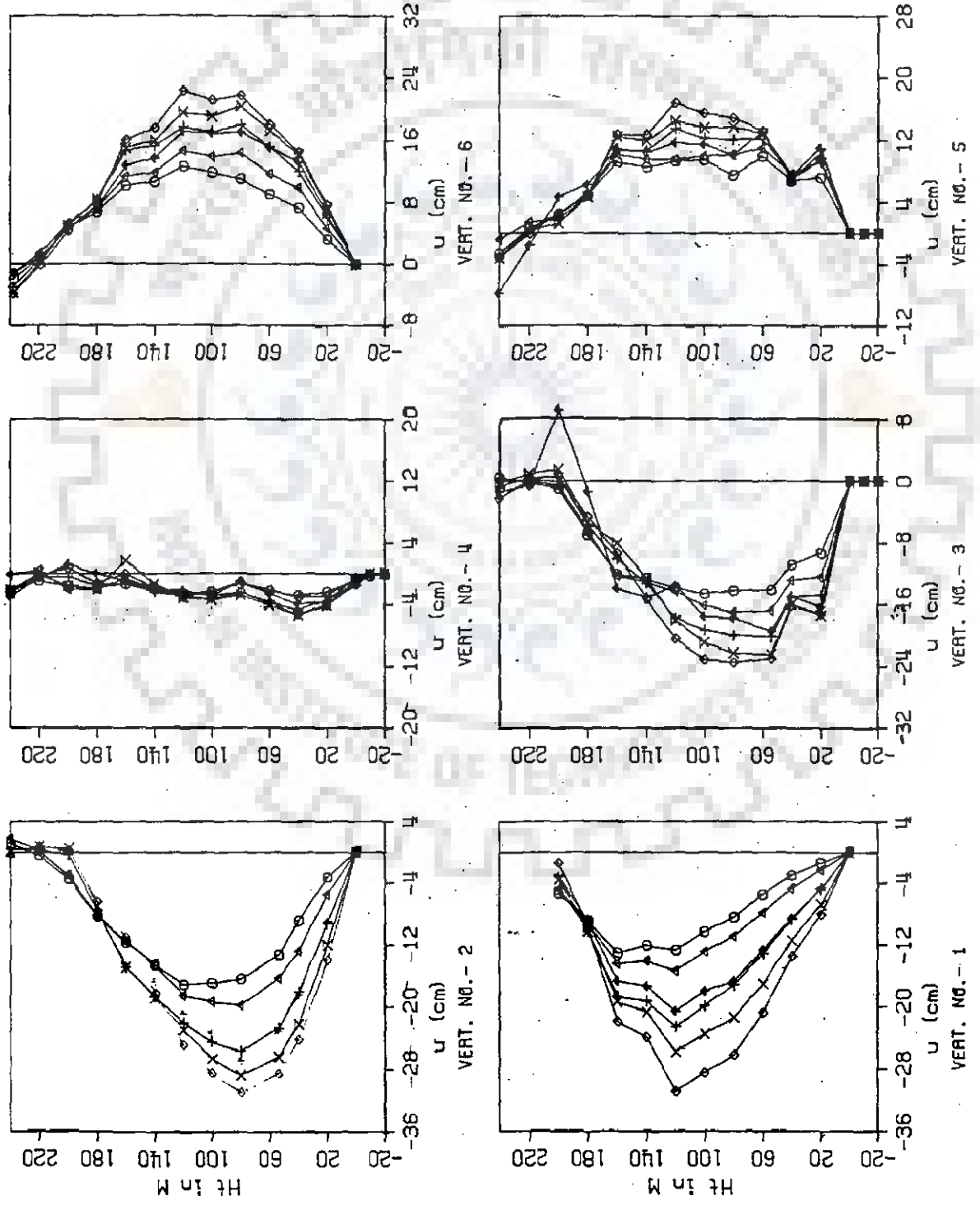








Fig 6.2 : Horizontal Movement - u Along Height Over Central Section

- LEGEND**
- CASE 1 
 - CASE 2 
 - CASE 3 
 - CASE 4 
 - CASE 5 
 - CASE 6 

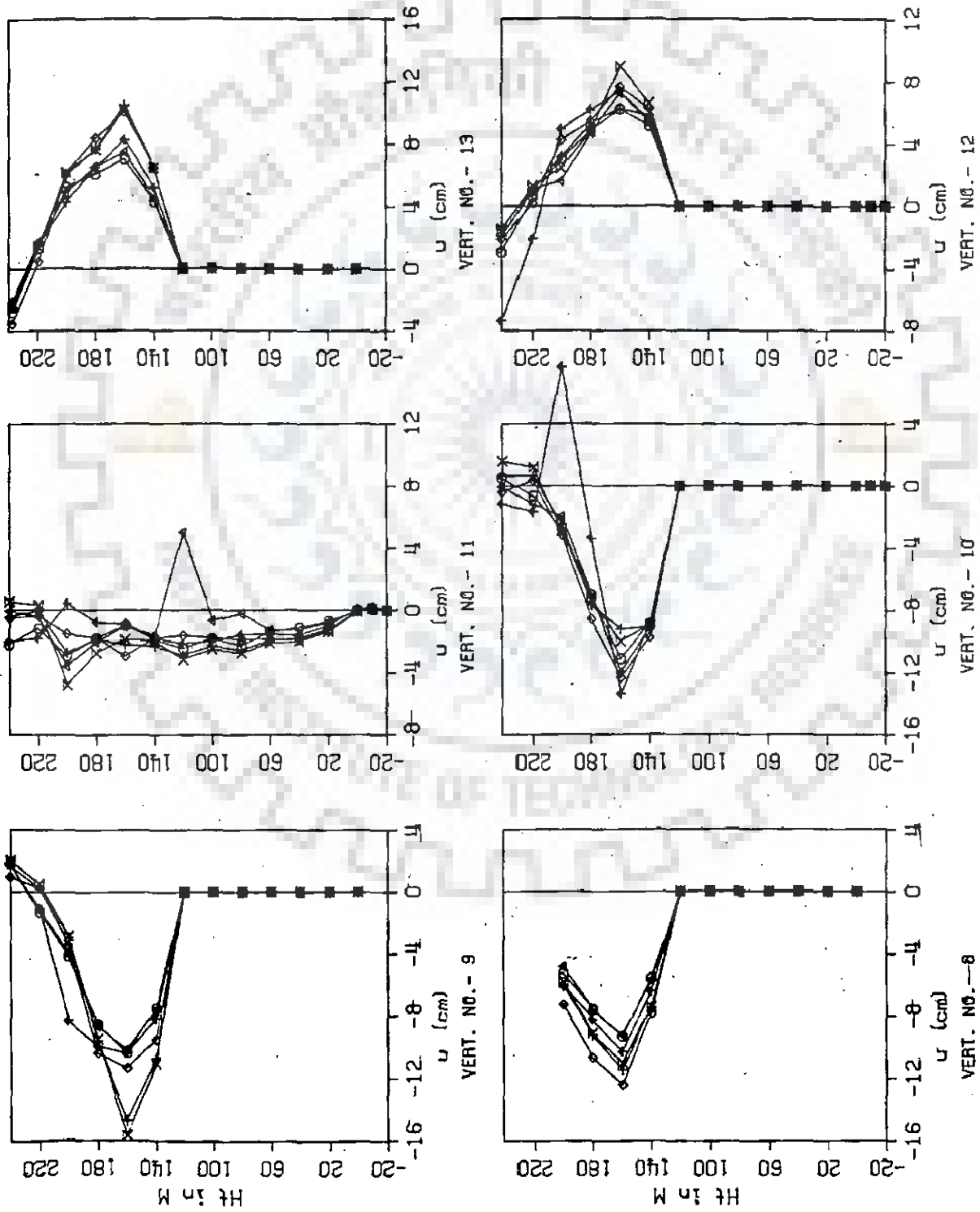


Fig 6.3 : Horizontal Movement - u Along Height Over Plane No. 2

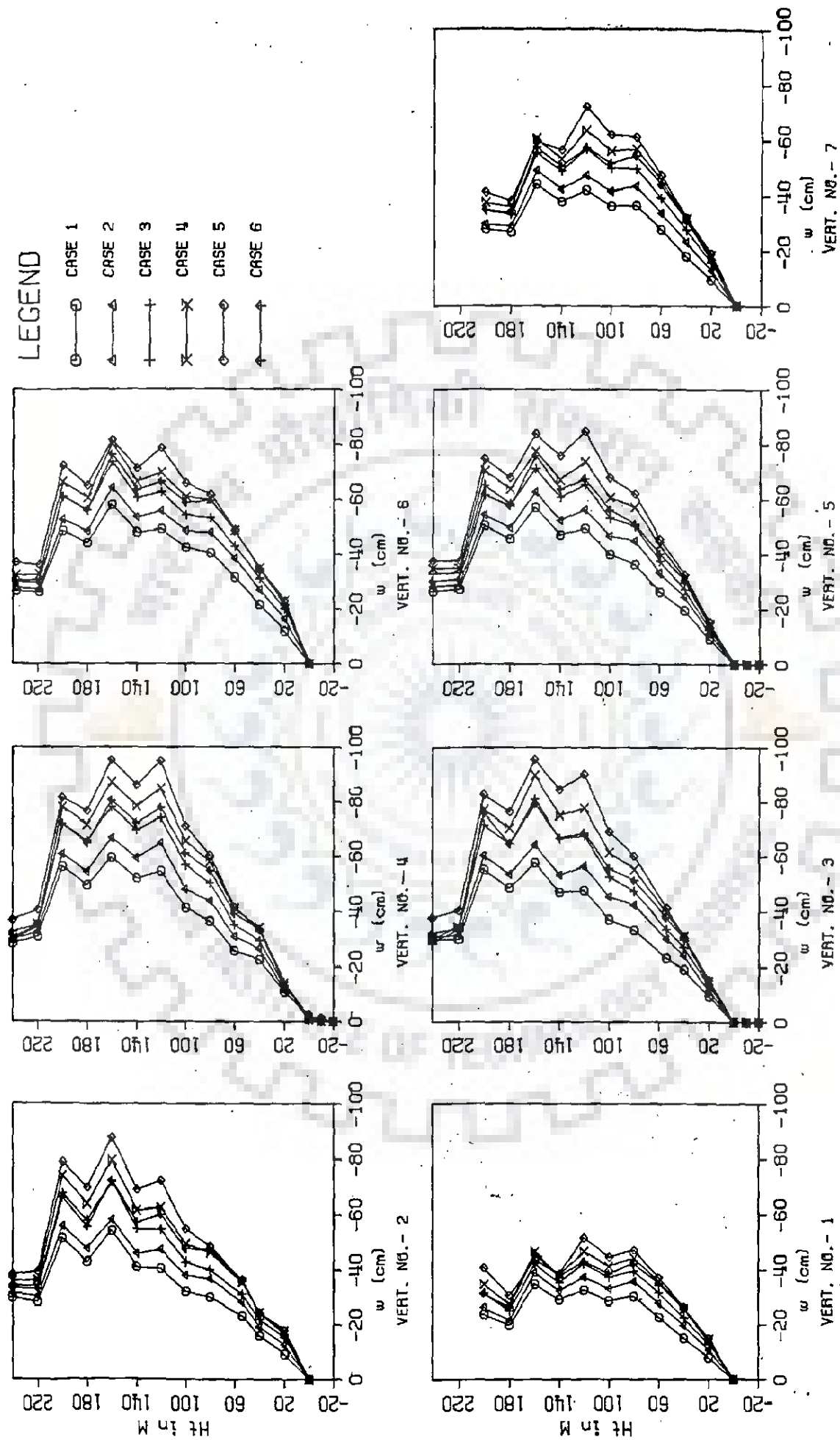








Fig 6.4 : Vertical Movement -w Along Height Over Central Section

LEGEND

- CASE 1 
- CASE 2 
- CASE 3 
- CASE 4 
- CASE 5 
- CASE 6 

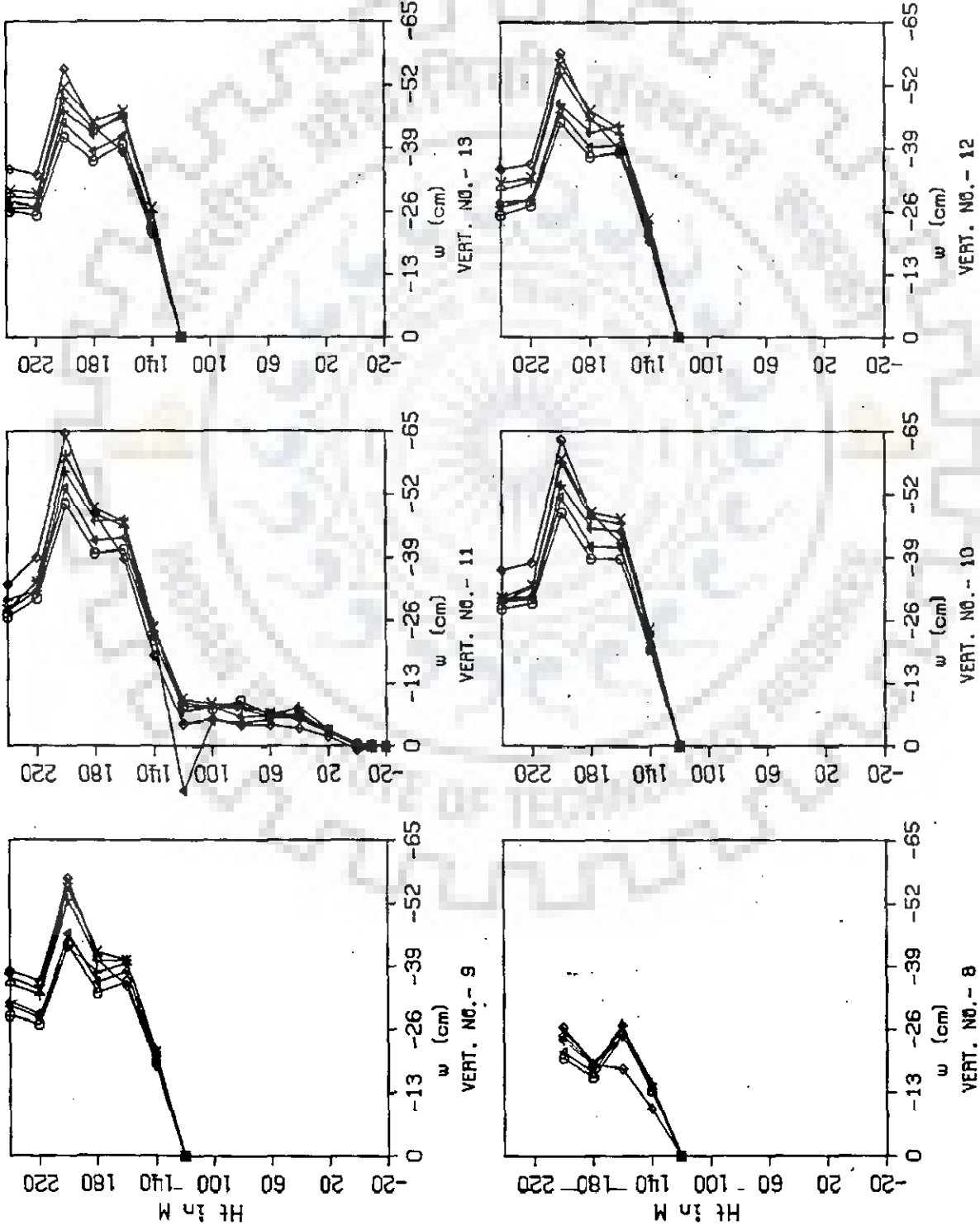








Fig 6.5 : Vertical Movement -w Along Height Over Plane No. 2

- LEGEND**
- CASE 1 
 - CASE 2 
 - CASE 3 
 - CASE 4 
 - CASE 5 
 - CASE 6 

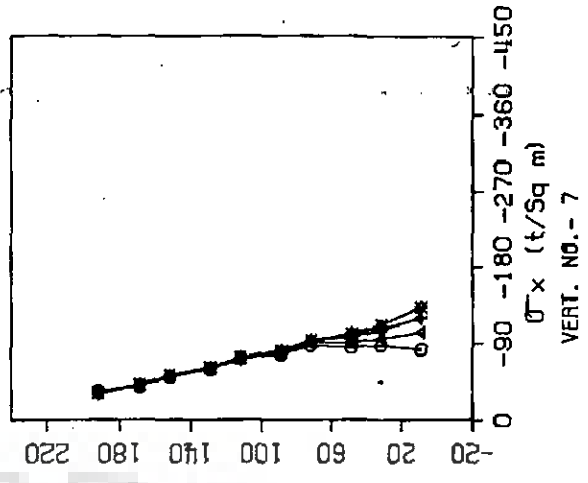
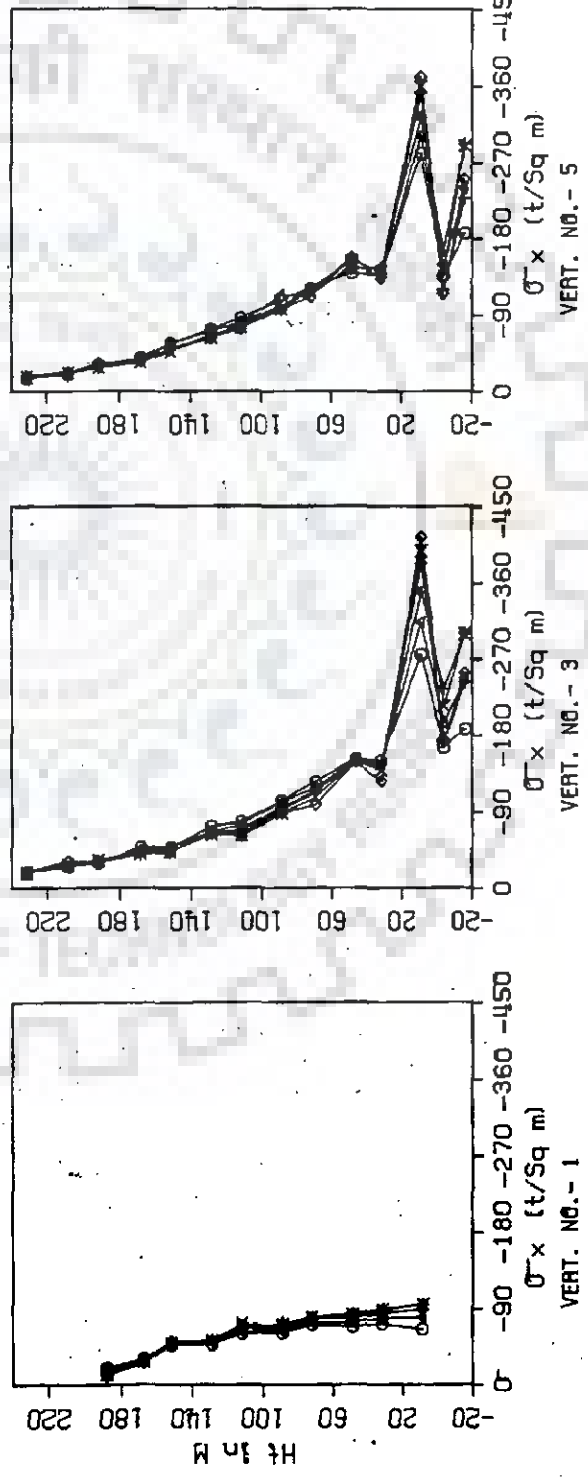
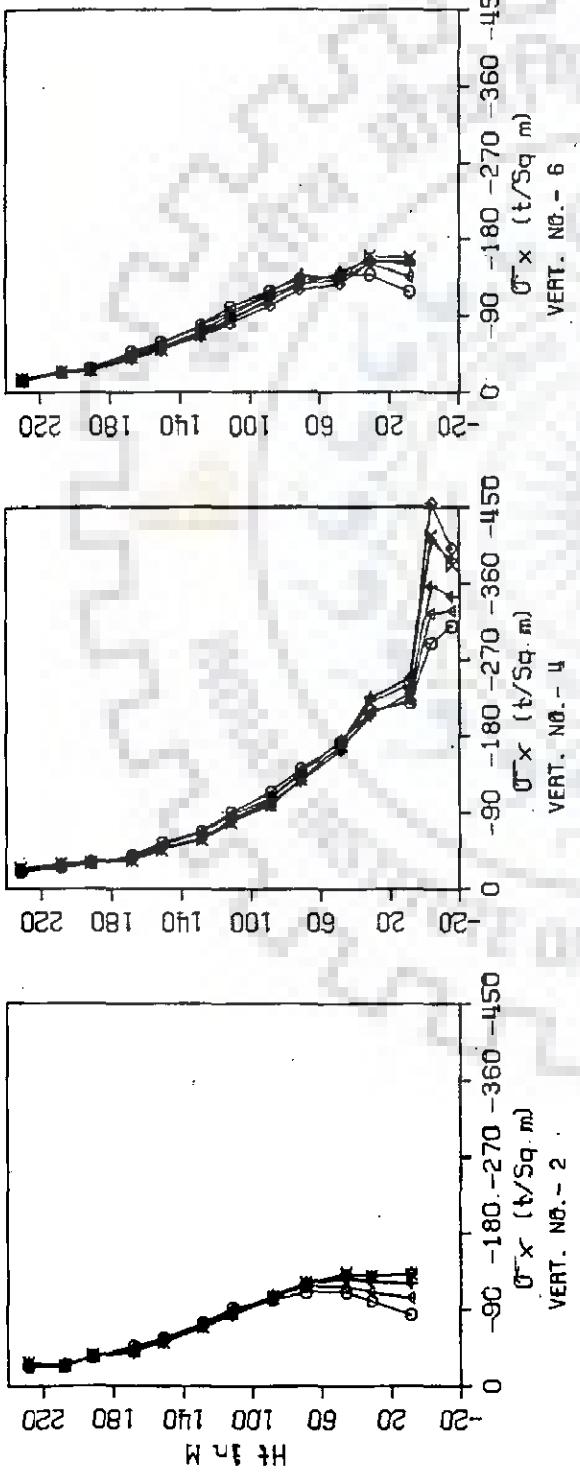


Fig 6.6 : Transverse Stress σ_x Along Height Over Central Section

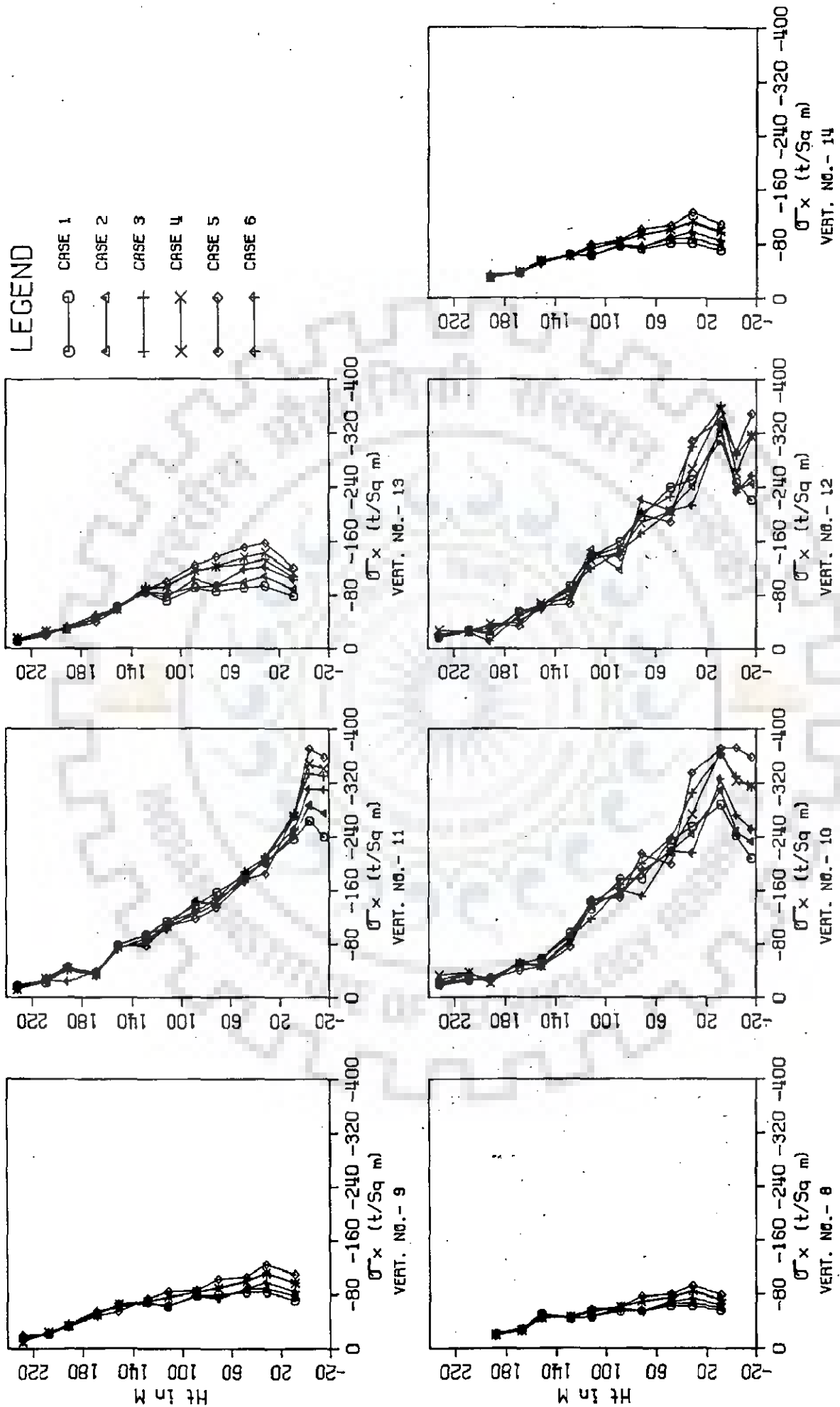


Fig 6.7 : Transverse Stress σ_x Along Height Over Plane No. 2

LEGEND
 CASE 1 ○
 CASE 2 △
 CASE 3 †
 CASE 4 ×
 CASE 5 ◇
 CASE 6 ‡

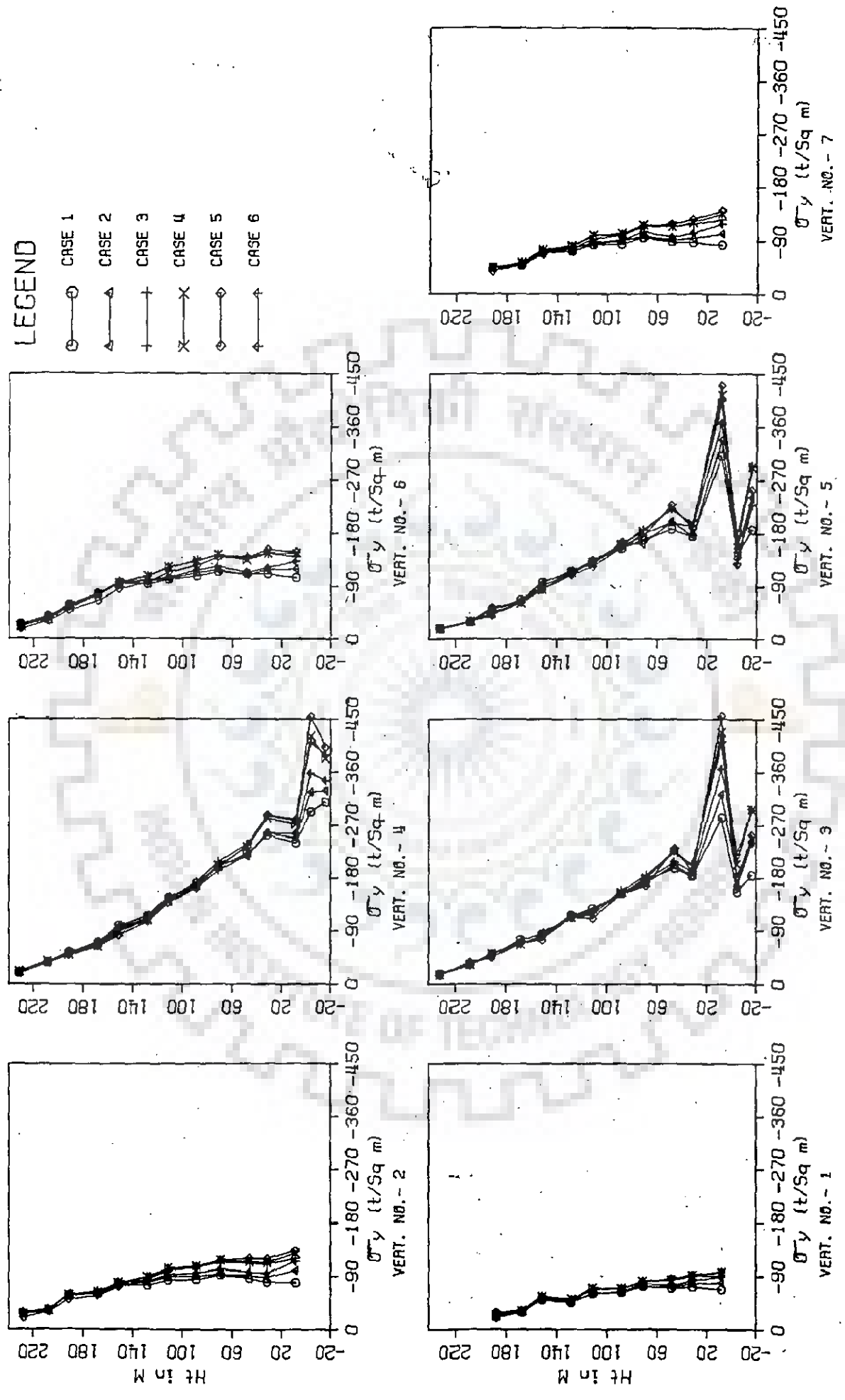


Fig 6.8.: Longitudinal Stress σ_y Along Height Over Central Section

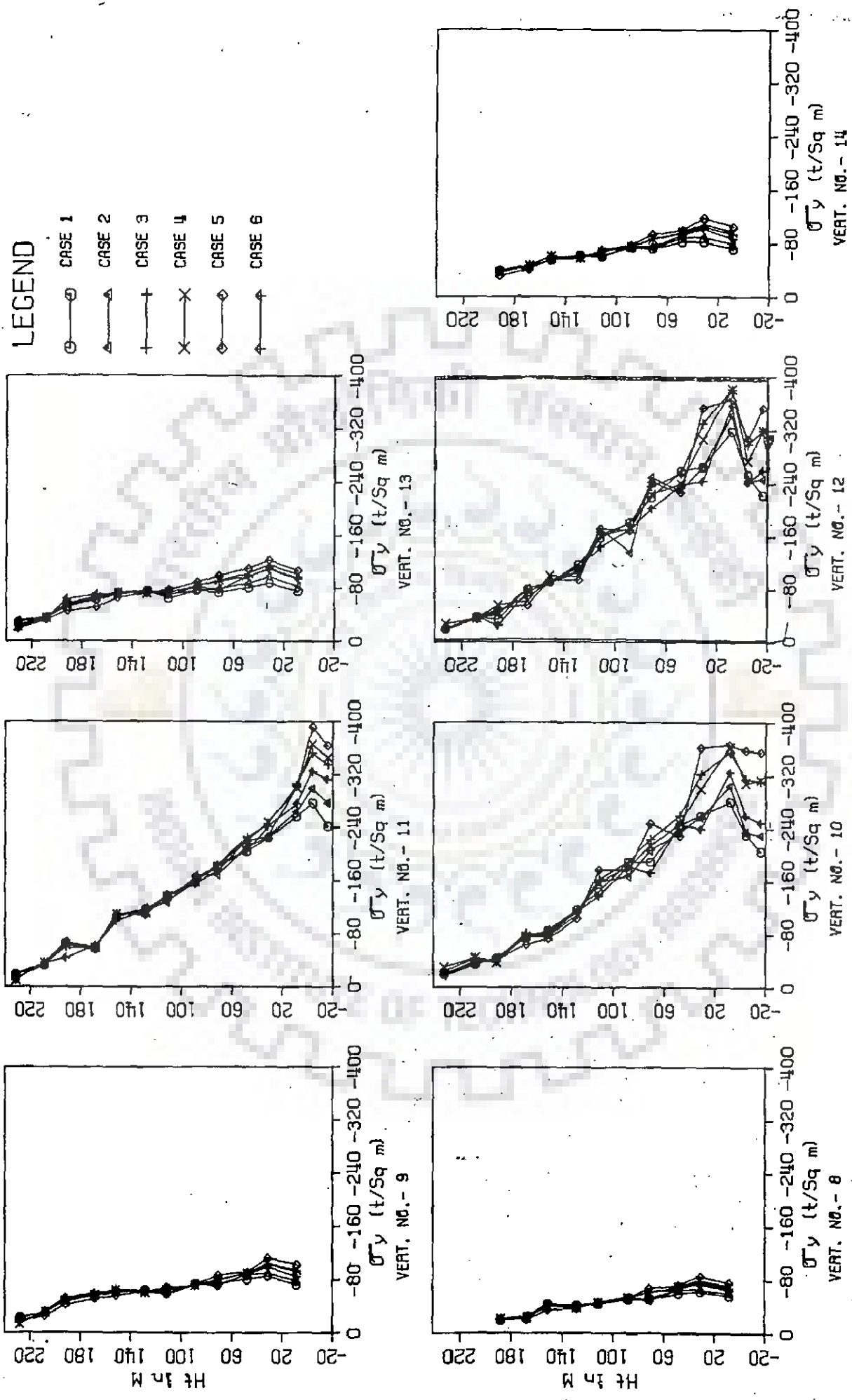




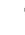



Fig 6.9 : Longitudinal Stress σ_y Along Height Over Plane No. 2

- LEGEND**
- CASE 1 
 - CASE 2 
 - CASE 3 
 - CASE 4 
 - CASE 5 
 - CASE 6 

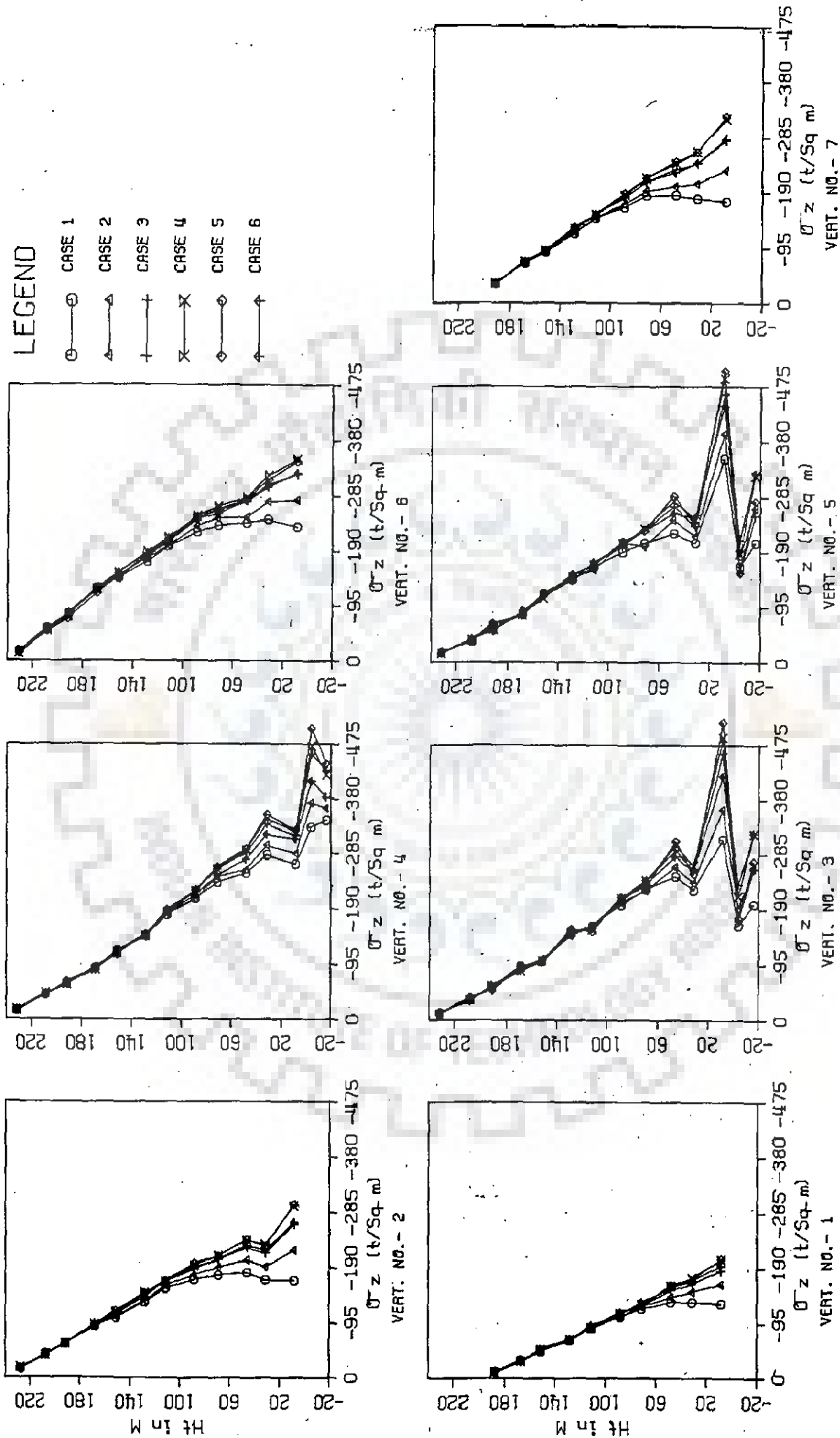


Fig 6.10 : Vertical Stress σ_z Along Height Over Central Section

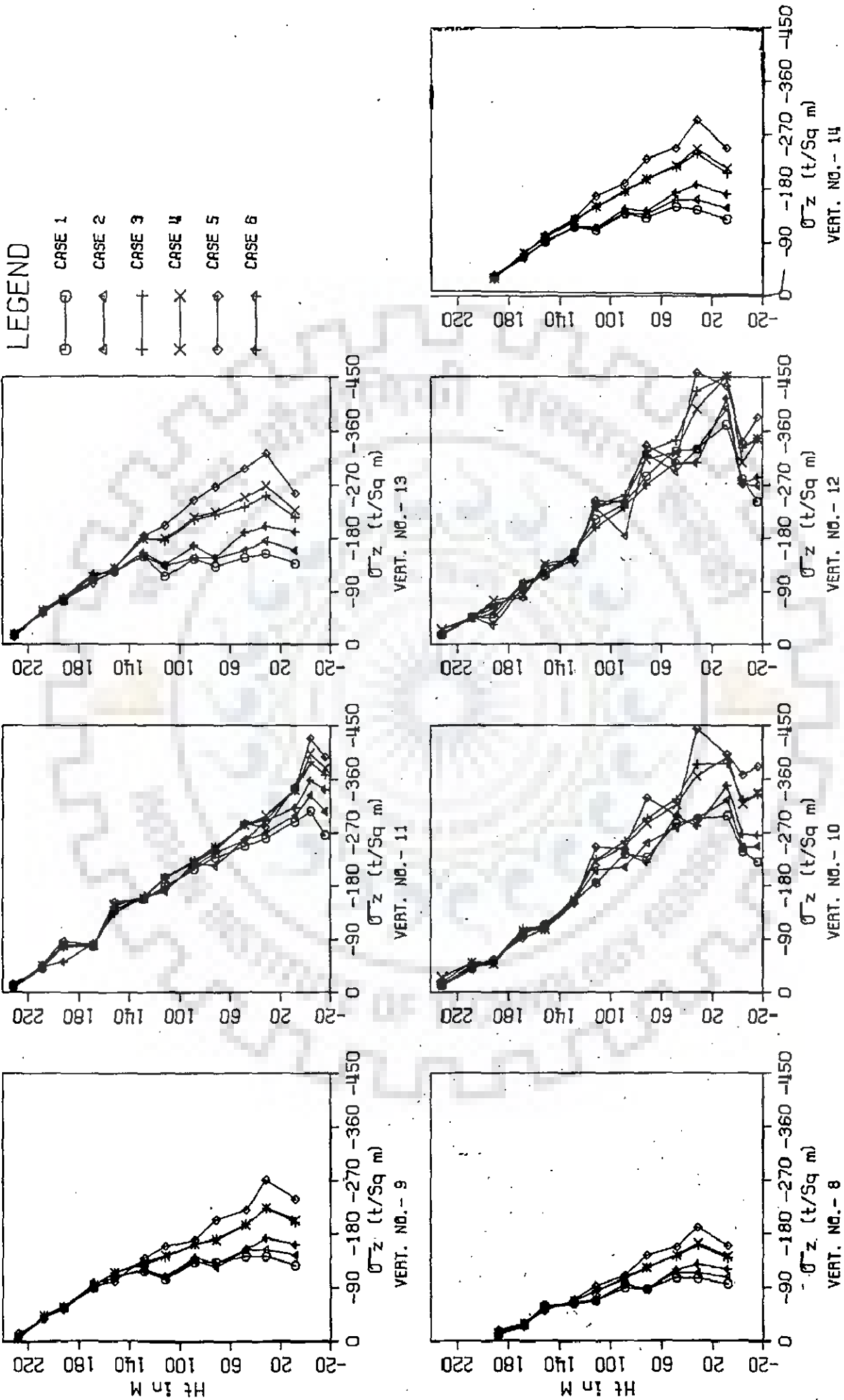


Fig 6.11 : Vertical Stress σ_z Along Height Over Plane No. 2

CHAPTER 7

EFFECT OF MATERIAL PROPERTIES ON DAM BEHAVIOUR

7.1 INTRODUCTION

The properties of the materials constituting the dam have an important bearing on the dam behaviour. A number of studies have confirmed the influence (21,38) of material properties on the performance of dams. All the studies reported so far are based on 2-D analysis of dams. No study has so far been reported on the influence of material properties on dams situated in narrow valleys in which 3-D effects can not be ignored.

To fulfill this gap, a study has been carried out to study the behaviour of the dam with different material properties. Since the core properties are likely to have greater variation and would also have greater influence on the safety of dam, in this study only the core properties have been varied. Three-Dimensional analyses have been done for four different values of stiffness modulus, K , of core, of a dam situated in a narrow valley. All other properties of core and other zones remain unchanged, as used in Chapters 5 and 6.

In Chapter 5 it has been found that the stresses and displacements in the dam increase with increase in the valley width factor. That study has been done for a given set of material properties. Since the material properties are going to affect the performance of the dam, the conclusions drawn with regard to the effect of valley width might be affected by the change in material properties. To ascertain this effect, a study has been made of the effect of valley shape at two different sets of material properties.

7.2 CASES STUDIED

(1) To assess the effect of core stiffness on the dam behaviour, the same valley has been used in all the analyses, with valley width factor, $\beta=2.25$. The values of modulus number, K , for core are taken as 100, 250, 400 and 1000. These values still represent a core softer than the shell.

(2) To study the effect of valley width at different material properties, the following cases have been studied :

(A) with $K = 400$: (i) $\beta=2.25$ (ii) $\beta=4.5$

(B) with $K = 1000$: (i) $\beta=2.25$ (ii) $\beta=4.5$

The dam section and the valley shapes are the same as in Chapter 5. The values of stresses and displacements have been studied along the 7 verticals in shells, transitions and core on central section and plane no. 2.

7.3 RESULTS

7.3.1 Different Values of K at Constant Valley Width, Case(1)

7.3.1.1 Stresses

The three normal stresses σ_x , σ_y and σ_z are plotted at different verticals over central section in Figs. 7.1 to 7.3. It is observed that all over the height in shells the stresses remain practically unaffected by the change in value of K for core; in transitions the stresses decrease with increase in value of modulus number K and in core the stress values increase with K . It is seen that the effect of K value on stresses is smallest for σ_x and maximum on vertical normal stress σ_z .

The typical maximum values of the stresses at different verticals and the general ratio of the stress values for

K=250, 400 and 1000 to the values with K=100 are given in Tables 7.1 to 7.3 for the three stresses.

Table 7.1: Horizontal Normal Stress σ_x Over Central Section

Vert No.	Maximum Values of σ_x for K of core				Ratio r^* (%) for K		
	100	250	400	1000	250	400	1000
1	-83	-81	-80	-78	98	97	94
2	-192	-167	-150	-120	87	78	63
3	-258	-292	-302	-310	113	117	120
4	-303	-329	-336	-347	109	111	115
5	-254	-284	-297	-328	112	117	129
6	-175	-173	-166	-151	99	95	86
7	-105	-105	-104	-103	99	99	98

* r = Stress at a given value of K expressed as percentage of the stress at K = 100

Table 7.2: Horizontal Normal Stress σ_y Over Central Section

Vert No.	Maximum Values of σ_y for K of core				Ratio r (%) for K		
	100	250	400	1000	250	400	1000
1	-83	-81	-80	-80	98	96	96
2	-122	-116	-111	-101	95	91	83
3	-251	-291	-304	-320	116	121	128
4	-304	-329	-337	-346	108	111	114
5	-263	-307	-331	-396	117	126	151
6	-136	-134	-129	-116	98	95	86
7	-107	-107	-107	-106	100	100	99

From a perusal of the tables along with those of the corresponding figures it is found that in shells, all the three

stresses decrease with increasing values of K . The decrease, however, is very small and is of no practical significance. On the upstream side of core, the stresses in shell decrease by about 5% for increase of K from 100 to 1000. In the downstream shell the corresponding stress decrease is less than 1 percent.

In transitions also the stresses decrease with increasing values of K . The reduction in stresses with K , on the upstream side is found to be maximum for σ_x and minimum in case of σ_z . The decrease varies from 5 to 15% in case of σ_z and from 15 to 35% in case of σ_x . In the downstream transition the case is just opposite i.e maximum reduction in case of σ_z (5 to 15%) and minimum reduction in case of σ_x (1 to 15%). In case of σ_y the reduction is same on both sides and ranges from 5 to 15% for an increase of K , from 100 to $K=1000$.

Table 7.3: Vertical Normal Stress σ_z Over Central Section

Vert. No.	Maximum Values of σ_z for K of core				Ratio r (%) for K		
	100	250	400	1000	250	400	1000
1	-174	-167	-164	-163	96	94	94
2	-256	-252	-245	-223	98	95	87
3	-265	-309	-323	-337	117	122	130
4	-335	-365	-374	-386	109	114	115
5	-289	-342	-374	-457	111	130	140
6	-297	-287	-277	-251	96	93	84
7	-236	-235	-235	-233	100	100	99

In core, the stresses increase with increase in the stiffness of core. The percentage increase is lowest in the core interior and highest on the downstream face of core. For

$K=250$ the stress increase is almost constant all through the core thickness. The stress increase is minimum for σ_x and maximum for σ_z . The percentage increase is of the order of 10 to 15% at the core centre, 15 to 45% on the downstream face of core and 15 to 30% on the upstream face of core, as the modulus number K is increased from 100 to 1000.

On plane no. 2 the stress reduction in pervious zones is found to be still lesser than that on central section but in core the stress increase is found to be more on plane no. 2 as compared to that on central section. The higher core stresses imply transfer of stress from shells to core and would provide added safety against hydraulic fracturing in the central portion of the dam.

7.3.1.2 Mobilisation Factors

The maximum values of mobilisation factors, which occur near the dam base in pervious zones and at about mid height above base in core, are given in Table 7.4 for different locations over central section.

Table 7.4: Typical Maximum Values of Mobilisation Factors

Vert No.	Value of Mobilisation Factor for $K =$			
	100	250	400	1000
1	0.37	0.36	0.36	0.36
2	0.44	0.41	0.39	0.37
3	0.14	0.31	0.39	0.57
4	0.13	0.23	0.29	0.41
5	0.23	0.26	0.32	0.48
6	0.55	0.53	0.51	0.48
7	0.37	0.38	0.38	0.38

It is seen from the table that the mobilisation factors follow the trend of stresses, i.e., in shells the mobilisation factors remain practically unaffected by the value of K , while in transitions the mobilisation factors decrease slightly with increase in core stiffness. The decrease in values of mobilisation factors vary from 5 to 15% of the value at $K = 100$, when K is increased from 100 to 1000. In core the mobilisation factors increase with the stiffness of the core. The increase is maximum on the upstream face and reduces towards the downstream face. The increase in mobilisation factors in core is substantial and varies from 100 to 300% of the values at $K=100$, for $K=250$ to $K=1000$. It, therefore, follows that a dam with a stiffer core will have lower factor of safety against sliding.

Plane no. 2 is also found to exhibit a similar behaviour with regard to the mobilisation factors. Even though the mobilisation factors have higher values on this plane as compared to those on central section, the effect of core stiffness is smaller. In transitions the decrease in mobilisation factors is of the order of 5 to 15%, while in core the increase is of the order of 60 to 180% over the values of mobilisation factors with $K=100$, when the value of K for core is increased from 100 to 1000.

It, therefore, follows that the mobilisation factors are affected by the stiffness of the core. As the core becomes stiffer, the mobilisation factors decrease slightly in pervious zones but increase considerably in core. The reduction in the value of mobilisation factors is negligible at the dam faces

and increases towards the interior.

7.3.1.3 Displacements

The horizontal displacements along the river, u and the vertical settlement, w are plotted along height at different locations of central section, for different values of the core modulus number in Figs. 7.4 and 7.5. It is seen that the displacements, both horizontal and vertical decrease at all locations as the K value of core is increased. It is also seen that influence of K on displacements increases from dam face upto the core centre line from both sides. The reduction in displacement is very sharp when K is increased from 100 to 250 after which it is gradual upto $K = 1000$. The influence of core stiffness is more on the upstream side as compared to that on the downstream side. The effect of the core stiffness on horizontal movement is more than that on vertical movements.

Tables 7.5 and 7.6 show the maximum movement values at different verticals of central section for analyses with different values of K . The movements for analyses with $K=250$, 400 and 1000 expressed as a percentage of the movement values at $K=100$ are also shown in these tables.

It is noted from the tables that the magnitudes of horizontal movement expressed as a percentage of the movement with $K=100$ decrease by about 5-25% in shells, 15-40% in transitions and 55-70% in core. The vertical movements decrease by about 5% in shells, 20-30% in transition and by about 30-60% in core.

On plane no. 2 the movement values are small but still the same trend is observed here as well. The effect of core stiffness, however, is observed more in the transition zones and

lesser in core as compared to that on central section.

Table 7.5: Horizontal Movement -u (cms) Over Central Section

Vert No.	Maximum Values of u for K of core				Ratio r* (%) for K		
	100	250	400	1000	250	400	1000
1	-22.4	-22.0	-20.3	-17.8	95	85	75
2	-31.7	-25.7	-21.6	-14.3	85	75	60
3	-65.9	-19.2	-19.2	-17.4	45	40	30
4	-22.6	-6.7	-4.8	-1.2	30	25	10
5	17.4	12.2	11.1	9.5	70	60	55
6	17.3	17.0	15.7	13.7	98	90	80
7	17.5	16.7	16.4	15.2	95	92	88

* $r = (\text{Displacement at a given value of } K / \text{Displacement for } K=100) * 100$

Table 7.6: Vertical Movement - w (cms) Over Central Section

Vert No.	Maximum Values of w for K of core				Ratio r (%) for K		
	100	250	400	1000	250	400	1000
1	-43.4	-42.9	-41.6	-41.5	98	95	95
2	-104.4	-86.7	-70.2	-57.1	70	65	50
3	-111.9	-92.7	-76.2	-60.0	70	65	50
4	-128.3	-81.9	-68.6	-50.7	65	55	40
5	-78.0	-69.1	-66.3	-58.4	90	85	75
6	-67.7	-63.6	-61.4	-55.0	92	90	80
7	-54.7	-54.4	-54.4	-53.7	99	98	96

The variation of the maximum longitudinal horizontal displacement, v at different verticals of plane no. 2, with stiffness modulus, K of core is given in Table 7.7.

Table 7.7: Cross Valley Movements-v (cms) at Plane No. 2

Vert No.	Maximum Values of v for K of core				Ratio r ^o (%) for K		
	100	250	400	1000	250	400	1000
1	-10.5	-7.4	-7.7	-7.3	70	73	70
2	-12.3	-15.1	-12.5	-11.4	123	103	93
3	-27.1	-12.4	-11.7	-10.3	46	43	38
4	-22.3	-12.6	-10.4	-6.8	56	47	31
5	-29.6	-12.7	-12.8	-11.9	43	43	40
6	-14.2	-12.6	-12.5	-11.7	89	88	83
7	-9.3	-9.4	-9.4	-9.2	101	101	99

It is noted from the table that the cross valley movements are towards the central section for all values of core modulus number, K. For a soft core with $K = 100$, the cross valley movements in core are substantially higher than those in pervious zones. As the value of K is increased, the magnitudes of cross valley movements generally decrease at all locations in the section. The decrease is quite sharp as the value of K is increased from 100 to 250. Beyond $K = 250$, the decrease in magnitudes is gradual. In the dam portion downstream of core central line, the reduction in magnitude of cross valley movements, as K increases, is smaller than the corresponding decrease on the upstream side. As with transverse horizontal movement and vertical settlement, for longitudinal movements also the reduction in movements, as K is increased, is minimum at dam faces and increases towards the centre of core. In core the reduction in longitudinal movements expressed as a percentage of the movement at $K = 100$, is of the order of 40 to

70 %. In pervious zones the longitudinal movements reduce by about 10-30 % on the upstream side and by 5 to 10 % on the downstream side.

7.3.2 Effect of Valley Shape at Different Core Stiffness, Case(2)

7.3.2.1 Stresses

The three normal stresses σ_x , σ_y and σ_z are plotted against height for all the four analyses at two valley shapes at different locations of central section in Figs. 7.6 to 7.8.

It is seen that at all locations the stresses increase as the valley width factor β increases from 2.25 to 4.5 for both values of core modulus number, namely 400 and 1000.

The maximum values of the stresses at diferent verticals over central section for all the four analyses are shown in Tables 7.8 to 7.10. The differetⁿial ratio Δr at all locations on plane no. 1 and at the corresponding locations over plane no. 2 are also given in these tables. The differential ratio Δr is defined as

$$\Delta r = r_1 - r_2$$

where $r_1 = \frac{\text{Value of stress at } \beta = 4.5}{\text{Value of stress at } \beta = 2.25} * 100$ for $K = 400$

while r_2 pertains to the ratio at $K=1000$

It is noted from the tables that the absolute differential ratios both at plane no. 1 and 2 are almost negligible and less than 4%. It can, therefore, be inferred that the influence of valley shape/width is practically independent of the material properties, i.e., as the valley width is increased, the stresses increase in the same proportion irrespective of the material

properties.

Table 7.8: Horizontal Normal Stress σ_x (t/m^2) at Central Section

Vert No.	Values of σ_x (t/m^2) for K				Difference between the ratios, Δr , for plane no.	
	400		1000		1	2
	$\beta=2.25$	$\beta=4.5$	$\beta=2.25$	$\beta=4.5$		
1	-78	-92	-78	-90	2	1
2	-129	-144	-110	-121	2	-4
3	-284	-352	-315	-383	2	-2
4	-336	-374	-346	-380	1	-1
5	-308	-342	-356	-402	2	-3
6	-144	-151	-131	-145	2	2
7	-104	-132	-103	-131	0	0

Table 7.9: Horizontal Normal Stress σ_y (t/m^2) at Central Section

Vert No.	Values of σ_y (t/m^2) for K				Difference between the ratios, Δr , for plane no.	
	400		1000		1	2
	$\beta=2.25$	$\beta=4.5$	$\beta=2.25$	$\beta=4.5$		
1	-80	-96	-80	-95	2	1
2	-119	-135	-107	-120	2	-3
3	-304	-368	-320	-380	2	-2
4	-337	-374	-346	-381	1	-2
5	-331	-370	-396	-451	2	-3
6	-129	-144	-116	-136	4	-2
7	-107	-138	-106	-137	1	1

Table 7.10: Vertical Normal Stress σ_z (t/m²) at Central Section

Vert No.	Values of σ_z (t/m ²) for k				Difference between the ratios, Δr , for plane no.	
	400		1000		1	2
	$\beta=2.25$	$\beta=4.5$	$\beta=2.25$	$\beta=4.5$		
1	-164	-208	-163	-203	2	1
2	-245	-273	-223	-254	-1	-4
3	-323	-397	-341	-413	2	-1
4	-374	-416	-386	-425	1	-1
5	-374	-426	-457	-536	-1	-4
6	-285	-350	-249	-306	-2	-2

7.3.2.2 Displacements

The horizontal and vertical displacements u and w are plotted along height at different locations over central section for all the four analyses in Figs. 7.9 and 7.10 respectively. It is seen from the figures that for analyses with both $K=400$ and $K=1000$, the displacements increase as the valley shape is changed by increasing the valley width factor β from 2.25 to 4.5.

The maximum displacement values at different verticals for all the analyses are given in Tables 7.11 to 7.12. The differential ratios Δr for displacements (as defined for stresses) at all locations on central section and corresponding locations at plane no. 2 are also given in these tables.

It is noted from the tables that the differential ratios of displacement are of the order of 1 to 10% in case of horizontal movements and 2 to 6% in case of settlements. It is also observed that the increase in movements due to valley widening is more for $K=1000$ as compared to that for $K=400$ as

indicated by the negative values of the differential ratios. The differential ratios at plane no. 2 are lesser than those at central section. It can, therefore, be said that the displacements increase due to the widening of valley is slightly more for dams with stiffer cores. The difference, however, is small and can, therefore, be neglected.

Table 7.11 : Horizontal Movement u (cms) Over Central Section

Vert No.	Values of u (cms) for K				Difference between the ratios, Δr , for plane no.	
	400		1000		1	2
	$\beta=2.25$	$\beta=4.5$	$\beta=2.25$	$\beta=4.5$		
1	-20.3	-30.0	-17.8	-28.3	-10	6
2	-21.6	-28.2	-16.1	-20.2	-3	8
3	-19.6	-22.1	-17.4	-21.2	-7	-
5	12.5	17.4	12.4	18.6	-10	-
6	15.4	21.6	15.8	22.1	1	-8
7	16.4	26.0	15.2	24.8	-4	-4

Table 7.12 : Vertical Movement w (cms) Over Central Section

Vert No.	Values of w (cms) for K				Difference between the ratios, Δr , for plane no.	
	400		1000		1	2
	$\beta=2.25$	$\beta=4.5$	$\beta=2.25$	$\beta=4.5$		
1	-41.6	-49.2	-41.5	-51.7	-6	4
2	-70.2	-89.7	-57.1	-75.7	-5	-3
3	-76.2	-90.4	-60.0	-78.3	-6	1
4	-72.2	-94.5	-57.0	-80.4	-6	1
5	-66.3	-86.3	-58.4	-78.7	-5	2
6	-65.4	-79.2	-60.2	-74.3	-2	-1
7	-54.2	-72.6	-53.7	-73.3	-2	-2

7.4 CONCLUSIONS

1. As the core becomes stiffer, the stresses in pervious zones slightly reduce while those in core increase substantially. The reduction in stresses is almost negligible on the dam face and increases towards the interior.
2. The increase in core stresses as the core stiffness increases is minimum on the core centre line and largest on the downstream face of core.
3. A stiffer core provides higher resistance against hydraulic fracturing as compared to a softer core.
4. For shallow failure planes involving only the pervious zones, a stiffer core offers comparatively higher safety against sliding. However, for deep failure planes passing through core a stiffer core offers lower resistance against sliding as compared to a softer core.
5. The effect of core stiffness gradually diminishes towards the abutments.
6. The movements in the dam, both in pervious zones and core decrease as the core becomes stiffer. The decrease of movements is smaller at dam face and increases towards the interior from both sides. The reduction in movements is substantial and the upstream half is more influenced by core stiffness, in comparison to the downstream half.
7. The stresses and displacements increase in magnitude as the valley width factor increases and this increase is practically independent of the material properties within the range studied.

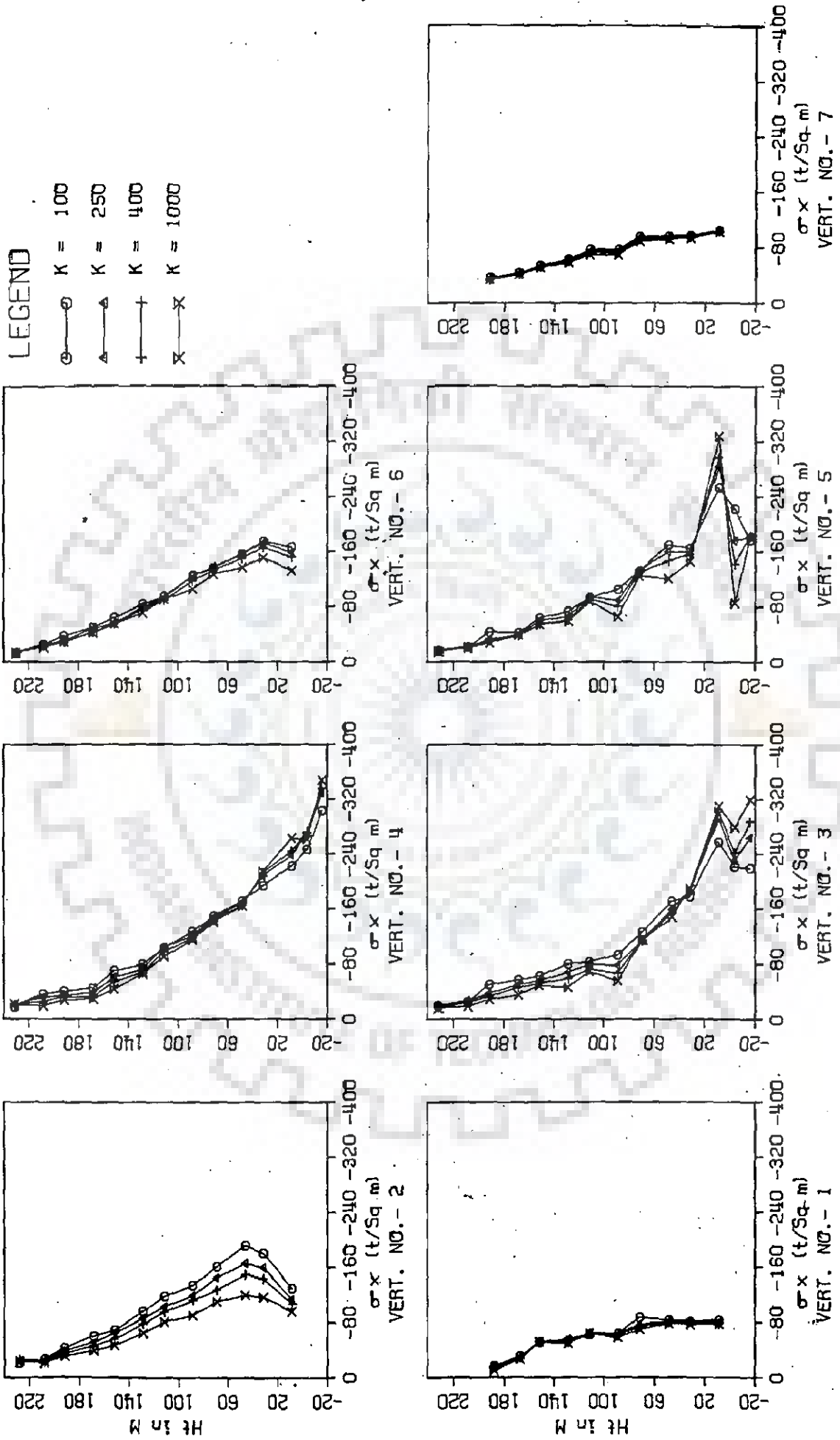


Fig 7.1 : Transverse Stress Over Central Section (Effect of K)

LEGEND

- K = 100
- △ K = 250
- † K = 400
- × K = 1000

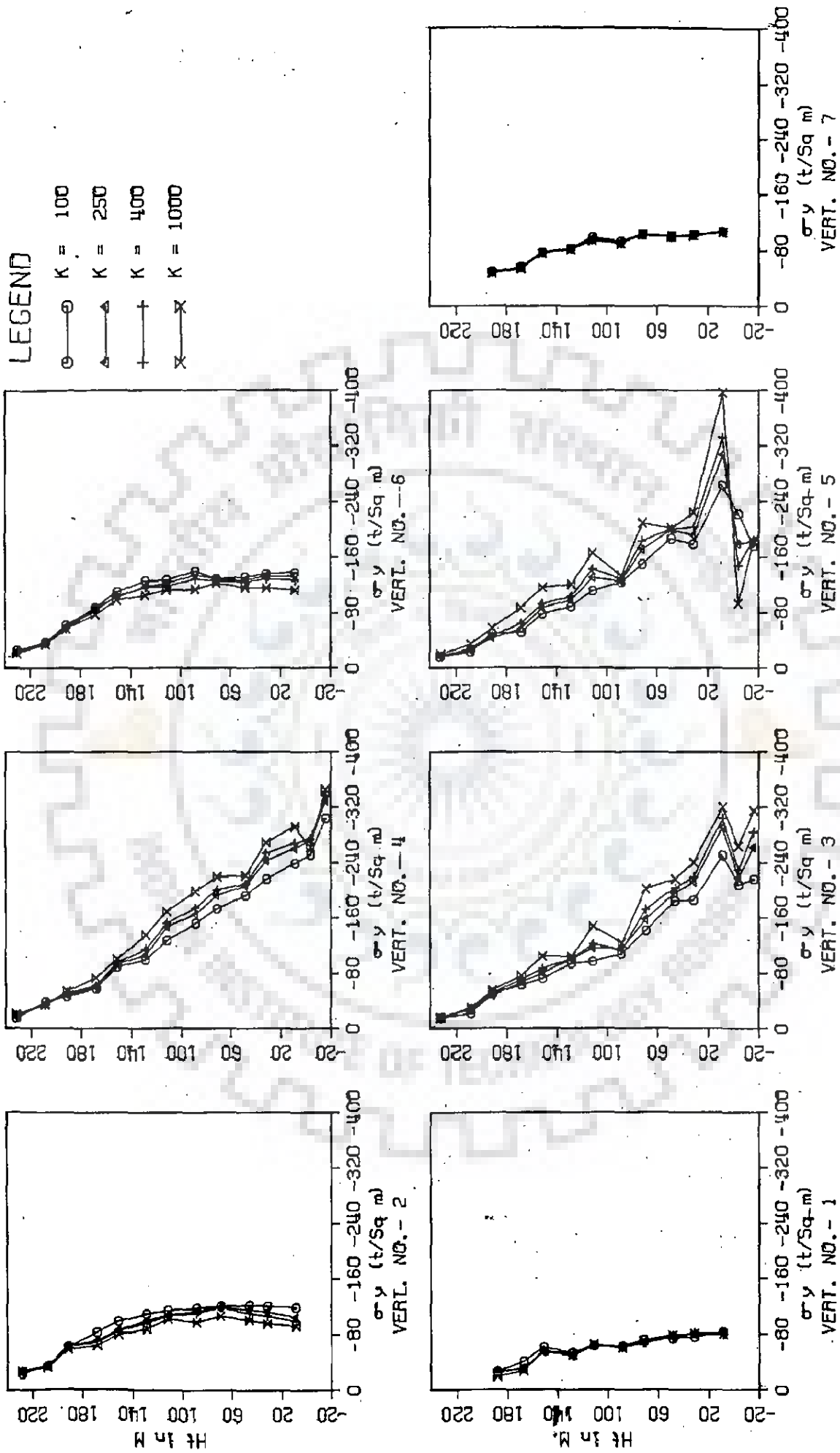


Fig 7.2: Longitudinal Stress Over Central Section (Effect of K)

LEGEND
 ○ K = 100
 △ K = 250
 + K = 400
 × K = 1000

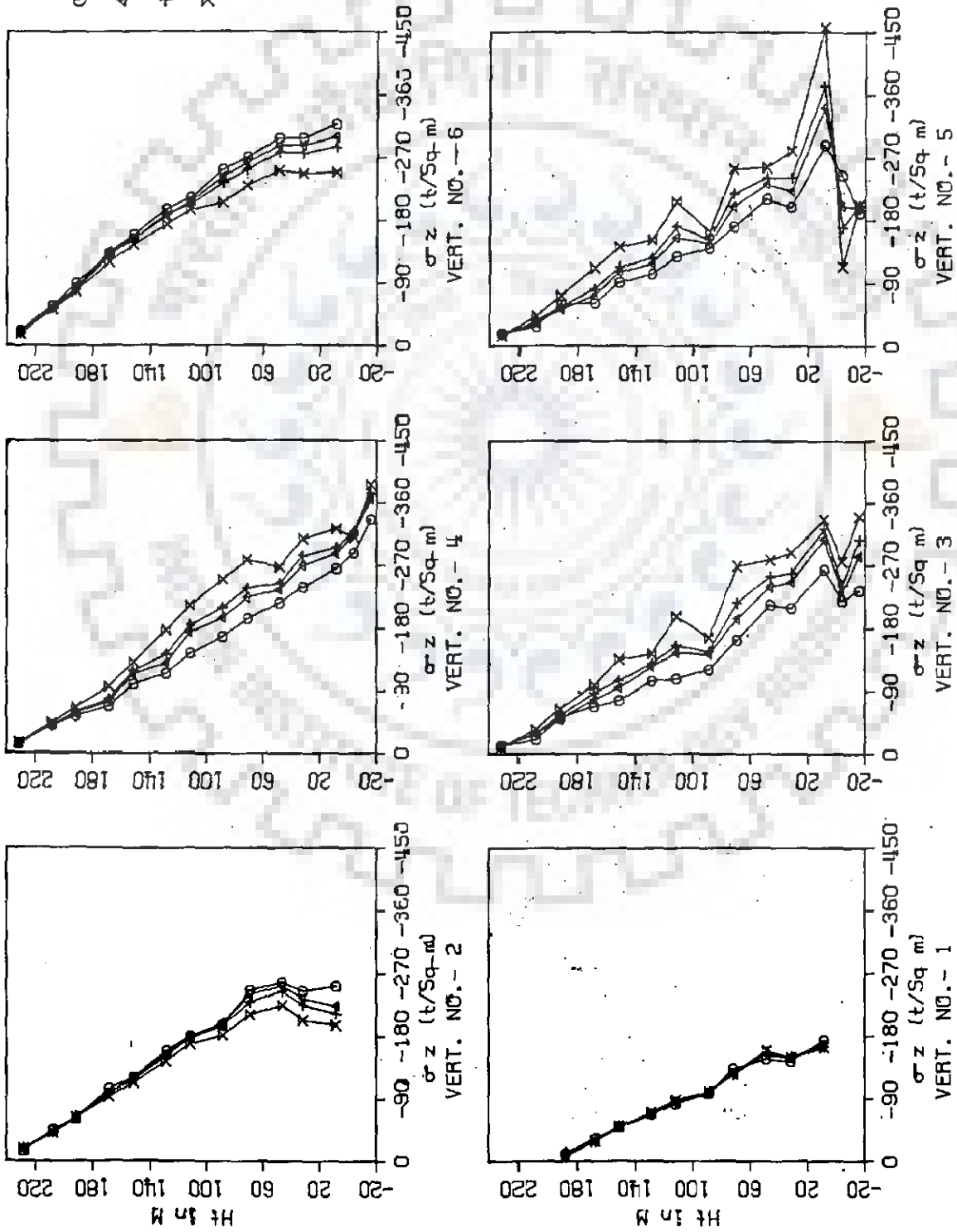
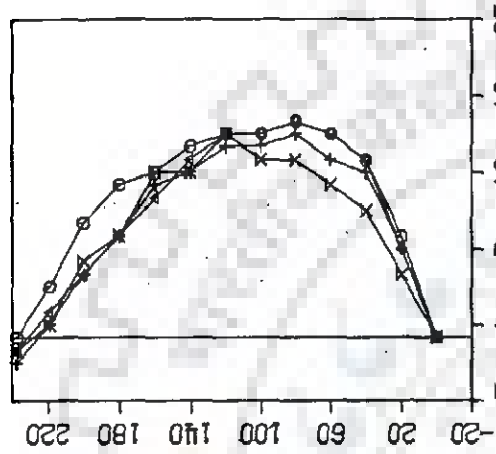


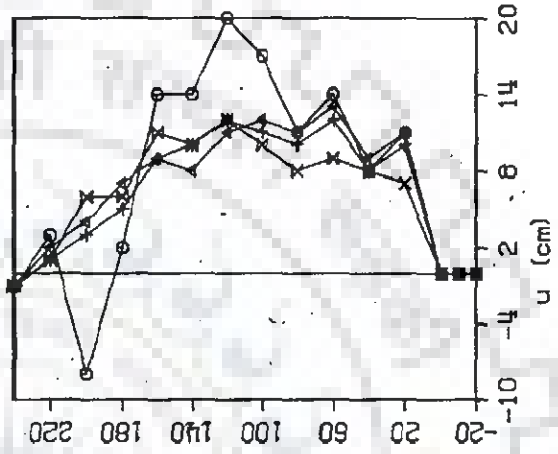
Fig 7.3: Vertical Stress Over Central Section (Effect of K)

LEGEND

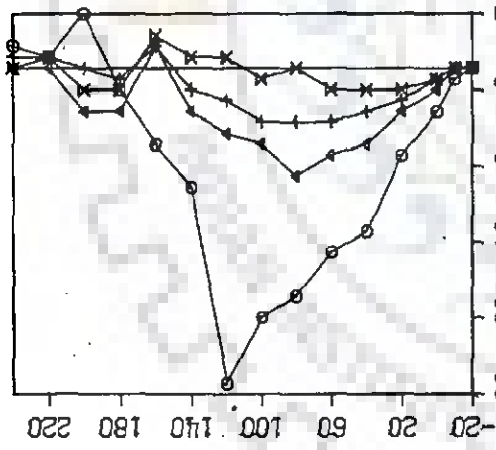
- K = 100
- △ K = 250
- † K = 400
- × K = 1000



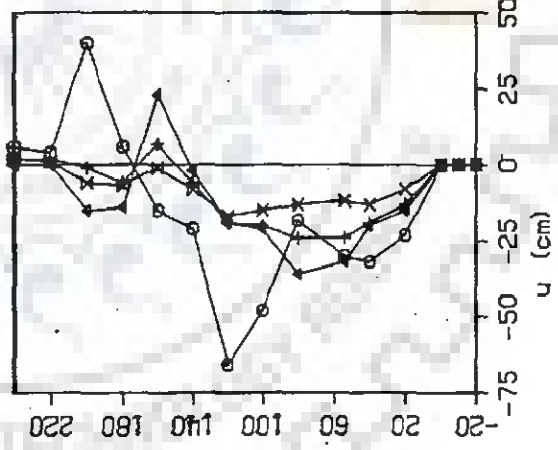
u (cm)
VERT. NO. - 6



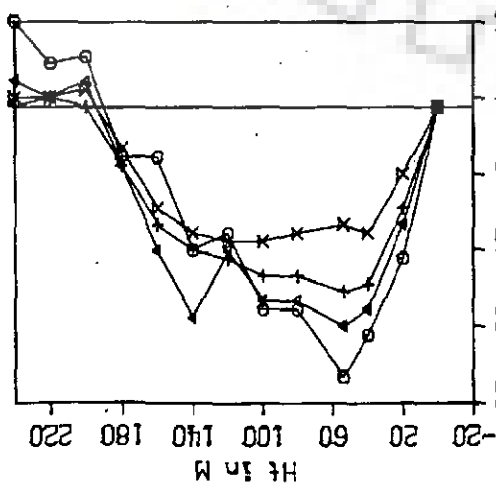
u (cm)
VERT. NO. - 5



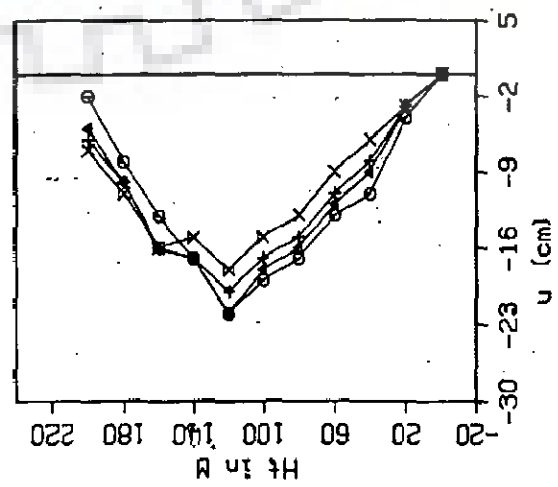
u (cm)
VERT. NO. - 4



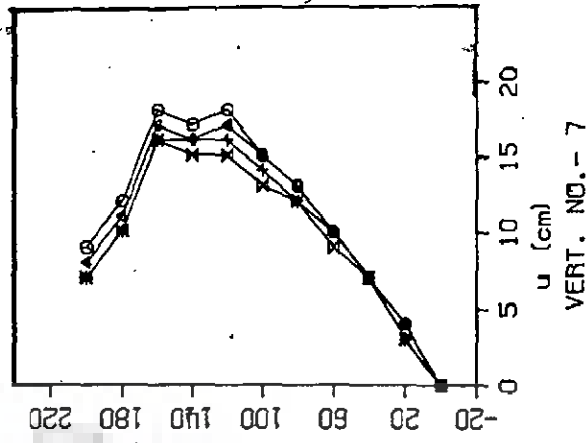
u (cm)
VERT. NO. - 3



u (cm)
VERT. NO. - 2



u (cm)
VERT. NO. - 1



u (cm)
VERT. NO. - 7

Fig 7.4: Horizontal Movement - u Over Central Section (Effect of K)

LEGEND

- K = 100
- △ K = 250
- † K = 400
- × K = 1000

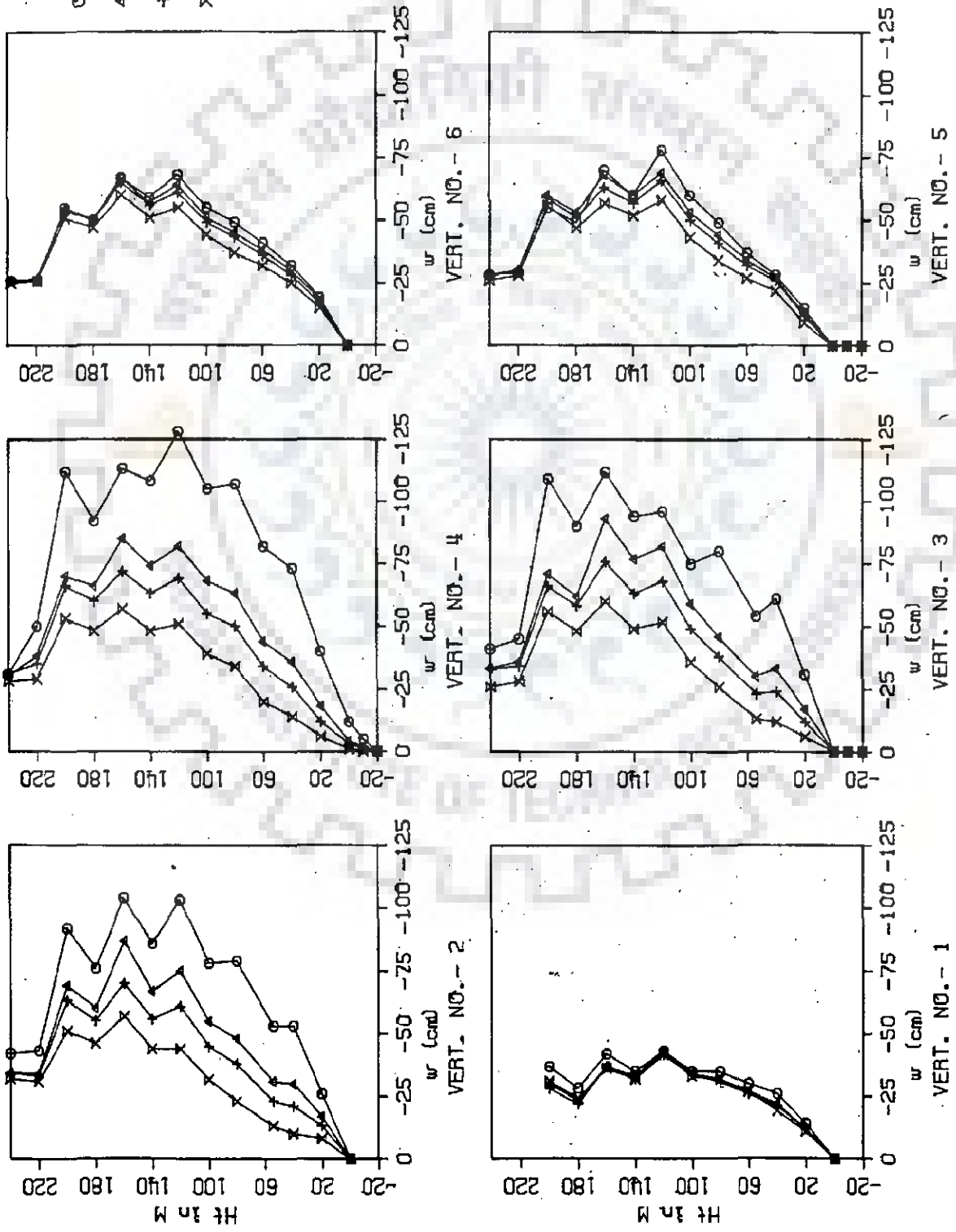


Fig 7.5: Vertical Movement -w Over Central Section (Effect of K)

LEGEND

- — $\beta = 2.25, K = 400$
- △ — $\beta = 4.50, K = 400$
- + — $\beta = 2.25, K = 1000$
- × — $\beta = 4.50, K = 1000$

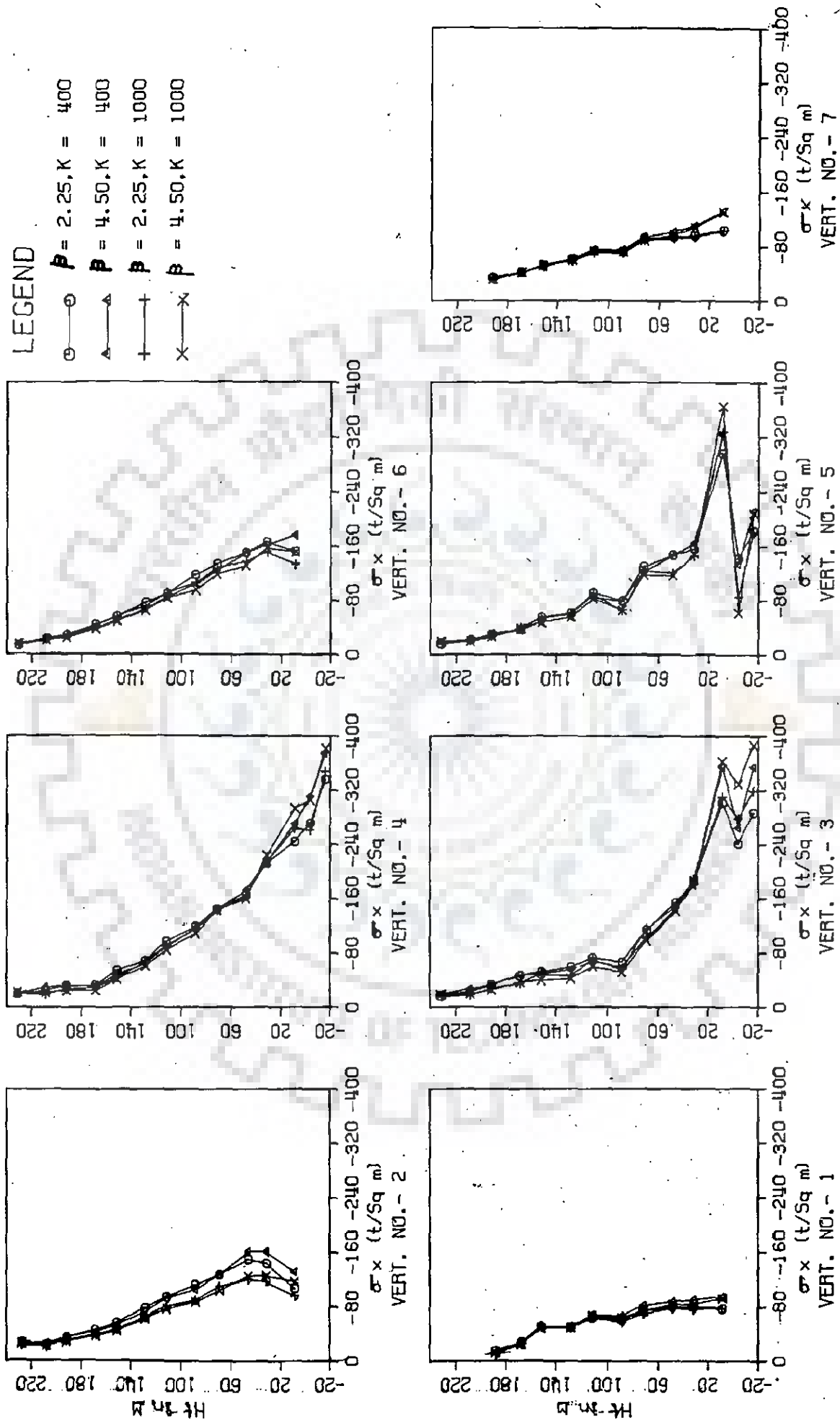


Fig 7.6: Transverse Stress Over Central Section (Effect of K and β)

LEGEND

- — $\beta = 2.25, K = 400$
- △ — $\beta = 4.50, K = 400$
- † — $\beta = 2.25, K = 1000$
- × — $\beta = 4.50, K = 1000$

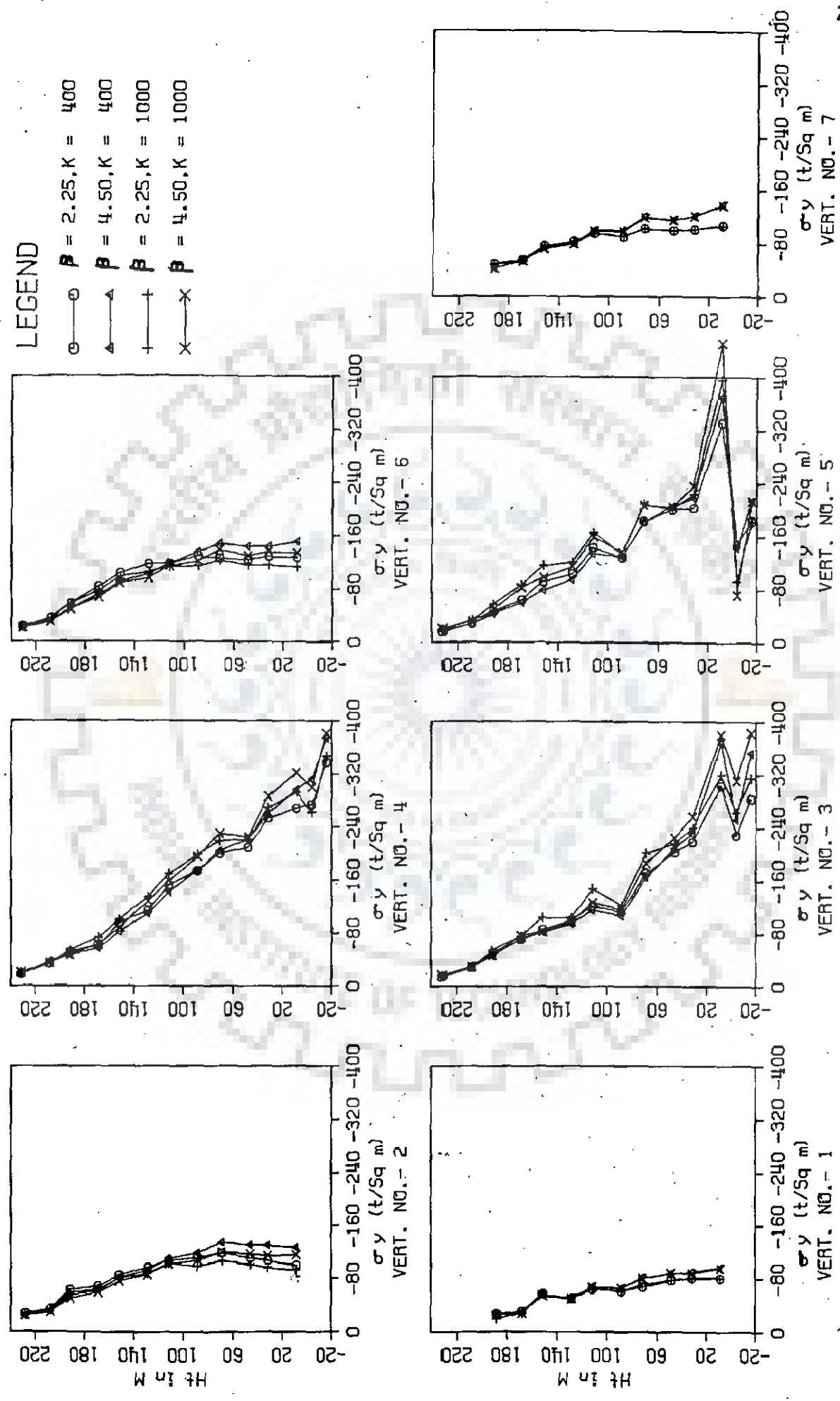


Fig.7: Longitudinal Stress Over Central Section (Effect of K and β)

LEGEND

- $\beta = 2.25, K = 400$
- △ $\beta = 4.50, K = 400$
- + $\beta = 2.25, K = 1000$
- × $\beta = 4.50, K = 1000$

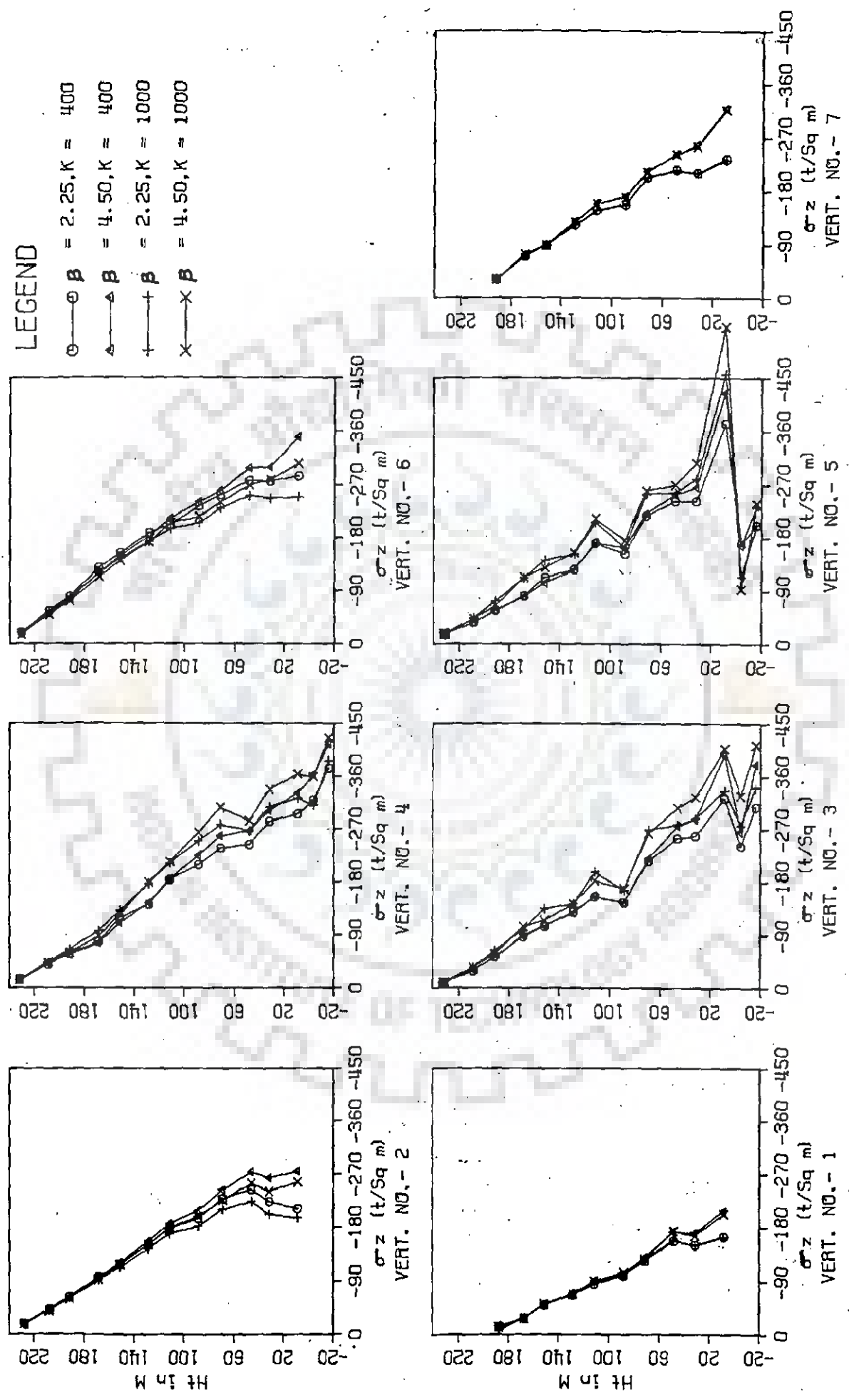


Fig. 7.8: Vertical Stress Over Central Section (Effect of K and β)

LEGEND

- $\beta = 2.25, K = 400$
- △ $\beta = 4.50, K = 400$
- + $\beta = 2.25, K = 1000$
- × $\beta = 4.50, K = 1000$

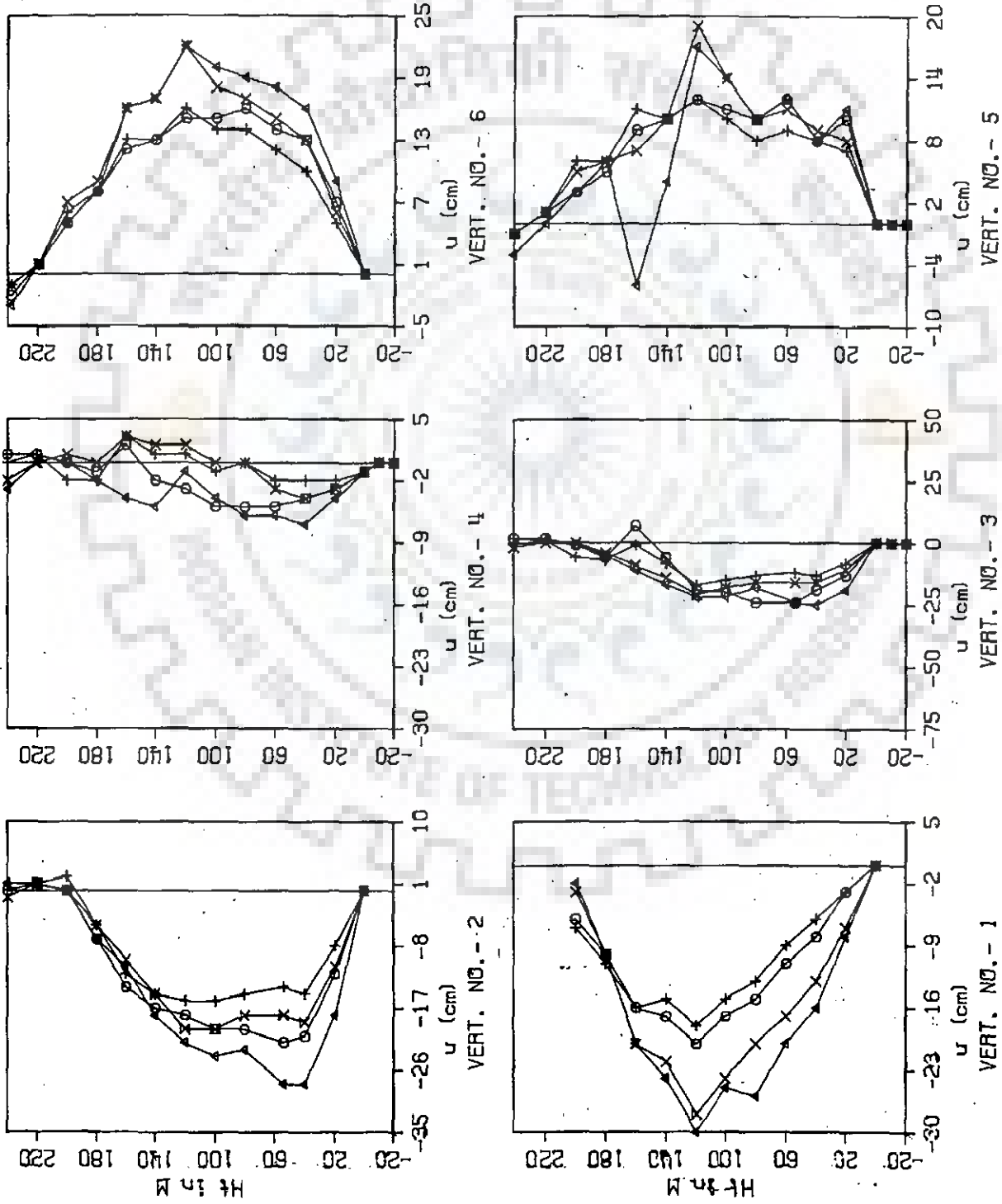


Fig 7.9: Horizontal Movement - u Over Central Section (Effect of β and K) 25

LEGEND

- = 2.25, K = 400
- △ = 4.50, K = 400
- = 2.25, K = 1000
- × = 4.50, K = 1000

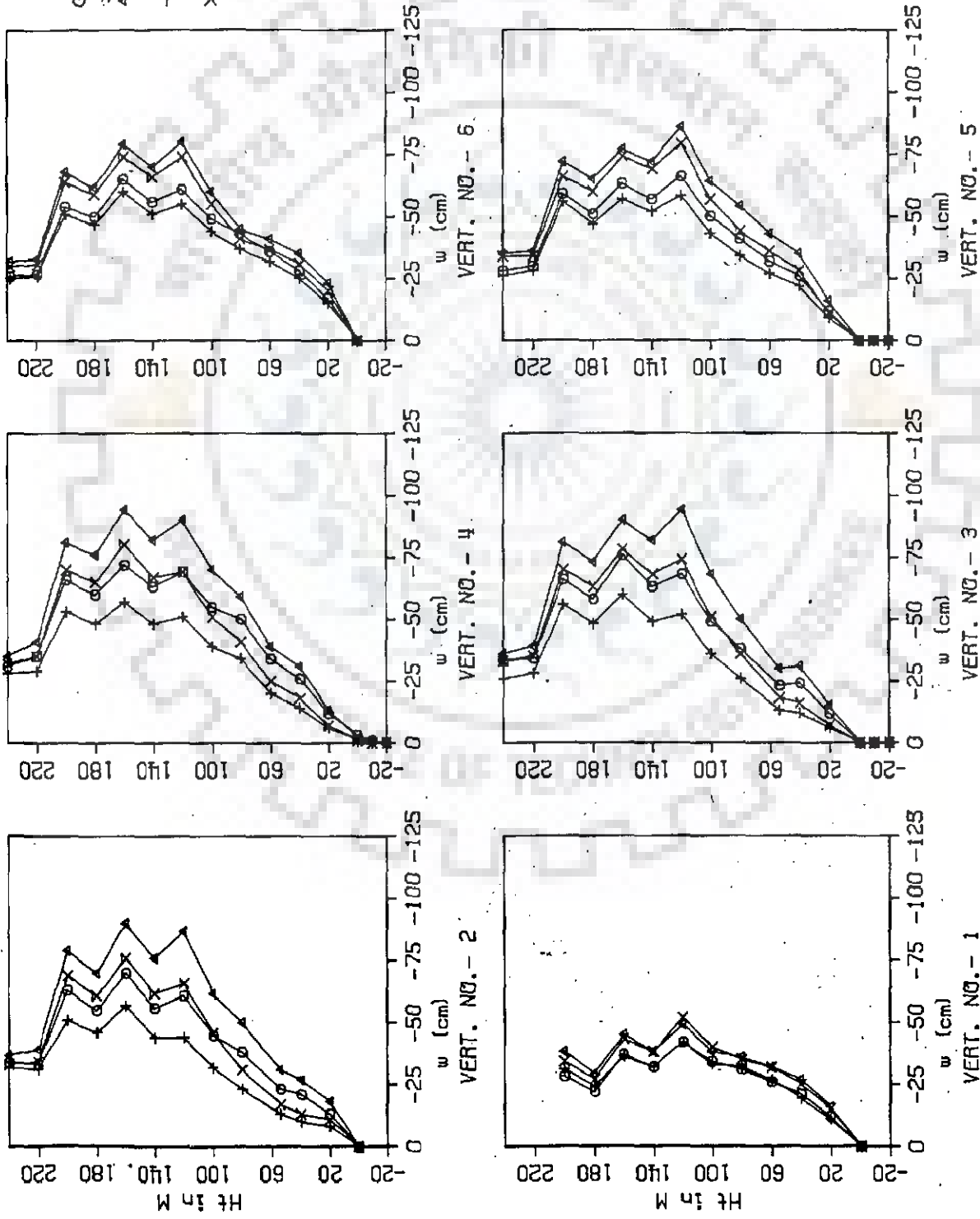


Fig 7.10: Vertical Movement -w Over Central Section (Effect of K and β)

CHAPTER 8

CONCLUSIONS

The following conclusions are drawn from this study

Effect of Valley Width factor

1. The displacements in the dam increase as the valley width factor β increases approaching plane strain values for valley width factor equal to 9. The effect of valley width factor on displacements is highest on the maximum transverse section and decreases towards the abutments.
2. On the maximum transverse section, the horizontal displacement values obtained from 3-D analyses with $\beta=1.12, 2.25, 4.5$ and 9 are about 25-40 %, 40-60 %, 55-80 % and 75-100 % of the plane strain values. In case of vertical displacements the corresponding figures are 35-40 %, 50-60%, 60-75 % and 90-98 % of the plane strain values.
3. Both the transverse horizontal and vertical displacements decrease sharply towards the abutments. The effect of valley width factor on displacements is negligible on planes near the abutments beyond valley width factor $\beta = 4.5$.
4. In the upper one third height of dam, the stresses obtained from 3-D analyses with different valley shapes are of nearly the same magnitude. In the lower two-third height of dam the effect of valley shape on stresses is substantial and the stresses increase with increasing valley width factor approaching plane strain values at $\beta = 4.5$.
5. Over the maximum transverse section the stresses obtained

from 3-D analyses with $\beta = 1.12, 2.25$ and 4.5 or more are about $50-60\%$, $70-80\%$ and $90-100\%$, of the corresponding plane strain values. The magnitudes of the stresses and the effect of valley width factor thereupon increase towards the abutments.

6. The distribution pattern of both stresses and displacements as well as the location of their maxima are same for all valley shapes. The distribution pattern along height for any stage of construction is almost similar to the distribution pattern for the full height of dam.
7. The principal stress ratios and mobilisation factors increase with valley width factor on the maximum transverse section. Both increase towards the abutments. However, the mobilisation factors in core decrease towards the abutments. The potential failure surfaces are wedge shaped on the central section and circular on planes away from it. The factor of safety against sliding decreases towards the abutments.

EFFECT OF VALLEY BASE WIDTH AND WALL SLOPES

1. Even though the increase in valley base width alone does not appreciably increase the valley width factor, the effect of base width on the increase in stresses and displacements is more than that of the increase in valley wall slope. This contribution of valley base width is maximum on central section and decreases towards the abutments.
2. The increase in stresses and displacements, due to the increase in valley wall inclination from vertical, at constant base width, reduces as the valley base width is

increased. The increase is least on central section and increases towards the abutments. At constant valley base width, the increase of valley wall slope alone beyond 1H:1V has no effect on stress magnitudes. As far as the displacements are concerned, at central section the displacements increase with increasing valley wall slope from the vertical but on plane no. 2, flattening the valley beyond 1H:1V does not increase the displacement magnitudes.

3. The mobilisation factors and the principal stress ratios increase with increase in valley base width at constant valley wall slope in all zones of dam at central section. On planes towards the abutments, in pervious zones of the dam, the mobilisation factors and principal stress ratios are not affected by the change in valley base width.

For a circular sliding surface passing largely through pervious zones, at central section a valley with narrow base width gives a higher factor of safety as compared to a valley with a wider base width. On planes towards the abutments the position is opposite to it. At constant base width a flatter valley gives a higher factor of safety as compared to a steep walled valley.

For a deep failure surface involving the core in the slide, the dam in a valley with smaller base width and steeper wall slope has a higher factor of safety against sliding as compared to the one in a wide and flatter valley. The influence of valley wall slope on sliding stability of the dam is substantial at central section

but decreases rapidly towards the abutments.

EFFECT OF MATERIAL PROPERTIES

1. As the core becomes stiffer, there is a decrease in the stresses in the pervious zones while the stresses in core increase. The reduction in stresses in pervious zones is least on the dam faces and increases towards the transitions. Over the stress values for K of core = 100, the reduction in shells varies from 1 to 5 %, and in transitions from 5 to 15 %, as K is increased from 100 to 1000. The increase in stresses in the core is of the order of 15-40 % of the corresponding stress values for $K = 100$.
2. Towards the abutments, the effect of core stiffness on stresses in pervious zones decreases and that in core increases.
3. For shallow sliding surfaces encompassing only the shells a stiffer core provides more resistance against sliding while for deep failure planes passing through core also, a softer core offers higher resistance against sliding in comparison to that offered by a stiffer core.
4. The displacements all over the dam decrease as the core becomes stiffer. The decrease in displacements is substantial and is least on dam faces and increases towards the core interior. At central section the decrease in displacements over the corresponding values for $K = 100$ is about 5-25 % in shells and 55-70 % in core for horizontal displacements and 5 % in shells to 30-60 % in core for vertical displacements, as the value of K of core increases from 100 to 1000.
5. The effect of valley width factor on stresses and

displacements is not affected by the value of core stiffness.



REFERENCES

1. Alberro, J., "Stress Strain Analysis of El-Infiernillo Dam", ASCE, Speciality Conference on Performance of Earth and Earth Supported Structures, Purdue University. June 1972
2. Al - Hussani, M.M. and Radhakrishnan, N., "Analysis of Plane Strain Tests Using the Finite Element Method" Application of the Finite Element Method in Geotechnical Engineering, Proc. of the Symposium held at Vicksburg, Mississippi, 1972
3. Anderson, K.H., "Skredet i Kimola Flotnings kanal, Finland, Norwegian Geotechnical Institute. Publication No 90
4. Bishop, A. W., "The Use of the Slip Circle in Stability Analysis of Slopes", Geotechnique, Vol 5, 1955, pp 7-17.
5. Botta, L. P., Varde, O. A., Paitovi, O. and Anderson, C. A., "Comparison between Predicted and Observed Behaviour of Alicura Dam, Argentina", Proc. of 15th ICOLD, Lausanne, June 1985, Q56, R43, pp 813-838.
6. Clough, R. W., "Comparison of Three Dimensional Finite Elements", Symp. on Appl. of Finite Element Methods in Civil Engg., ASCE-Vanderbilt Univ., Nashville., Nov 1969.
7. Clough, R.W., and Woodward, R.J., "Analysis of Embankment Stresses and Deformations, " JSMFD, ASCE, Vol 93, No SM4, July 1967.
8. Clough, R. W., and Zienkiewicz, O. C., "Finite Element Method in Analysis And Design of Dams " Proc of Symposium on Criteria and Assumptions for Numerical Analysis of Dams, Swansea, 1975, pp 286-307
9. Cole, K.W. and Burland, J.B., "Observations of Retaining Wall Movements Associated With a Large Excavation" , Proc. of the 5th European Conference on Soil Mechanics and Foundation Engg, Madrid, April 1972
10. D'Appolonia, D.J., and Lambe, T.W., " Method for Predicting Initial Settlements", Journal of SMFD, ASCE, VOL 98, NO SM2, Proc. paper 7167, March 1970
11. Desai, C.S., " Non linear Analysis using Spline Functions", JSMFD, Vol 97, No SM10, Oct. 1971
12. Desai, C. S and Abel, J. E " Introduction to the Finite Element Method " Van Nostrand - Reinhold, N. Y., 1972
13. Desai, C.S and Christian, J.T., "Numerical Methods in Geotechnical Engineering", MC Graw-Hill Book Co., New York, 1977

14. Domaschuk, L. and Wade, N.H., " A Study of Bulk and Shear Moduli of Sand", JSMFD, ASCE, Vol 95, No SM2, March 1969, pp 561-582
15. Domaschuk, L. and Valliappan, P., " Nonlinear Settlement Analysis by Finite Element", Journal of Geotech. Engg. Div, ASCE, Vol 101, No. GT7, July 1975, pp 601-614
16. Duncan, J.M. and Chang, C.Y., " Nonlinear Analysis of Stress and Strains in Soils", JSMFD, ASCE, Vol 96, No. SM5, Proc paper 7513, Sept 1970, pp 1629-1653
17. Duncan, J.M., "Finite Element Analysis of Stresses and Movements in Dams, Excavation and Slopes, State of the Art," Application of the Finite Element Method in Geotechnical Engineering, Proc of the Symposium held at Vicksburg, Mississippi, Vol 1, 1972
18. Duncan, J.M., Byrne, P., Wong, K.S. and Marby, P., "Strength, Stress-Strain and Bulk Modulus Parameters for Finite Element Analysis of Stresses and Movements in Soil Masses", Report No. UCB/GT/78-02, University of California, Berkeley, April 1978
19. Dunlop, P. and Duncan J.M., and Seed, H.B., " Finite Element Analysis of Slopes in Soil", Geotechnical Engineering, University of California, Berkeley, Report no TE-68-3, May, 1968
20. Dunlop, P. and Duncan, J.M., "Development of Failure Around Excavated Slopes", JSMFD, ASCE, Vol 96, No SM2, Proc. paper 7162, March 1970, pp 471-493
21. Eisenstein Z., Krishnayya A.V.G., Morgenstern, N.R., "An Analysis of Cracking in Earth Dams ", Application of the Finite Element Method in Geotechnical Engineering, Proc of the Symposium held at Vicksburg, Mississippi, Vol 1, 1972 ,pp 431-454
22. Eisenstein, Z. , Krishnayya, A.V.G., and Morgenstern, N.R. , "An Analysis of Cracking at Duncan Dam" , Proc of ASCE Speciality Conf on Performance of Earth and Earth Supported Structures, Purdue University, Lafayette, Indiana, Vol I, pp 765-777
23. Eisenstein, Z and Simmons, J.V., " Three Dimensional Analysis of Mica Dam" , Proc of Symposium on Criteria and Assumptions for Numerical Analysis of Dams, Swansea, 1975, pp 1051-1069
24. Fellenius, W., "Calculation of the Stability of Earth dams", Trans. 2nd Cong. on Large Dams, Vol 4, Washington, 1936.
25. Hansen, T.B., " Discussion-Hyperbolic Stress-Strain Relationship for Cohesive Soil" , JSMFD, ASCE, Vol 89, No SM4, 1963, pp 241-242

26. Hølemberg, S., " Preliminary Finite Element Analysis of Two Test Embankments in Thailand". Norwegian Geotechnical Institute, Internal Report, Dec, 1971
27. Irons, B. M., " A Frontal Solution Program for Finite Element Analysis", Int J. Num Meth in Engg., 2, 5-32, 1970.
28. Izumi, H., Kamemura, K. and Sato, S., " Finite Element Analysis of Stresses and Movements in Excavations", Numerical Methods in Geomechanics, ASCE, 1976, pp 701-712
29. Janbu, N., "Earth Pressures and Bearing Capacity Calculations by Generalized Procedure of Slices", Proc. 4th Int. Conf. Soil Mech. Found. Eng, London, 1957, Vol 2 ,pp 207-212.
30. Janbu, N., "Soil Compressibility as Determined by Oedometer and Triaxial Tests, " Proceedings, European Conference on Soil Mechanics and Foundation Engineering, Vol I, Weisbaden, 1963, pp. 19-25
31. Jaworski, W.E., " An Evaluation of the Performance of a Braced Excavation", Sc. D. Thesis, Deptt. of Civil Engg., M.I.T, Cambridge Mass, 1973
32. Justo, J.L and Saura, J., " Three Dimensional Analysis of Infiernillo Dam During Construction and Filling of the Reservoir", Int. Journal of Numerical and Analytical Method in Geomechanics, Vol 7, 1983, pp 225-243
33. Knight, D.J. , Naylor, D.J., and Davis, P.D., " Stress-Strain Behaviour of the Mona Savu Soft Core Rockfill Dam Prediction, Performance and Analysis" Proc of 15th ICOLD, Lausanne, June 1985.
34. Kondner, R.L., " Hyperbolic Stress-Strain Response: Cohesive Soils". JSMFD, ASCE, Vol 89, No SM1, Feb, 1963, p115
35. Kulhawy, F. H., Duncan, J. M. and Seed, H. B., "Finite Element Analyses of Stresses and Movements in Dams During Construction", Report No. TE-69-4, Office of Research Services, University Of California, Berkeley, 1969.
36. Kulhawy, F.H. and Duncan, J.M., "Nonlinear Finite Element Analysis of Stresses and Movements in Oroville Dam". Geotechnical Engg. Univ. of California, Report No. TE-70-2
37. Kulhawy, Fred H. and Duncan, James M., "Stresses and Movements in Oroville Dam" JSMFD, ASCE, SM7, July 1972.
38. Kulhawy, Fred H. and Gurtowski, Thomas M., "Load Transfer and Hydraulic Fracturing in Zoned Dams", JGTE, ASCE, GT9, Sept 1976, pp 963-974.

39. Lefebvre, G., Duncan, J.M. and Wilson, E.L., "Three Dimensional F.E. Analysis of Dams", JSMFD, ASCE, SM7, Vol-29, pp 495-507
40. Lee, K.L. and Idriss, I.M., "Static Stresses by Linear and Nonlinear Methods", J.Geotech Engg Div, Proc ASCE, Vol 101, pp 871-877
41. Marsal, R.J. and Moreno, E.G., "Investigations of the Design and Performance During Construction of Chicoasen Dam, Maxico", Contribution to the XIII ICOLD, New Delhi, 1979
42. Mejia, Lelio H. and Seed, Botton H., "Comparison of 2-D and 3-D Dynamic Analyses of Earth Dams", Journal of Geotechnical Engg., ASCE, Vol 109, No. 11, Nov 1983.
43. Morgenstern, N. R. and Price, V. E., "The Analysis of the Stability of General Slip Surfaces", Geotechnique, Vol 3, Sept 1958.
44. Nayak, G. C and Zienkiewicz, O. C. "Elasto - Plastic Stress Analysis. Generalisation for Various Constitutive Relations Including Strain Softening", Int. J. Num Meth Engg, 5, 113-135, 1972.
45. Naylor, D.J. and Pande, G.N., "Finite Elements in Geotechnical Engineering", Pineridge Press, Swansea, U.K, 1981
46. Nobari, E. S and Duncan, J. M., "Movements in Dams Due to Reservoir Filling ". Proc. ASCE speciality Confrence on Performance of Earth and Earth - Supported Structures, Purdue University, Lafayette, Indian, pp. 797-815.
47. Palmerton, J. B., "Application of Three Dimensional Finite Element Analysis", Proc., WES Symp on Appl. of Finite Element Method in Geotechnical Engg., Vicksburg, Miss., May 1972.
48. Pare, J. J., Verma, N. S., Keira, M. S and McConnell, A. D., "Stress Deformation Prediction for the LG-4 Main Dam", Canadian Geotechnical Journal, Vol 21, No. 2, 1984, pp 213-222.
49. Penman, A, and Charles, A., "Constructional Deformations in Rockfill Dam" ,JSMFD, ASCE, SM2, VOL 99,1973
50. Pinto, P.S. Seico E., Noves, E. Maranha Das, "Hydraulic Fracturing in Zoned Earth and Rockfill Dams", Proc. of XIth Int. Conf. on Soil Mech and Found. Engg, San Francisco, Aug 85, pp 2025-2030.
51. Priscu, D., Stematiu, D. and Dobrescu, D., "Capabilities of Mathematical Models to Predict Dam Behaviour During Erection of Riusor Rockfill Dam", Proc. 15th ICOLD, Lausanne, June 1985, Q56, R34.

52. Resendiz, Daniel and Romo, Miguel P. "Analysis of Embankment Deformations" Proc of Speciality Conf on Performance of Earth & Earth Supported Structures, Purdue University, Lafayette, India, June 1972.
53. Seed, Bolton H. ; Duncan, J. M. and Idriss, I. M., "Criteria and Methods for Static and Dyanamic Analysis of Earth Dams " Proc of Symposium on Criteria and Assumptions for Numerical Analysis of Dams, Swansea, 1975, pp563-588
54. Seed, H. B.,and Sultan ,H.A., "Stability Analysis of Sloping Core Earth Dams", JSMFD, ASCE, Vol 93, No SM4, 1967.
55. Sharma, H. D., Nayak, G.C. and Maheshwari, J. B., "Non-Linear Stress Analysis of Rickfill Dam by Finite Element Methods", Proc. Int. Conf. on Finite Element Methods in Engineering, Dec 1974, Coimbtore, India.
56. Sharma, H. D., Nayak, G. C. and Maheshwari, J. B., "Nonlinear Analysis of Rockfill Dam with Vertical and Inclined Cores, International Symposium on Criteria and Assumptions for Numerical Analysis of Dams, 8-11 Sept. 1975, University of Wales, Swansea, U. K.
57. Sherard , J. L., Woodward, R. J., Gizienski, S. F. and Clevenger, W. A., "Earth and Earth Rock Dams", John Wiley and Sons, Inc., New York, 1963, pp 367, 350, 359.
58. Singh, B. , Nayak, G.C. and Puri, N., "Abutment Slopes on Stress and Strain Distribution in clay Cores" , Irrigation and Power Journal , India, April 1976.
59. Singh, R. P., Gupta, S. K. and Saini, S. S., "Three Dimensional Analysis of Tehri Dam", Proc. Indian Geotechnical Confrence, Roorkee, India, Dec. 16-18, 1985, Vol. 1, pp. 481-486.
60. Tanaka, T. and Nakano, R., "Finite Element Analysis of Miyano Rockfill Dam, "Numerical Methods in Geomechanics, Vol II, Virginia Polytechnic Institute and State University, Blacksburg, Virginia, USA, June 76, pp 650-651.
61. Taylor, Donald W., "Fundamentals of Soil Mechanics", John Wiley and Sons, London, 1948.
62. Vagneron, J., Lada, P.V. and Lee, K.L., " Evaluation of Three Stress-Strain Models for Soils", Numerical Methods in Geomechanics, ASCE, 1976, pp 1329-1351
63. Wong, I.H., " Analysis of Braced Excavations, Sc. D Thesis, Deptt. of Civil Engg., M.I.T. , Cambridge, Mass, 1971

64. Yasunaka, M., Tanaka, T. and Nakano, R., "The Behaviour of Fukado Dam During Construction and Impounding of the Reservoir", Proc. of 15th ICOLD, Lausanne, June 1985, Q56, R24, pp 491-518
65. Zienkiewicz, O. C., "The Finite Element Method ", McGraw Hill, 1979
66. Zienkiewicz, O. C., Irons, B. M., Ergatoudis, J., Ahmad, S. and Scott, F. C., "Isoparametric and Associated Element Families for Two and Three - Dimensional Analysis," Proc. course on Finite Element Method in stress Analysis (Ed. by I. Holand and R. Bell), Tech. Univ., Trondheim, 1969
67. Zienkiewicz, O. C., Valliappan, S., and King, I.P., "Elasto-Plastic Solutions of Engineering Problems :Initial Stress, Finite Element Approach "., Int Journal for Num. Meth in Engg, Vol I, 1969, pp 75-100

